TECHNISCHE UNIVERSITÄT MÜNCHEN

FAKULTÄT FÜR CHEMIE

LEHRSTUHL FÜR ORGANISCHE CHEMIE II

Investigation of the role of VAT-1 as a target of the natural product neocarzilin A in tumor cell migration

DISSERTATION ZUR ERLANGUNG DES AKADEMISCHEN GRADES EINES

DOKTORS DER NATURWISSENSCHAFTEN VON

Carolin Marie-Luise Gleißner

München, 2020

TECHNISCHE UNIVERSITÄT MÜNCHEN
FAKULTÄT FÜR CHEMIE
LEHRSTUHL FÜR ORGANISCHE CHEMIE II

Investigation of the role of VAT-1 as a target of the natural product neocarzilin A in tumor cell migration

Carolin Marie-Luise Gleißner

Vollständiger Abdruck der von der Fakultät für Chemie der Technischen Universität München zur Erlangung des akademischen Grades eines

Doktors der Naturwissenschaften (Dr. rer. nat.)

genehmigten Dissertation.

Vorsitzender: Prof. Dr. Matthias Feige

Prüfer der Dissertation: 1. Prof. Dr. Stephan A. Sieber

                              2. Prof. Dr. Kathrin Lang

Die Dissertation wurde am 27.04.2020 bei der Technischen Universität München eingereicht und durch die Fakultät für Chemie am 22.06.2020 angenommen.

- Meiner Familie gewidmet -

"Die Definition von Wahnsinn ist, immer wieder das Gleiche zu tun und andere Ergebnisse zu erwarten."

- Albert Einstein -

DANKSAGUNG

Die drei Jahre meiner Promotion am AK Sieber waren eine wunderbare Zeit, in der ich fachlich und vor allem persönlich sehr viel gelernt habe und an die ich mich immer gerne erinnern werde. Das alles habe ich natürlich nicht allein geschafft und möchte mich hiermit bei allen für ihre große Unterstützung bedanken.

Zu allererst möchte ich mich bei PROF. STEPHAN SIEBER für die Möglichkeit bedanken, die Promotion an seinem Lehrstuhl anfertigen zu können. Ich bedanke mich für alle fachlichen Gespräche mit ihm, sein Interesse am Neocarzilin Projekt, seine zahlreichen Ideen und seine Vorschläge für neue Kooperationen. Es war super, in einem so gut ausgestatteten Labor arbeiten zu können. Ich bin außerdem froh über sein Talent, mit zahlreichen Anträgen und auch dem Neocarzilin Projekt eine sehr gute Finanzierung des Laboralltags zu ermöglichen. Am meisten danke ich ihm für die Freiheit, die er mir bei der Planung der Experimente gegeben hat, um ein selbstständiges und kreatives Arbeiten zu ermöglichen. Ich bin ihm weiterhin auch sehr dankbar für die Möglichkeit, auf internationalen Konferenzen meine Ergebnisse präsentieren zu können und auf Workshops mein Wissen zu erweitern.

Ich bin für das Korrekturlesen dieser Arbeit bin ich MARTIN PFANZELT, DR. VOLKER KIRSCH, DR. CAROLIN PYKA, DR. STEPHAN HACKER und DIETRICH MOSTERT sehr, sehr dankbar für die investierte Zeit.

Ein besonderer Dank gilt allen Kooperationspartnern, die mich während meiner Promotion unterstützt haben. Ich möchte mich vor allem bei PROF. ANGELIKA VOLLMAR, DR. SIMONE BRAIG und DR. CAROLIN PYKA von der LMU für die tolle Neocarzilin Kooperation bedanken. Die Kommunikation und Zusammenarbeit mit euch hat mir sehr viel Spaß gemacht. Für die zahlreichen Telefonate und Treffen für die Neocarzilin Publikation möchte ich vor allem bei dir, CARO, bedanken. Die Zusammenarbeit war großartig mit dir, das Ergebnis war super und ich wünsche dir nur das Beste. ADRIAN JAUCH als Nachfolger des LMU Neocarzilin Teams wünsche ich viel Erfolg für die kommenden Jahre. Zusätzlich möchte ich mich sehr bei DR. SABINE SCHNEIDER für die Kooperation bezüglich der VAT- 1 Proteinaufreinigung und Kristallisation bedanken.

ABSTRACT

The burden of cancer in the world is still growing. Importantly, tumor metastases reduce survival rates and, therefore, represent one of the biggest challenges in cancer therapy. Consequently, there is an urgent need for new drug candidates targeting cell migration in tumor cells, which is a crucial step in cancer metastasis. Anti-cancer drugs are often inspired by natural products, which are secondary metabolites with unique, complicated scaffolds. Since these lead structures are usually identified by phenotypic screening and their molecular targets are therefore initially not known, identification of the mode-of-action of so far unexplored natural compounds gained attention in drug discovery.

The natural product neocarzilin A (**NCA**) from *Streptomyces carzinostaticus* was discovered decades ago and despite its potent cytotoxic effects in leukemia cells, no mode-of-action studies were performed to date. Recently, synthesis of neocarzilins A, B, C also provided access to a probe for activity-based protein profiling (ABPP) studies, which identified the synaptic vesicle membrane protein VAT-1 homolog (VAT-1) as a covalent target of neocarzilin A in the human liver cancer cell line HepG2. VAT-1 is a largely uncharacterized enzyme, which has been assigned a role in tumor cell migration in glioblastomas in a previous study.

In this thesis, the anti-migratory and anti-proliferative potential of the polyenone **NCA** was studied *in vitro* and *in vivo*. The interaction between **NCA** and VAT-1 and the resulting effects on a human breast cancer cell line (MDA-MB-231) were investigated. A probe of **NCA** containing a terminal alkyne tag, termed **NC-1**, was applied for *in situ* profiling in MDA-MB-231 cells. The protein VAT-1 was confirmed as a covalent cellular target of **NCA** by MS/MS analysis with both stable isotope labeling with amino acids in cell culture (SILAC) and label-free quantification (LFQ).

For binding site identification of **NCA** in human cells, *in vitro* mutagenesis of cysteine residues was performed, however, no reactivity towards cysteines was detected. A proteomics approach for active site peptide profiling (ASPP) with desthiobiotin-azide identified a peptide unique for VAT-1 isoform 1, which might be relevant for **NCA** binding. Subsequent *in vitro* mutagenesis of all nucleophilic residues of this peptide showed E113 to be involved in **NCA** binding, but the exact binding mode is still unclear.

The importance of the chemical structure of the neocarzillins for target protein binding and biological activity was analyzed by structure activity relationship (SAR) studies with the natural products **NCA**, **NCB** and **NCC**, related derivatives as well as different probes for

protein profiling. **NCA** turned out to be the most potent member of the neocarzilin family regarding VAT-1 binding and inhibition of cell migration.

In accordance with the phenotype observed after **NCA** treatment, a corresponding knockout (KO) or an siRNA (small interfering RNA) mediated silencing of the target protein VAT-1 confirmed the phenotype of a reduced cell motility, whereas cell proliferation was unaffected after downregulation.

A co-immunoprecipitation (co-IP) approach revealed VAT-1 to be involved in a network of cell adhesion proteins such as Talin-1 (TLN1), which mediates contacts between the actin cytoskeleton and the extracellular matrix (ECM) by integrin activation. In this context, **NCA** seemed to strengthen the interaction between VAT-1 and TLN1 and increase the integrin surface expression and activation, leading to an enhanced cell adhesion and a reduced cell migration. To facilitate insights into **NCA**-affected cellular pathways, a global proteome analysis was performed in MDA-MB-231 cells treated with and without **NCA**, but no significant changes were detected. When different expression levels of VAT-1 were studied, overexpression yielded an upregulation of proteins involved in cell adhesion or migration, whereas silencing of VAT-1 resulted in a downregulation of those proteins. In contrast, complete VAT-1 KO led to an upregulation of proteins involved in cell adhesion and cell migration, suggesting a feedback-loop for compensation of VAT-1 function.

Since VAT-1 is the target protein of **NCA** that is relevant for inhibition of cell migration but not cell proliferation, screening for alternative protein targets was performed in VAT-1 KO cells. Moreover, an optimized probe, which is structurally more similar to **NCA** than **NC-1**, termed **NC-4**, was generated and applied for ABPP studies in breast cancer cells. However, no further proteinogenic targets of **NCA**, which could be relevant for inhibition of cell proliferation were detected.

Since VAT-1 is linked to tumor migration and might therefore be a promising candidate for the development of selective migration inhibitors inspired by natural products, its cellular function and interaction with **NCA** should be elucidated in detail in further studies. Overall, we introduce VAT-1 as a promising novel target for future anti-metastatic drugs, which will be of high importance for general public health.

ZUSAMMENFASSUNG

Die Krebserkankungen nehmen weltweit immer mehr zu und die Bildung von Metastasen verschlechtert die Überlebensraten drastisch und stellt deshalb in der Krebstherapie die größte Herausforderung dar. Deshalb werden Medikamente, die in die Zellmigration in Tumorzellen eingreifen, dringend benötigt, da sie die Grundlage für die Bildung von Metastasen bildet. Krebsmedikamente basieren oft auf Naturstoffen. Dabei handelt es sich um sekundäre Stoffwechselprodukte mit einzigartigen und komplexen Strukturen. Da diese Leitstrukturen oft durch phänotypische Screening-Ansätze identifiziert werden, sind die molekularen Interaktionspartner anfangs oft nicht bekannt. Deshalb gewinnt die Identifizierung der molekularen Wirkmechanismen der bis jetzt unerforschten Naturstoffe in der Wirkstoffentdeckung immer mehr an Aufmerksamkeit.

Der Naturstoff Neocarzilin A (**NCA**) aus *Streptomyces carzinostaticus* wurde vor Jahrzehnten entdeckt. Trotz seiner potenten Zytotoxizität in Leukämiezellen wurden bis jetzt keine Studien zum Wirkmechanismus durchgeführt. Vor kurzem wurde durch die Synthese von Neocarzilin A, B und C die Entwicklung einer Sonde für funktionelle ABPP (Aktivitäts-basiertes Protein-Profiling) Studien ermöglicht, welche das synaptic vesicle membrane protein VAT-1 homolog (VAT-1) in der humanen Krebszelllinie HepG2 als kovalentes Target **NCA** identifizierten. VAT-1 ist ein größtenteils uncharakterisiertes Enzym, welchem in einer neueren Studie eine Rolle in der Zellmigration in Glioblastomen zugeschrieben wurde.

In dieser Arbeit wurde die Fähigkeit des Polyenons **NCA**, die Zellmigration zu hemmen, *in vitro* und *in situ* untersucht. Insbesondere die Interaktion zwischen **NCA** und VAT-1 und die resultierenden Folgen für Brustkrebszellen (MDA-MB-231) wurden untersucht. Eine Neocarzilin-Sonde mit einer terminalen Alkin-Funktionalität (**NC-1**) wurde in MDA-MB-231 in einem *in situ* ABPP-Experiment zur Bestätigung von VAT-1 als zelluläres Target verwendet. VAT-1 wurde als Target durch MS/MS mit einer anschließenden SILAC und „label-free" Quantifizierung bestätigt.

Für die Identifizierung der Bindestelle von **NCA** an VAT-1 in humanen Zellen wurde eine *in vitro* Mutagenese der Cysteinreste durchgeführt. Dabei wurde jedoch keine Reaktivität gegenüber Cysteinen detektiert. Ein neuer Proteomik Ansatz für die Detektion des Peptids mit der aktiven Bindungsstelle basierend auf einer Desthiobiotinazid-Funktionalität identifizierte ein Peptid, welches einzigartig für die VAT-1 Isoform 1 ist. Mutationen der nukleophilen Reste zeigte, dass E113 in der **NCA** Bindung beteiligt war, der genaue

Bindungsmodus jedoch noch unklar ist. Wie essenziell die Neocarzilin Struktur für die Bindung des Zielproteins und die biologische Aktivität ist, wurde sowohl durch Struktur-Aktivitäts-Beziehungsstudien mit den Naturstoffen **NCA**, **NCB**, **NCC** und unterschiedlichen Derivaten als auch verschiedenen Sonden untersucht. Dabei stellte sich **NCA** bezüglich der Bindung an das Zielprotein und Hemmung der Migration als aktivstes Mitglied der Neocarzilin Familie heraus.

Übereinstimmend mit dem Effekt von **NCA** auf die Zellmigration, konnte ein entsprechender Knockout des Target Proteins VAT-1 oder ein Knockdown den Phänotypen einer reduzierten Zellmigration bestätigen, während die Zellproliferation nicht beeinträchtigt wurde. Eine Ko-Immunopräzipitation zeigte, dass VAT-1 in einem Netzwerk von Zelladhäsionsproteinen verwickelt ist, unterem anderem mit Talin-1 (TLN-1), welches Kontakte zwischen dem Aktin-Zytoskelett und der extrazellulären Matrix durch Integrin-Aktivierung vermittelt. In diesem Kontext scheint **NCA** die Interaktion zwischen VAT-1 und TLN1 zu verstärken und die Integrin-Oberflächenexpression und Aktivierung zu erhöhen, was zu einer erhöhten Zelladhäsion und in einer verminderten Migration führt. Für ein besseres Verständnis der **NCA**-Effekte auf zelluläre Signalwege wurde eine globale Proteomanalyse in MDA-MB-231 durchgeführt, jedoch wurden keine nennenswerten Veränderungen detektiert. Als unterschiedliche Expressionslevel von VAT-1 auf das globale Proteom untersucht wurden, führte eine VAT-1 Überexpression zu einer Hochregulierung von Proteinen, die in der Zellmigration und Zelladhäsion involviert sind, wobei ein Knockdown in einem reduzierten Level dieser Proteine resultierte. Im Gegensatz dazu führte ein kompletter VAT-1 Knockout zu einer Hochregulierung von Proteinen, die in der Zelladhäsion und Migration involviert sind. Deshalb wird ein Kompensationseffekt der Funktion von VAT-1 vorgeschlagen. Da VAT-1 nur das Target von **NCA** darstellt, das für die Hemmung der Zellmigration verantwortlich ist, nicht aber für die Proliferation, wurde ein Screening-Ansatz nach neuen Targets in VAT-1 Knockout Zellen durchgeführt. Außerdem wurde eine optimierte Sonde, die **NCA** ähnlicher ist als **NC-1**, **NC-4**, entwickelt und in ABPP Studien in Brustkrebszellen eingesetzt. Es wurden keine weiteren Proteine detektiert, die **NCA** kovalent binden und somit relevant für die Hemmung der Proliferation sein könnten.

Da VAT-1 mit der Zellmigration in Verbindung gebracht wurde und womöglich einen vielversprechenden Kandidaten für die Entwicklung selektiver Migrationsinhibitoren inspiriert von Naturprodukten darstellt, ist die Aufklärung der zellulären Funktion von VAT 1 und die Interaktion mit **NCA** in weiteren Studien von wesentlicher Bedeutung. Insgesamt wurde VAT-1 als vielversprechender Angriffspunkt für zukünftige Medikamente zur Bekämpfung invasiver Tumore eingeführt, welche zukünftig für das Gesundheitswesen von hoher Bedeutung sein werden.

INTRODUCTORY REMARKS

The present doctoral dissertation was accomplished between May 2017 and May 2020 under the supervision of Prof. Dr. Stephan A. Sieber at the Chair of Organic Chemistry II of the Technische Universität München.

Parts of this thesis are based on the following publications:

Journal publications:

Gleissner, C.M.L.*, Pyka, C.L.*, Heydenreuter, W.*, Gronauer, T.F., Atzberger, C., Korotkov, V.S., Cheng, W., Hacker, S., Vollmar, A., Braig, S., Sieber, S.A., *"Neocarzilin A is a potent inhibitor of cancer cell motility targeting VAT-1 controlled pathways"*, *ACS Cent. Sci 5,7, 1170-1178, 2019*

* contributed equally to this publication

Figures from the publication were adapted for this thesis and are reprinted with permission. https://pubs.acs.org/doi/10.1021/acscentsci.9b00266.

Conference presentations:

Gleissner, C.M.L.*, Pyka, C.L.*, Heydenreuter, W.*, Gronauer, T.F., Atzberger, C., Korotkov, V.S., Cheng, W., Hacker, S., Vollmar, A., Braig, S., Sieber, S.A., *"Neocarzilin A is a potent inhibitor of cancer cell motility targeting VAT-1 controlled pathways"*, *Gordon research seminar and conference Bioorganic chemistry, 2019*

* contributed equally to this publication

Contributions:

W. Heydenreuter and T. Gronauer performed all the synthetic procedures for obtaining the natural products and probes, W. Heydenreuter performed target ID experiments in HepG2 for the publication in ACS central science. C. Pyka (LMU) performed all proliferation and migration assays, confocal microscopy experiments and Western blot-based co-IPs.

This thesis was written in Microsoft Word (latest version of 21.4.2020) and all structures were assembled with ChemDraw Professional 19.1 under the ACS document 1996 guidelines. Processing of gel scans was performed with Fujifilm Multi Gauge 3.0 and Photoshop CS5 12.0. Processing and plotting of data were performed with GraphPad Prism 6.05 or 8.0 and Adobe Illustrator CS5 15.0.0 was applied for creation of Figures.

X

TABLE OF CONTENTS

LIST OF TABLES

XVI

LIST OF FIGURES

1.

INTRODUCTION

Since cancer metastasis imparis survival rates, drugs targeting cell migration as crucial proccess of the metastatic cascade are of urgent need. Drugs are often inspired by natural products. This is why the natural product neocarzilin A known for its potent cytotoxicity was applied for target discovery studies. The identified target protein VAT-1 has already been linked to cell migration before. For deeper insights, protein interactions of the target protein were investigated.

Contents:

1.INTRODUCTION

1.1. Cancer therapy as a challenge in the modern world

According to the WHO project GLOBOCAN the global burden of cancer is still increasing with 18.1 million new cancer cases and 9.6 million cancer deaths in 2018. This increase is linked to an aging and growing world population and a higher degree of development which is associated with a cancer-promoting lifestyle. The most frequent cancer and the leading cause of death is lung cancer for males and breast cancer for females.[1] While cardiovascular diseases are still the major factor for mortality in middle-aged patients (35-70) globally, cancer has replaced cardiovascular diseases as the leading cause of death in high-income countries.[1, 2] However, cancer also displays one of the most prominent causes of mortality in low- and middle-income countries promoting cancer to one of the biggest public health challenges worldwide.[1, 3]

The complex molecular pathways underlying cancer development are not completely understood so far, but Hanahan and Weinberg developed a rational concept describing the main characteristics which are acquired by healthy cells on their way to a neoplasia. These include the resistance of cell death, genome instability, induction of angiogenesis, activation of invasion and metastasis, tumor promoting inflammation, replicative immortality, avoiding immune destruction, evading growth suppressors, sustaining proliferative signaling and deregulating cellular energetics (Figure 1).[4, 5] The hallmarks of cancer illustrate not only the complex nature and heterogeneity[6] of tumors, but also show the challenges that therapies are confronted and the number of possible attacking points that can be targeted by new drugs.
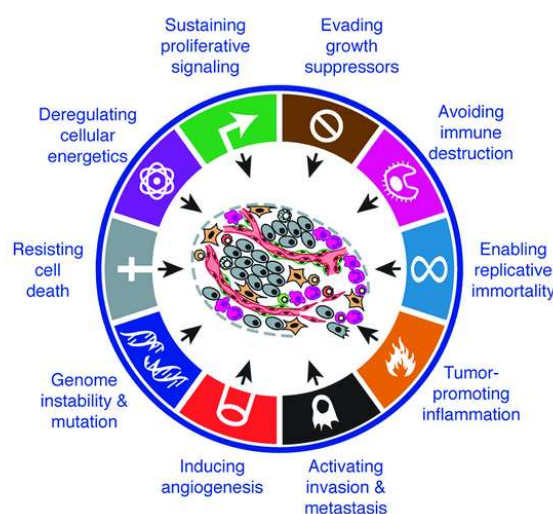
Figure 1: Schematic illustration of the hallmarks of cancer. Figure is adapted from Hanahan and Weinberg.[4] Reprinted with permission.

Depending on the severity of the tumor, treatment options of cancer can be divided into local and systemic therapies. Initial local treatment options consist of surgical removal of the tumors and local radiotherapy for the reduction of tumor size.[7] For metastatic or very aggressive forms of tumors, a systemic application of anti-proliferative chemotherapy (5-fluorouracil, cis-platin or taxol)[8], targeted and immunotherapy (small molecules such as imatinib or monoclonal antibodies such as trastuzumab) or hormonal therapy (tamoxifen) is required.[9, 10] In addition, combinations of different chemotherapeutic agents[11] or combined targeted and immunotherapy are used.[12] The responsiveness to treatments is dependent on various factors such as the receptors the tumor is expressing and the appearance of resistances. Chemotherapeutic agents inhibit the cell proliferation by interfering directly with the cell cycle and cell mitosis.[11] However, cytotoxic chemotherapy is often accompanied by severe and long-lasting side effects since the drugs are not tumor specific and also target normal tissue due to the same origin of both tumor and healthy cells.[9, 11]

Fortunately, over the past two decades, cancer therapy has developed from relatively non-specific chemotherapeutic agents to selective, mechanism-based drugs.[12] Due to earlier diagnosis possibilities, better prevention and awareness as well as improved treatment options, cancer survival rates are augmenting in the industrialized states.[3, 10, 13, 14] However, metastases with their unpredictable and aggressive nature are often associated with a poor prognosis due to a decreased responsiveness to chemotherapeutics and are therefore responsible for 90% of all cancer-caused mortalities.[5, 15] So far, inhibition of cell proliferation remains the focus of drug development and only a minority of targets linked to migration, the crucial step of metastasis, have been investigated therapeutically, since the design of anti-metastatic drugs is challenging and most of the clinical trials, to date, have failed. However, further development of anti-metastatic drugs for controlling the spread of cancer is worthwhile since this strategy is expected to exhibit less toxicity associated adverse effects, one of the major struggles of modern medicine.[16, 17]

1.2. Tumor cell migration and cell adhesion in metastasis process

Malignant, aggressive populations of tumor cells often leave the primary tumor and spread into surrounding tissue by a multistep metastatic cascade. The main steps for metastatic process constitute the detachment of tumor cells from the primary tumor, invasion into the surrounding tissue, entry into blood or lymphatic vessels, dissemination in the vessel system, exit of the vessels and finally colonization of a distant site (Figure 2).[15, 18, 19] An early step for tumor cells on their way to motile population displays the endothelial-mesenchymal transition (EMT) to overcome the basement membrane by formation of invadopodia for matrix degradation. Crucial processes which are directly connected to metastasis formation represent the loss of cell adhesion, an increased cell motility by directed cell migration and a higher invasive behavior.[19,20]
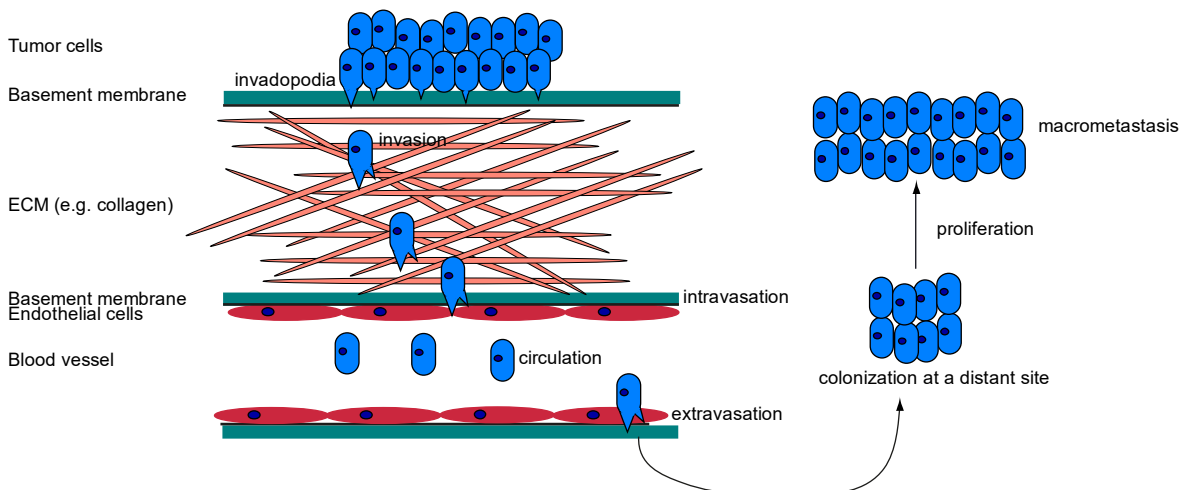
Figure 2: Metastatic cascade of tumor cells. Tumor cells form invadopodia for transition of the basement membrane and invasion in the ECM. Intravasation and circulation of tumor cells in the vessel system is followed by extravasation and colonization of distant sites as well as proliferation to macrometastasis.

The multi-cycle process of cell migration is regulated by various soluble factors (e.g. growth factors and chemokines) and remodeling of the extracellular matrix (ECM). Cell migration is initiated by directed membrane trafficking and cell polarization including the formation of lamellipodia and filopodia at the leading edge of cell. Lamellipodia display a broad membrane protrusion containing a branched two-dimensional network of actin filaments regulated by the small Rho-GTPase Rac-1 whereas filopodia are small extensions controlled by Cdc42. While lamellipodia act as the main cellular engine, filopodia fulfill the sensory and guidance role for cell migration.[21] The major driving force of migration is the extension of a leading-edge protrusion for the establishment of new focal adhesions attachment sites initiated by integrins and a subsequent cell body contraction by reorganization of actin cytoskeleton regulated by myosin II and the Rho GTPase RhoA.[22] Afterwards, the process is repeated several times till the cell has arrived at a desired site.

The key players in migration are Rho GTPases such as Rho, Rac and Cdc42 since they are involved in the regulation of actin cytoskeleton, cell polarity, gene expression, microtubule dynamics as well as vesicular transport pathways.[19, 22] Further, microtubule stabilization which is promoted by the PI3K/Akt pathway is crucial for cell polarization and migration.[23]

Additionally, cell adhesion to the ECM plays a critical role in cell migration and therefore for the progression of metastatic cancers. Cell adhesion to the ECM, which is composed of a network of proteins such as collagens, fibronectin, laminin glycoproteins and vitronectin is mediated by specific cell surface receptors such as integrins. Integrins are heterodimeric glycoproteins composed of an α and β subunit connecting the ECM to the cytoskeleton.[24] Further, they are known for their transmembrane signaling. Integrins are activated by a conformational change from the closed to the open state leading to a higher affinity to the ECM ligand. This integrin activation is controlled by TLN1 binding to the tails of integrin-β subunits.[25, 26] TLN1 is a cytoplasmic protein with three actin binding sites with which the protein connects integrins to the actin cytoskeleton. It serves as adaptor protein for signal transduction induced by alteration in the cytoskeleton and modulates the contact to the ECM by integrins and therefore cell adhesion.[27] Moreover, integrins are not only essential for cell migration and invasion due to cell adhesion to the ECM as well as signal transduction cascades regulating cytoskeleton remodeling, but they are also involved in the activation of MMPs (matrix metalloproteinase). MMPs modulate the tumor microenvironment by degrading the basement membrane, the first barrier to surrounding tissue.[24]

Due to their important role in cell adhesion and cell migration, integrins and MMPs are among the limited number of targets for anti-migration drugs which undergo clinical trials at the moment.[28-31] Targeting of other proteins involved in crucial pathways in the cell migration process by small molecules might constitute a breakthrough in anti-metastatic therapies. For elucidation of further critical molecular pathways of migration and for expanding the library of druggable targets, new chemical entities are required. Here, natural products could serve as valuable handles for the identification of crucial processes in cell migration and might further inspire new lead structures for the anti-metastatic therapy.[32]

1.3. Drug development based on natural products

Historically, natural products from plants and animals were the major source for all medicinal preparations for the treatment of many diseases.[33] Today, natural products from terrestrial and marine sources play an indispensable role in drug discovery for the therapeutic areas of oncology or infectious diseases.[34] The bioactive secondary metabolites with abundant scaffold diversity are derived from plants, bacteria, fungi or marine sources. They are mainly used by the organisms as self-defense mechanisms for an enhancement of their survival and competitiveness in difficult environmental conditions.[35] Natural products cover various functions depending on the organisms of origin and their habitat due to a high biodiversity. Further, the specificity of natural products is unique due to a natural selection over millions of years.[36] The highly diverse structures of natural products are frequently characterized by their complex chemical entities as well as stereochemistry based on diverse structural classes such as non-ribosomal peptides, glycopeptides, alkaloids, isoprenoids and polyketides.[37]

Due to their unique structural diversity adapted over the evolution of time in comparison to standard combinatorial chemistry, natural products and their direct derivatives have a high impact on drug discovery and lead structure identification.[33, 38, 39] Approximately 50% of all FDA-approved therapeutics have a natural origin and many new drug candidates are inspired by natural products.[35, 40] Nature, bearing a high biodiversity, still displays a rich source of new lead structures.

To date, only a small percentage of all organisms has been investigated. This means there is still a vast pool of unidentified novel natural compounds with high bioactivity waiting to be investigated.[41] So far, most of the natural product-based therapeutics are of plant origin. However, microorganisms show a higher degree of biodiversity compared to eukaryotes. They can survive under the most extreme environmental conditions because of their high metabolic adaptability. Therefore, microbes represent a very promising source for new bioactive small molecules. However, less than 1% of the microbial biodiversity has been investigated yet. This lack of identification of the "hot spots" of biodiversity mainly results from the fact that microorganisms are very difficult to cultivate in the laboratory. But with the help of new methods and strategies such as metagenomic and heterologous-expression techniques, these barriers could be overcome allowing these new fruitful sources for lead structures to be exploited.[38]

Due to the different functions and activity of these novel molecules, many specific targets in human cells are addressed by them. Many of which focus on DNA-affecting proteins[42], tyrosine kinases[40] and cytoskeletal proteins[43]. Some of these targets have already been successfully covered by therapeutics with natural origin such as taxol. Isolated from the bark of the *Taxus Brevifolia*, taxol has been applied for the treatment of lung, ovarian and breast cancer.[33] Taxol is a mitotic inhibitor which stabilizes microtubules and interferes with microtubule organization during cell division.[34] Another prominent example is Doxorubicin, a member of the anthracycline family from *Streptomyces*, which has been used for the treatment of various tumors and leukemia.[41]

However, despite of their big contribution to new medicines, natural products-based compounds were neglected by pharma industry during the last two decades due to their incompatibility for high-throughput assays against molecular targets. In addition, there were concerns about the regulation of the international access to natural products and technical challenges such as high synthetic complexity and low extraction rates from the organisms of origin. Therefore, the pharma industry focused on synthetic libraries and combinational chemistry approaches for drug discovery.[38, 44] However, the success of identifying new lead structures by synthetic libraries was limited. With new methods in the fields of metabolomics and metagenomics as well as the pharma industry noticing these benefits of natural products over synthetic compounds, these molecules will feature more prominently in drug discovery in the future.[38]

1.4. *Streptomyces* - a fruitful source for natural products with anti-cancer properties

It is of general interest to screen microorganisms for new natural products which can serve as new lead structures as well as to improve the methods for overproduction of natural products. Therefore, *Streptomyces* attracted attention due to its high reservoir of bioactive natural compounds and its unique properties distinguishing them from *E. coli* or yeast.[45] Streptomycetes are aerobe, gram-positive bacteria with a high genomic GC content belonging to the family Streptomycetaceae and the class of Actinobacteria. The *Streptomyces* genus consists of more than 800 species which can survive in extreme climate conditions and colonize uncommon habitats such as the deep-sea, the desert or in cryo and volcanic environments.[46] They have unique characteristics among soil bacteria due to the formation of filamentous mycelia, aerial hyphae, and conidial spores during their life cycle. Furthermore, the most interesting feature of this genus displays the capability to generate secondary metabolites with many pharmaceutical applications. These secondary metabolites are characterized by a high structural diversity and an assortment of different bioactivities such as antibacterial, antifungal, antiviral, antihypertensive, immune suppressant, and antitumor.[47]

Notably, *Streptomyces* species produce a considerable portion (39%) of all known microbial metabolites. Within the Streptomycetaceae family, this genus is known to generate nearly 80% of all bioactive molecules.[46] Secondary metabolites in Actinomycetes are mainly produced by Biosynthetic gene clusters (BGC) containing a group of genes that encode the natural product biosynthetic pathways. The size of the biosynthetic gene clusters in *Streptomyces* chromosome ranges from a few kb to 100 kb. For example, nonribosomal peptide synthetases (NRPS) and polyketide synthase (PKS) are known to be involved in the synthesis of many of the bioactive metabolites in Actinomycetes.[46] Additionally, streptomycetes represent promising organisms for natural product overproduction because they distinguish themselves by highly developed post modification systems for phosphorylation, acetylation, farnesylation, and glycosylation of natural products to guarantee their activity.[45]

Interestingly, S*treptomyces* is the largest genus regarding antibiotic-production. However, there are also a remarkable number of anti-cancer agents on the market with *Streptomyces* origin (Figure 3). The first antibiotic shown to have anticancer activity was the polyketide actinomycin isolated from *Streptomyces parvulus* in 1940. Its directly related derivative actinomycin D, also known as dactinomycin, is an approved FDA-drug which has been widely applied as a DNA intercalating agent. Other examples for DNA intercalating drugs

represent the anthracyclines, a family of polyketides generated by *Streptomyces* species by iterative PKS pathways including daunorubicin, doxorubicin, aclacinomycin A and nogalamycin. Both daunorubicin and doxorubicin have been FDA-approved drugs for cancer therapy since the 1960s. Further, streptomycetes produce the glycopeptide bleomycin which causes DNA-strand breakages and mithramycin which interacts with the DNA in a non-intercalative way.[48] [49] [37]
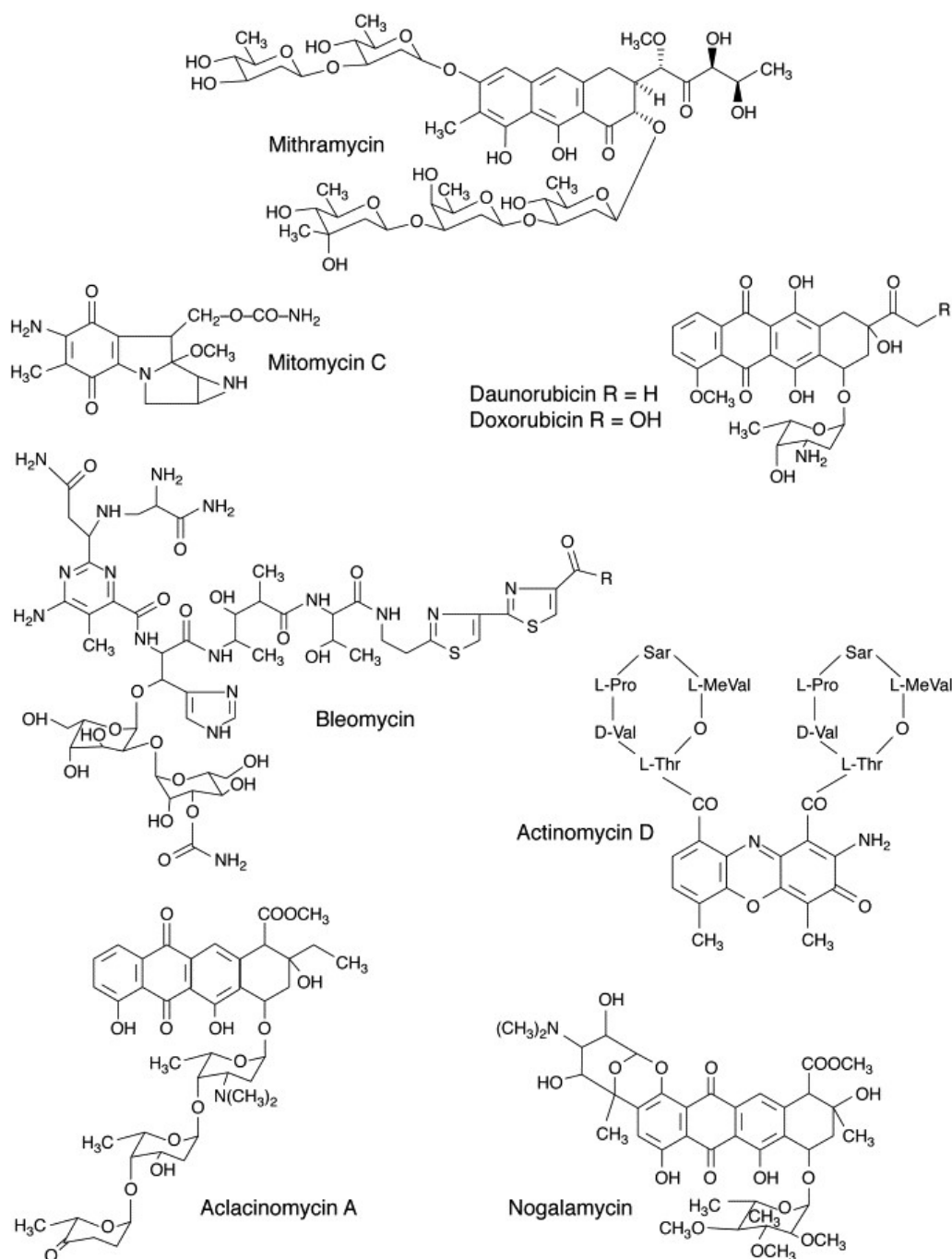
Figure 3: Chemical structures of antitumor drugs produced by *Streptomyces* species with clinical application in cancer chemotherapy. Reprinted with permission.[49]

Interestingly, another important antitumor agent from *Streptomyces* which exert its cytotoxic action by interfering with DNA function is zinostatin also known as neocarzinostatin, which was first isolated in 1965. This complex natural product consisting of two noncovalently bound components is produced by the strain *Streptomyces carzinostaticus*.[50] Neocarzinostatin contains a labile bicyclodiynene chromophore which is responsible for its activity and a protein component (apoprotein) for stabilization of the chromophore (Figure 4).[50, 51] It belongs to the enediyne antibiotics which are among others the strongest anti-tumor agents, but they are also known for their high toxicity due to an induction of apoptosis in healthy cells as well as in tumor cells.[37] Neocarzinostatin is generated by the biosynthetic gene cluster localized in 130 kb continuous DNA from *Streptomyces carzinostaticus* ATCC15944 including two distinct type I polyketide synthases.[52]

neocarzinostatin
(PDB ID = 1NCO)

neocarzinostatin
chromophore
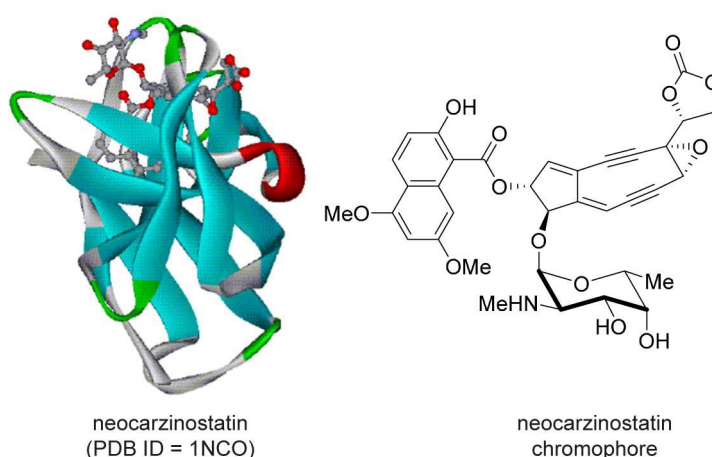
Figure 4: Structure of neocarzinostatin on the left and its chromophore on the right adapted from Jean *et al*.[51]

There are a plenty of anti-cancer natural products from the *Streptomyces* species with already known mode of actions which are already introduced to the pharmaceutical market. However, the genus of *Streptomyces* still represents a treasure for natural products with so far unknown modes of actions, which can be further elucidated.

1.5. Neocarzilin - a promising natural product from *Streptomyces*

As already mentioned above, neocarzinostatin is generated by *Streptomyces carzinostaticus*.[50] The same actinomycete was discovered to produce the natural products neocarzilins A and B (**NCA**/**NCB**), which were first isolated in 1992 by Nozoe *et al.* from an extract of the mycelium of *Streptomyces carzinostaticus* var. F41 and structurally analyzed by NMR/MS spectroscopy (Figure 5). Neocarzilins (**NC**) display trichlorinated polyenones with a slightly acidic character due to the enolic hydroxyl group which is stabilized by an intramolecular hydrogen bond.[53, 54] In 2004, the biosynthesis of neocarzilins involving a novel type I PKS system was elucidated and neocarzilin C (**NCC**), the dichloro derivative of **NCA** and most likely its biosynthetic precursor, was identified (Figure 5).[55] Further, a total synthesis of **NCA** was reported by Nozoe *et al.*[56]

The natural **NCA** isolated from *Streptomyces carzinostaticus* showed high cytotoxic activity against K562 chronic myelogenous leukemia cells with an IC_{50} of 0.06 µg/mL (186 nM).[53] Synthetic **NCA** displayed the same cytotoxicity as the natural product against K562 chronic myelogenous leukemia cells. These findings show that the activity of **NCA** is as potent as neocarzinostatin with an IC_{50} of 0.09 µg/mL whereas the acute toxicity in mice was diminished compared to neocarzinostatin. In regard to antibiotic effects, **NCA** was found to be only weakly active in gram-positive strains such as *micrococcus luteus* and *bacillus megaterium*.[56]

The acidic hydroxyl group seems to be crucial for the biological activity in human cells since the corresponding methylether of **NCA** was revealed to cause only a moderate cytotoxic effect with an IC_{50} of 2 µg/mL (6 µM).[53] Further, the chloromethyl groups are required for the biological activity of neocarzilins.[55] Despite the known impact of distinct structural moieties in the structure of the neocarzilins on biological activity, no SAR (structure-activity relationship) studies in human cancer cells have been published so far.

In contrast to the detailed characterization of the structures and their biosynthesis, only one study detecting a cytotoxic effect of **NCA** was reported several years ago. However, the detailed biological activity, the mode of action and the molecular target within human cancer cells have not been studied until now.

Neocarzilin A (NCA)   Neocarzilin B (NCB)   Neocarzilin C (NCC)
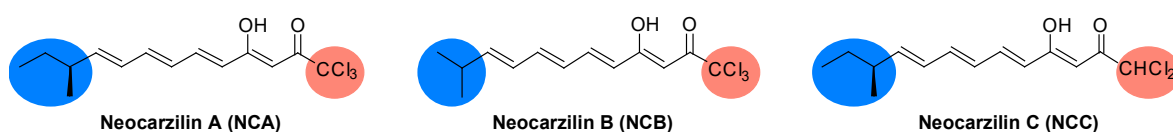
Figure 5: Chemical structures of necarzilins.

1.6. VAT-1: a synaptic vesicle membrane protein

1.6.1. Origin of VAT-1 and its role in *T. californica*

The synaptic vesicle membrane protein VAT-1 (VAT-1) was first discovered to be specifically expressed in the electric organ of the pacific ray *Torpedo californica* (*T. californica*) by Linial *et al.* in 1989.[57] The protein with a molecular weight of 41,572 daltons was isolated from synaptic vesicle membranes. Due to its localization and its hydrophobic character, it was proposed to represent an integral membrane protein with the region between residues 163-184 to be membrane bound. However, membrane spanning helical regions could not be clearly defined since the length of the hydrophobic regions was too short for membrane spanning.[57] Later, VAT-1 was suggested to play a central role in nerve signal transmission.[57] Consistent with this suggestion, VAT-1 was linked to neuronal and brain development in zebrafish.[58]

In regard to the protein sequence, similarities to the protein from *T. californica* were detected in alcohol dehydrogenases, translocases, protein kinase C, nucleotide binding proteins, ATPases, and some viral membrane proteins.[57] Furthermore, a homology to ζ-crystallin from guinea pig lens was revealed by a Swissprot database search with the highest similarity detected for domains conserved in zinc-dependent dehydrogenases of the alcohol dehydrogenase family. Additionally, the cofactor-binding domain of oxidoreductases was found to be conserved in VAT-1 and in ζ-crystallin. It was demonstrated that VAT-1 preferably binds NADPH in the presence of divalent Zn^{2+} ions whereas Mg^{2+} only poorly supported this interaction.[59] Further, VAT-1 was revealed to exhibit a specific ATPase activity whereas a supportive effect on this activity was shown by divalent ions like Mg^{2+} and Ca^{2+}. Therefore, VAT-1 was proposed to have effects on ATP-dependent reactions in Torpedo nerve terminals, e.g. phosphorylation and dephosphorylation of proteins.[60]

Notably, a formation of a globular, high-molecular-mass complex with a size of 176 kDa consisting of 3-4 VAT-1 subunits was detected, which is stable under solubilizing conditions by various detergents.[61] A higher oligomeric state of VAT-1 between 90-160 kDa was also confirmed by SDS-PAGE with nonreducing conditions.[57] Moreover, the protein was found to be a low-affinity Ca^{2+}-binding protein, whereas mainly the C-terminus is responsible for Ca^{2+} binding.[62] Interestingly, an influence of the Ca^{2+} concentration on the VAT-1 complex was proposed since the complex partially dissociates in the presence of chelating calcium ions.[61] [63]

1.6.2. The mammalian homolog of VAT-1: sequence and localization

VAT-1 and the mammalian VAT-1 homologs belong to the protein superfamily of medium-chain dehydrogenases/reductases. There is a 26-27% sequence identity between the VAT-1 protein and the mammalian ζ-crystallins or the *E. coli* quinone oxidoreductase. Part of VAT-1 shows a similarity with the enoyl reductase of the fatty acid synthase.[64] Other studies report an ATPase activity of both VAT-1 and VAT-1 homolog.[60, 65]

Since the region which was observed to be membrane bound[57] corresponds to the coenzyme-binding region and VAT-1 has been reported to have nucleotide-binding capacity, Persson *et al.* disagreed with the assumption of VAT-1 to be membrane associated. In general, VAT-1 localization to the membrane seems to be improbable due to the homology to the cytosolic alcohol dehydrogenases and no obvious transmembrane domains within the protein.[64, 66] The reason for VAT-1 association to the cell membrane might be a complex formation with other membrane bound proteins.[64] Recent studies confirm that the human VAT-1 homolog is mainly found in the cytosol[67, 68], perinuclear regions[69] and to a small extent in association with the outer mitochondria or ER membrane.[66, 67]

1.6.3. Function of VAT-1 in human cells

The cellular function of VAT-1 is still not clear. However, several studies in the last years have assigned VAT-1 to play a role in mitochondria morphology, cell migration and phospholipid transport.[66, 69, 70]

The rat homologue of VAT-1 was proposed to be crucial for cell growth by regulating mitochondrial membrane dynamics in cooperation with mitofusin proteins localized in the mitochondrial outer membrane. VAT-1 turned out to be a negative regulator of mitochondria fusion, meaning that high expression of VAT-1 induced mitochondria network fragmentation and VAT-1 knockdown led to network extension.[66] In this context, the AAA ATPase ATAD3A, which is an anti-apoptotic marker localized to mitochondria[71] and is essential for mitochondrial network organization, mitochondrial metabolism and cell growth[72], was later identified as a VAT-1 interaction partner.[68]

Furthermore, Junker *et al.* showed that VAT-1 plays a role in the phosphatidylserine (PS) transport from ER to mitochondria. Therefore, VAT-1 was suggested to be involved in the control of the lipid composition of mitochondria thereby affecting mitochondria morphology.[66, 68] Moreover, VAT-1 was revealed to bind phosphatidic acid (PA) or phosphatidylserine with the same affinity. PA has been recognized to be a bioactive lipid involved in cell growth, proliferation, membrane trafficking and cytoskeleton

reorganization.[73] Just recently, VAT-1 was confirmed to be a soluble phospholipid transport protein binding to phosphatidylserine but also other acidic phospholipids. Further, a phospholipid binding cavity was discovered in the crystal structure of a dimeric VAT-1 (Figure 6). [70]
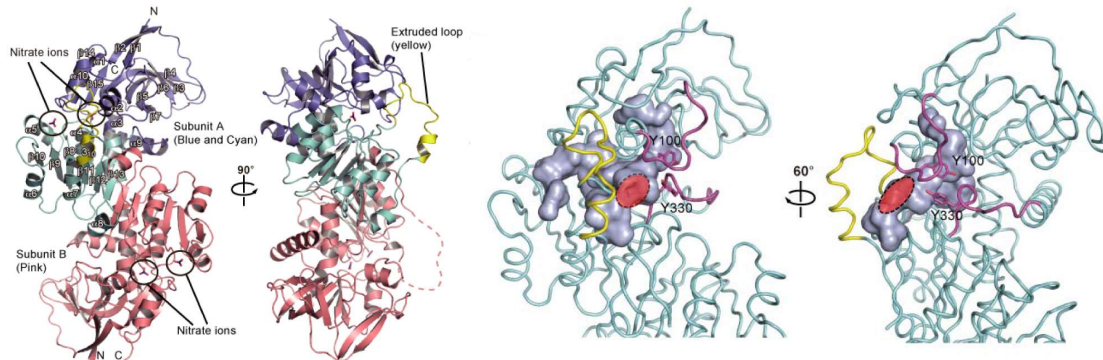
Figure 6: Structure of VAT-1 and structure of the phospholipid binding cavity. Reprinted with permission.[70]

Moreover, phosphorylation of VAT-1, which was shown to be PKC (Protein kinase C) - dependent, and its recruitment to intracellular membrane compartments was identified in neutrophils to be regulated by Src kinases.[74]

In addition, an involvement of VAT-1 in a Ca^{2+} dependent processes in keratinocyte physiology was found. VAT-1 expression was detected to be a Ca^{2+} regulated process with high calcium concentrations leading to decreased VAT-1 expression. This fact might indicate VAT-1 to be involved in cell signaling cascades that are negatively regulated by calcium.[67]

1.6.4. Role of VAT-1 in cancer

In the context of cancer, research has been focused on the human synaptic vesicle membrane protein VAT-1 homolog (VAT-1) since its gene has been localized on chromosome locus 17q21 in the neighborhood of the breast cancer gene BRCA.[75] Chromosomal instability in this gene region leads to an inherited predisposition for breast and ovarian cancer.[76]

A study by Mertsch *et al*. revealed VAT-1 to be overexpressed in certain glioblastoma cell lines. Elevated levels of this protein were directly linked to increased tumor migration but did not affect cell proliferation.[69] As already mentioned, VAT-1 was shown to be a calcium binding protein. Interestingly, several proteins involved in glioma migration are Ca^{2+} dependent due to the fact that glioma cell migration is regulated by Ca^{2+} levels for modelling shape and volume of cells *via* ion channels.[69, 77] Furthermore, VAT-1 was identified to be a pathogenic, upregulated factor in progressive benign prostatic hyperplasia (BPH). By si-RNA (small interfering RNA) knockdown, a significant suppression of cell growth was

detected in three different prostate cancer cell lines. [78] In conclusion, the involvement of VAT-1 in migration of cancer cells promoted this protein to an interesting candidate for further studies.

1.7. Protein-Protein interactions: detection and therapeutic targets

Proteins can act independently as single molecules as well as functional complexes with other proteins leading to a higher protein diversity. Protein-protein interactions (PPIs) play a decisive role for biological processes like signal transduction, cell division, apoptosis and protein homeostasis. Due to the high impact of PPIs, it is of considerable importance to study these interactions and their effects on cellular pathways. There are various methods to study PPIs, amongst others pull-down with antibodies, yeast-two-hybrid, Förster resonance energy transfer (FRET), surface plasmon resonance spectroscopy (SPR) and cryo-EM.[79]

However, it is challenging to detect interactions in complexes with only weak binding affinities and a transient nature.[80] Protein interactions are often investigated by co-immunoprecipitation (co-IP), meaning the enrichment of a protein of interest and its respective binding partners by specific antibodies in cell lysate[81]. These interactions can often be validated by orthogonal methods or reverse co-IP experiments, but there are limitations such as false positive results and artificial effects due to cell lysis or a loss of low-affinity protein interactions. Therefore, it was established to apply chemical crosslinking *in situ* to catch the protein interactions within the native cell environment before pull-down experiments.[82] With this strategy, analysis of complex protein networks and protein dynamics is also enabled. Compared to conventional co-IPs, this technique can guarantee more reliable results regarding false positive hits and a better performance in regards to preserving native interactions.[80]

Notably, PPIs also offer the attractive possibility for a drug-mediated intervention.[83] The success of biologicals for the inhibition of PPIs is powerful and there are already inhibitors in the area of autoimmune diseases and cancer with clinical applications.[84] In case of small molecules which are easier and cheaper in production compared to biologicals, antagonists exist which directly bind to the protein-protein interface or rather bind allosteric sites to interfere with PPIs.[83] However, it is very challenging to design small molecule inhibitors to disturb PPIs since the clear binding pockets are often unknown, the protein interface can be very flat and large as well as there being a lack of small-molecule starting points for drug design.[83, 84] There are rare examples that existing drugs can represent a starting point for the design of small molecule inhibitors such as the cytotoxic vinca alkaloids, which were

later discovered to affect the polymerization of tubulin.[83] During the last decade, some progress has been recorded regarding small molecules targeting PPIs. For example, for induction of growth arrest and apoptosis in cancer cells, the interaction between MDM2 and p53 is inhibited by Nutlin-3 and idasanutlin, which are currently being tested in advanced clinical trials.[84] Small molecules based on natural products which interfere with PPIs would be beneficial for disrupting cellular pathways which are linked to a pathological potential.

1.8. Target identification in drug discovery

1.8.1. Target identification methods in drug discovery

Target identification is crucial in drug discovery since the effect of drugs is dependent on the efficiency and strength of therapeutics binding to their molecular targets. However, target identification of small molecules in cells is challenging and there is a broad spectrum of methods for shedding light into the dark. Approaches for target identification range from direct biochemical methods (affinity purification, high throughput screening (HTS) combined with recombinant proteins), proteomics methods (liquid chromatography-mass spectrometry (LC-MS) platforms for shotgun analysis, yeast two-hybrid strategies, protein microarrays)[85, 86], genomic technologies (phenotypic screening based on RNAi, gene expression microarrays[87]) and computational methods. Nevertheless, a combination of methods often delivers more detailed results regarding off-target effects and mode of actions.[88] Genomic approaches were very prominent two decades ago and also built the foundation for proteomics. However, proteomics evolved as the new leading platform since mass spectrometry (MS) based proteomics approaches caught up very rapidly with genomics and have broader applications such as analysis of PTMs[85], cellular compartments and organelles and their time-resolved dynamics. Particularly the development of mass spectrometers to highly sensitive instruments and the discovery of protein ionization methods like matrix-assisted laser desorption/ionization (MALDI) and electrospray ionization (ESI) displayed a milestone for proteomics methods in the post-genomics era.[89-91]

At the beginning of proteomic approaches, it was only possible to identify proteins by MS after 2D gel electrophoreses resulting in a low protein coverage.[89] Further, it was only possible to monitor protein-drug interactions in the cell lysate or directly *in vitro* on recombinant proteins. In the last years, quantitative proteomics methods coupled directly to MS have evolved[89] which enable *in situ* profiling of covalent binding small molecules such as activity-based proteome profiling (ABPP) as well as non-covalent interactions such as affinity based proteome profiling (AfBPP).[92] These approaches require a functionalized,

bioactive probe which is structurally similar to the small molecule based drug and target protein binding can be monitored indirectly by competitive approaches with small molecules and probe in parallel. However, if no suitable analytical handle is accessible for a small molecule or if the probe is not active enough, these powerful approaches reach their limitations.

Consequently, one downside for determination of the efficiency of drugs constitutes the fact that there was no capture-free method for a direct measurement of drug-target interactions within cells. In 2013, a biochemical method for profiling of drug-target engagement directly in cells and tissue samples based on the induced thermal stabilization of target proteins upon ligand binding with Western blot-based read-out was developed by Molina *et al.* which is known as the cellular thermal shift assay (CETSA). The method has a broad application profile which ranges from a detection of drug transport and activation, off-target effects to drug resistance in cancer cells.[93] With the combination to multiplexed quantitative MS, there is also the possibility to identify unbiased, unexpected hits, which completely revolutionized the method termed thermal proteome profiling (TPP).[94, 95]

In conclusion, MS-based chemical proteomics occupies a leading role for target identification in drug discovery today and further strategies will evolve in the future in this field with the constant improvement of MS instruments and data analysis tools leading to an ever more detailed look into previous unknowns.

1.8.2. Activity-based protein profiling (ABPP) - from the beginning to the current state

In the field of chemical proteomics, ABPP has emerged as an innovative and powerful key technology for profiling the activity of enzymes directly in native biological environment on a global level.[85, 96] The main goal of proteomics is the characterization of the expression levels of proteins and their function in complex networks in physiological as well as pathological biological pathways such as cancer-related processes.[97]

However, the activity of enzymes is not only controlled by their abundance in the cells, but is regulated by complex mechanisms such as PTMs, proteolytic cleavages in zymogens or allosteric activators or inhibitors.[97-101] The strength of ABPP lies in the enrichment of target proteins by small molecule probes as well as monitoring of enzyme activities in complex proteomes since the probes are designed to bind directly to the active sites of proteins.[85, 97, 102] ABPP has gained high popularity as a multidisciplinary approach which finds application in biochemistry, molecular and cellular biology, medicinal chemistry, pathology, physiology and pharmacology.[96] The method has proven to be very valuable for discovery of targets and inhibitors as well as for the identification of enzyme active sites.[86, 103]

The ABPP technology was first reported by Powers and Walkers,[104, 105] and was then stepwise established by Cravatt *et al.*[85, 100, 103, 106] and Boygo *et al.*[97, 107] The method has been increasingly evolved over the last decade. In the early days of this technology, only easy targetable enzyme classes were hit, whereas now, even difficult enzyme classes or low abundant enzymes can be targeted.[96] Generally, the concept of ABPP relies on the treatment of a complex protein sample with an active site directed covalent probe with target selectivity containing a reporter tag for detection. Scaffolds for chemical probes include mechanism-based inhibitors, protein-reactive natural products, and general electrophiles.[85, 86]

An ABPP probe is composed of two entities: a moderate reactive group (or warhead), which is often an electrophilic residue which covalently binds to a nucleophilic residue in the active site of the target, and a reporter tag which enables the visualization (fluorescence dye) or enrichment (biotin tag) of the labeled proteins (Figure 7A).[85, 101-103] For non-covalent probes, photoreactive groups are incorporated into the probe that label residues in the proximity of enzyme active sites by covalently linking to the target protein upon UV irradiation.[85] A binding group is also often applied for directing the reactive groups to different enzyme active sites and to support probe interactions with enzyme active sites.[85, 102, 103]

The reactivity of entire enzyme classes such as proteases, kinases, phosphatases, glycosidases, and oxidoreductase were profiled.[85, 86, 101, 106, 108] For targeting, various reactive chemical groups have been harnessed for ABPP probes such as fluorophosphonates[106], vinylsulfones[109], epoxides[107] or β-lactones[110].[86] Further, an iodoacetamide alkyne probe was used for determination of the global reactivity profile of cysteine thiols across the entire human proteome by isoTOP-ABPP (isotopic tandem orthogonal proteolysis-activity-based protein profiling).[96, 111]

One of the main benefits of ABPP represents its application in intact cells (*in situ*) for profiling of the *status quo* of a cell with all proteins being in their native environment. For targeting enzymes in their complex biological system, the use of smaller tags or tag-free rather than bulky reporter tags is of advantage due to an improved cell permeability and distribution within the cells[100, 103] as well as a higher structural similarity to the corresponding natural product which often goes along with a more comparable activity between probe and the natural product.[97, 112]

To overcome these challenges, biorthogonal reactions such as the copper-mediated 1,3- dipolar cycloaddition (Click-chemistry) are taken advantage of. Small reporter tags like terminal alkynes (or azides) can be "clicked" to reporter groups such as fluorescent tags for visualization or biotin for enrichment after cell lysis.[100] The copper(I)-catalyzed azide-alkyne cycloaddition is the most commonly applied reaction for linking alkynes to azides which is characterized by high bioorthogonality, selectivity and solid reaction rates due to its broad pH and temperature tolerance range and universal applicability in aqueous solutions.[102, 113-116]
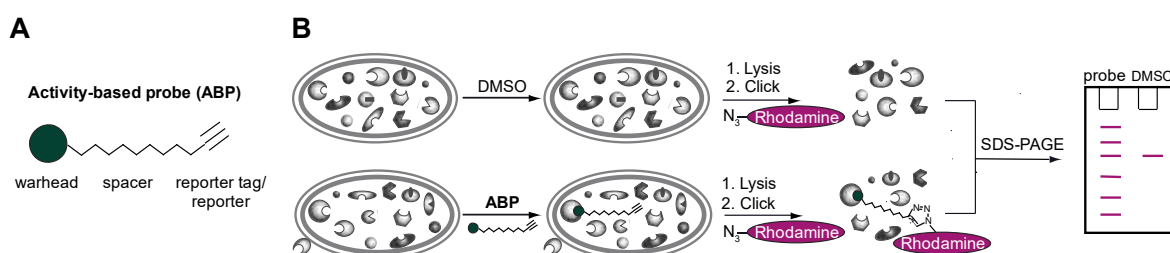
Figure 7: Schematic overview of ABP structure and gel-based ABPP. **A,** Structure of activity-based probe (ABP) with a reporter tag. **B,** Overview of gel based ABPP workflow with application of click chemistry.

In the ABPP workflow, cells are treated *in situ* with the cell-permeable, alkyne-tagged probe or a vehicle control before cell lysis. Labeled proteins are linked to an azide-containing reporter group in the cell lysate by click chemistry. The reporter group displays either a fluorophore for SDS-PAGE read-out, a trifunctional linker (TFL) with biotin and a fluorophore for a combination of SDS-PAGE and MS-based readout[117] or a biotin tag for a direct LC-

MS read-out.[86, 97] For SDS-PAGE analysis, probe treated and vehicle control treated protein samples are compared in fluorescence intensity (Figure 7B).

For MS-based proteomics, proteins are enriched *via* the biotin tag on avidin beads to reduce the complexity of the samples. A few years ago, proteins were again eluted from the beads by SDS for separation by gel electrophoreses, isolated and digested for analysis by LC-MS. Today, with highly developed MS instruments and data analysis tools, proteins are directly reduced, alkylated and digested on the beads. Digested peptides are desalted and applied for LC-MS/MS. Unspecific binding is detected by comparison of probe treated samples with a vehicle control.

Gel based methods are known to have a high robustness and throughput. [85, 86, 103] However, SDS PAGE readout has several limitations such as the resolution, sensitivity and no direct accessibility of the protein identity.[85, 86, 118] For gel-coupled MS techniques, there are also several drawbacks such as the risk of missing targets with a low abundance, membrane-associated proteins[101] or the lack of reproducibility.[102, 119] Complete gel-free approaches, enabled by technological advances in high resolution MS with a higher sensitivity[89], have many upsides such as more quantitative insights into the target proteins.[120]

However, MS is not quantitative *per se* and quantification is therefore performed by a comparison between different samples by either stable-isotope-labeling approaches or label-free quantification (LFQ) strategies.[118] For isotopic based approaches, quantification relies on the extracted ion chromatograms of MS full scans containing the pair of heavy and light peptides whereas for LFQ, spectral counting or peptide intensities are used.[118] Every approach has its advantages and drawbacks depending on the experimental setup.[121, 122]

Methods based on isotopic labels have been developed and applied for several years. These include metabolic labeling, for instance, stable isotope labeling of amino acids in cell culture (SILAC)[123], chemically labeling such as isotope-coded affinity tags (ICAT),[124,97] multiplexed chemical labeling methods like dimethyl labeling[125], isobaric tags for relative and absolute quantification (iTRAQ labels)[126] and tandem mass tags (TMT labels) [122]. These approaches especially convince with their high peptide identification rates as well as their robustness and accuracy since even small changes in the whole proteome can be detected.[127]

In the SILAC approach (Figure 8), different labeling states of the cells can be identified by metabolic incorporation of amino acids with unnatural isotope patterns into the proteomes.[120, 121] A benefit over other methods with late stage application of chemical modifications or LFQ strategies is the early combination of the samples in the workflow leading to a reduction of technical variations between the replicates.[120] However, SILAC is not suitable for clinical tissues or samples since direct metabolic labeling is not possible.[127] Further, upon incorporation of amino acid isotopes, cells react with metabolic and proteomic alterations, which can be avoided by the application of LFQ approaches.
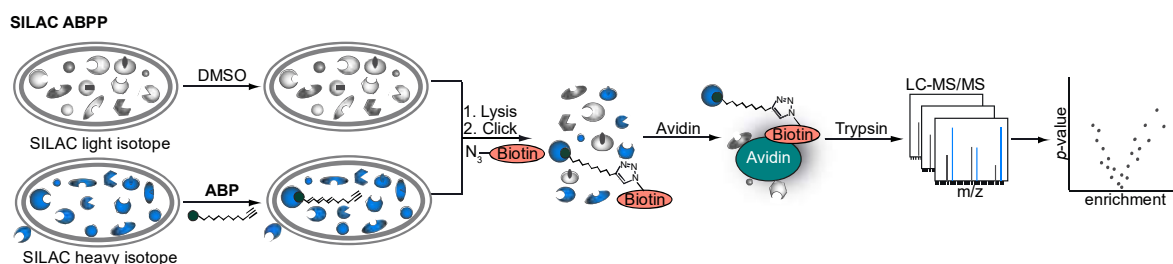
Figure 8: Workflow of SILAC-ABPP.

Generally, label-free approaches (Figure 9) are more simple and economical in regard to sample preparation, are applicable to every type of cells or tissues and the sample number is unlimited.[127] With improved tools for data evaluation such as MaxQuant[128, 129] and the implemented MaxLFQ algorithm[127], challenges such as the robust and accurate proteome wide quantification of peptides in LFQ approaches could be overcome and the strategy became very popular over the last years (Figure 4).[127, 130-132] LFQ has been applied in many proteomic approaches such as whole proteome analysis, ABPP approaches or protein-protein interaction studies to date.[133-135] In contrast to SILAC, samples are processed in a separate workflow. Therefore, a reliable mass spectrometer performance is required to avoid variations in ion intensities and to achieve precise reproduction of retention times. LFQ methods particularly excel due to a considerable proteome coverage, a high analytical depth and a dynamic range.[118]
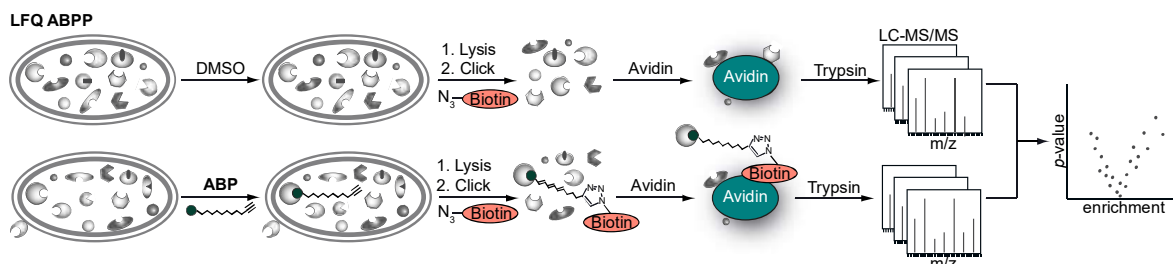
Figure 9: Workflow of label-free ABPP experiment. Adapted from Gleissner *et al.*[134]

1.9. Scope of this work

Since the burden of cancer is still increasing and cancer metastasis impairs the survival rates, it is a valuable approach to target and inhibit cellular proteins which impair the cell migration representing the crucial step for tumor metastasis. For drug discovery, natural products display an indispensable source for new lead structures, which are characterized by a broad range of functions and specificity in targeting proteins.

In a recent study, the natural product **NCA** from *S. carzinostaticus* was considered for target protein profiling and investigation of the biological effects due to its published cytotoxicity. VAT-1 was shown to be the molecular target in the liver cancer cell line HepG2 and there were first hints of an anti-migratory phenotype after **NCA** treatment.[54]

The scope of this thesis was the further characterization of the **NCA**-VAT-1 interaction and its biological consequences within human breast cancer cells. The main goal was the confirmation of the target protein in the breast cancer cell line MDA-MB-231 and the identification of the mode of action. For this investigation, SILAC as well as LFQ quantification based ABPP was applied for target protein validation and a MS-based active-site peptide profiling (ASPP) approach[85] was harnessed for the identification of the binding site peptide. In order to find a response for the reactive, functional groups important for VAT-1 binding, SAR studies in a competitive labeling format were used and different probes were designed for reactivity profiling in cooperation with Thomas Gronauer. In order to enlighten the biological function of VAT-1, a network of interaction partners was established by different co-immunoprecipitation approaches. In addition, specificity was guaranteed by performing a co-IP in VAT-1 KO cells for investigation of unspecific antibody binding. Moreover, for elucidation of the biological process, whole proteome analysis of **NCA** treated, VAT-1 KO, si-VAT-1 cells and cells overexpressing VAT-1 were performed.

In cooperation with Carolin Pyka, the anti-migratory and anti-proliferative effects of the **NC**s were studied.[136] By establishing a stable VAT-1 knockout (KO) HEK cell line by CRISPR/Cas, the role of VAT-1 in cell migration and proliferation was investigated. Since VAT-1 was found to only be involved in migration, the identification of an alternative target protein of **NCA** responsible for inhibition of the proliferation was tackled by labeling in VAT- 1 KO cells and *in situ* profiling with a new probe **NC-4** which more resembles **NCA**.

2.

BIOLOGICAL ACTIVITY

NCA was found to be the most active member of the neocarzilin family in inhibition of cell proliferation and migration with no induction of apoptosis at relevant concentrations. For ABPP studies, the probes **NC-1** and **NC-4** were designed. **NC-4** showed comparable activity to the natural product, whereas **NC-1** turned out to be mainly appropriate for identification of the target protein responsible for migration.

Contents:

2.BIOLOGICAL ACTIVITY

Since decades, natural products display a valuable source of bioactive compounds for drug discovery.[40, 135] So far, the potential biological activity of **NCA** was only investigated in a study by Nozoe *et al*. after its first isolation from *Streptomyces carzinostaticus*. Here, **NCA** exhibited a high cytotoxicity in the human chronic myelogenous leukemia cell line K562 with an IC_{50} of 186 nM.[53] Despite of its cytotoxicity, **NCA** attracted only little attention since its discovery in 1991. Therefore, no further studies regarding the bioactivity or the mode of action of the neocarzilins have been published up to date.

In this thesis, the biological activity of all known natural appearing neocarzilins **NCA**, **NCB** and **NCC** and two corresponding opposite enantiomers **NCA'** and **NCC'** for investigation of the relevance of the stereocenter at C11 position were determined (Figure 10A). Chemical structures of neocarzilins are relatively easy to access in contrast to other natural products characterized by complex chemical scaffolds and stereochemistry, making their synthesis often very challenging and leading to low chemical yields.[38] As a first step, neocarzilins were synthetized according to the procedures described by Nozoe *et al.* by Wolfgang Heydenreuter and Thomas Gronauer.[54, 56] (Scheme S1-S4, appendix).

Neocarzilins were investigated regarding their effects on cell proliferation and cell migration of cancer cells, due to those being the key elements addressed in cancer therapy. Since the impact on cells which are characterized by an aggressive cell proliferation and migration should be elucidated, the highly invasive human triple negative breast adenocarcinoma cells MDA-MB-231 were chosen as standard cell line for all experiments in this thesis.[137] A convincing analytical labeling profile had already been established before in this cell line.[54] Further, 4T1-luc2 cells were applied for cytotoxicity and migration studies, since the *in vivo* efficiency in mice was investigated with 4T1 murine cells.

2.1. Biological activity of natural products

First, cytotoxicity screens of neocarzilins in MDA-MB-231 were performed by measuring the cell metabolic activity corresponding to the number of viable cells with MTT (3- (4,5- dimethylthiazol-2-yl)-2,5-diphenyltetrazolium bromide) assays. The assay is based on NAD(P)H-dependent mitochondrial oxidoreductase enzymes, which can reduce the tetrazolium dye MTT to its water-insoluble form formazan, which can be detected photometrically.[138, 139] An IC_{50} value of 608.7 nM was identified for **NCA** cytotoxicity after 24 h treatment (Figure 10B), which is in the same range of the previously determined cytotoxicity with an IC_{50} of 186 nM in leukemia cells K562.[53] It must be considered that the determined IC_{50} values in MTT assays are subjected to small fluctuations in dependence of stock dilutions and differences in the DMSO stock activity, which were detected after repeated freeze-and thaw cycles. Further, the difference between the detected and the published cytotoxicity can also be explained by an application of different cell lines, incubation times and cytotoxicity assay formats.

For the stereoisomer of **NCA**, termed **NCA'**, an IC_{50} value of 852.4 nM was detected after 24 h treatment (Figure 10C). Therefore, the cytotoxicity potential is reduced to a small extent in comparison to **NCA** only by inversion of the stereocenter at C11, which seems to be important for a high cytotoxicity. The same effect could be investigated for **NCB** with a less pronounced activity with an IC_{50} of 1.19 µM (Figure 10D), which also bears a trichloromethyl group but slightly differs to **NCA** at the conjugated, unsaturated carbon chain. Consequently, the stereocenter and the length of the carbon chain is important for cytotoxic activity but is not decisive for the activity. The crucial impact of the trichloromethyl group for the biological cytotoxic activity was confirmed by the investigation of the dichloro-compounds **NCC** and **NCC'** (Figure 10D, appendix Figure 45).[55] **NCC** which is probably the biosynthetic precursor of **NCA** bears the same chemical structure as **NCA** apart from one chloride atom and shows a 10-fold weaker cytotoxic activity with an IC_{50} of 8.01 µM compared to **NCA**. For **NCC'** which is the opposite stereoisomer of **NCC**, activity in MTT assays was even more impaired with an IC_{50} of 15.79 µM. As a conclusion, **NCA** turned out to be the most potent compound in reducing the metabolic activity of MDA-MB-231 cells followed by **NCA'** and **NCB** with a moderate activity whereas **NCC** and **NCC'** only provided weak activity. Consequently, the trichloromethyl group displays the essential functional group for the biological activity, but the stereo position and the length of the conjugated, unsaturated carbon chain contribute as well to the cytotoxicity to a smaller extent.
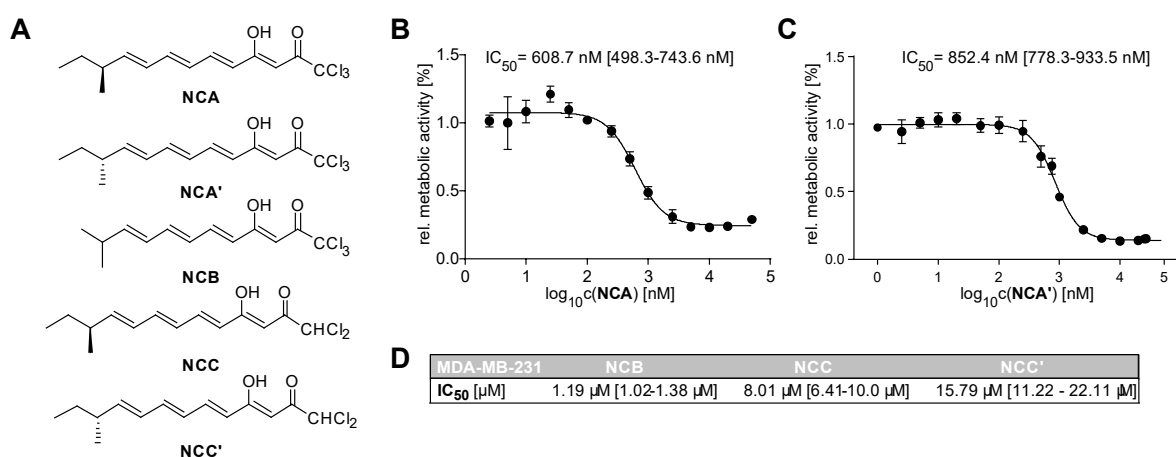
Figure 10: Cytotoxicity of natural products in MDA-MB-231. A, Chemical structures of **NCA**, **NCA'**, **NCB**, **NCC** and **NCC'**. **B**, MTT assay of **NCA** in MDA-MB-231 for 24 h. **C,** MTT assay of **NCA**' in MDA-MB-231 for 24h. **D,** IC_{50} values of **NCB**, **NCC**, **NCC**' determined by MTT assay. **B-D,** One representative replicate out of three independent experiments is shown and 95% confidential intervals are indicated in brackets.

MTT assays are relevant for the investigation of cell proliferation, cell viability and cytotoxicity. However, only the metabolic activity is detected, but it is not differentiated between cell proliferation, cell migration or apoptosis. Therefore, these cellular pathways were investigated separately in suitable assays for distinguishing between the effects.

First, the anti-proliferative potency of the neocarzilins was measured by crystal violet staining[140] against MDA-MB-231 (Figure 11A) and a panel of cancer cell lines (appendix Figure 46A). **NCA** exhibited an IC_{50} value of 373 nM in MDA-MB-231 and again displayed the most active compound in inhibition of cell proliferation. For different cancer cell lines, IC_{50} values ranging from 300 to 800 nM were detected for **NCA** corroborating previous literature data.[53] In contrast, the effects observed for **NCA'**, **NCB** and **NCC** were less strong with IC_{50} values ranging from 1-6 µM for human MDA-MB-231 (Figure 11A) and murine 4T1-luc2 breast cancer cells (appendix Figure 46B). The results obtained from crystal violet assays are in good accordance with the results from MTT assays described before, especially for the compounds **NCB** and **NCC**. Based on this data, it is proposed that already minor structural changes in stereochemistry and in the trichloromethyl group, respectively, affect the bioactivity in regard to cell proliferation.

Up to date, most anti-tumor agents provide anti-proliferative activity, but do not inhibit the cell motility and therefore do not interfere with metastasis formation.[141] The impairment of tumor cell migration might be crucial for success in cancer therapy and new compounds with anti-migratory characteristics are thus of high importance.[142]

Consequently, the anti-migratory behavior of cells treated with neocarzilins was investigated, too. Therefore, migration was monitored in Boyden chamber assays. In the breast cancer cell line MDA-MB-231, **NCA** significantly reduced cell migration (Figure 11B)

whereas in 4T1-luc2 cells, a reduced potency of **NCA** was detected (appendix Figure 46C). Further, the diminished cell migration behavior was also confirmed by single-cell chemotaxis assays. Here, a significant reduction of the forward migration index, a measure of directed migration, as well as directness of cells migrating towards a chemoattractant was obtained (Figure 11C). Besides cell migration, **NCA** also impaired cell invasion of breast cancer cells determined in Boyden chamber assays (appendix Figure 46D). Whereas an anti-migratory phenotype was triggered by **NCA**, the neocarzilins **NCA**', **NCB** and **NCC** exhibited only minimal anti-migratory effects in MDA-MB-231 (Figure 11D). However, **NCA'** again pertained as the second most active member of the natural compounds, which only differs to **NCA** in the stereocenter at C11. Here again, the results illustrate that the trichloromethyl group is indispensable for neocarzilin's biological effects, while small changes in the stereocenter also contribute to the activity. Since **NCA** turned out to be the most active member of the neocarzilins regarding inhibition of cell proliferation and migration in the nanomolar range, further biological activity studies were only focused on the potential of **NCA**.
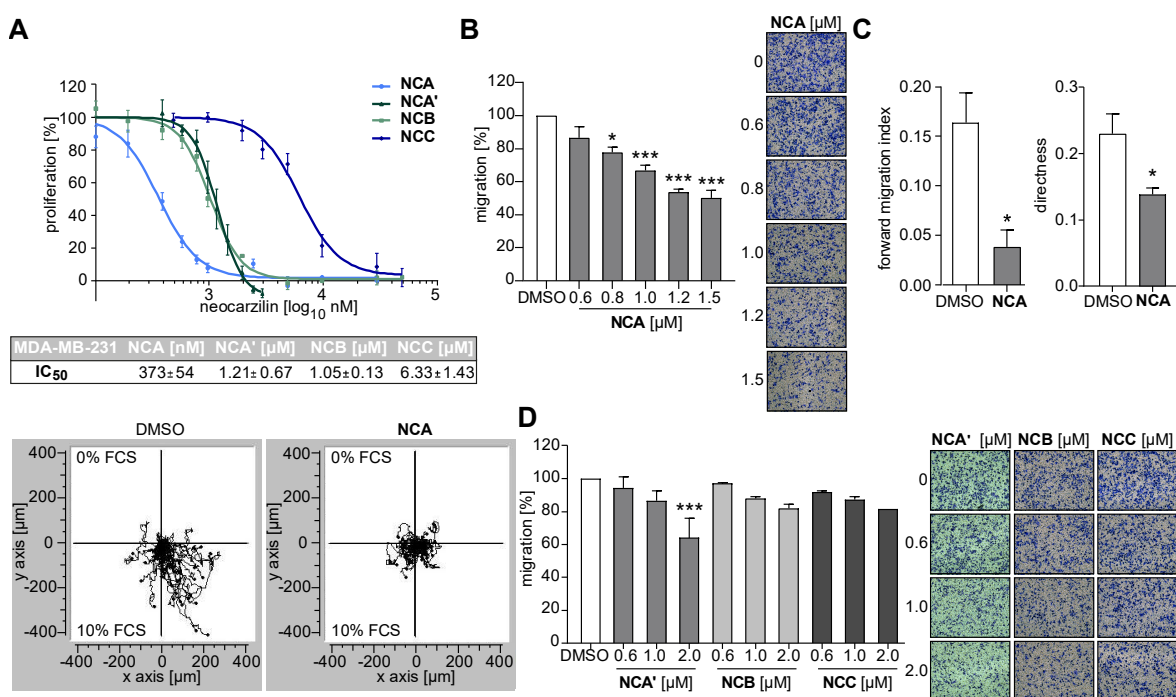
Figure 11: Anti-cancer effects of neocarzilins. A, Proliferative capacity of MDA-MB-231 cells treated with **NCA**, **NCA**', **NCB** and **NCC** and IC_{50} values determined by crystal violet staining after 72 h. **B**, Transwell migration of MDA-MB-231 cells treated with **NCA** determined by Boyden Chamber assay. **C**, Trajectory blots, forward migration index and directness as measure of directed chemotactic migration of MDA-MB-231 cells determined by chemotaxis assay. 30 cells per condition were monitored over 20 h. Bars always represent the mean ± SEM of 4 independent experiments, two-tailed unpaired Student's *t* test, *P < 0.033. **D**, Transwell migration of MDA-MB-231 cells treated with **NCA', NCB** and **NCC** determined by Boyden Chamber assay. **B,D,** Bar diagrams showing the number of migrated cells normalized to the control are presented, one-way ANOVA, Dunnett's test, *P < 0.033, ***P < 0.001 compared with DMSO control. **A,B,D**, Bars always represent the mean ± SEM of at least three independent experiments performed in duplicates/triplicates. Experiments were performed by Dr. Carolin Pyka (LMU München). Adapted from Gleissner *et al.* [134]

Since the observed phenotypes of reduced cell migration and proliferation can be also caused by apoptosis mediated cell death, the induction of apoptosis by **NCA** needs to be excluded at relevant concentrations. Apoptosis was monitored by permeabilizing and staining with propidiumiodide using the method described by Nicoletti *et al*.[143] Notably, there were no apoptotic effects on MDA-MB-231 cells detected at concentrations which are considered as relevant for inhibition of migration after 24 and 48 h (appendix Figure 46E), whereas for **NCA** treated 4T1-luc2, cells revealed a higher sensibility with an induction of cell death at concentrations and time ranges relevant for inhibition of cell migration. Therefore, apoptotic cells might slightly influence the anti-migratory readout in 4T1-luc2 cells (appendix Figure 46F). Since all experiments except the *in vivo* experiment were performed with MDA-MB-231 and no induction of apoptosis was revealed for this cell line for relevant time points, it can be stated that the anti-migratory and anti-proliferative phenotype is not considered as a side-effect of cell death but is a real effect. Moreover, the influence of **NCA** on cell cycle progression and microtubule network organization was investigated since these cellular pathways are crucial for cell migration and proliferation. However, no effect of **NCA** on cell cycle progression and microtubule network organization was observed (appendix Figure 46G+H).

Finally, the *in vivo* efficacy of **NCA** was investigated with an injection of luciferase tagged 4T1 murine cells into the tail vein of Balb/c mice.[144] A diminished tumor size was detected, however, the significance was not sufficient due to statistical outliers in the control group. Due to ethical guidelines, the experiment was not repeated. The tendency which was observed suggested that a treatment with 10 mg/kg **NCA** reduced tumor cell dissemination into the mouse lungs compared to solvent control treated animals after five days (appendix Figure 46I). Notably, the body weight of the mice increased for both groups during the experiment, therefore proposing a suitable safety profile of **NCA** (appendix Figure 46I). Therefore, it is worth to exploit the therapeutic potential of **NCA** and to decipher the mode of action of the compound.

It is concluded, that particularly **NCA** of the neocarzilin family from *Streptomyces carzinostaticus* has a high potency for inhibition of cell migration and proliferation in the nanomolar range without a parallel induction of apoptosis at relevant concentrations. Since metastasis still impairs cancer survival rates and is responsible for 90% of cancer-related deaths, the development of anti-metastatic drugs has emerged as a promising strategy in cancer therapy.[141, 142] The goal is the impairment of cell migration, since the metastatic cascade is closely linked to this process.[142] With anti-migratory drugs, the application of highly aggressive cytostatic agents with severe side effects can be reduced.[141] Therefore,

the anti-migratory potential of **NCA** attracts attention and merits an in detail characterization. Further, a high synergistic effect of inhibition of proliferation and migration in cancer therapy for treatment of metastasis was suggested recently[145], underlining the excellent potential of **NCA** as a lead structure for anti-metastatic drugs. Consequently, the elucidation of the mode of action and the identification of the cellular target of **NCA** is of high impact.

The biological activity of **NCA** again shows that natural products are clearly a rich source of drugs and drug lead structures. However, the cellular target and the mode of action of natural products are often unknown since they are challenging to identify. This is even the case for compounds that are currently tested in clinical trials or are already FDA approved pharmaceuticals. The exact cellular targets are crucial for docking studies of the protein and the natural product to improve the therapeutic potential of natural compounds. Consequently, target identification of natural products is of urgent need for the design and development of optimized drugs.[146]

2.2. Biological activity of ABPP probes

Despite its early discovery, the protein target of the neocarzilins has not been identified yet. Since no mode of action studies of the neoarzilins have been reported so far, it is of crucial impact to elucidate the target protein within human cancer cells and the biological pathways which are affected by **NCA**. Therefore, an ABPP approach has already been considered for target discovery of **NCA** in the liver cancer cell line HepG2.[54] In ABPP experiments, probes based on the natural products bearing an alkyne tag as a visualization tool are applied *in situ* for target discovery.[147] In order to unravel the mode of action of **NCA**, the small molecule probe **NC-1** with an alkyne tag was designed and synthetized by Wolfgang Heydenreuter and Thomas Gronauer.[54] Considering that the trichloromethyl group is essential for biological activity, this strongly electrophilic structural element was suggested to covalently interact with the dedicated protein target. Therefore, **NC-1** was designed as trichlorinated compound which is structurally similar to **NCA** apart from the length of the unsaturated chain and removal of the stereocenter at C11 (Figure 12A). The resemblance of the natural product and the ABPP probes are crucial for the biological activity and reactivity with the target protein.[112] Therefore, changes should be as minimal as possible in probe design.

Due to the slight variations between **NCA** and **NC-1** and keeping in mind that the stereocenter is also relevant for the **NCA** activity, another probe termed **NC-4** which was chemically not as easily accessible as **NC-1** was designed later in the project which is composed of **NCA** with an alkyne tag (Figure 12A).

For testing the suitability for ABPP of **NC-1** and **NC-4** as probes of **NCA**, the metabolic activity after probe treatment was measured by MTT assays. While **NC-1** showed a diminished IC_{50} compared to **NCA** with 2.56 µM, **NC-4** turned out to be highly active with an IC_{50} of 454.8 nM (Figure 12B+C). **NC-4** is comparably active as **NCA** in the MTT assay considering the 95% confidential intervals. Therefore, the probe **NC-4** with a higher structural similarity to **NCA** is proposed to be more suitable for ABPP approaches compared to **NC-1**. However, since the probe was synthetized at a very late phase of the project, most of the experiments were performed with **NC-1**. But it should be kept in mind, that **NC-4** can provide a deeper insight into the mode of action of **NCA** for future experimental design. **NC- 1** cytotoxicity monitored in MTT assays was 4-fold reduced compared to **NCA**, which is appropriate for ABPP approaches.
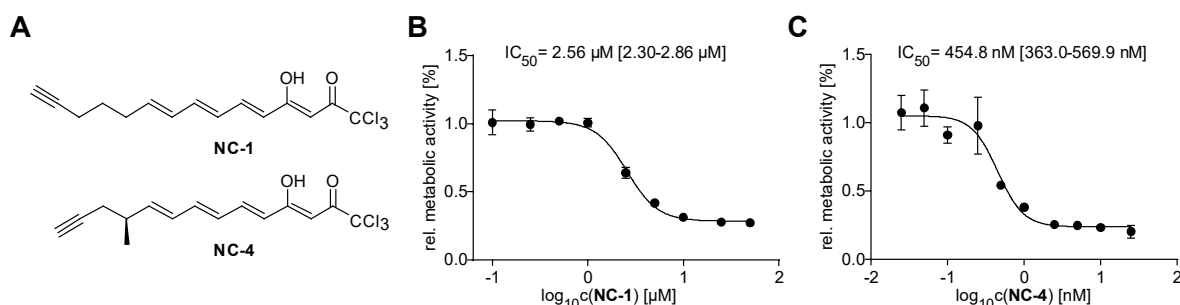
Figure 12: Cytotoxicity of NCA probes. **A,** Chemical structures of probes **NC-1** and **NC-4**. **B,** MTT assay of **NC-1** in MDA-MB-231 for 24h. **C,** MTT assay of **NC-4** in MDA-MB-231 for 24 h. **B-C,** One representative replicate out of three independent experiments is shown.

According to the natural products, the probe **NC-1** was further tested for inhibition of the cell migration and proliferation as well as induction of apoptosis for distinguishing the effect which leads to a moderate cytotoxicity in MTT assays. As shown in Figure 13A, the anti-proliferative activity significantly dropped in MDA-MB-231 and 4T1-luc2 cells (IC_{50} values of 24-34 µM) compared to **NCA**. The stereocenter and the length of the carbon chain might be crucial for the antiproliferative effect of neocarzilins. The removal of the stereocenter in **NC- 1** might interfere with the correct binding to the target protein relevant for cell proliferation.

In contrast, the anti-migratory activity of **NC-1** was only slightly reduced compared to **NCA** with visible effects at 2.5 µM comparable to MTT assays (Figure 13B). These results suggest the probe being a suitable tool for profiling of the target proteins of **NCA** linked to cell migration but not to cell proliferation. Moreover, according to the results obtained for **NCA**, no induction of apoptosis was observed upon treatment with **NC-1** for relevant concentrations and time points considered for migration or proliferation assays (appendix Figure 47).
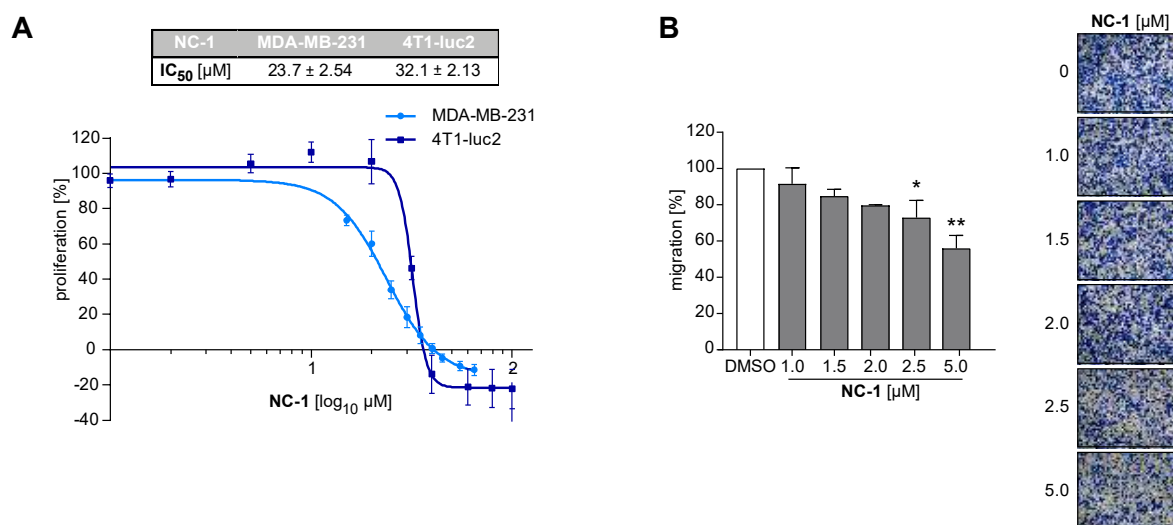
Figure 13: Anti-cancer effects of probe NC-1. A, Proliferative capacity of human MDA-MB-231 and murine 4T1-luc2 breast cancer cells treated with the activity-based probe **NC-1** determined by crystal violet staining after 72 h. **B,** Transwell migration of MDA-MB-231 cells treated with **NC-1** determined by Boyden Chamber assay. Bar diagram showing the number of migrated cells normalized to the control is presented. **A-B**, Bars represent the mean ± SEM of three independent experiments performed in duplicates/triplicates, one-way ANOVA, Dunnett's test, *$P < 0.033$, **$P < 0.002$ compared with DMSO control (**B**). Experiments were performed by Dr. Carolin Pyka (LMU München). Adapted from Gleissner *et al.* [134]

To sum up, **NC-1** severely loses activity particularly in inhibition of the metabolic activity and the cell proliferation while the antimigratory effects are still present in a slight diminished manner. The removal of the stereocenter might therefore be critical for inhibition of cell proliferation. The activity of the new probe **NC-4** should be definitely investigated regarding inhibition of cell proliferation and migration, since the strong activity comparable to **NCA** in the MTT assays is very convincing. Overall, **NC-4** might be more suitable for ABPP studies due to its high similarity to **NCA** and therefore its stronger activity. The potential of **NC-4** should be exploited for unraveling the targets of **NCA** important for inhibition of cell migration and particularly of cell proliferation. However, the results propose that the probe **NC-1** is appropriate for ABPP especially for detecting the anti-migratory target of **NCA**, which is described in the next two chapters.

3.

LABELING EFFICIENCY IN HUMAN CELLS

Probe **NC-1** showed a very specific labeling of a protein in the range of 40 kDa. **NCA**, **NCA'** and **NCB** showed a high competition of **NC-1**, which directly correlates with the observed anti-migratory and anti-proliferative activity of the compounds. Further, the trichloromethyl group was found to be essential for specific labeling in the nanomolar range.

Contents:

3. LABELING EFFICIENCY IN HUMAN CELLS

3.1. Analytical labeling with probe **NC-1**

Since particularly **NCA** showed a high bioactivity in human breast cancer cells, the target protein of the natural product was investigated by ABPP approaches for optimization of the compounds in regard to their therapeutic potential. First, gel-based ABPP approaches were applied for *in situ* target discovery with the alkyne tagged probe **NC-1** (Figure 14A). Analytical SDS-PAGE based experiments don't provide the in-depth information about the target protein identity and binding site compared to MS based experiments. Nevertheless, they have been applied a long time since a lot of samples can be analyzed in parallel for first insights into the labeling pattern and reactivity of the probe. Gel-based strategies are suited for optimizing the probe concentration and incubation times before MS/MS analysis.

Therefore, prior to MS studies, the most convincing labeling conditions were figured out *via* gel-based analysis of **NC-1** probe treated cells. The three breast cancer cell lines MDA-MB-231, MCF-7, T24 and liver cancer cell line HepG2 were applied for labeling. Cells were incubated for 1 h with probe **NC-1** *in situ* followed by cell lysis and click chemistry with rhodamine azide for subsequent fluorescent SDS-PAGE (Figure 14). In MDA-MB-231, only one intense band in the range of 40 kDa was observed with a low fluorescence background at concentrations ranging from 10 to 100 nM after 1 h of probe incubation. In case of 500 nM, the background labeling was slightly increased and the intensity of the 40 kDa band was reduced to a small extent meaning that more off targets were hit by the probe at higher concentrations (Figure 14B). For MCF-7, HepG2 and T24 cells, the same labeling pattern was obtained with a higher specificity at a concentration of 500 nM (Figure 14C). Overall, the probe delivered an extremely specific labeling profile in the nanomolar range, which was not expected for the highly electrophilic trichloromethylacyl group

As mentioned in the chapter before, the probe **NC-4** which is closely related to **NCA** shows a higher bioactivity as **NC-1** in MTT assays. This is a hint that **NC-4** is better suitable for ABPP than **NC-1** since it is structurally more similar to **NCA** and shows the same activity. However, so far, the are no results for inhibition of cell migration and proliferation of the probe. The first experiments were focused on **NC-1** since all bioactivity data were collected with this probe. **NC-1** turned out to be a good candidate for elucidation of the anti-migratory protein target of **NCA** since it still triggers an anti-migratory phenotype. Nevertheless,

labeling efficiency and target protein identification with probe **NC-4** is described in chapter 8 for identification of the target protein for cell proliferation

The identity of the **NC-1** labeled protein in the range of 40 kDa can be analyzed by MS-coupled experiments. But first, a similar reactivity of the probe **NC-1** and **NCA** to the same target protein was evaluated by competitive labeling approaches.
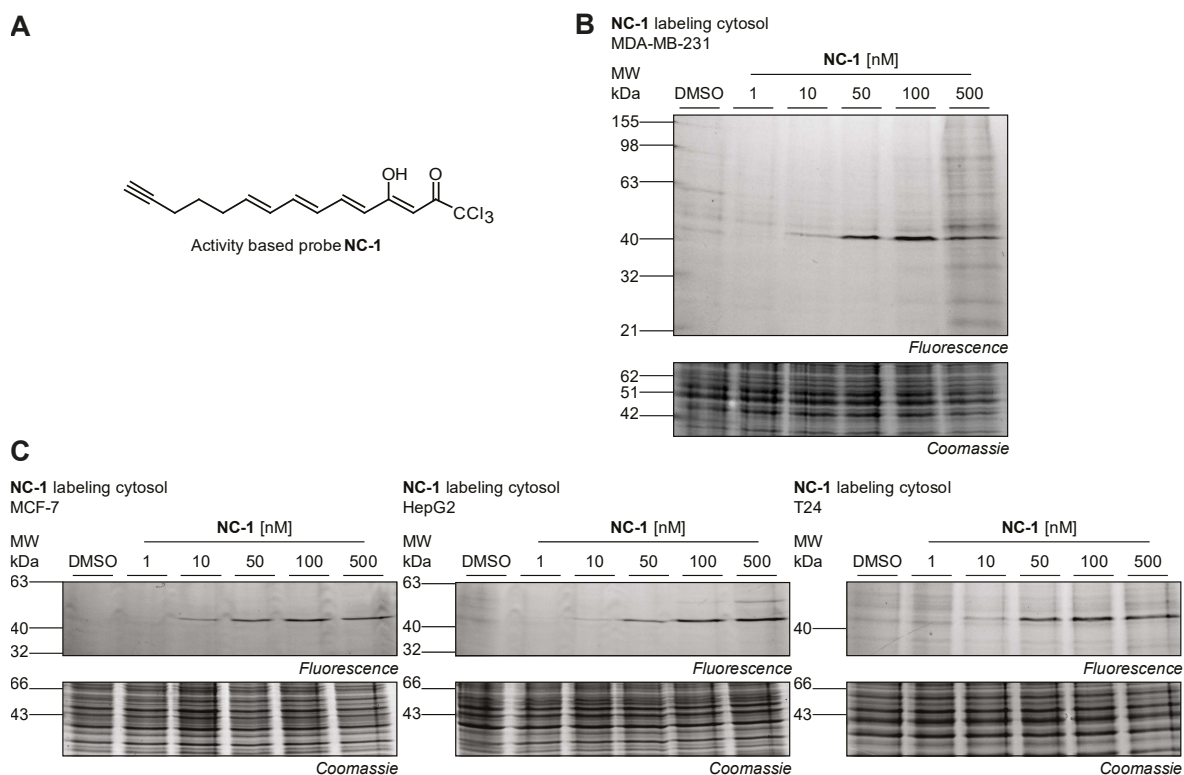
Figure 14: Analytical *in situ* labeling with probe NC-1 in different cell lines. **A,** Chemical structure of probe **NC-1**. **B,** SDS-PAGE analysis of cytosolic fraction of MDA-MB-231 after *in situ* labeling with **NC-1** for 1 h (0.1% DMSO). **C,** SDS-PAGE analysis of cytosolic fraction of analytical *in situ* labeling with **NC-1** (0.1% DMSO) in three different cell lines for 1 h. **B-C,** One representative gel out of three independent experiments is shown. Adapted from Gleissner *et al.* [134]

3.2. Competitive analytical labeling with probe **NC-1**

In order to confirm that the natural product and the probe target the same protein, competition experiments with 1- and 5-fold excess of natural products were performed. The 40 kDa band was outcompeted by addition of 1- and 5-fold **NCA** and **NCB** in HepG2 and MDA-MB-231 while for **NCC**, only a slight competition effect at a 5-fold access was observed (Figure 15A+B). Similar results were obtained for the opposite stereoisomers in MDA-MB-231, in detail, **NCA'** showed a good competition effect whereas for **NCC'**, no competition was detected (Figure 15C). According to the results obtained for bioactivity, **NCA**, **NCA'** and **NCB** pertained again as the most active members in competition experiments and therefore in target protein binding. For both the inhibition of proliferation and migration, **NCA** was revealed as the most active member followed by **NCA'** and **NCB** which showed quite comparable effects. Consequently, target protein binding is suggested to directly correlate with the observed effects on bioactivity. With the optimized labeling conditions obtained by analytical labeling in hand, MS based approaches were applied for elucidation of the target protein in the next chapter.
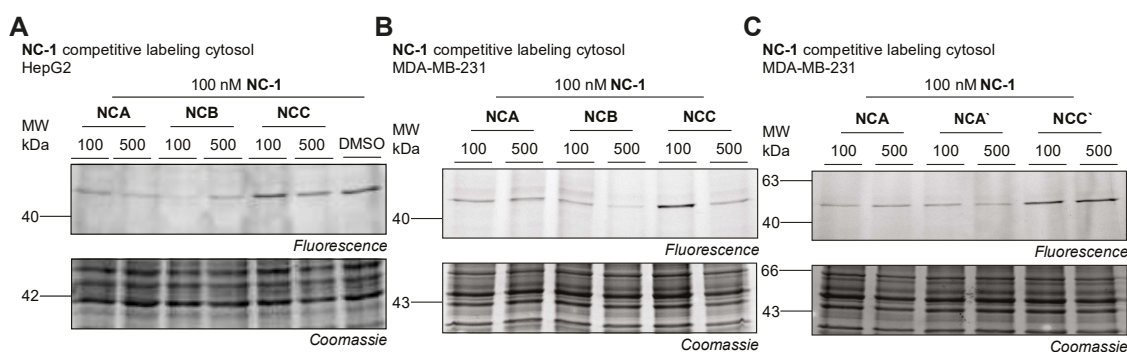
Figure 15: Competitive analytical *in situ* labeling in MDA-MB-231. A, SDS-PAGE of competitive analytical labeling for 1 h in HepG2 cells with natural products **NCA**, **NCB**, **NCC** and DMSO control (0.1% DMSO). **B,** SDS-PAGE of competitive analytical labeling for 1 h in MDA-MB-231 cells with natural products **NCA**, **NCB** and **NCC** (0.1% DMSO). **C,** SDS-PAGE of competitive analytical labeling for 1 h in MDA-MB-231 cells with natural products **NCA**, **NCA'**, and **NCC'** (0.1% DMSO). **A-C,** Natural products were applied in concentration ratios 1:1 and 5:1 (natural product:probe). One representative gel out of three independent experiments is shown. Adapted from Gleissner *et al.* [134]

.

3.3. Importance of the trichloromethly group

Further, the importance of the trichloromethyl group for target protein binding was investigated with two different variants of the alkyne-tagged probe **NC-1.** Probes were designed with a trifluoromethyl group, namely **NC-5**, and a dichloromethyl group termed **NC-2** (Figure 16A). With these probes in hand, the labeling efficieny was tested in a gel-based ABPP approach. After 1 h of probe incubation and click reaction with rhodamine azide, no labeling could be observed for concentrations relevant for **NC-1** labeling meaning a range of 10-500 nM (Figure 16B). For higher concentrations starting at 1 µM or 5 µM, an unspecfic labeling was found for probe **NC-5.** In the case of **NC-2**, a slight labeling pattern was obtained for 1 µM probe concentration and an unspecific labeling pattern was detected at 10 µM. For both probes, the labeling is shifted to much higher probe concentrations in the µM range with an unspecific pattern compared to **NC-1** since the trichloromethyl group was exchanged by different functional groups. Taken together, the trichloromethyl group is reported to be crucial for a highly efficient and specific target protein binding in the nanomolar range.
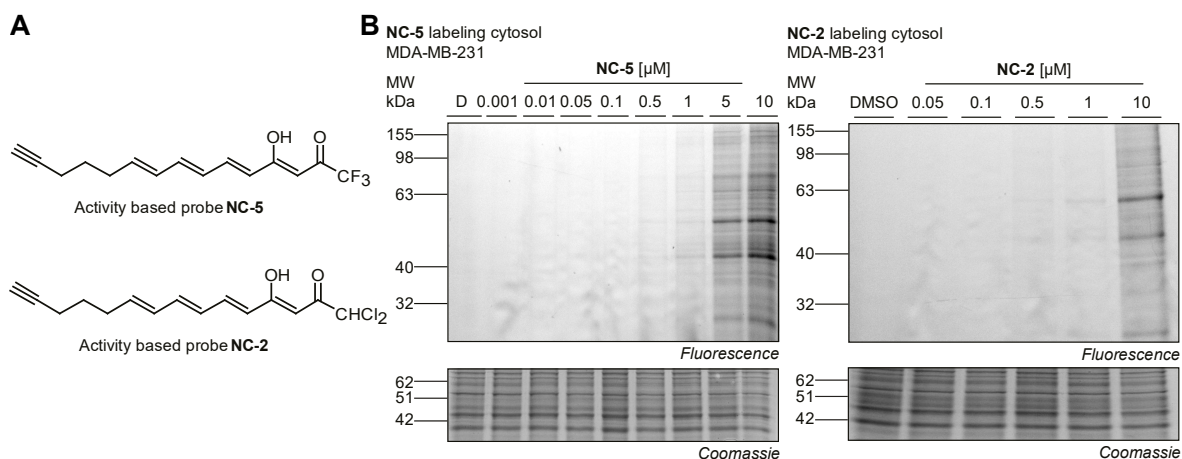
Figure 16: Analytical *in situ* labeling with probe NC-5 and NC-2 in MDA-MB-231. A, Chemical structure of probe **NC-5** and **NC-2**. **B,** SDS-PAGE analysis of cytosolic fraction of MDA-MB-231 after *in situ* labeling with **NC-5** and **NC-2** (0.1% DMSO) for 1 h. One representative gel out of three independent experiments is shown.

4.

TARGET IDENTIFICATION AND VALIDATION

VAT-1 was identified as the only reproducible target protein of **NC-1** by LFQ and SILAC ABPP approaches in human breast cancer cells. Binding of **NCA** to the target protein was detected and the protein was confirmed as a confidential target by orthogonal methods.

Contents:

4.TARGET IDENTIFICATION AND VALIDATION

4.1. Application of ABPP for target identification

To unravel the identity of the target protein, MS-based ABPP approaches with two complementary quantification strategies namely SILAC and LFQ were applied for an improved confidence of the enriched hits.[123, 148] For MS experiments, proteins labeled by the probe are clicked to analytical handles for enrichment and are digested to peptides which can be analyzed by MS/MS and identified by comparison to databases performed software tools. In first labeling approaches reported before, the synaptic vesicle membrane protein was identified as a protein target of **NC-1** in the liver cancer cell line HepG2.[54]

For MS-based ABPP, MDA-MB-231 cells were incubated with either 100 or 500 nM **NC-1** or DMSO as a control and clicked to biotin-azide for a subsequent enrichment on avidin beads. Proteins were directly reduced by DTT (dithiothreitol) and alkylated by IAA (iodoacetamide) on the beads and processed for LC-MS/MS proteome analysis. Detected proteins were identified by the software MaxQuant and are visualized with Perseus in volcano plots displaying enrichment over background log_2 enrichment > 2 on the x-axis and significance ($p < 0.05$) on the y-axis. In the SILAC approach, the synaptic vesicle membrane protein 1 (VAT-1) with a size of 41.9 kDa pertained as the most significant enriched protein among others such as reticulon 3 (RTN3), heme oxygenase (HMOX2) or cytochrome 5B (CYB5B) (Figure 17A, Table 1). Notably, the LFQ approach provided the same results with VAT-1 as the most prominent hit in the volcano plot, which enhanced the confidence of VAT-1 being the most prominent target protein of **NC-1** (Figure 17B, Table 2). Overall, both SILAC and LFQ ABPP approaches demonstrate a reproducible readout, which can be quite good compared in case of **NC-1**. The results obtained support each other and confidently deliver the target protein of **NC-1**.

To further confirm VAT-1 as a protein target of **NCA**, competitive studies with an excess of 5-fold **NCA** were performed *via* LFQ in MDA-MB-231 (Figure 17C, Table 2). The DMSO control samples should behave similarly to samples treated with **NCA** and **NC-1** in parallel since for both cases, **NC-1** is not bound to VAT-1 and therefore, it cannot be clicked to a biotin tag for enrichment. In the LFQ competition experiment, VAT-1 was again revealed as the most prominent hit in the volcano plot showing enrichment of **NC-1** treated cells against competition background (Figure 17C). Accordingly, the profile plot of the absolute LFQ

intensity of VAT-1 also showed a drop in signal intensity for the competition samples comparable to that of the DMSO control (Figure 17D). The only protein which pertained sufficient competition in the LFQ approach was the HMOX2, which is a protein of high abundance and is frequently targeted by electrophilic compounds (Figure 17C).

The other proteins which showed high enrichment factors in Figure 17B were discarded from further analysis due to insufficient competition results. In contrast, VAT-1 was considered as promising target protein and selected for further validation experiments.
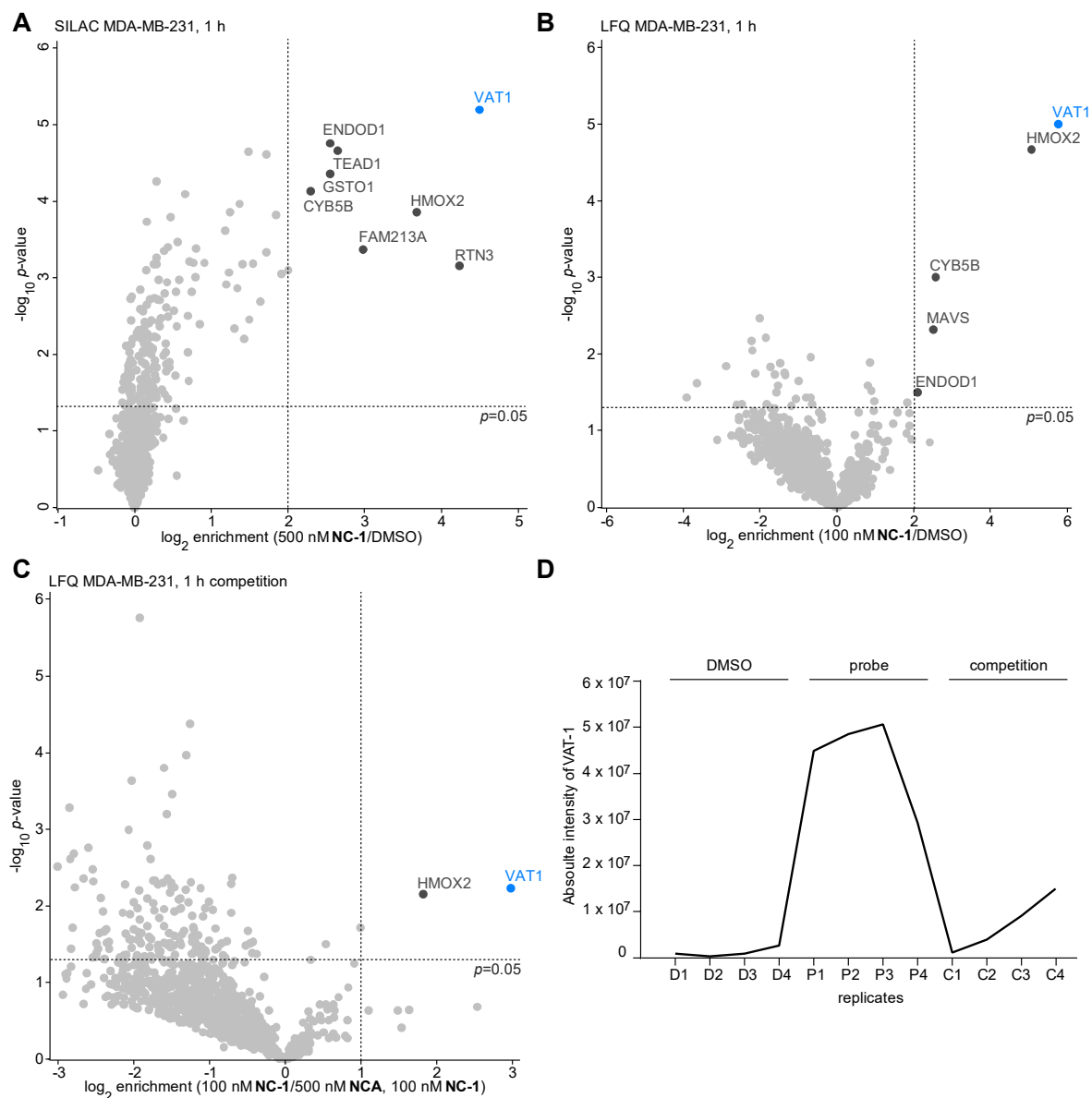
Figure 17: Identification of VAT-1 as cellular target protein of NCA by competitive LC-MS/MS-based ABPP in MDA-MB-231. A, Volcano plot of *in situ* SILAC ABPP experiment with 500 nM **NC-1** (n=6). Hits matching the criteria log$_2$ enrichment > 2, *p*-value < 0.05 are highlighted in dark grey and the protein with the highest enrichment factor (VAT-1) is shown in blue. **B,** Volcano plot of *in situ* LFQ ABPP experiment with 100 nM **NC-1** (n=5). Hits matching the criteria log$_2$ enrichment > 2, *p*-value < 0.05 are highlighted in dark grey and the protein with the highest enrichment factor (VAT-1) is shown in blue. **C,** Volcano plot of *in situ* competitive label-free ABPP experiment (n=5) (log$_2$ enrichment > 1, *p*-value < 0.05). **D,** Profile plot of absolute intensities shown for DMSO, probe and competition samples. **A-D,** Results were already generated in my master thesis, but were re-evaluated for this thesis.[149] Adapted from Gleissner *et al.* [134]

Table 1: Significantly enriched proteins from SILAC **NC-1** target ID shown in Figure 17 A with corresponding $\log_2$ enrichment and significance. (blue = most prominent **NC-1** target protein, dark grey = proteins matching the criteria $\log_2$ enrichment > 2, p-value < 0.05).

gene name	protein name	$\log_2$ fold change	$-\log_{10}$ p-value	coverage [%]
VAT1	Synaptic vesicle membrane protein VAT-1 homolog	4.49	5.19	57
RTN3	Reticulon	4.23	3.16	22
HMOX2	Heme oxygenase 2	3.68	3.85	66.8
FAM213A	Redox-regulatory protein FAM213A	2.97	3.37	29.3
TEAD1	Transcriptional enhancer factor TEF-1	2.65	4.65	23
GSTO1	Glutathione S-transferase omega-1	2.55	4.36	49
ENDOD1	Endonuclease domain-containing 1 protein	2.55	4.76	16.2
CYB5B	Cytochrome b5 type B	2.29	4.13	50.7

Table 2: Significantly enriched proteins from LFQ **NC-1** target ID shown in Figure 17B+C with corresponding $\log_2$ enrichment and significance. (blue = most prominent **NC-1** target protein, dark grey = proteins matching the criteria $\log_2$ enrichment > 2 for target ID and $\log_2$ enrichment > 1 for competition, p-value < 0.05).

gene name	protein name	$\log_2$ fold change	$-\log_{10}$ p-value	coverage [%]
LFQ target ID (100 nM NC-1/DMSO)				
VAT1	Synaptic vesicle membrane protein VAT-1 homolog	5.77	5.00	27
HMOX2	Heme oxygenase 2	5.07	4.67	34.5
CYB5B	Cytochrome b5 type B	2.58	3.00	18
MAVS	Mitochondrial antiviral-signaling protein	2.52	2.32	19.8
ENDOD1	Endonuclease domain-containing 1 protein	2.11	1.50	23.4
LFQ competition (100 nM NC-1/500 nM NCA, 100 nM NC-1)				
VAT1	Synaptic vesicle membrane protein VAT-1 homolog	2.98	2.23	27
HMOX2	Heme oxygenase 2	1.82	2.16	34.5

Since the biological activity was measured over longer time periods such as 24 or 48 h, the time stability of the target protein labeling was investigated. Time dependence was monitored in an MS-based and gel-based approach. Extended incubation times with 500 nM **NC-1** for 24 h in MDA-MB-231 did not change the results presented in Figure 17 (Figure 18A). VAT-1 still turned out to be highly significantly enriched in **NC-1** treated samples against background amongst other proteins which were not detected after 1 h labeling (Table 3). A further competition experiment with **NCA** for 24 h could exclude these hits as target proteins.

Since in analytical labeling experiments, only a selective labeling of VAT-1 in the range of 40 kDa was obtained, a further competition study was not required. In analytical gel-based experiments, the protein labeling showed a high stability over extended incubation times of 24 and 48 h proposing sufficient stability upon binding of the protein target (Figure 18B). The results show that longer incubation times for screening of the biological activity are applicable since the labeling pattern does not change over time. For the obtained phenotypes, VAT-1 is the only plausible protein target which is relevant for the caused effects.
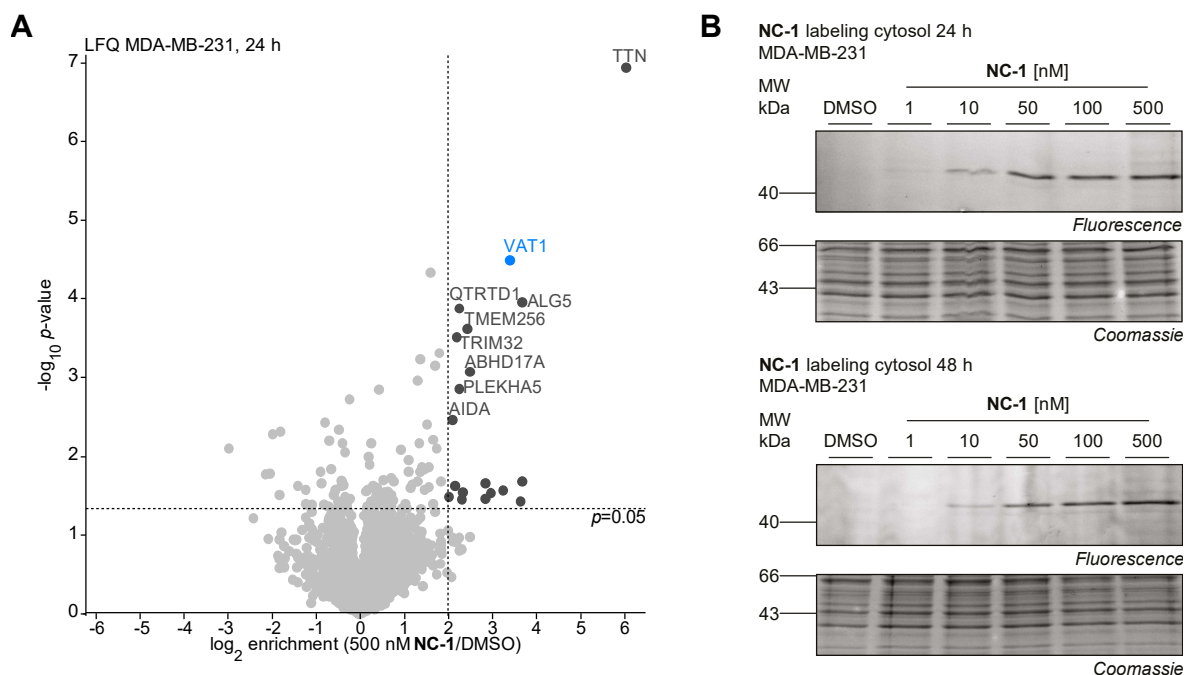
Figure 18: Time dependence of target ID in MDA-MB-231: **A,** Volcano plot of *in situ* label-free ABPP experiment in MDA-MB-231 cells which were incubated for 24 h with 500 nM **NC-1** (n=4). Hits matching the criteria log$_2$ enrichment > 2, *p*-value < 0.05 are highlighted in dark grey and the target protein VAT-1 is shown in blue. **B,** SDS-PAGE analysis of cytosolic fraction of MDA-MB-231 after *in situ* labeling with **NC-1** for 24 or 48 h (0.1% DMSO). Adapted from Gleissner *et al.* [134]

Table 3: Significantly enriched proteins from LFQ **NC-1** target ID for 24 h shown in Figure 18A with corresponding log$_2$ enrichment and significance. (blue = most prominent **NC-1** target protein, dark grey = proteins matching the criteria log$_2$ enrichment > 2, *p*-value < 0.05).

gene name	protein name	log$_2$ fold change	-log$_{10}$ *p*-value	coverage [%]
TTN	Titin	6.05	6.95	0.2
ALG5	Dolichyl-phosphate beta-glucosyltransferase	3.69	3.96	18.3
U2AF1L4	Splicing factor U2AF 26 kDa subunit	3.68	1.68	44.4
SEC61G	Protein transport protein Sec61 subunit gamma	3.64	1.43	23.5
VAT1	Synaptic vesicle membrane protein VAT-1 homolog	3.41	4.49	45.5
FAM126A	Hyccin	3.26	1.57	6.5
LMAN2	Vesicular integral-membrane protein VIP36	2.97	1.53	11.2
TUBA4A	Tubulin alpha-4A chain	2.85	1.66	43.8
RINT1	RAD50-interacting protein 1	2.84	1.46	5.7
ABHD17A	Alpha/beta hydrolase domain-containing protein 17A	2.50	3.08	6.1
TMEM256	Transmembrane protein 256	2.43	3.62	22
SPCS1	Signal peptidase complex subunit 1	2.35	1.55	26.5
TIMP2	Metalloproteinase inhibitor 2	2.32	1.45	11.7
PLEKHA5	Pleckstrin homology domain-containing family A member 5	2.26	2.86	9.5
QTRTD1	Queuine tRNA-ribosyltransferase subunit QTRTD1	2.26	3.88	8.4
TRIM32	E3 ubiquitin-protein ligase TRIM32	2.20	3.51	5.1
PPIF	Peptidyl-prolyl cis-trans isomerase	2.16	1.62	32.4
AIDA	Axin interactor, dorsalization-associated protein	2.10	2.46	23
MRPL24	39S ribosomal protein L24, mitochondrial	2.02	1.48	28.7

Further, ABPP with LFQ quantification was repeated to guarantee the same activity of the old stock of **NC-1** and the newly synthetized probe **NC-1** (appendix Figure 48). Again, VAT-1 turned out to be the most prominent hit in volcano plots. Further proteins were enriched, which did not appear amongst the enriched proteins shown in Figure 17 and 18. Thus, it is suggested that only VAT-1 is a reproducible hit in enrichment experiments with LFQ. Moreover, MS-based ABPP was repeated for the comparison of the target protein binding of **NCA'** and **NCA**. In the reference enrichment plot showing **NC-1** against background, VAT-1 turned out to be again the most enriched hit amongst a few other proteins which were not detected in the approaches before (Figure 19A). Together with results obtained before, this data also confirms that VAT-1 is the only reproducible hit detected over all enrichment experiments.

For competition experiments, a 5-fold excess of **NCA** or **NCA'** was applied. For both approaches, a highly competitive effect was revealed for VAT-1 and some other proteins, which were not amongst the enriched hits in the reference **NC-1**/DMSO volcano plot and were thus excluded from further analysis (Figure 19B+C). **NCA** and **NCA'** show quite comparable competition according to the results obtained for competitive analytical labeling. Furthermore, the profile plot of VAT-1 over all intensities detected for each sample showed a drop in intensities for competition samples comparable to the DMSO control (Figure 19D).

The data obtained for MS-based competition ABPP for **NCA** and **NCA'** are in accordance to the analytical labeling results shown in the chapter before. In case of bioactivity assays, for both the inhibition of proliferation and migration, **NCA** pertained as the most active member of the neocarzilins followed by **NCA'.** However, the competitive effect in ABPP experiments of both compounds was completely similar for VAT-1 with no stronger effect of **NCA**. It was already mentioned that **NC-1** is an appropriate probe for investigation of the target responsible for cell migration but no proliferation, since it showed only little effects on cell proliferation and might therefore only weakly bind to the protein target for cell proliferation.

In parallel, **NCA'** itself showed stronger effects on cell migration compared to cell proliferation comparable to **NC-1** while it was more active than **NC-1**. This means that it also binds to the target for cell migration to a higher extent as **NC-1**. Therefore, it can be explained that **NCA',** which triggers an anti-migratory phenotype at lower concentrations than **NC-1**, shows the same competition than **NCA** for the target protein VAT-1, which probably is only responsible for inhibition of cell migration. Further, it might be that both compounds are bound to the target protein, but **NCA** is stronger in inhibiting the activity of the protein due to its structure. Additionally, **NCA** might in contrast to **NCA'** also hit different

proteins or non-proteinogenic targets, which we did not detect with our ABPP approaches, but are relevant for bioactivity effects. This might especially be the case for the targets of cell proliferation, since **NCA** showed ten-fold higher activity than **NCA'** in inhibition of cell proliferation.
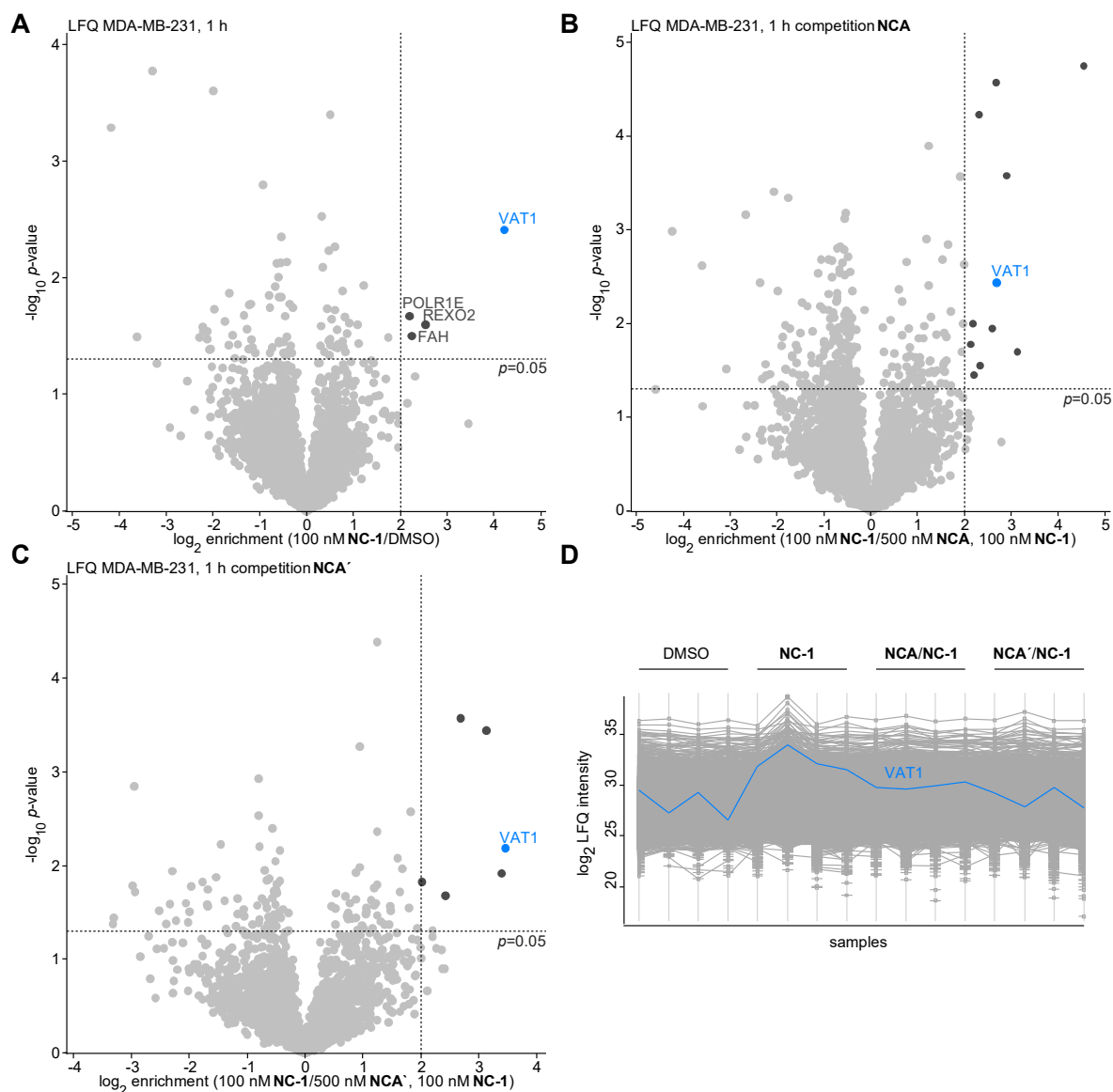
Figure 19: Identification of VAT-1 as cellular target protein of NCA and NCA' by competitive LC-MS/MS-based ABPP in MDA-MB-231. **A,** Volcano plot of *in situ* LFQ ABPP experiment with 100 nM **NC-1** (n=4). **B,** Volcano plot of *in situ* competitive LFQ ABPP experiment with 5-fold excess of **NCA** and 100 nM **NC-1** (n=4). **C,** Volcano plot of *in situ* competitive label-free ABPP experiment with 5-fold excess of **NCA** and 100 nM **NC-1** (n=4). **A-C,** Hits (log$_2$ enrichment > 2, *p*-value < 0.05) are highlighted in dark grey and the protein with the highest enrichment factor (VAT-1) is shown in blue. **B-C,** Proteins in dark grey with no indication of the gene name did not appear as enriched in **A** and were neglected for further analysis. **D,** Profile plot of log$_2$ LFQ intensities shown for DMSO, probe and **NCA/NC-1** or respectively **NCA'/NC-1** competition samples. Profile plot of VAT-1 is highlighted in blue.

4.2. Target protein validation by orthogonal methods

For confirmation of VAT-1 as the target protein, analytical labeling in si-VAT-1 treated cells was performed. No protein labeling could be observed in si-VAT-1 treated MDA-MB-231 whereas for the control treated with non-targeting (nt) si-RNA, the VAT-1 labeling pattern was still detected for 100 and 500 nM probe concentration (Figure 20A). These results confidently validate the identity of VAT-1 as the probe labeled protein which is visible on the gel in the range of 40 kDA. Further, a selective labeling of VAT-1 isoform 1 is obtained in the presence of all three VAT-1 isoforms present in human cells.

Additionally, an analytical labeling with a subsequent immunoprecipitation (IP) was performed to confidently validate the identity of the protein with a complementary approach. Therefore, cells were first incubated with the probe *in situ* and VAT-1 was pulled down with a specific antibody, enriched on Protein A/G beads- meaning beads coated with a recombinant fusion protein that combines Fc-IgG binding domains of both Protein A and Protein G- and again eluted after click chemistry. In the IP eluate, one fluorescent band derived from VAT-1 was detected for both acidic elution and elution by detergents (Figure 20B). Consequently, the protein providing fluorescence intensity on the gel represents VAT-1, since the signal could be still detected after a specific pulldown strategy.

Moreover, to verify VAT-1 as target of **NCA** directly, we overexpressed and purified the recombinant protein in *E. coli*. Labeling was performed in cell lysates after VAT-1 overexpression as well as directly with the purified, recombinant protein. For cell lysate labeling, *E. coli* lysate was incubated with 2 µM of probe **NC-1** after induction of protein expression by IPTG and without IPTG (Isopropyl β-d-1-thiogalactopyranosideas) a control. Gel-based labeling with **NC-1** revealed a clear protein band for *E. coli* lysate after VAT-1 overexpression, which was absent in the control (Figure 20C). Further, fluorescent labeling was also detected for the recombinant protein in a concentration dependent manner, while for heat inactivation of the protein prior to labeling, signal intensity was strongly reduced (Figure 20D). These results demonstrate a direct binding of the probe **NC-1** to VAT-1 *in vitro.* The reduction of the protein binding for the heat control shows a selective binding of the probe only to the correctly folded protein.

However, it still has to be figured out if the protein binding of **NC-1** in *E. coli* cell lysates or to the recombinant protein occurs in the same manner as in human cells. For example, a metabolic modification of the probe or a selective transport of the probe to the protein can take place in human cells which are absent *in vitro* or in bacteria.
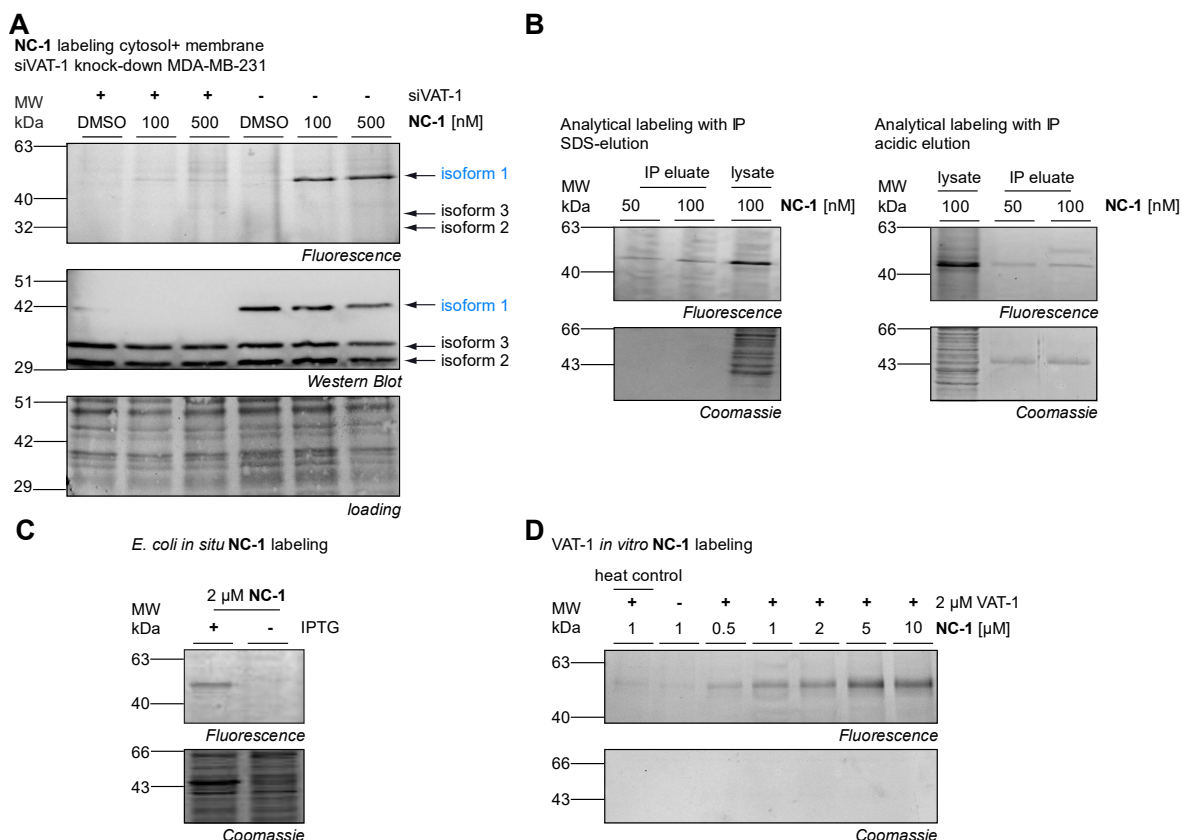
Figure 20: Confirmation of VAT-1 identity of target protein of probe NC-1. A, SDS-PAGE and Western blot of analytical labeling of si-VAT-1 treated MDA-MB-231 cells in comparison to nt si-RNA treated cells. Cells were transfected for 2 days and were labeled *in situ* for 1 h with probe **NC-1**. **B**, SDS-PAGE and Western blot of analytical labeling in MDA-MB-231 with a subsequent immunoprecipitation with VAT-1 antibody with acidic or respectively SDS elution. **C,** SDS-PAGE of *E. coli* cell lysate of *in situ* labeling with **NC-1** after VAT-1 overexpression induced by IPTG. **D,** SDS-PAGE of *in vitro* labeling of recombinant *E. coli* VAT-1 with increasing **NC-1** concentrations. Heat control and no enzyme control are included. Adapted from Gleissner *et al.* [134]

4.3. Conclusion

In conclusion, it was deciphered that VAT-1 is the most prominent target protein of **NC-1** in both SILAC and LFQ ABPP approaches. In further LFQ studies, VAT-1 was revealed as the only reproducible hit. Moreover, in competition experiments, a selective binding of neocarzilins, in particular of **NCA** and **NCA**', could be shown for VAT-1. Since the probe **NC-1** is only suitable for the detection of the target protein relevant for inhibition of cell migration, VAT-1 might be the target of **NCA** which provides a link to cell migration.

VAT-1 was further confirmed as the highly confidential protein target of **NC-1** by labeling in si-VAT-1 cells and immunoprecipitation. Finally, overexpression of the protein in *E. coli* and recombinant protein labeling experiments again revealed VAT-1 as the target protein of neocarzilins, which can be further validated in context of the neocarzilin binding mode.

Overall, the data demonstrates the power of chemical proteomics for identification of the cellular target of a natural compound which has been discovered decades ago. The target validation by orthogonal methods underlines the high reliability of chemical proteomics approaches with different quantification strategies.

5.

BINDING SITE IDENTIFICATION

By an active-site peptide profiling (ASPP) approach and by re-evaluation of the target ID data, it was proposed that the binding site peptide of VAT-1 is located in a region of the protein which is unique for isoform 1. Further, E113 was shown to be involved in neocarzilin binding in human cells, which could not be confirmed for *E. coli*. Consequently, a different binding mode is suggested between human cells and bacteria.

Contents:

5. BINDING SITE IDENTIFICATION

5.1. Detection of binding site peptide and residues involved in binding

VAT-1 was figured out as the protein target of neocarzilins in human breast cancer cells. However, the clear binding mode of the compound and the corresponding binding site was not elucidated so far. Intact protein MS approaches failed to detect the mass shift caused by **NCA** binding since the spectral quality of the purified protein was insufficient on a LTQ- FT instrument (data not shown). Consequently, the exact mass adduct was unknown, thus, the binding site analysis by software tools became more complex. Tools for the identification of unknown modifications such as MaxQuant dependent peptides mode and Byonic software wildcard search[150] were taken into account to gain deeper insights into the binding mode.

The detection of the binding site was first approached by MS/MS fragmentation of the purified, recombinant protein labeled with **NCA,** which provided insufficient results. Further, co-IP and whole proteome samples treated with **NCA** were evaluated with the software MaxQuant in dependent peptides mode and the Byonic software with a wildcard search[150] for the identification of an unknown modification. However, we were not able to find the binding site or a plausible mass shift matching with **NCA**. Further, an ABPP strategy with **NC-1** using a TEV protease (Tobacco Etch Virus nuclear-inclusion-a endopeptidase) cleavable linker to detect the modified binding site peptide was applied. Here, proteins were digested on the beads with trypsin and subsequently with TEV protease for elution of the binding site peptides. The approach provided a high protein enrichment of VAT-1 after trypsin digestion as well as after TEV protease digestion again underlining VAT-1 to be a highly confidential target protein of **NC-1**. However, the approach did not deliver the binding site peptide with MaxQuant dependent peptide search (data not shown).

Finally, a strategy based on active-site peptide profiling (ASPP) was performed, which has already been described by Cravatt *et al*. The principle involves the digestion of the probe-treated proteomes before enrichment of the peptides bearing the binding site on affinity resins.[85] For example, active-site peptides have been enriched by pull-down with anti-rhodamine antibodies for LC/MS-MS analysis before.[151] Here, an approach with a digestion step before enrichment on avidin beads with a desthiobiotin tag and subsequent elution of the peptides by organic solvents was exploited. Only the peptides bound to the probe are

enriched after the digestion and in contrast to the biotin-avidin interaction, desthiobiotin can be eluted from avidin beads by MeCN (acetonitrile) and FA (formic acid) (Figure 21A). Recently, isotopically labeled desthiobiotin azide (isoDTB) tags which were also eluted from the beads were applied for reactive cysteine profiling of proteomes.[152]

Again, we were not able to elucidate either the binding site or the chemical mode of action for binding. Nevertheless, an unmodified tryptic peptide for VAT-1 (residues 103-128 or respectively 97-128) was detected by MaxQuant which was eluted from the beads after desthiobiotin enrichment (Figure 21B). It is suggested that the probe was detached during the MS preparation procedure or rather the MS measurement since the stability of the probe-protein interaction was confirmed for protein precipitation by acetone with a subsequent MeOH washing step and for elution buffer (MeCN/FA) applied for protein desalting (appendix Figure 49A). Again, a mass shift corelating with **NCA** was not detected by MaxQuant dependent peptide search.

Notably, the corresponding peptide is only present in isoform 1 out of three native VAT-1 isoforms which are all expressed in MDA-MB-231, as confirmed by Western Blot (Figure 20A). Isoform 2 and 3 are shorter than isoform 1 with missing parts at the beginning of the protein sequence. Since only isoform 1 with 41.9 kDa is labeled by **NC-1** but not isoform 2 and 3, it is suggested that only the initial part until residue 128 is relevant for **NC-1** binding. Particularly the region unique for isoform 1 between residue 61-128 is critical for neocarzilin binding. Consequently, the peptide detected by MS/MS with the desthiobiotin approach which is directly located in this region is considered as an interesting candidate as binding site peptide.

For further confirmation of the binding site peptide and for investigation of the residue, which is involved in **NCA** binding, we mutated all nucleophilic residues in the protein sequence (Figure 21B). The point mutants were established in a human plasmid bearing the sequence for His-TEV-tagged VAT-1 for a direct labeling in human cells after transfection. The resulting His-TEV-VAT-1 constructs were labeled in MDA-MB-231 and fluorescent gel bands were detected for all point mutants except for E113Q mutant (Figure 21C+D). E113Q is highly overexpressed in human cells after the transfection, which was detected by Western blot, but is not labeled by the probe. These results further narrow down the residues important for neocarzilin binding and suggest that E113 is somehow involved the binding mechanism.

Further, for R128, the results were first not clear. The point mutations R128Q and R128N delivered ambiguous results since no fluorescent intensity was detected for them, which would be a hint for a possible involvement in neocarzilin binding. However, in parallel, only

a weak overexpression was achieved after protein transfection according to the Western blot results (appendix Figure 49B). Therefore, another point mutant (R128K) was created, which showed a stabile overexpression in human cells and labeling by **NC-1** (Figure 21D, appendix Figure 49B). Therefore, R128 was excluded as a possible binding site candidate and only E113 was considered as relevant for neocarzilin binding.
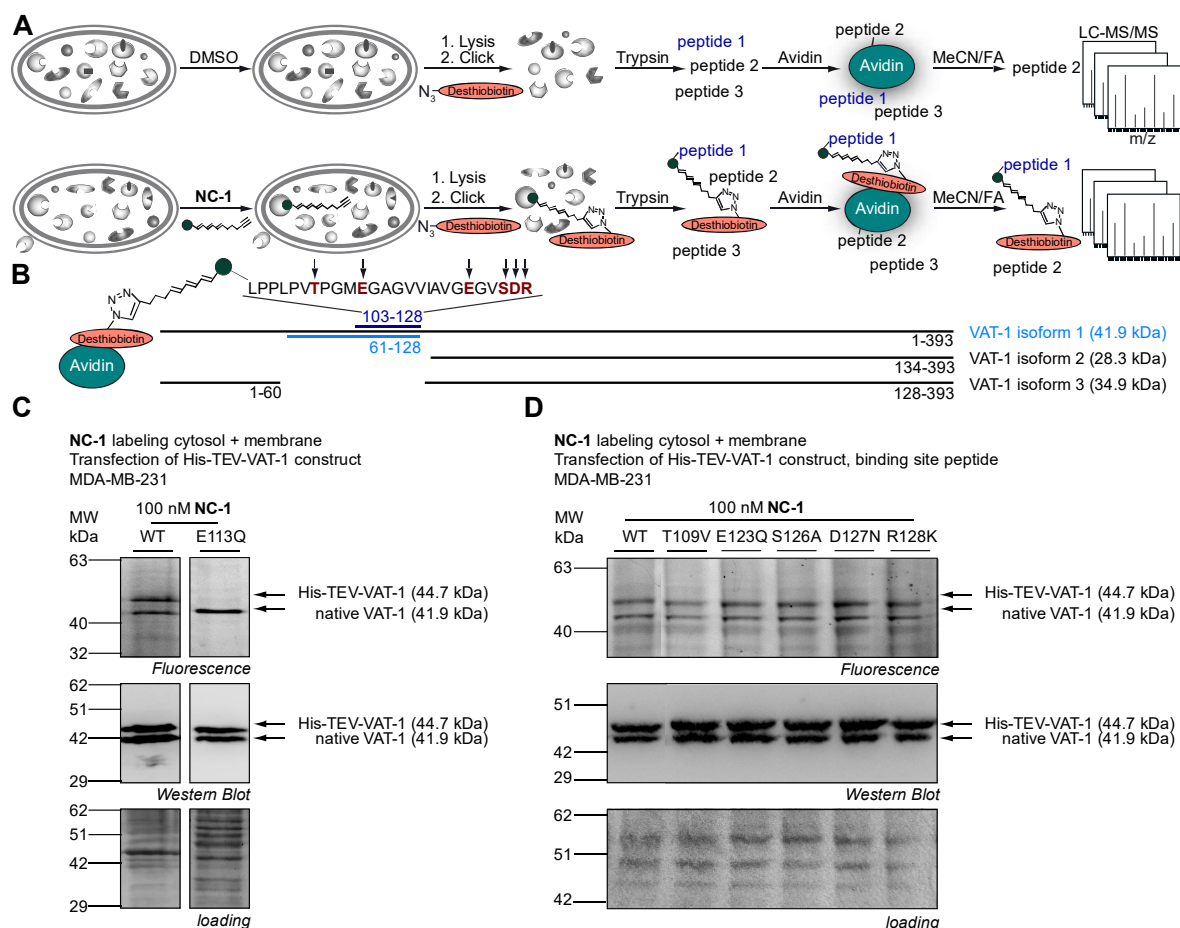
Figure 21: Verification of VAT-1 binding site. **A,** Schematic overview of ABPP based approach to identify binding site peptides. After protein digestion, only peptides bound to the probe are enriched on avidin beads and eluted with acetonitrile (MeCN) and formic acid (FA) for MS/MS detection. B, Identified binding site peptide (aa 103-128) in **NC-1** treated cells and location of the peptide in the part of VAT-1 which is unique to isoform 1. Mutated residues are shown in red. **C,** *In situ* labeling of MDA-MB-231 which were transfected with His-TEV-VAT-1 construct expressing wildtype (WT) or the point mutant E113Q. SDS PAGE and Western blot are shown. **D,** Western blot and SDS-PAGE of *in situ* labeling of transfected VAT-1 wildtype (WT) and point mutants with an additional His-TEV tag compared to native VAT-1 in MDA-MB-231 cells for binding site identification. Adapted from Gleissner *et al.* [134]

Of note, another hint corroborating the correct localization of the **NCA** binding site peptide constitutes the fact that the peptide ranging from residue 103 to 128 or respectively 97-128 found in the desthiobiotin approach was not detected in all LFQ target ID experiments, which revealed an overall protein coverage of around 50%. For target ID experiments, the peptide directly bound to the probe and therefore the avidin beads is always missing for MS/MS analysis, since it remains bound to the beads and is not eluted.

For illustration, a heat map showing log$_2$ enrichment (**NC-1**/DMSO) over seven independent LFQ target ID experiments was generated. Decisive for analysis was mainly the detection of the peptides in **NC-1** samples and not the significant enrichment compared to DMSO samples. Therefore, also log$_2$ enrichment factors smaller than 0 were accepted since the absence or presence of the peptides in **NC-1** samples is relevant for analysis and not only the enrichment.

Interestingly, the first part of VAT-1 unique for isoform 1 which is relevant for **NC-1** binding is completely covered in seven independent LFQ target ID experiments apart from residue 97-128 (Figure 24). However, also some peptides in the end region of the protein sequence of VAT-1 are missing which were in contrast found in co-IP or whole proteome analysis experiments. If the peptides are also involved in **NCA** binding or are located near the binding site in the three-dimensional structure of VAT-1 needs to be figured out in future studies. The region ranging from residue 140-210 (70 residues) cannot be detected by MS/MS due to its length since the optimal peptide length after digestion is distributed between 7 to 35 residues.[153]
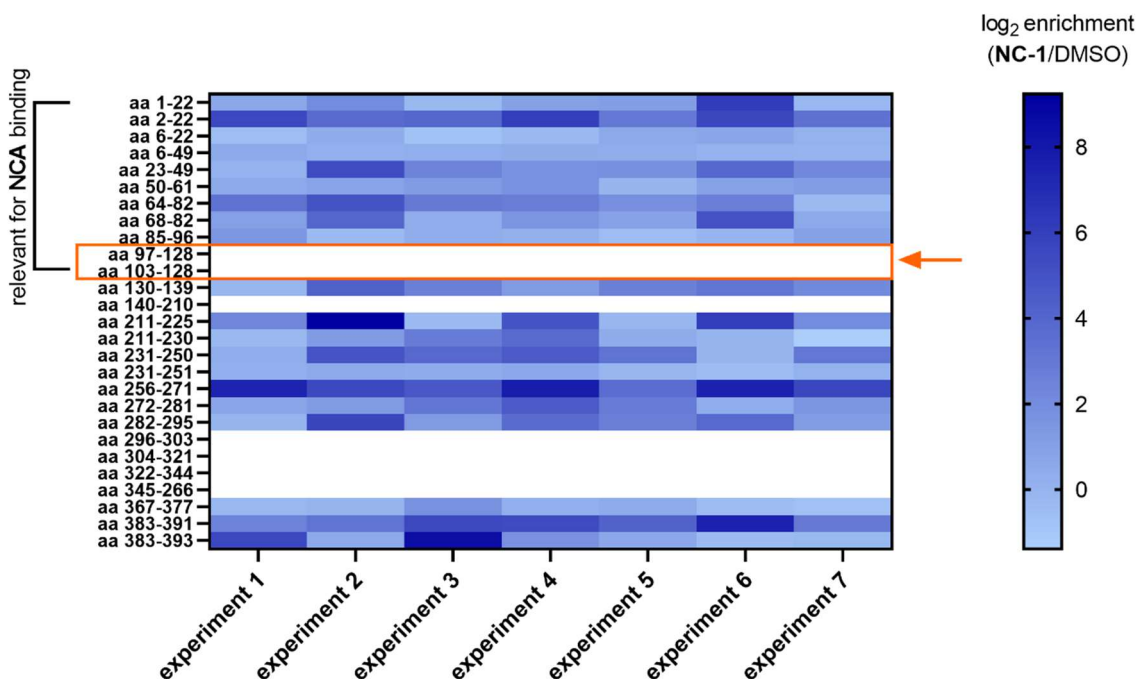
Figure 24: Peptides of VAT-1 identified in independent LFQ enrichment experiments. Heat map showing log$_2$ enrichment (**NC-1**/DMSO) of all detected VAT-1 peptides identified in seven independent enrichment experiments. Peptides only identified in co-IP or whole proteome experiments, but not in target ID approaches, are included in the heat map and are shown as colorless. Peptides found in **NC-1** samples which were not significantly enriched versus DMSO samples are also considered as relevant due to their presence and are highlighted according to the color code indicated on the right. Binding site peptide is highlighted in orange und was not detected in target ID experiments. Two sample students *t*-test and missing value imputation was performed in Perseus software.

Overall, it was proposed that the binding site peptide of VAT-1 is located in a region of the protein which is unique for isoform 1. Further, E113 was shown to be involved in neocarzilin binding since no labeling was detected for the point mutant E113Q in human cells. The residue could be confirmed to be involved in binding by a creation of further point mutants. The crystal structure of VAT-1 published recently shows that E113 is directly located near the hydrophobic pocket which was shown to bind phospholipids.[70] As neocarzilin also bears a fatty-acid-like unsaturated side chain, it is proposed that the binding occurs in a similar way as revealed for phospholipids. However, this hypothesis still needs to be supported by further data and the exact mode of action still has to be figured out. A crystal structure of VAT-1 in combination with **NCA** will help to understand the exact binding mode and to detect residues involved in neocarzilin binding *in vitro*.

5.2. **NC-1** reactivity towards cysteines

Further, as the target ID experiments provided several additional enriched proteins which display proteins with highly electrophile-sensitive cysteine residues [e.g. GSTO1 (C32), HMOX2 (C265, C282), FAM213A (C85,C88)], it is proposed that the trichloromethyl ketone group of **NCA** has some potential for reacting with cysteine residues as well.[154-156] Consequently, the reactivity of neocarzilin towards the four present cysteines in VAT-1 were investigated by further mutagenesis studies. Therefore, the four present cysteines in VAT-1 were mutated to serines and the point mutants were transfected in human cells. Labeling by **NC-1** was detected for each of the point mutants apart from the variant with all four cysteines mutated in parallel (Figure 22). Consequently, it is proposed that the protein structure is completely disrupted after mutation of all four cysteines since the residues are required for a correct protein folding, for example for formation of disulfide bonds. Overall, the data indicate that neocarzilin is not binding to a cysteine of VAT-1 in human cells.
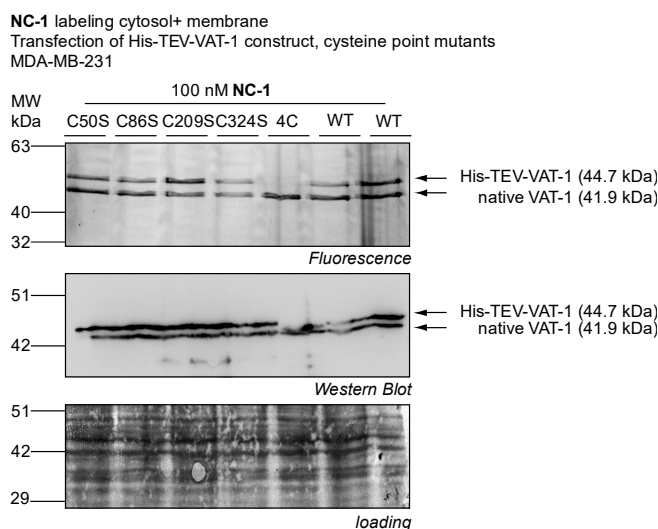
Figure 22: Cysteine mutant labeling in MDA-MB-231. *In situ* labeling of MDA-MB-231 which were transfected with His-TEV-VAT-1 construct expressing wildtype (WT) or cysteine point mutants.

5.3. Verification of residues of VAT-1 involved in **NC-1** binding in *E. coli*

The residues involved in neocarzilin binding should be directly verified in VAT-1 after overexpression in *E. coli*. Therefore, the point mutants for residues which were first considered as possible binding sites namely E113 and R128 were inserted in the bacterial vector pET300. VAT-1 point mutants were overexpressed in *E. coli* and labeled in *E. coli* lysates after IPTG induction. Fluorescence labeling could be detected for each of the investigated point mutants, whereas in human cells, no labeling was obtained for E113 (Figure 23A). Further, cysteine point mutants were also brought in bacterial vectors for analytical labeling in *E. coli*. According to the results obtained for human cells, labeling could be monitored for each of the cysteine mutants with a slight reduction of signal intensity for the four-cysteine mutant (Figure 23B).
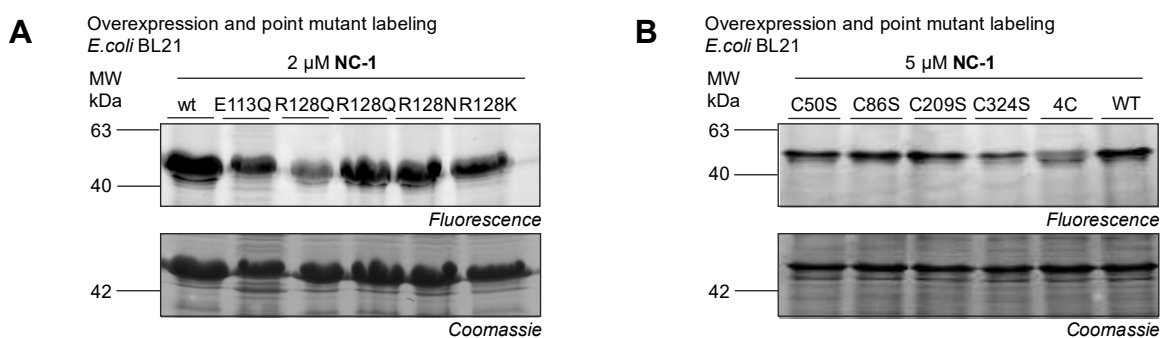
Figure 23: Analytical labeling of binding site mutations in *E. coli*. A, SDS-PAGE of *in situ* labeling of *E. coli* BL21 cells overexpressing VAT-1 wildtype (WT) and E113 and R128 point mutants for binding site identification. **B,** SDS-PAGE of *in situ* labeling of *E. coli* BL21 cells overexpressing VAT-1 wildtype (WT) and cysteine point mutants.

In contrast to human cells, labeling of the E113Q point mutant was observed in *E. coli*, suggesting a different binding mechanism in human cells. It is suggested that neocarzilin is metabolically modified in human cells for correct binding to VAT-1. The binding mode might therefore be different between human and bacterial cells. Here, a metabolomics approach could be considered for investigation of a metabolic modification of neocarzilin in human cells. Further, a selective transport of **NCA** after chemical modification to the target protein binding site is possible, which might not occur in bacteria. Moreover, the results can be explained by specific binding to VAT-1 in human cells after transfection, but an unspecific binding to the most abundant, overexpressed protein in *E. coli* due to a wrong protein folding. Consequently, the amount of the overexpressed VAT-1 should be reduced for Figure 23A to avoid unspecific binding to the most abundant protein in *E. coli* cells or to diminish incorrect protein folding.

6.

VAT-1 PROTEIN INTERACTIONS

VAT-1 protein interactions were studied by conventional and *in situ* crosslink co-IP, whereby the crosslinking co-IP revealed more confidential hits. VAT-1 was detected to be intricated in a network of proteins involved in cell adhesion such as TLN1, which mediates the connection between the ECM and the actin cytoskeleton by integrin activation. Since cell adhesion is crucial for cell migration, the VAT-1-TLN interaction was confirmed by orthogonal methods, while unspecific antibody binding was excluded by a co-IP in VAT-1 KO cells.

Contents:

6. VAT-1 PROTEIN INTERACTIONS

An anti-migratory phenotype was detected in cells upon treatment with **NCA**, particularly. Since VAT-1 was revealed as the target protein of **NCA**, the role of VAT-1 in tumor cell migration was investigated. VAT-1 was earlier linked to cell migration in glioblastomas but there were no further studies elucidating the role of VAT-1 in tumor cell migration.[69] Otherwise, VAT-1 is a largely uncharacterized enzyme which shows an ATPase activity and calcium dependency.[60, 67, 157] Furthermore, a homology to *E. coli* quinone oxidoreductases as well as eye lens zeta-crystallin has been published.[158]

Thus, for gaining deeper insights into the cellular pathways VAT-1 is involved in, the molecular interaction networks of VAT-1 were elucidated by MS based co-IP.

Protein-protein interactions display an essential subject to study for investigation of protein-mediated biological processes and cellular functions.[159] By performing conventional co-IPs, protein interactions can be monitored in cell lysates. Here, VAT-1 and bound interaction partners were isolated from the MDA-MB-231 cell lysate by a specific VAT-1 antibody. For elimination of nonspecifically bound proteins, control samples treated with an isotype antibody were included. Antibodies were immobilized on beads bearing protein A/G which binds to the Fc domain of antibodies. Captured proteins were digested on the beads and analyzed by LC-MS (Figure 25A).[159]

6.1. Comparison of conventional co-IP and crosslink co-IP

We started with a conventional co-IP without crosslinker and performed a VAT-1 pulldown using an VAT-1 antibody with a high specificity, which was first investigated in Western blots. We detected a very high and significant enrichment of VAT-1 in the volcano plot showing fold change of VAT-1 antibody treated lysates against isotype background in Figure 25B. Hits represent proteins matching the criteria of $\log_2$ enrichment > 1 on the x-axis and significance of $p < 0.01$ on the y-axis.

Interestingly, among the most reliable hits, subunits of the phosphatidylinositol 3-kinase (PI3K) complex were identified such as PI3K catalytic subunit 3 (PIK3C3) as well as regulatory subunit 4 (PIK3R4). However, the interaction of PIK3C3 and VAT-1 was so far unknown according to a network of PIK3C3 created by cytoscape[160] (data not shown). Some interaction partners of PIK3C3 such as Beclin-1 (BCN) and Beclin 1-associated autophagy-related key regulator (ATG14) were also found among VAT-1 interaction partners, which highlights the power of a co-IP to enrich whole networks of interacting

proteins. The proteins shown in green in Figure 25B form together the PI3K complex, which is involved in autophagy, membrane trafficking and endocytosis.[161] Endosomal trafficking contributes in various forms to cell migration and cell adhesion, for example by internalization of chemokines, integrin trafficking or ECM reorganization.[162] Consequently, interactions of VAT-1 with the PI3K complex might contribute to the anti-migratory phenotype triggered by **NCA** treatment.

Further, some enriched proteins cluster functionally together with cell adhesion such as Talin-1 (TLN1), Vinculin (VCL), Fibronectin (FN1), Thrombospondin1 (THBS1) and Gelsolin (GSN). While FN1 and THBS1 are glycoproteins of the ECM, TLN and VCL link the actin cytoskeleton to the ECM by binding to integrins.[27] GSN displays an actin binding protein which is relevant for actin nucleation und is associated with the GO term[163] *regulation of cell adhesion*.[164] Cell adhesion and cell migration are closely linked together, since contacts to the ECM are crucial for cell migration.

Moreover, proteins connected to the cytoskeleton such as the microtubule cross-linking factor 1 (MCTL1) which plays a role in epithelial polarization and microtubule dynamics organization important for cell migration.[165, 166] Additionally, collagen alpha-1(XIII) chain (COL13A) as a constituent of the ECM which is involved in cell-matrix and cell-cell adhesion interactions was detected. Collagens XIII are known to bind to FN1, which was also detected amongst most enriched hits.[167]

Overall, several candidates for VAT-1 interaction partners were detected which provide a link between cell migration and VAT-1. For validation of the interaction partners, Western blots or reverse co-IPs could be considered. However, the protein background of the co-IP experiment was very strong suggesting that a lot of proteins were detected as interaction partners which displays unspecific hits. In order to avoid false positive hits and for catching also transient interactions as shown previously, a DSSO (disuccinimidyl sulfoxide) crosslinker was applied for co-IP. By performing co-Ips combined with crosslinker, protein interactions can be captured in their physiological state with proteins being in native conformations and post-translationally modified.[80, 168]

In a recent study, it was already demonstrated that the crosslinking strategy provides protein interaction partners with a higher confidence compared to conventional co-IPs.[82] Therefore, the cells were incubated *in situ* with DSSO crosslinker before cell lysis and co-IP procedure (Figure 25A). Subsequent analysis of pulled down proteins *via* LC-MS/MS revealed several significantly enriched hits in MDA-MB-231 cells (Figure 25C). Again, VAT-1 was found with a high enrichment factor shown in the volcano plot in Figure 25C. The overlap between the

enriched hits of the conventional co-IP and the crosslink co-IP is shown in Figure 25D (Table 4). Several proteins were detected as enriched in both volcano plots; however, the number of hits was strongly reduced in crosslink co-IP. Interestingly, Rac2 was detected only in the crosslink co-IP which is relevant for lamellipodium organization (Figure 25C). In accordance to the conventional co-IP, several proteins involved in cell adhesion were again detected such as TLN1, VCL, FN1, THBS1 and GSN (Figure 25C+D, Table 4). In front, TLN1, which displays one of the key proteins for activating integrin signaling, linking integrins to the cytoskeleton, formation of focal adhesions and subsequently promoting migration,[169] protruded as one of the strongest hits. Directly in this context, integrin beta-1 (ITGB1) was revealed as VAT-1 interaction partner (Figure 25C). TLN1 was confirmed as enriched hit in an independent VAT-1 DSSO co-IP, however, with a lower enrichment factor compared to Figure 25C (appendix, Figure 50).

Proteins linked to cell adhesion were highlighted in both Figure 25B and C. Here, it was observed that some proteins such as TLN1 were also detected in Figure 25B, however, the enrichment was more pronounced in the crosslink co-IP. These results show that the native protein interactions are better preserved by *in situ* crosslinking compared to the conventional strategy. However, some proteins which were proposed to be candidates linking VAT-1 to cell migration pathways from the conventional co-IP strategy such as the PI3K complex were not detected among the enriched hits. Accordingly, PIK3C3-VAT-1 interaction could not be validated by Western blot (data not shown). Thus, it is suggested that these proteins only display false positive hits which nonspecifically bind to the VAT-1 antibody or the protein A/G beads. To sum up, the hits between the conventional and crosslink co-IP overlap to a certain extent, but a reduced number of proteins was detected for the crosslink co-IP, suggesting a diminished unspecific background and more confidentially enriched hits compared to conventional approaches (Figure 25D).

A cytoscape[160] BINGO[170] analysis of the enriched proteins from the crosslink co-IP was performed and GO terms for the categories cellular compartment, biological activity and molecular function which were linked to cell migration or rather cell adhesion are illustrated in Figure 25E. These terms were found overrepresented in the analyzed data set consisting of all significantly enriched proteins matching the criteria $\log_2$ enrichment > 1 and *p*-value < 0.05 in Figure 25C. The bars in the Figure 25E show the direct comparison of frequency of appearance of each term in the data set against the overall frequency of the terms in the global proteome.

For the category biological compartment, GO terms like *focal adhesions*, *adherens junction*, *actin cytoskeleton*, *collagen containing ECM* and *lamellipodium* were found overrepresented in the investigated data set. In case of molecular function, *cell adhesion*

molecule binding, *actin binding*, *collagen binding* or *fibronectin binding* were detected as GO terms with overrepresentation. For the category biological process, *regulation of cell adhesion*, *regulation of actin cytoskeleton organization*, *regulation of ECM organization*, *cell matrix adhesion* or *integrin activation* were found among the overrepresented GO terms.
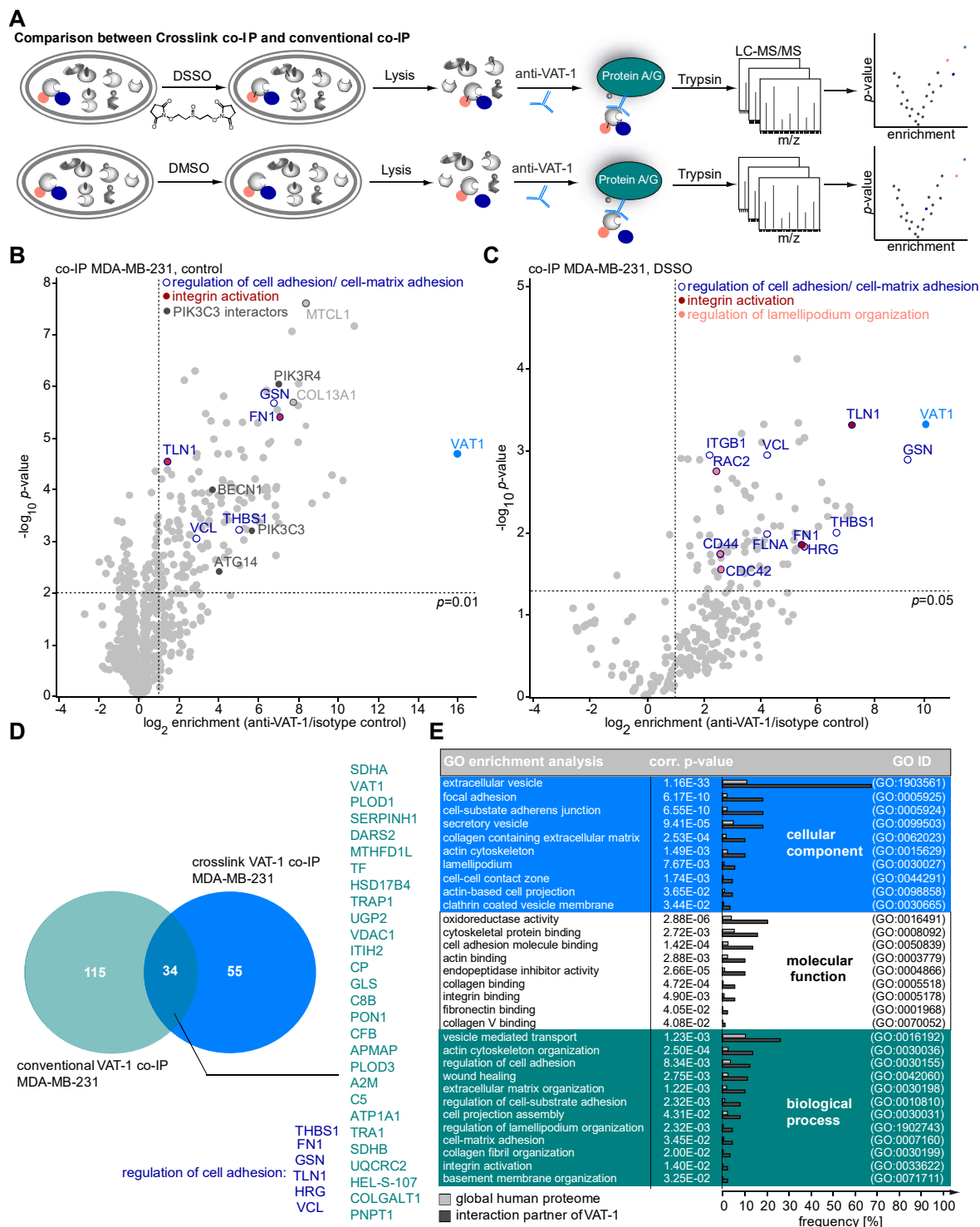
Figure 25: Cellular interaction partner of VAT-1 in context of cell migration. A, Schematic representation of the comparison between a crosslink co-IP with DSSO crosslinker and a conventional co-IP. **B.** Volcano plot of co-IP of VAT-1 in MDA-MB-231 (n=5). **C,** Volcano plot of co-IP of VAT-1 with 2 mM DSSO in MDA-MB-231 (n=3). **D,** Venn diagram showing the overlap between the enriched proteins of both co-IPs. The common proteins are indicated in green and common proteins involved in cell adhesion are highlighted in blue. **E,** GO enrichment analysis of hits (log$_2$ enrichment > 1, *p*-value < 0.05) was performed with Cytoscape[160] BINGO[170] app whereas frequencies of enriched GO terms are compared between the co-IP and the global proteome. [134]

Table 4: Proteins significantly enriched in the crosslink co-IP which are involved in cell adhesion are shown in the same color code as in Figure 25C and proteins enriched in both conventional and crosslink co- IP are shown in green according to Figure 25D.

gene names	protein names	$\log_2$ fold change	$-\log_{10}$ p-value	coverage [%]
VAT1	Synaptic vesicle membrane protein VAT-1 homolog	10.03	3.33	70.5
GSN	Gelsolin	9.17	2.89	37.2
TLN1	TLN1	7.19	3.32	44.6
THBS1	Thrombospondin-1	6.67	2.01	15.9
HRG	Histidine-rich glycoprotein	5.52	1.83	1.9
FN1	Fibronectin	5.44	1.86	6.4
VCL	Vinculin	4.22	2.95	17.8
FLNA	Filamin-A	4.21	1.99	39.6
CDC42	Cell division control protein 42 homolog	2.60	1.56	52.4
CD44	CD44 antigen	2.57	1.74	29.1
RAC2	Ras-related C3 botulinum toxin substrate 2	2.44	2.75	31.2
ITGB1	Integrin beta-1	2.20	2.95	8.3
C5	Complement C5	7.13	2.24	5.4
A2M	Alpha-2-macroglobulin	7.11	2.31	6
DARS2	Aspartate–tRNA ligase, mitochondrial	7.10	2.32	44.7
ITIH2	Inter-alpha-trypsin inhibitor heavy chain H2	6.62	2.33	9.4
PON1	Serum paraoxonase/arylesterase 1	6.34	2.20	8.5
UGP2	UTP–glucose-1-phosphate uridylyltransferase	6.33	2.39	46.7
HSD17B4	Peroxisomal multifunctional enzyme type 2	6.02	2.08	53.4
TRAP1	Heat shock protein 75 kDa, mitochondrial	5.52	3.16	27.5
SDHA	Succinate dehydrogenase flavoprotein subunit, mit.	5.33	3.11	47.9
CP	Ceruloplasmin	5.20	2.00	14.1
TRA1	Endoplasmin	5.16	1.92	67
SERPINH1	Serpin H1	4.78	1.62	40.2
PNPT1	Polyribonucleotide nucleotidyltransferase 1, mit.	4.69	2.09	32.6
MTHFD1L	Monofunctional C1-tetrahydrofolate synthase, mitochondrial	4.63	2.44	23.7
C8B	Complement component C8 beta chain	4.44	2.09	14.4
UQCRC2	Cytochrome b-c1 complex subunit 2, mitochondrial	4.17	1.55	44.2
CFB	Complement factor B	3.96	1.59	4.8
COLGALT1	Procollagen galactosyltransferase 1	3.88	2.03	17.7
GLS	Glutaminase kidney isoform, mit.	3.78	1.91	39.5
PLOD3	Procollagen-lysine,2-oxoglutarate 5-dioxygenase 3	3.65	1.57	33.9
SDHB	Succinate dehydrogenase iron-sulfur subunit, mit.	3.45	1.77	20
TF	Serotransferrin	3.26	1.33	7.5
APMAP	Adipocyte plasma membrane-associated protein	2.82	1.77	21.8
ATP1A1	Sodium/potassium-transporting ATPase subunit alpha-1	2.60	1.84	34.6
PLOD1	Procollagen-lysine,2-oxoglutarate 5-dioxygenase 1	2.38	1.53	18.2
VDAC1	Voltage-dependent anion-selective channel protein 1	2.12	1.32	67.5
HEL-S-107	Endoplasmic reticulum resident protein 29	1.49	1.84	14.6

Taken together, proteome analysis to unravel the role of VAT-1 in cellular migration revealed that VAT-1 interacts with a network of proteins associated with the ECM or cytoskeleton organization. Functional analysis of proteins enriched in the crosslink co-IP hits provided a link to cell adhesion which is closely linked to cell migration. In front, TLN1 displays an important mediator in cell adhesion since it activates the integrins and thereby connects the actin cytoskeleton to the ECM. Overall, it was shown that the crosslink co-IP provided more confidential interaction partners of VAT-1 as the conventional VAT-1 co-IP, which was already observed in previous studies.[80, 82] Artificial interactions in the cell lysate might be the reason for the detection of false positive hits such as the PI3K complex in the conventional approach.

6.2. Effect of **NCA** on VAT-1 protein interactions

Since small molecules like **NCA** are interesting candidates to interfere with protein-protein interactions, the effect of **NCA** on VAT-1 protein interaction was further studied by co-IP upon previous treatment with **NCA**. Natural compounds can interfere with binding of specific interaction partners, resulting in a loss of protein interactions (Figure 26A)

For proteomics experiments, LFQ intensities illustrated in profile plots over each sample were exploited for showing the effects of **NCA** on VAT-1 interactions (Figure 26B). However, it was revealed with intensity plots that protein interactions between VAT-1 and TLN1, VCL and ITGB1 were not affected by **NCA** treatment. The intensities were in the same range for **NCA** or DMSO treatment before *in situ* crosslinking. A clear drop of the intensities for the isotype controls compared to specific antibody treated samples was registered, demonstrating the strong pulldown of named proteins.

The effect of **NCA** on the interaction of VAT-1 and TLN1 was further probed by Western-blot-based co-IP. First, the interaction with TLN1 shown in Figure 25 could be independently verified by Western blot-based co-IP, in which VAT-1 was pulled down from whole cell lysates (Figure 26C). Of note, it was also revealed that treatment of the cells with **NCA** seemed to even further enhance the interaction of VAT-1 with TLN1 (Figure 26C). Moreover, immunostaining revealed co-localization of both proteins in lamellipodia at the leading edge of migrating cells (Figure 26D). In contrast, the proteins were not detected at the leading edge of the cells after **NCA** treatment. These results are contradicting the Western blot data showing the enhancement of the VAT-1-TLN1 interaction. The amount of pulled-down TLN1 is also dependent on the overall expression levels of the protein. Therefore, the TLN1 protein levels after **NCA** treatment were investigated after 4 and 24 h. However, the overall levels of TLN1 did not change after **NCA** treatment thereby supporting the Western blot data of Figure 26 C to show a stronger protein interaction (Figure 26E). Nevertheless, the profile plots obtained for **NCA** coupled co-IP (Figure 26B) disagree with the Western blot- based co-IP (Figure 26C). The proteomics data did not confirm the increased protein interaction between VAT-1 and TLN1, leading to ambiguous, unclear results, which need to be further clarified.
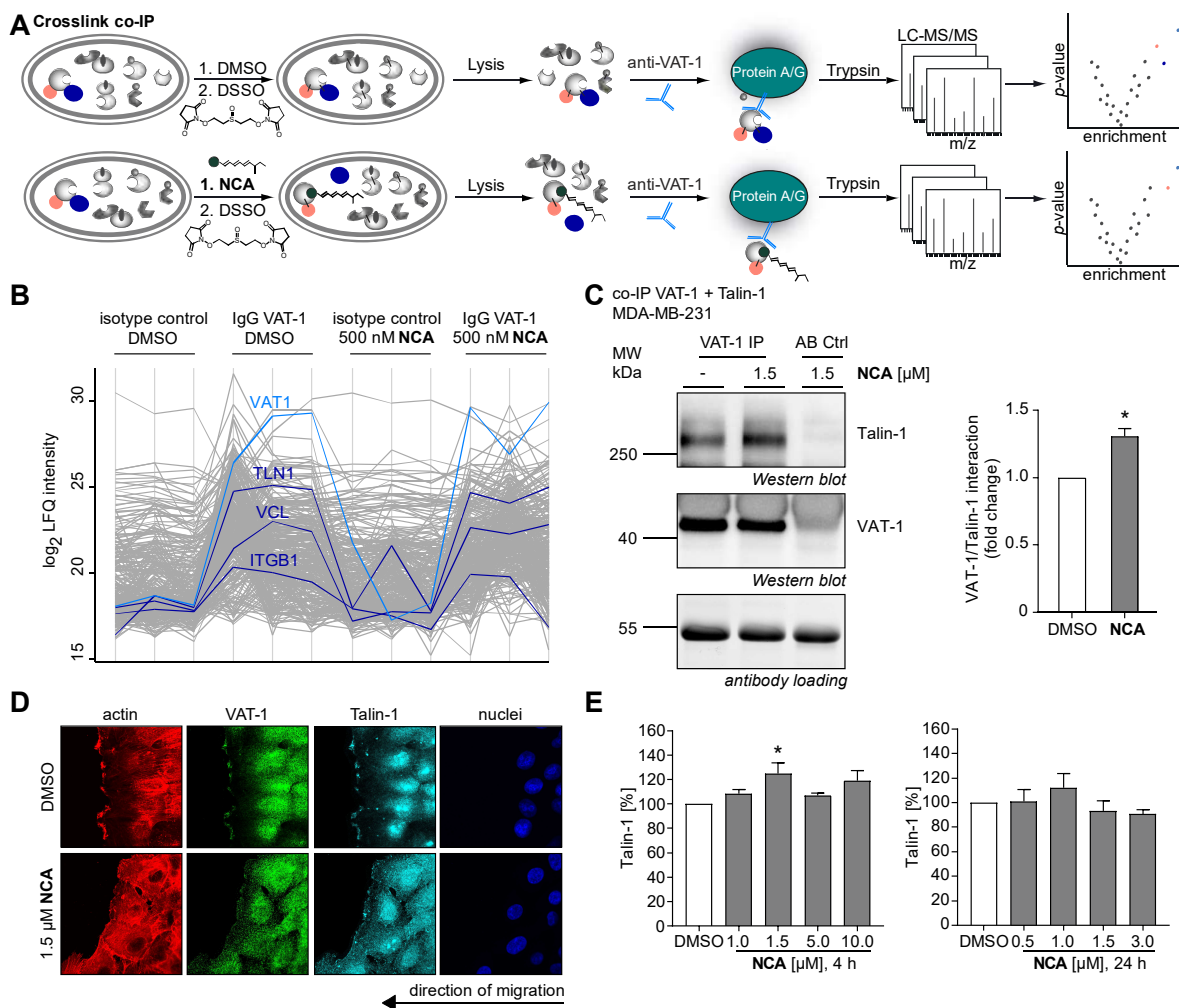
Figure 26: Effect of NCA on VAT-1 interaction partner in context to cell adhesion. **A,** Schematic overview of effect of natural product treatment on protein-protein interactions. **B,** Profile plot of $\log_2$ intensities of VAT-1, TLN1, VCN and ITGB1. **C,** Co-IP of VAT-1 and TLN1. VAT-1 was precipitated from MDA-MB-231 cell lysates after 24 h stimulation with **NCA**. Amount of TLN1 determined by Western blot was normalized to VAT-1 and results were normalized to the control. Bars represent the mean ± SEM of two independent experiments, two-tailed unpaired Student's t test, *P < 0.033. **D,** T24 cells treated with **NCA** were engaged in a Scratch assay and co-stained for VAT-1 (green), TLN1 (cyan) and actin (red). Nuclei were stained with Hoechst 33342. **C-D,** A representative experiment out of 3 independent experiments is shown. **E,** Effect of **NCA** on the cellular level of TLN1. MDA-MB-231 cells were treated with the indicated concentrations of **NCA** or DMSO for 4 h or 24 h, respectively. Cellular protein levels were detected by Western blot analysis and results normalized to DMSO treated cells. Bars represent the mean ± SEM of three independent experiments, one-way ANOVA, Dunnett's test, *P < 0.033 compared with DMSO control. **C-D,** Experiments were performed by Dr. Carolin Pyka (LMU). Adapted from Gleissner *et al.* [134]

Further, the effect of **NCA** on protein interactions was visualized by volcano plots showing the enrichment of VAT-1 pull-down after **NCA** treatment against DMSO background. For conventional co-Ips, the loss of several protein interactions highlighted in blue was shown after **NCA** treatment (Figure 27A). However, these proteins were not relevant for cell migration. In case of crosslink co-IP, only one protein was shown as a lost interaction partner, namely the mitochondrial dicarboxylate carrier (SLC25A10), which is not relevant for cell adhesion (Figure 27B). Consequently, the proteomics results point to no effects of **NCA** on VAT-1 protein interactions, which is directly in contrast with the Western-blot results. Consequently, further studies are required to shed light into the dark.
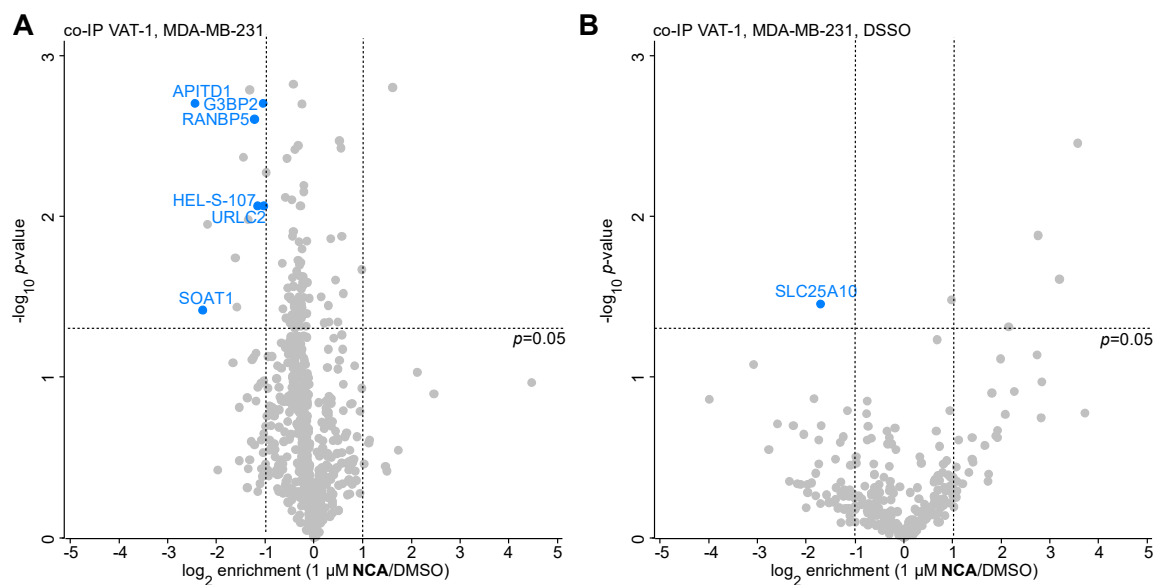
Figure 27: Effect of NCA on VAT-1 interactions. **A,** Volcano plot of VAT-1 pull-down in MDA-MB-231 treated with 1 µM **NCA** for 24 h or respectively DMSO (n=5). **B,** Volcano plot of VAT-1 pull-down with DSSO crosslinker in MDA-MB-231 treated with 1 µM **NCA** for 24 h or respectively DMSO (n=3).

6.3. Validation of interaction partners by reverse co-IP

The PI3K complex was detected in the conventional co-IP as highly enriched interaction partner of VAT-1 and this interaction might be promising to link VAT-1 to cell migration. The interaction was not confirmed by crosslink co-IP. Thus, the interaction was attempted to validate by a reverse co-IP with a PIK3C3 antibody. In this case, no crosslinker was applied, since the interaction between VAT-1 and PIK3C3 was also shown without crosslinker.

In the co-IP volcano plot, PIK3C3 and PIK3R4 were among the most prominent hits, confirming that the co-IP procedure was successful (Figure 28). Further, several known interaction partner of PIK3C3 forming the PI3K complex were found amongst the most enriched proteins and are shown in dark blue such as BCN1, UVRAG and ATG14, which are all involved in autophagy and membrane trafficking. The detection of already known interaction partners supports the confidence of the co-IP data.[161] Some proteins involved in cell migration were also among enriched proteins shown in green. However, VAT-1 was not detected as an interaction partner of PIK3C3. This result points to a non-specific interaction between PIK3C3 and VAT-1 in the VAT-1 conventional co-IP, which is further supported by the crosslink co-IP of VAT-1 with PIK3C3 being not detected. Consequently, PIK3C3 represents a false positive or artificial hit, which could be avoided by a pull-down with *in situ* application of DSSO crosslinker, which preserves the protein interactions in their native state and reduces the unspecific background.
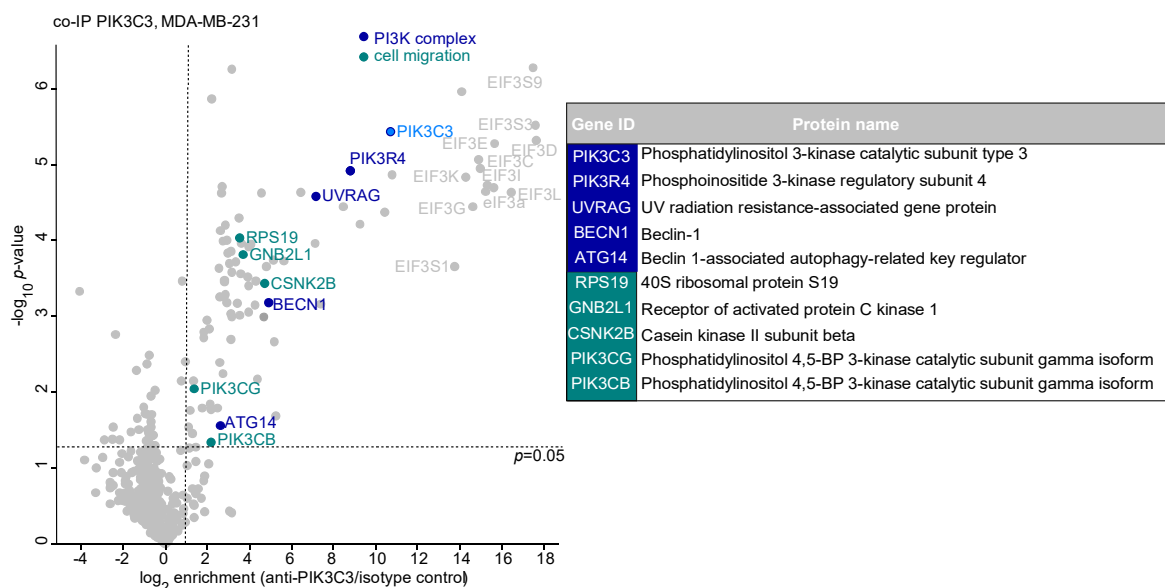
Figure 28: Validation of PIK3C3 as target protein from conventional co-IP. PIK3C3 interactions were investigated by reverse co-IP (n=4). Volcano plot of reverse co-IP of PIK3C3 is shown with known interaction partners shown in blue and proteins involved in cell migration shown in green.

Moreover, the interactions detected in the DSSO co-IP of VAT-1 were also verified by reverse co-IP by application of a crosslinker. The most interesting interaction partners in context of cell migration were TLN1 and therefore also VCL and ITGB1 which are directly linked to TLN1, FN1 as component of the ECM and Rac1 as regulator of lamellipodia formation. Consequently, co-Ips with *in situ* application of DSSO in MDA-MB-231 were performed with TLN1 antibodies, a FN1 antibody and a Rac-1 antibody.

The interaction between TLN1 and VAT-1 has already been confirmed by co-localization of the proteins at the leading edge of the cell and a Western blot-based co-IP. TLN1 displays therefore a promising candidate for a highly confidential VAT-1 interaction partner.

For TLN1 co-IP, two different antibodies were tested to avoid a disruption of the interaction between the proteins, since the antibody can exactly bind to the region which is important for protein interaction. The TLN1 co-IP was successful for both antibodies and TLN1 was detected as one of the most prominent hits with a high enrichment factor (Figure 29A). In both co-Ips, Vinculin was validated as an interaction partner of TLN1, however, with a small enrichment factor and significance (Figure 29A+B). Further, the SEPT proteins, which display filament-forming GTPases required for organization of the actin and microtubule cytoskeleton[171], were found as hits in the co-IP which could not be confirmed as interaction partners by STRING database. However, VAT-1 could not be validated as interaction partner of TLN1 by reverse co-IP experiments with two different TLN1 antibodies. In contrast to VAT-1 MS-based co-IP, which was validated by Western blot-based co-IP and confocal microscopy, the reverse co-IP did not reveal the interaction between the two proteins. The disruption of the interaction interface can be excluded due to the application of two different antibodies. The question is now, if TLN1 did only appear as VAT-1

interaction partner due to unspecific binding to the antibody or if it is a confident interaction partner, which would provide a link between VAT-1 and migration. Thus, further interaction studies are required.

Moreover, reverse co-IP was performed against FN1 as a component of the ECM. The co-IP was successful, however, no interaction between FN1 and VAT-1 or FN1 and TLN1 could be observed in the volcano plot shown in Figure 29C. Similar results were obtained for Rac1, for which the interaction with VAT-1 couldn't be confirmed (Figure 29D). However, the antibody for Rac1 was not specific enough for a confidential co-IP output, since a high number of proteins achieved higher enrichment factors than Rac1. Consequently, these proteins are no interaction partners of Rac1, but of other, non-specifically bound proteins.
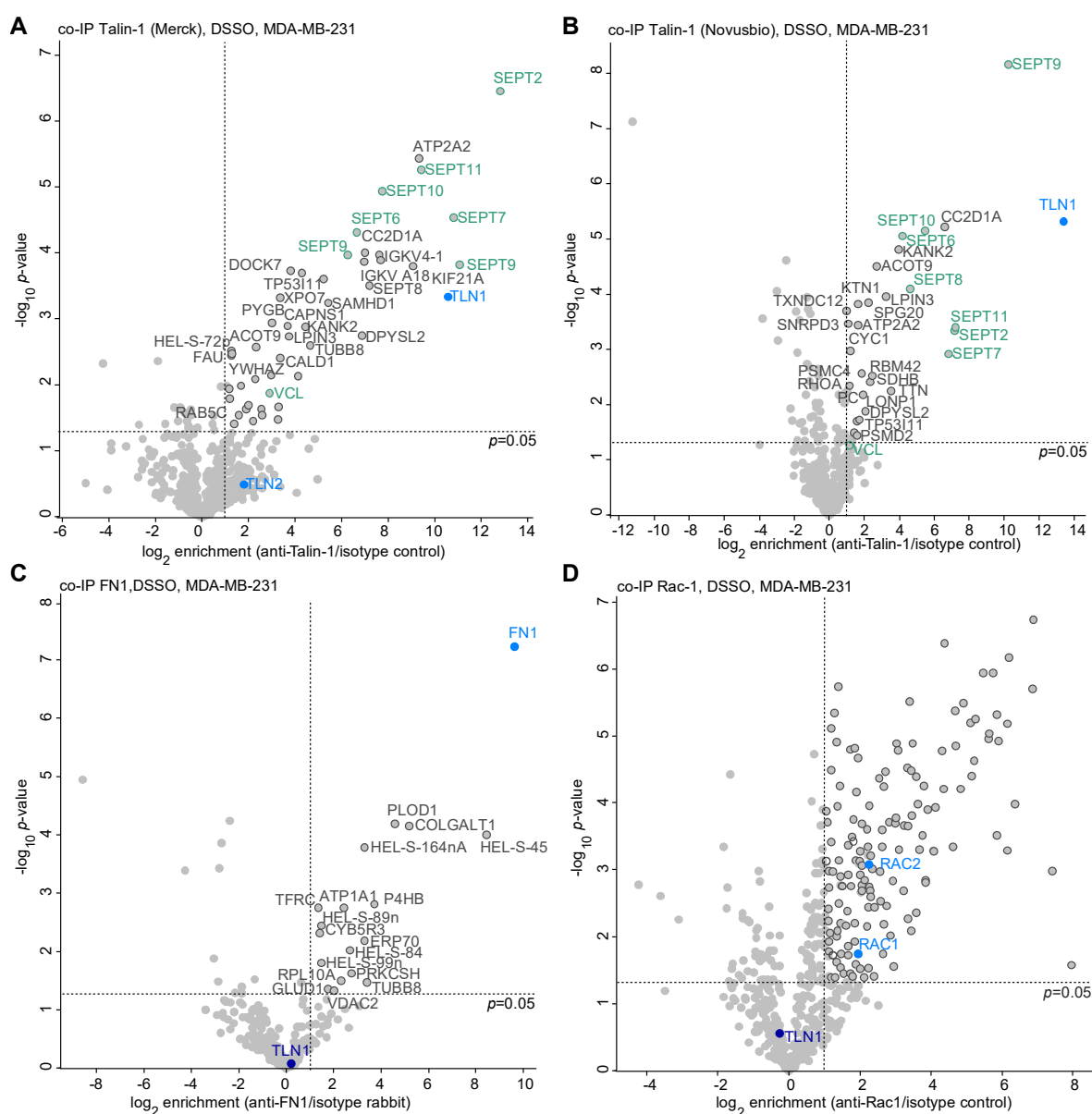
Figure 29: Validation of target proteins from crosslink co-IP by reverse co-IP. A, Volcano plot of reverse co-IP of TLN1 with Merck antibody (n=4). **B,** Volcano plot of reverse co-IP of TLN1 with Novusbio antibody (n=3). **C,** Volcano plot of reverse co-IP of FN1 (n=4). **D,** Volcano plot of reverse co-IP of Rac1 (n=4). **A-D,** Hits matching the criteria log$_2$ enrichment > 1 and p-value < 0.05 are highlighted and indicated in dark grey or green.

In conclusion, the reverse co-IP experiments didn't confirm the interactions revealed in VAT-1 DSSO co-IP, which might either be caused by disruption of the interactions by the antibodies in some cases or a nonspecific detection of the interaction in the VAT-1 co-IP. For TLN1, the reverse-coIP results together with the Western-blot, confocal microscopy and VAT-1 proteomics data are in conflict regarding the TLN1-VAT-1 interaction in cell migration. Therefore, an approach for the detection of unspecific binding of TLN1 to the VAT-1 antibody was figured out und is described in the next section.

6.4. co-IP in VAT-1 knockout cells for detection of unspecific interactions

In order to guarantee that the interactions obtained in the crosslink VAT-1 co-IP illustrated in Figure 25C are of specific nature and are not caused by unspecific binding of TLN to the VAT-1 antibody, a crosslink co-IP was conducted in HEK VAT-1 knockout (KO) cells. This HEK KO cell line was generated for detecting the role of VAT-1 in cell migration and was established by CRISPR/Cas (see next chapter). In the absence of VAT-1 in HEK cells, the antibody only hits proteins which are unspecific binders and do not interact with VAT-1. The proteomics results for the VAT-1 co-IP with *in situ* DSSO crosslinking are shown in Figure 30A. VAT-1 was not among enriched hits, which verified its knockout in this cell line. However, several proteins were detected as highly significant, enriched hits, which might bind unspecifically to the VAT-1 antibody. The appearance of these proteins in the VAT-1 crosslink co-IP in breast cancer cells needs to be clarified for elimination of the proteins as possible VAT-1 interaction partners.

For comparison of the co-IP in VAT-1 KO cells with the co-IP in MDA-MB-231 (Figure 25C), both volcano plots are depicted next to each other in Figure 30 for means of direct visualization. Notably, the majority of the proteins hit by the VAT-1 antibody which are shown in green were also detected in the VAT-1 co-IP in Figure 25C (Figure 30B+C). However, these proteins can't be interaction partners of VAT-1, since VAT-1 is not present in the KO cells and did not appear among enriched hits. Also, proteins such as FN1, GSN, FLNA were detected as enriched in Figure 30A and can definitely be excluded as VAT-1 interaction partners (Figure 30C). However, TLN1, VCL, ITGB1 and THBS1 as well as CDC42 highlighted in dark blue pertained as VAT-1 interaction partners and can be considered as real hits (Figure 30B+D). These results for TLN1 again disagree with the reverse co-IP data. However, we have obtained a lot of different data from orthogonal experiments as already mentioned which support the VAT-1-TLN1 interaction. There might be another challenge for the detection of the interaction by reverse-co-IP, which is unclear till now. Since most of the data point towards an interaction between VAT-1 and TLN1, the interaction will be further investigated in detail.

Additionally, the enriched proteins which were revealed as confidential interaction partners in the crosslink co-IP (Table 5) were subjected to a STRING database analysis (minimum required interaction score: 0.7) for investigation of the functional networks the proteins are involved in (Figure 30E). Notably, the proteins are linked to each other and form three large clusters and four smaller clusters with some proteins which did not match to any cluster. The biggest network displayed the one with a link to metabolism and the cluster related with cell adhesion or actin filament binding. The cluster connected to cell adhesion, which also

contained TLN1, VCL and ITGB1 and some ECM constituents and Rab GTPases, attracts attention since it provides a link between VAT-1 and cell adhesion or rather cell migration. The two large clusters are also connected with each other, underlining the complexity of the network, in which VAT-1 is intricated.
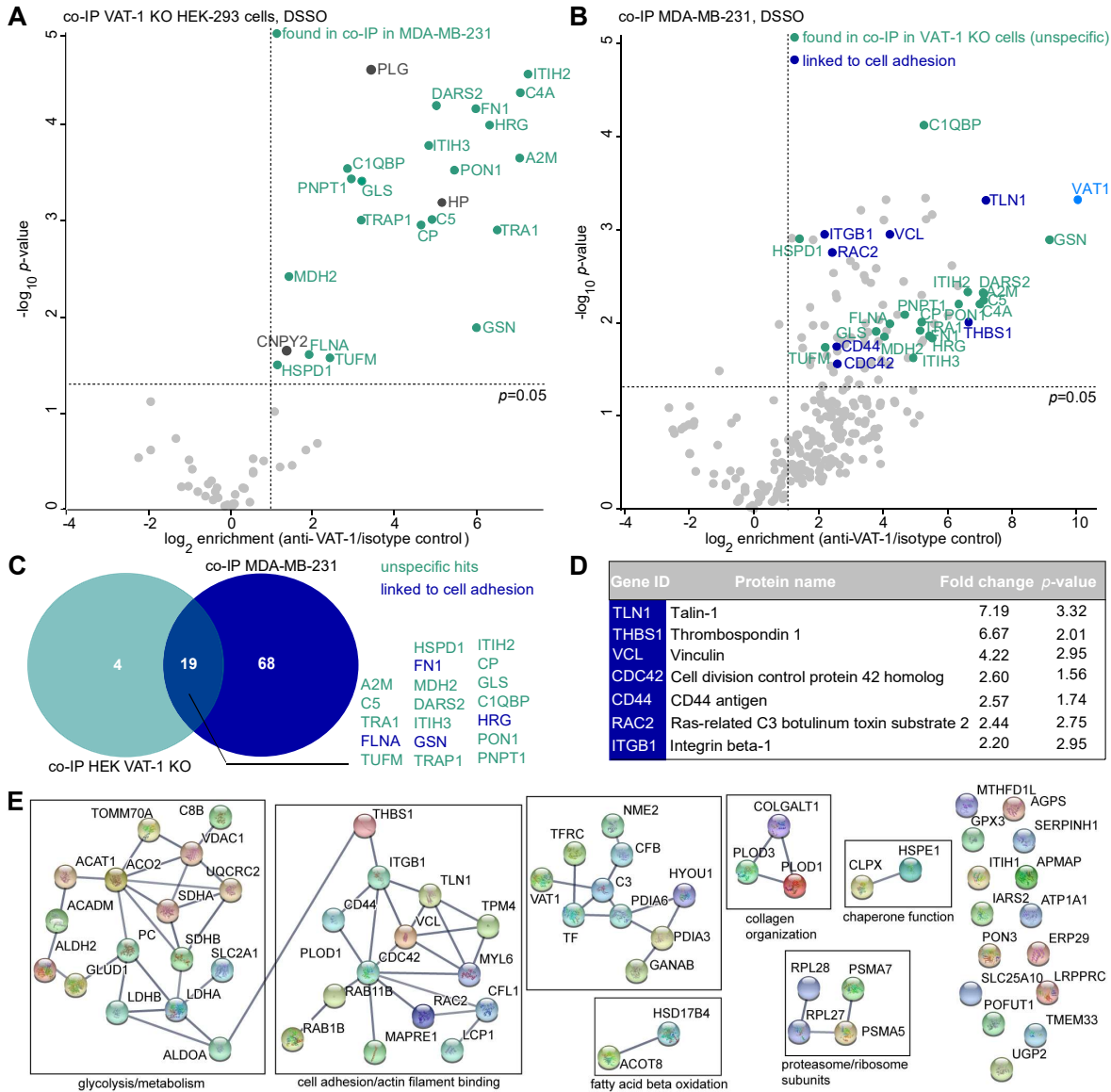
Figure 30: Specific interaction partner of VAT-1. A, VAT-1 co-IP in VAT-1 KO HEK-293 cells with DSSO crosslinker (n=3). Proteins also found in co-IP in MDA-MB-231 are highlighted in green and display unspecific proteins bound to the VAT-1 antibody. Volcano plot represents results of two-sample *t*-test showing the enrichment of proteins with corresponding significance (*p*-values) **B,** Volcano plot of co-IP of VAT-1 with DSSO in MDA-MB-231 (n=3). Unspecific proteins are bound to the antibody are highlighted in green und are excluded for further validation. **C,** Venn diagram showing the overlap between both co-IP experiments. **D,** Most confidential VAT-1 interaction partners involved in cell adhesion. **E,** STRING 11.0 database analysis for multiple proteins of specific VAT-1 interaction partners matching the criteria log₂ difference > 1.5 and *p*-value > 0.05 excluding proteins highlighted in green from **B**. A minimum required interaction score of 0.7 and confidence network edges were applied for analysis.

Table 5: Most confident interaction partners of VAT-1 from co-IP in VAT-1 KO cells. Proteins which only appeared in Figure 30B as significantly enriched but not in Figure 30A are listed. (blue = protein, which was pulled-down, dark blue = proteins involved in cell adhesion, grey = remaining hits matching the criteria log$_2$ enrichment > 1, *p*-value < 0.05).

gene names	protein names	log$_2$ fold change	-log$_{10}$ *p*-value	coverage [%])
VAT1	Synaptic vesicle membrane protein VAT-1 homolog	10.03	3.33	70.5
TLN1	TLN1	7.19	3.32	44.6
THBS1	Thrombospondin-1	6.67	2.01	15.9
VCL	Vinculin	4.22	2.95	17.8
CDC42	Cell division control protein 42 homolog	2.60	1.56	52.4
CD44	CD44 antigen	2.57	1.74	29.1
RAC2	Ras-related C3 botulinum toxin substrate 2	2.44	2.75	31.2
ITGB1	Integrin beta-1	2.20	2.95	8.3
C4A	Complement C4-A	7.01	2.20	7.5
UGP2	UTP-glucose-1-phosphate uridylyltransferase	6.33	2.39	46.7
LDHA	L-lactate dehydrogenase	6.13	2.62	74.7
HSD17B4	Peroxisomal multifunctional enzyme type 2	6.02	2.08	53.4
C3	Complement C3	5.60	1.99	4.6
SDHA	Succinate dehydrogenase flavoprotein subunit, mit.	5.33	3.11	47.9
LDHB	L-lactate dehydrogenase	5.32	3.34	46.4
ITIH1	Inter-alpha-trypsin inhibitor heavy chain H1	5.25	1.81	3.6
GPX3	Glutathione peroxidase	5.20	1.78	10.7
CFL1	Cofilin-1	5.20	2.29	61.4
TRA1	Endoplasmin	5.16	1.92	67
SERPINH1	Serpin H1	4.78	1.62	40.2
MTHFD1L	Monofunctional C1-tetrahydrofolate synthase, mit.	4.63	2.44	23.7
C8B	Complement component C8 beta chain	4.44	2.09	14.4
UQCRC2	Cytochrome b-c1 complex subunit 2, mitochondrial	4.17	1.55	44.2
PC	Pyruvate carboxylase	4.12	1.91	40.7
NME2	Nucleoside diphosphate kinase	4.10	3.33	55.1
AGPS	Alkyldihydroxyacetonephosphate synthase, peroxisomal	4.03	3.10	34.5
MYL6	Myosin light polypeptide 6	4.01	2.19	65.1
CFB	Complement factor B	3.96	1.59	4.8
COLGALT1	Procollagen galactosyltransferase 1	3.88	2.03	17.7
LRPPRC	Leucine-rich PPR motif-containing protein, mitochondrial	3.87	1.39	49
ALDOA	Fructose-bisphosphate aldolase	3.87	1.80	54.4
RAB1B	Ras-related protein Rab-1B	3.78	2.58	66.2
PLOD3	Procollagen-lysine,2-oxoglutarate 5-dioxygenase 3	3.65	1.57	33.9
TMEM33	Transmembrane protein 33	3.63	2.42	26.3
LCP1	Plastin-2	3.54	1.90	15.6
TPM4	Tropomyosin alpha-4 chain	3.46	2.46	52.4
PON3	Serum paraoxonase/lactonase 3	3.46	1.99	11
SDHB	Succinate dehydrogenase iron-sulfur subunit, mit.	3.45	1.77	20
POFUT1	GDP-fucose protein O-fucosyltransferase 1	3.45	1.51	11.9
ACOT8	Acyl-coenzyme A thioesterase 8	3.42	1.84	25.7
ACO2	Aconitate hydratase, mitochondrial	3.41	2.51	18.8
ALDH2	Aldehyde dehydrogenase, mitochondrial	3.32	1.56	29.8
ACADM	Medium-chain specific acyl-CoA dehydrogenase, mitochondrial	3.31	3.21	30.9
TF	Serotransferrin	3.26	1.33	7.5
PSMA5	Proteasome subunit alpha type	3.15	2.61	17
TOMM70A	Mitochondrial import receptor subunit TOM70	3.02	1.84	20.7
SLC25A10	Mitochondrial dicarboxylate carrier	2.99	2.67	16.7
RPL28	60S ribosomal protein L28	2.87	1.31	32.9
APMAP	Adipocyte plasma membrane-associated protein	2.82	1.77	21.8
PSMA7	Proteasome subunit alpha type	2.78	1.80	28.2
ATP1A1	Sodium/potassium-transporting ATPase subunit alpha-1	2.60	1.84	34.6
RPL27	60S ribosomal protein L27	2.59	1.69	22.2
ACAT1	Acetyl-CoA acetyltransferase, mitochondrial	2.56	2.26	25.1
SLC2A1	Solute carrier family 2, facilitated glucose transporter member 1	2.53	2.30	8.4
PTPN1	Tyrosine-protein phosphatase non-receptor type	2.49	1.47	16.8
CLPX	ATP-dependent Clp protease ATP-binding subunit clpX-like, mit	2.48	2.53	22.7
PLOD1	Procollagen-lysine,2-oxoglutarate 5-dioxygenase 1	2.38	1.53	18.2
GLUD1	Glutamate dehydrogenase	2.26	1.64	52.3
ITGB1	Integrin beta-1	2.20	2.95	8.3

IARS2	Isoleucine–tRNA ligase, mitochondrial	2.19	1.97	13.6
RAB11B	Ras-related protein Rab-11B	2.16	1.31	50
VDAC1	Voltage-dependent anion-selective channel protein 1	2.12	1.32	67.5
HYOU1	Hypoxia up-regulated protein 1	1.84	2.89	20.4
GANAB	Neutral alpha-glucosidase AB	1.83	1.97	32.8
MAPRE1	Microtubule-associated protein RP/EB family member 1	1.77	1.61	31.5
TFRC	Transferrin receptor protein 1	1.75	2.16	33.2
HSPE1	10 kDa heat shock protein, mitochondrial	1.74	1.54	55.9
PDIA6	Protein disulfide-isomerase A6	1.52	1.73	35.5
HEL-S-107	Endoplasmic reticulum resident protein 29	1.49	1.84	14.6
PDIA3	Protein disulfide-isomerase	1.19	2.90	51.2

Further, a cytoscape[160] BINGO app[170] analysis was carried out for investigation of overrepresentation of specific GO terms in the data set compared to the global proteome. Therefore, GO enrichment analysis was performed with a hypergeometric test with a Benjamini&Hochberg false discovery rate (FDR) correction and a significance level of 0.05. Output for namespaces biological process, molecular function and cellular compartment in terms of cell migration and cell adhesion are listed in Table 6. Several GO terms involved in cell adhesion and migration such as *actin cytoskeleton organization*, *integrin mediated signaling pathway*, *regulation of lamellipodia organization*, *collagen binding* and cell contacts such as *adherens junction* and *focal adhesion* were overrepresented in the analyzed dataset, meaning that the frequency of appearing GO terms in the dataset was higher than for the global proteome. Further, GO terms involved in metabolic pathways were overrepresented such as *fatty acid metabolism* and *succinate dehydrogenase activity*, which is in accordance to the detected cluster linked to metabolism by STRING database analysis (Figure 30E).

Table 6: Functional enrichment analysis performed by Cytoscape BINGO app for most confident VAT-1 interaction partners listed in Table 5. GO terms involved in cell adhesion and cell migration are listed for analysed categories with corresponding corrected *p*-values and frequencies.

GO-ID	description	corr. *p*-value	frequency global proteome [%]	frequency co-IP dataset [%]
biological proccess				
GO:0030036	actin cytoskeleton organization	1.19E-03	2.7	14.7
GO:0007015	actin filament organization	2.00E-03	1.3	10.3
GO:0007229	integrin-mediated signaling pathway	1.00E-02	0.5	5.9
GO:1902743	regulation of lamellipodium organization	1.50E-02	0.3	4.4
GO:0007265	Ras protein signal transduction	3.35E-02	1.3	7.4
GO:0010592	positive regulation of lamellipodium assembly	3.59E-02	0.1	2.9
molecular function				
GO:0050839	cell adhesion molecule binding	8.50E-04	2.7	14.7
GO:0005296	cadherin binding	1.21E-03	1.8	11.8
GO:0005518	collagen binding	2.31E-03	0.4	5.9
GO:0005178	integrin binding	1.74E-02	0.7	5.9
GO:0051015	actin filament binding	2.96E-02	1.0	5.9
cellular compartment				
GO:0005925	focal adhesion	3.71E-09	2.1	20.6
GO:0005924	cell-substrate adherens junction	3.73E-09	2.1	20.6
GO:0030055	cell-substrate junction	3.90E-09	2.1	20.6
GO:0005912	adherens junction	8.42E-08	2.8	20.6
GO:0030054	cell junction	9.93E-07	6.7	27.9
GO:0031252	cell leading edge	2.66E-03	2.1	10.3
GO:0030027	lamellipodium	2.93E-03	1.0	7.4
GO:0015629	actin cytoskeleton	5.44E-03	2.4	10.3
GO:0031253	cell projection membrane	5.55E-03	1.8	8.8
GO:0031258	lamellipodium membrane	1.14E-02	0.1	2.9
GO:0098858	actin-based cell projection	2.02E-02	1.1	5.9
GO:0034665	integrin alpha1-beta1 complex	2.22E-02	0.0	1.5
GO:0062023	collagen-containing extracellular matrix	2.39E-02	1.8	7.4

Taken together, unspecific binding of TLN1 and its direct interaction partners such as VCL and ITGB1 to the VAT-1 antibody was excluded by performing a co-IP in VAT-1 KO cells. This strategy turned out to be highly valuable for the detection of false-positive interactions, since nearly one quarter of the detected interaction partners could be excluded for further analysis due to unspecificity. Interestingly, protein clusters within the VAT-1 network were detected by functional analysis providing links to cell adhesion, metabolism and collagen organization. The cluster connected to cell adhesion attracts attention since it provides a link between VAT-1 and cell adhesion or rather cell migration. Interestingly, TLN1 was a member of the cell adhesion cluster together with several other proteins. Therefore, the interaction between VAT-1 and TLN1 should be further studied. On top, the effects of **NCA** on the formation of lamellipodia and activation of integrins are an attractive subject to study, since some identified interaction partners of VAT-1 established a connection to the corresponding GO terms *integrin activation* and *regulation of lamellipodium organization*. So far, **NCA** was only deciphered to bind VAT-1 and inhibit cell migration, however, details for the mode of action leading to a reduced anti-migratory phenotype are still missing. Consequently, based on these results and with the VAT-1 KO cells in hands, the role of VAT-1 and **NCA** in cell adhesion and cell migration was further investigated in parallel in the next chapter.

6.5. Detection of interaction partners by application of crosslinkers for target-ID

For an independent investigation of VAT-1 interaction partners, a different strategy based on ABPP was tested. Since **NC-1** selectively pulled-down VAT-1 comparable to an antibody, the ABPP workflow was combined with the DSSO crosslinker for catching the protein-protein interactions. Cells were incubated *in situ* with probe **NC-1** and afterwards with DSSO crosslinker whereas controls were included without crosslinker for correct interpretation of the data. After click chemistry to biotin-azide, VAT-1 was pulled-down comparable to target-ID procedures on avidin beads (Figure 31A).

Volcano plots with and without crosslinker were compared for the detection of interaction partner. Control volcano plot showing the enrichment of **NC-1** versus DMSO without crosslinker is shown in the appendix in Figure 51 (Table 30). Proteins which were only detected with the crosslinker illustrated in the volcano plot in Figure 31B are highlighted in green and are possible interaction partners of VAT-1 which were only pulled-down after *in situ* crosslinking (Table 7). Additionally, a different presentation of the data is shown in the volcano plot in Figure 31C illustrating the enrichment between **NC-1** treated cells with DSSO and **NC-1** treated samples without crosslinker. Some enriched proteins which are possible interaction partners of VAT-1 are overlapping between the two different visualizations (Table 8). However, no protein involved in cell adhesion was detected in contrast to the VAT-1 crosslink co-IP. Further, there were no common hits between the co-IP and the crosslinking ABPP approach.

The results obtained for **NC-1** target ID combined with *in situ* crosslinking are not as promising as the results gained by crosslinking co-IP. The methods are quite different regarding enrichment strategies. However, the protein interactions should be preserved for both methods by *in situ* crosslinking. It might be that the probe **NC-1** affects protein interactions to a higher degree than **NCA**. Therefore, some interactions might be lost compared to the co-IP since the cells were treated with the probe prior to crosslinking. Overall, the method requires some optimization since the buffers and enrichment conditions were completely different and the comparison of the obtained interaction partners with orthogonal methods is thus difficult. Nevertheless, enrichment of a desired protein by a specific probe after *in situ* crosslinking constitutes a valuable strategy for the detection of interaction partners and might be more successful for other probes.
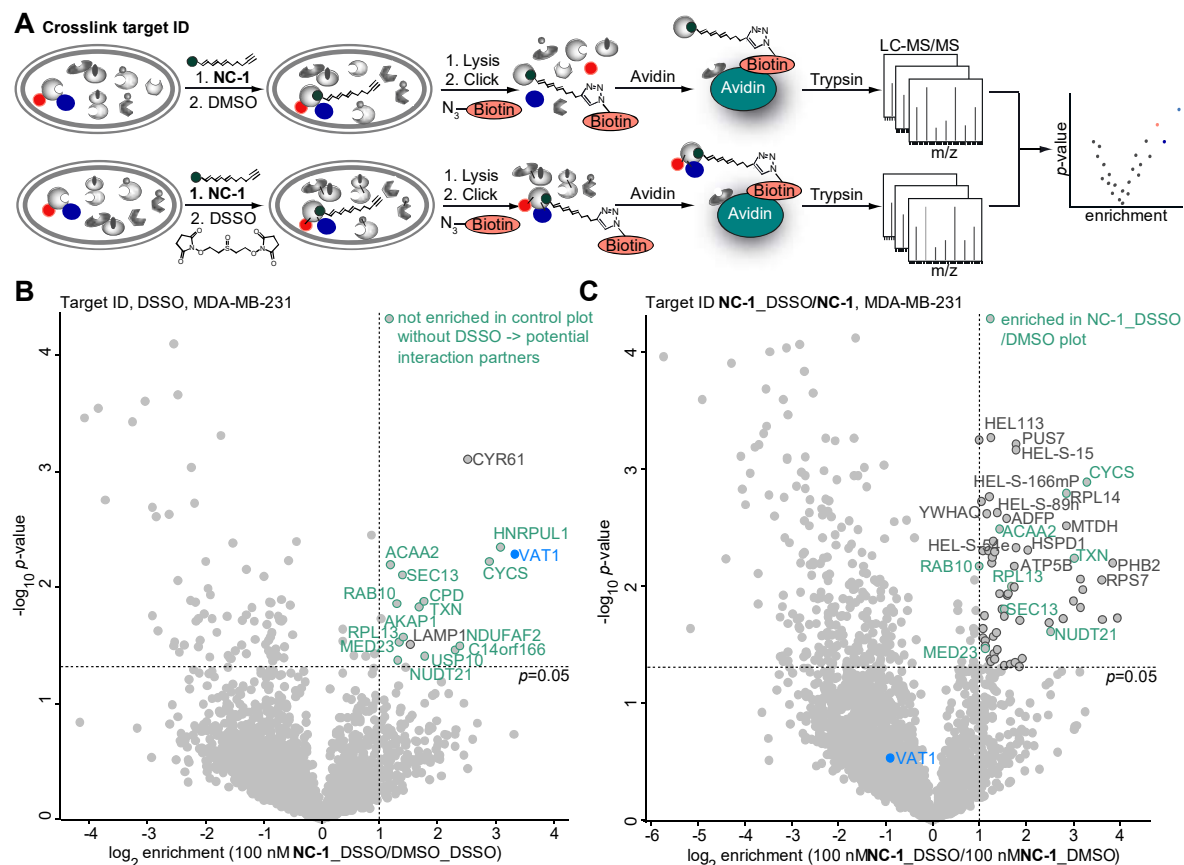
Figure 31: Target-ID with crosslinking for identification of VAT-1 interaction partner. A, Schematic overview of target ID with DSSO crosslinker for pull down of target protein and interaction partner (n=3). **B,** Volcano plot of **NC-1** enrichment with DSSO crosslinker. Proteins which did not appear in plot without crosslinker are highlighted in green and display potential interaction partner of VAT-1 (n=3). **C,** Volcano plot of **NC-1** enrichment with DSSO compared to **NC-1** enrichment without DSSO as a control. Proteins which also appeared in **B** amongst hits are highlighted in green.

Table 7: Significantly enriched proteins from Figure 31B with corresponding $\log_2$ enrichment and significance. (blue = **NC-1** target protein, green = proteins, which were not enriched in target ID control without DSSO (Figure 51), dark grey = proteins, which also appeared as significantly enriched in control).

gene names	protein names	$\log_2$ fold change	$-\log_{10}$ p-value	coverage [%]
VAT1	Synaptic vesicle membrane protein VAT-1 homolog	3.34	2.28	41.2
HNRPUL1	Heterogeneous nuclear ribonucleoprotein U-like protein 1	3.09	2.35	17.7
CYCS	Cytochrome c	2.89	2.22	21.8
NDUFAF2	Mimitin, mitochondrial	2.38	1.49	24.3
C14orf166	UPF0568 protein C14orf166	2.30	1.46	20.5
USP10	Ubiquitin carboxyl-terminal hydrolase 10	1.78	1.41	11.7
CPD	Carboxypeptidase D	1.77	1.88	13
TXN	Thioredoxin	1.69	1.83	31.4
RPL13	60S ribosomal protein L13	1.41	1.57	24.6
SEC13	Protein SEC13 homolog	1.39	2.10	18
MED23	Mediator of RNA polymerase II transcription subunit23	1.34	1.53	9.4
NUDT21	Cleavage and polyadenylation specificity factor subunit 5	1.31	1.37	17.2
RAB10	Ras-related protein Rab-10	1.30	1.86	30
ACAA2	3-ketoacyl-CoA thiolase, mitochondrial	1.19	2.19	40.4
AKAP1	A-kinase anchor protein 1, mitochondrial	1.02	1.73	7.1
CYR61	Protein CYR61	2.52	3.10	15.1
LAMP1	Lysosome-associated membrane glycoprotein 1	1.53	1.50	4.6

Table 8: Significantly enriched proteins from Figure 31C with corresponding $\log_2$ enrichment and significance. (blue = **NC-1** target protein, green = proteins, which were significantly enriched in Figure 31B and were simultaneously not enriched in target ID control without DSSO (Figure 51), dark grey = proteins, which were not enriched in Figure 31B).

gene names	protein names	$\log_2$ fold change	$-log_{10}$ p-value	coverage [%]
CYCS	Cytochrome c	3.29	2.89	21.8
TXN	Thioredoxin	3.02	2.24	31.4
NUDT21	Cleavage and polyadenylation specificity factor su. 5	2.53	1.61	17.2
ACAA2	3-ketoacyl-CoA thiolase, mitochondrial	1.43	2.49	40.4
RPL13	60S ribosomal protein L13	1.68	2.00	24.6
SEC13	Protein SEC13 homolog	1.48	1.80	18
MED23	Mediator of RNA polymerase II transcription subunit 23	1.13	1.49	9.4
PGRMC1	Membrane-associated progesterone receptor comp. 1	3.95	1.73	35.4
PHB2	Prohibitin-2	3.84	2.20	31.1
OCIAD1	OCIA domain-containing protein 1	3.63	1.72	15.5
RPS7	40S ribosomal protein S7	3.61	2.05	14.4
NACA	Nascent polypeptide-associated complex subunit α	3.20	1.97	41.9
SDCBP	Syntenin-1	3.16	1.82	37.9
ACOT7	Cytosolic acyl coenzyme A thioester hydrolase	3.16	2.06	27.9
HIST1H2BC	Histone H2B;	3.01	1.87	46
RPL14	60S ribosomal protein L14	2.86	2.79	24.1
MTDH	Protein LYRIC	2.86	2.52	33.2
HIST2H2AC	Histone H2A type 2-C	2.78	1.72	44.2
KRT18	Keratin, type I cytoskeletal 18	2.48	1.68	64.7
HSPD1	60 kDa heat shock protein, mitochondrial	2.03	2.30	60.9
HEL-S-71	Ubiquitin-conjugating enzyme E2 N	1.92	1.38	34.9
CAPZA2	F-actin-capping protein subunit alpha-2	1.86	1.70	37.1
PDIA6	Protein disulfide-isomerase A6	1.84	1.31	25.9
PUS7	Pseudouridylate synthase 7 homolog	1.79	3.22	14.4
HEL-S-54e	Prohibitin	1.79	2.33	51.8
HEL-S-15	Cofilin-1	1.78	3.17	57.8
ETFA	Electron transfer flavoprotein subunit alpha, mit.	1.77	1.35	45.2
ATP5B	ATP synthase subunit beta	1.75	2.17	50.6
STX18	Syntaxin-18	1.74	1.99	12.4
ANXA11	Annexin;Annexin A11	1.67	1.34	15.3
EIF2S2	Eukaryotic translation initiation factor 2 subunit 2	1.61	1.94	39.6
DKFZp686J1372		1.59	1.92	48.7
ADFP	Perilipin	1.57	2.58	19
SNRP70	U1 small nuclear ribonucleoprotein 70 kDa	1.53	1.81	32
ITGA3	Integrin alpha-3	1.53	1.32	10.7
CANX	Calnexin	1.52	1.74	34.3
SLC3A2	4F2 cell-surface antigen heavy chain	1.46	1.30	37.7
PTPN1	Tyrosine-protein phosphatase non-receptor type	1.43	1.93	29
HIST1H1C	Histone H1.2	1.38	1.46	30.5
HEL-S-89n	78 kDa glucose-regulated protein	1.38	2.62	51.7
CALU	Calumenin	1.36	1.60	19.7
HEL-S-68p	Phosphoglycerate kinase	1.34	2.29	51.8
NME1-NME2	Nucleoside diphosphate kinase	1.33	1.38	53.1
YBX1	Nuclease-sensitive element-binding protein 1	1.31	1.42	42
RPL19	Ribosomal protein L19	1.30	2.38	18.1
DPYSL2	Dihydropyrimidinase-related protein 2	1.30	1.57	47.1
TPD52L2	Tumor protein D54	1.28	2.25	61.2
SYNPO	Synaptopodin	1.26	2.20	9.8
HEL113	Vimentin	1.25	3.26	79
NCEH1	Neutral cholesterol ester hydrolase 1	1.24	1.35	22
PLS3	Plastin-3	1.23	1.37	33.7
HEL-S-166mP	Aflatoxin B1 aldehyde reductase member 2	1.21	2.76	21.4
HSPA9	Stress-70 protein, mitochondrial	1.20	2.30	55.3
HEL-S-64p	Glutathione synthetase	1.18	1.31	39.9
YWHAQ	14-3-3 protein theta	1.17	2.62	49.4
HEL-S-70	Transitional endoplasmic reticulum ATPase	1.13	1.53	43.5
CCT4	T-complex protein 1 subunit delta	1.13	1.46	41
HEL-S-269	Protein disulfide-isomerase	1.12	1.75	44.4
VDAC1	Voltage-dependent anion-selective channel protein 1	1.09	1.55	62.5
UBB	Ubiquitin-60S ribosomal protein L40	1.08	1.64	43
MGEA5	Protein O-GlcNAcase	1.08	2.30	12.1
HEL-S-87p	Fructose-bisphosphate aldolase	1.05	2.72	64.6

7.

BIOLOGICAL PATHWAYS

Upon **NCA** treatment, inhibition of the formation of lamellipodia was detected, whereas protein levels in whole proteome analysis did not significantly change. Further, activation of integrins and therefore an enhanced cell adhesion mediated by **NCA** was shown. Since VAT-1 is the target protein of **NCA** and it was linked to cell adhesion by co-IP approaches, the effects of VAT-1 downregulation on cell migration were investigated. A reduced anti-migratory phenotype was detected in si-VAT-1 and VAT-1 KO cells. Overexpression of VAT-1 in human cancer cells led to an upregulation of proteins involved in cell adhesion and migration, while downregulation led to a depletion. However, a complete KO of the protein resulted in an overexpression of proteins involved in cell adhesion and migration, suggesting a functional compensation of VAT-1 loss.

Contents:

7. BIOLOGICAL PATHWAYS

Since no studies in terms of the role of **NCA** in cell migration have been published, the effects of **NCA** and its target protein on this process were elucidated. In case of VAT-1, increased mRNA and protein levels of VAT-1 were detected in glioblastomas and benign prostatic hyperplasia compared to healthy tissue in previous studies.[157, 172] Further, a corresponding siRNA based VAT-1 knockdown significantly impaired glioma cell migration but not proliferation.[157] The functional link between VAT-1 and cell migration demonstrated in this study is in accordance with the observed anti-migratory phenotype upon **NCA**-treatment described in chapter 2. However, this study yields a prelimary evidence for VAT- 1 being not the proteinogenic target of **NCA** which triggers an anti-proliferative phenotype.

In this context, the role of VAT-1 in cell migration and cell proliferation was studied with bioactivity assays upon VAT-1 downregulation and several whole proteome analysis approaches upon VAT-1 up- and downregulation. To link the effect of **NCA** to VAT-1, a further whole proteome analysis of **NCA** treated MDA-MB-231 was conducted for comparison of the results of VAT-1 up- and downregulation and **NCA** treatment.

7.1. Biological activity after VAT-1 downregulation or knockout

For biological activity assays, MDA-MB-231 as well as 4T1-luc2 cells were transfected with si-VAT-1 and non-targeting (nt) si-RNA as a control for investigation of the effects on cell proliferation and cell migration. VAT-1 knockdown in MDA-MB-231 and 4T1-luc2 cells had no effect on apoptosis (appendix Figure 52A) while it triggered 50-80% inhibition of cell migration investigated in Boyden chamber assays (Figure 32A). Further, at the same time, VAT-1 silencing didn't affect cell proliferation (Figure 32B). These results indicate that VAT- 1 is required for a proper cell migration but not for cell proliferation. Successful knockdown of VAT-1 in MDA-MB-231 and 4T1-luc2 cells was verified by Western blot shown in the appendix (appendix Figure 52B).

However, with si-VAT-1 transfected cells, only a knockdown (KD) of the protein is achieved but not a stable and complete knockout (KO) of the protein. Consequently, CRISPR/Cas9 VAT-1 knockout clones were generated as mentioned before by deleting exon 2 of VAT-1 in HEK-293 cells for a complete KO of isoform 1. In comparison to wildtype HEK-293 cells and mock-transfected cells (CRISPR control), the VAT-1 knockout clones revealed a strong reduction of migration which was comparable to that caused by **NCA** treatment, whereas the proliferative behavior of the cells was not affected (Figure 32C+D). Successful knockout

of VAT-1 in HEK-293 cells was confirmed by Western blot (appendix Figure 52C). These data confirmed the results obtained for si-VAT-1 treated cells and of previous studies.

Taken together, in terms of effects of VAT-1 on cell migration, it was found that both knockdown and knockout of the protein resulted in a diminished cell migration, supporting the hypothesis that the cell motility phenotype caused by **NCA** is predominantly mediated through VAT-1 inhibition. Further, based on the results obtained for cell proliferation, it is suggested that the anti-proliferative effect could be caused by a different target protein. However, the link between VAT-1 and cell migration merits further investigation in detail. Therefore, changes on global proteome were studied after VAT-1 down- or upregulation described in this chapter. A further goal of future experiments should be the detection of the role of VAT-1 in cell adhesion, since it was found to be involved in a network of cell adhesion molecules by co-IP approaches.
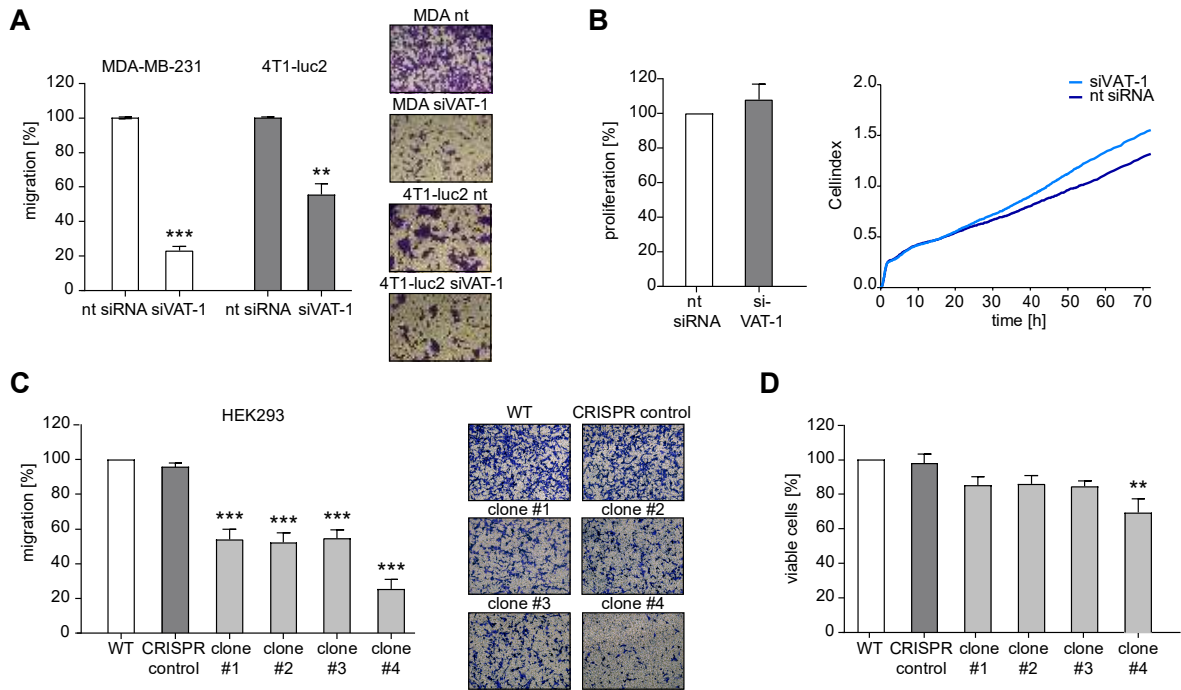
Figure 32: Effects of VAT-1 on cell migration and proliferation. **A**, Transwell migration of (non-targeting) nt and VAT-1 siRNA transfected MDA-MB-231 and 4T1-luc2 cells determined by Boyden Chamber assay. Bar diagrams show the number of migrated siVAT-1 cells normalized to nt siRNA cells. Bars represent the mean ± SEM of at least three independent experiments performed in duplicates, two-tailed unpaired Student's t test, **P < 0.002, ***P < 0.001. **B,** Proliferation of nt and VAT-1 siRNA transfected MDA-MB-231 cells determined by crystal violet staining after 72 h. Bar diagram showing the proliferation capacity of siVAT-1 cells normalized to nt siRNA cells is presented. Bars represent the mean ± SEM of three independent experiments performed in triplicates, two-tailed unpaired Student's t test. **C**, Transwell migration of HEK-293 CRISPR-Cas9 VAT-1 knockout clones determined by Boyden Chamber assay. Bar diagrams show the number of migrated VAT-1 knockout cells normalized to WT cells. Unsuccessfully altered WT cells were included as additional control (CRISPR control). Bars represent the mean ± SEM of at least three independent experiments performed in duplicates, one-way ANOVA, Dunnett's test, ***P < 0.001 compared with DMSO control. **D,** Proliferative capacity of WT and VAT-1 knockout clones was determined by measuring metabolic activity using CellTiter-Blue® Cell Viability Assay after 72 h. As additional control WT cells which were subjected to the complete CRISPR-Cas9 procedure but did not result in successful knockout of VAT-1 were included in the experiment (CRISPR control). Bars represent the mean ± SEM of three independent experiments performed in triplicates, one-way ANOVA, Dunnett's test, **P < 0.002 compared with DMSO control. Experiments were performed by Dr. Carolin Pyka (LMU). Adapted from Gleissner *et al.* [134]

7.2. Effects of **NCA** on lamellipodia formation and integrin activation

In co-IP experiments (see chapter 6), overrepresentation of the GO terms *organization of lamellipodia* and *activation of integrins* was found for the potential VAT-1 interaction candidates within the detected network. Since **NCA** binds to VAT-1, it might also interfere with pathways in which VAT-1 is involved. Directly in this context, for elucidation of the role of **NCA** on cell migration, the effect of **NCA** on the formation of lamellipodia at the leading edge of the cells was investigated first, which represents one of the initial steps in cell migration. Lamellipodia organization is mediated by the small GTPase Rac1, which translocates from the cytosol to the cell membrane in the activated, GTP bound state. Arrived at the cell membrane, Rac1 induces cortactin to localize to the cell membrane and bind to F-actin and actin-related protein (Arp) 2/3 complex in parallel.[173] Consequently, the activation of Rac-1, which is necessary for location to the cell membrane and lamellipodia formation, was investigated by pull-down of the GTP bound Rac1 and detection by a Western blot.

It was obtained, that the activation of the small Rho GTPase Rac1 was strongly impaired in **NCA** treated cells as shown by Rac1 pulldown assays (Figure 33A). In addition, the localization of Rac1 within the cells and the formation of lamellipodia can be observed by confocal microscopy. It was demonstrated that upon **NCA** treatment of migrating T-24 cancer cells, Rac1 was not localized to the cell membranes indicating an impaired formation of lamellipodia (Figure 33B). These results show that the cell migration is inhibited by **NCA** at one of the initial steps. In order to confirm that VAT-1 downregulation mediates the same effect than **NCA**-treatment, lamellipodia formation should be investigated after downregulation of VAT-1. Since HEK-231 VAT-1 KO cells are not a suitable model for monitoring lamellipodia formation, the generation of a stable VAT-1 KO cell line in breast cancer cells such as MDA-MB-231 or T-24 cells would be of high value.
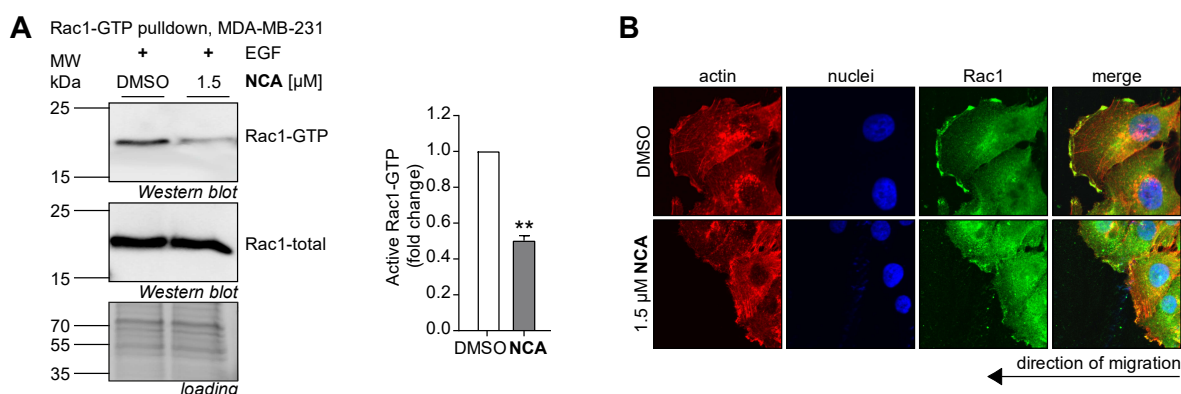
Figure 33: Effects of NCA on Rac1 levels and lamellipodia formation. A, Active Rac1 pull-down assay was conducted upon 5-minute EGF stimulation (100 ng/mL). A representative experiment out of 3 independent experiments is shown. Amount of Rac1-GTP determined by Western Blot was normalized to total Rac1 and results were normalized to the control. Bars represent the mean ± SEM of 3 independent experiments, two-tailed unpaired Student's *t* test, **P < 0.002. **B,** T24 cells treated with **NCA** were engaged in a Scratch assay and stained for Rac1 and F-actin. Nuclei were stained with Hoechst 33342. Representative images out of 3 independent experiments are shown. Experiments were performed by Dr. Carolin Pyka (LMU). [134]

Moreover, integrin activation and surface overexpression were investigated upon **NCA** treatment, since TLN1, VCL and ITGB1 were detected among the most confident interaction partners of VAT-1, which is the cellular target of **NCA**. Further, the GO terms *regulation of cell adhesion* and *integrin activation* were overrepresented in a STRING database analysis of the significant co-IP hits compared to the global humane proteome, also pointing to an effect of **NCA** on integrin levels. This data attracts attention since adhesion of cells to the ECM mediated by integrins is of crucial importance in cell migration and metastasis. Integrins form focal adhesions contacts between the cell and the ECM during cell migration and TLN1 is a mediator of integrin signaling.

For analysis of the effects of **NCA** on the integrin surface expression in MDA-MB-231 cells, antibody staining with a subsequent FACS (Fluorescence Activated Cell Sorting) analysis was conducted. Here, an increased surface expression of ITGB1, ITGB3 and ITGA5 was obtained in a concentration dependent manner (Figure 53A). Due to the fact that the overexpression itself is not decisive for the strength of the cell adhesion, the integrin activation was investigated, in which TLN1 is involved. Thus, the activation was monitored by immunostaining with a primary antibody specifically detecting the activated form ITGB1. It was shown that **NCA** led to a significant activation of ITGB1 in MDA-MB-231 cells (Figure 53B). Finally, cell adhesion to two components of the ECM, namely collagen I and FN1 was investigated, revealing an increased cell adhesion to both extracellular ligands was obtained (Figure 53C+D).

Overall, an integrin activation and increased surface overexpression was detected upon **NCA** treatment, leading to an enhanced cell adhesion. In chapter 2, inhibition of the cell migration in a dose dependent manner was shown for **NCA**. It has already been demonstrated before that a stronger cell adhesion disturbs the detachment of the cells and therefore interferes with cell migration.[174] Thus, it can by hypothesized that **NCA** inhibits the cell migration by an enhancement of the cell adhesion, resulting in a diminished detachment of the cells to the ECM preventing proper cell migration. However, the role of VAT-1 in this hypothesis is not yet clear, since a reduced cell adhesion of the HEK-293 VAT-1 KO clones was recognized, proposing VAT-1 to be crucial for cell adhesion. Consequently, if VAT-1 is relevant for the increased cell adhesion mediated by **NCA**, its function or its interaction with TLN might be enhanced instead of inhibited upon **NCA** treatment. The Western blot data showing a strengthened interaction between VAT-1 and TLN1 contributes to this hypothesis. For confirmation of the supportive role of VAT-1 in cell adhesion, integrin activation should be observed in si-VAT-1 transfected breast cancer cells or in VAT-1 KO clones generated for MDA-MB-231, since HEK-293 cells are not suitable for cell adhesion experiments. Further, it was investigated if a downregulation of VAT-1 and a treatment with **NCA** provoke similar changes on the global proteome of cancer cells.

7.3. Effects of **NCA** on global proteome of breast cancer cells

In addition to bioactivity experiments and confocal microscopy, the effect of **NCA** was also investigated on the expression levels of all proteins in a whole proteome analysis. Cells were treated with 500 nM of **NCA** for 24 h before cell lysis. The changes on the protein levels were analyzed in the complete, complex peptide solution without any pre-fractionation as well as in HILIC-fractionized samples on a peptide level (Figure 33A and B). Depleted hits were defined as proteins matching the criteria of $\log_2$ fold change > -1 and a significance of $p < 0.05$ whereas upregulated hits were defined as proteins matching the criteria of $\log_2$ fold change > 1 and a significance of $p < 0.05$. For both volcano plots showing the fold change of **NCA** treated samples against DMSO background, some upregulated and depleted proteins were detected. However, no proteins appeared simultaneously in both volcano plots, showing the low reproducibility of the whole proteome analysis with LFQ for **NCA** treatment. For SILAC, no protein changes matching the criteria mentioned above were detected at all upon **NCA** incubation (data not shown). The results implicate that **NCA** causes no relevant protein changes with a high fold changes or significance since the LFQ results are not reproducible and the SILAC results show no effects at all. In human whole proteome analysis, only the most abundant proteins in the cells are detected due to the complexity of the protein samples. The detected upregulated and depleted hits might be background proteins with a high abundance which appear upregulated or depleted in dependence of the whole proteome coverage, the recovery rates of proteins in each replicate, instrument performance and number of replicates. For fractionated samples, the coverage is higher and the results should be more reliable compared to more complex data.

With the whole proteome data in hand, the protein levels of the most interesting hits obtained by co-IP approaches which provided a link to cell migration and cell adhesion were also investigated. However, no significant effects on protein levels of TLN1, VCN, Rac1 and all integrins were obtained. These results were further validated independently by Western-blot analysis (Figure 26E, appendix Figure 54).

For gaining information about the cellular pathways which were affected by **NCA** treatment and to connect the proteins hits based on their function, up- and downregulated proteins were subjected to a STRING database (v.11.0) enrichment analysis for multiple proteins with high confidence interaction score (0.7) and network edges representing confidence. Upregulated and depleted proteins were analyzed separately (results are not shown) as well as together (Figure 34C+D). Networks created by STRING database revealed that there is hardly any connection between analyzed proteins, which confirms further that **NCA**

had no influence on proteins levels of particular cellular pathways in whole proteome analysis. Additionally, no relevant enrichment of GO terms was detected. Overall, the response obtained for **NCA** treatment was very limited in regard to cell proliferation and cell migration.

To sum up, these data indicate, that **NCA** didn't change the overall expression of proteins, but might affect the activity of these proteins rather than their expression levels by altering PTMs or interaction of proteins. To complement these whole proteome results obtained for **NCA**, the effect of up-or downregulation of VAT-1 on the global protein expression levels should be investigated, since a strong impact on cell migration was revealed upon VAT-1 silencing or rather KO.
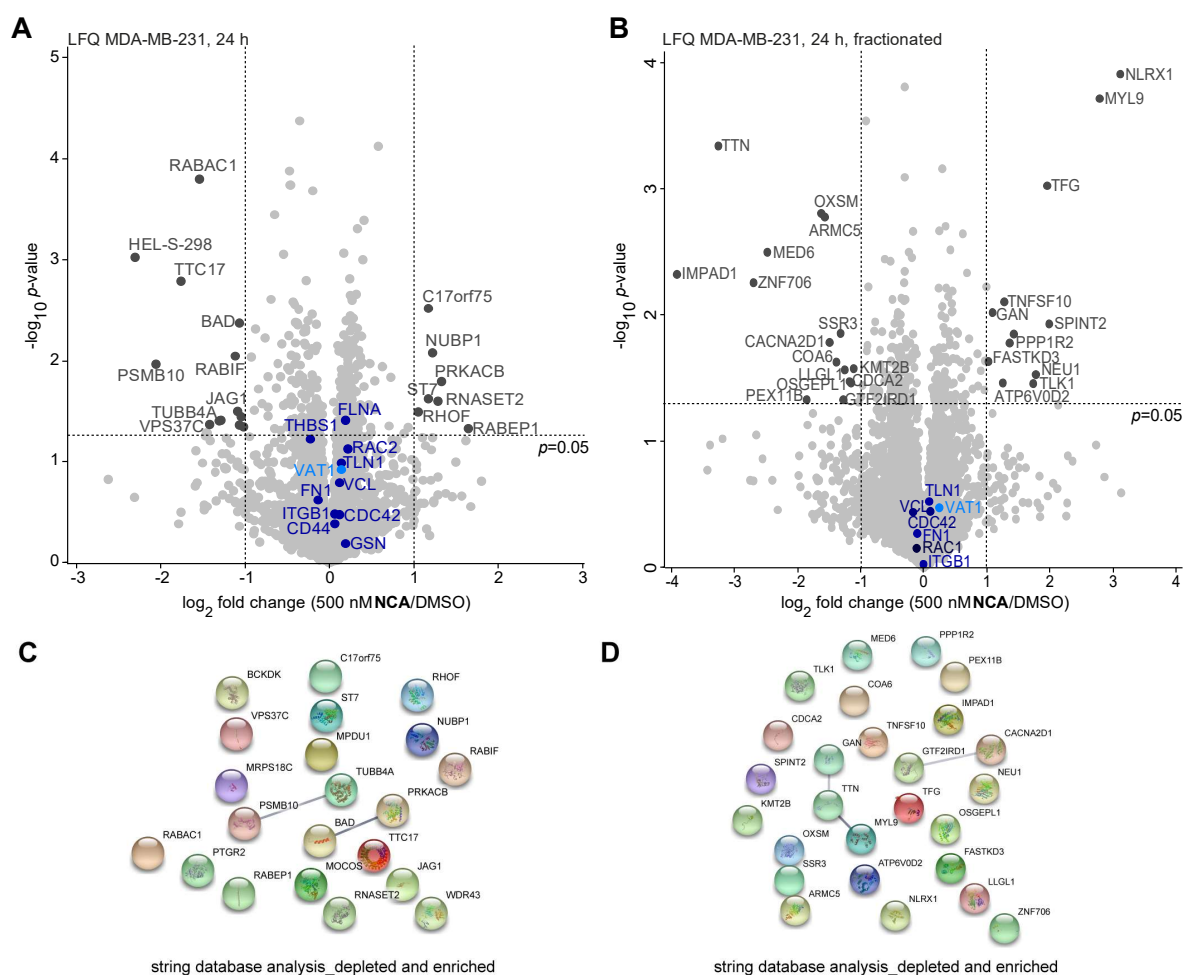
Figure 34: Whole proteome analysis in MDA-MB-231 after NCA treatment. A, Volcano plot of global proteome analysis with LFQ in MDA-MB-231 treated with 500 nM **NCA** for 24 h (n=4). Most relevant hits of co-IP are highlighted in blue. **B,** Volcano plot of global proteome analysis with LFQ with sample fractionation in MDA-MB-231 treated with 500 nM **NCA** for 24 h (n=3, 8 fractions). Proteins identified in the co-IP Figure 25C are shown in blue. **C,** STRING database analysis of depleted and upregulated proteins obtained by volcano plot shown in Figure 34A. **D,** STRING database analysis of depleted and upregulated proteins of volcano plot shown in Figure 34B. High confidence (0.7) was set as interaction score and network edges represent the confidence of an interaction. Adapted from Gleissner *et al.* [134]

7.4. Effects of VAT-1 upregulation of global proteome

It was found that **NCA** didn't alter the expression levels of proteins involved in cell migration and proliferation. Since VAT-1 is the protein target of **NCA** responsible for inhibition of cell migration, the effect of upregulation of VAT-1 on overall protein expression levels in MDA- MB-231 was investigated. Therefore, VAT-1 was overexpressed in MDA-MB-231 by a lipofectamine mediated plasmid transfection. For whole proteome analysis, cells overexpressing VAT-1 were compared to control cells which were only treated with lipofectamine. Two independent experiments were performed (Figure 35A+B), whereby the overlap of the upregulated proteins between both experiments represented seven proteins (Figure 35C). Further, VAT-1 overexpression in MDA-MB-231 after 2 days was confirmed by Western-blot analysis (Figure 35D).

Global proteome analysis revealed several upregulated proteins matching the criteria $\log_2$ fold change > 1 and a significance of $p < 0.05$ with some of them being assigned to GO terms cell migration and adhesion (Figure 35A+B, Table 9+10). In contrast, no protein involved in cell adhesion or migration was detected with significantly decreased expression levels. These results point to an upregulation of proteins involved in cell adhesion after VAT- 1 overexpression, which is consistent with the observed reduced cell adhesion of HEK-293 VAT-1 KO cells.

For both experiments shown in Figure 35A+B, PTGS2 (Prostaglandin G/H synthase 2) was detected among the upregulated hits which converts arachidonate to prostaglandin H2 and is therefore responsible for production of inflammatory prostaglandins. The enzyme is better known as cyclooxygenase 2 (COX2).[175] Of note, in cancer cells, PTGS2 produces the prostaglandin E2 (PGE2), which plays a crucial role in modulating motility and enhanced cell adhesion.[176] Moreover, SDC4 (Syndecan-4) displayed an upregulated protein in both experiments, which represents a cell surface proteoglycan that bears heparan sulfate involved in the assembly of the focal cell adhesions which connect the actin cytoskeleton to parts of the ECM.[177]

A STRING database (v.11.0) analysis was performed for upregulated proteins with a minimum required interaction score of 0.7 (high confidence) and network edges representing the confidence, however, only one cluster of several proteins involved in anti-viral defense was detected. Further, the GO term *defense response to virus* (FDR 3.31E-05) in the category biological process was overrepresented among upregulated proteins. Accordingly, several proteins upregulated in both experiments correlate with defense mechanisms against viruses such as IFIT1 IFIT3 IFIT2 (Interferon-induced antiviral RNA-binding protein)[178] and OASL (2'-5'-oligoadenylate synthase-like protein)[179], since external

plasmid DNA is transferred in human cells for protein expression by Lipofectamine which can be compared to a virus infection (Figure 35 C). For Figure 35A, STRING database provided a functional enrichment of KEGG pathways *Cell adhesion molecules* (*CAMs*) (FDR 1.82E-2) and biological processes such as *positive regulation of cell matrix adhesion* (FDR 4.83E-2) for upregulated proteins. However, no enrichment of cell adhesion processes was detected for functional analysis of upregulated proteins shown Figure 35B except the *defense response to virus* (FDR 2.41E-14).

Moreover, the expression levels of the most promising proteins detected in co-IP approaches (chapter 6) which provided a link to cell adhesion such as TLN1 and ITGB1 remained unaffected after VAT-1 overexpression. To sum up, some proteins involved in cell adhesion and cell migration were upregulated after VAT-1 overexpression. For deeper insights into the role of VAT-1 in cell adhesion, the effects of VAT-1 downregulation on the global proteome were investigated as a next step.
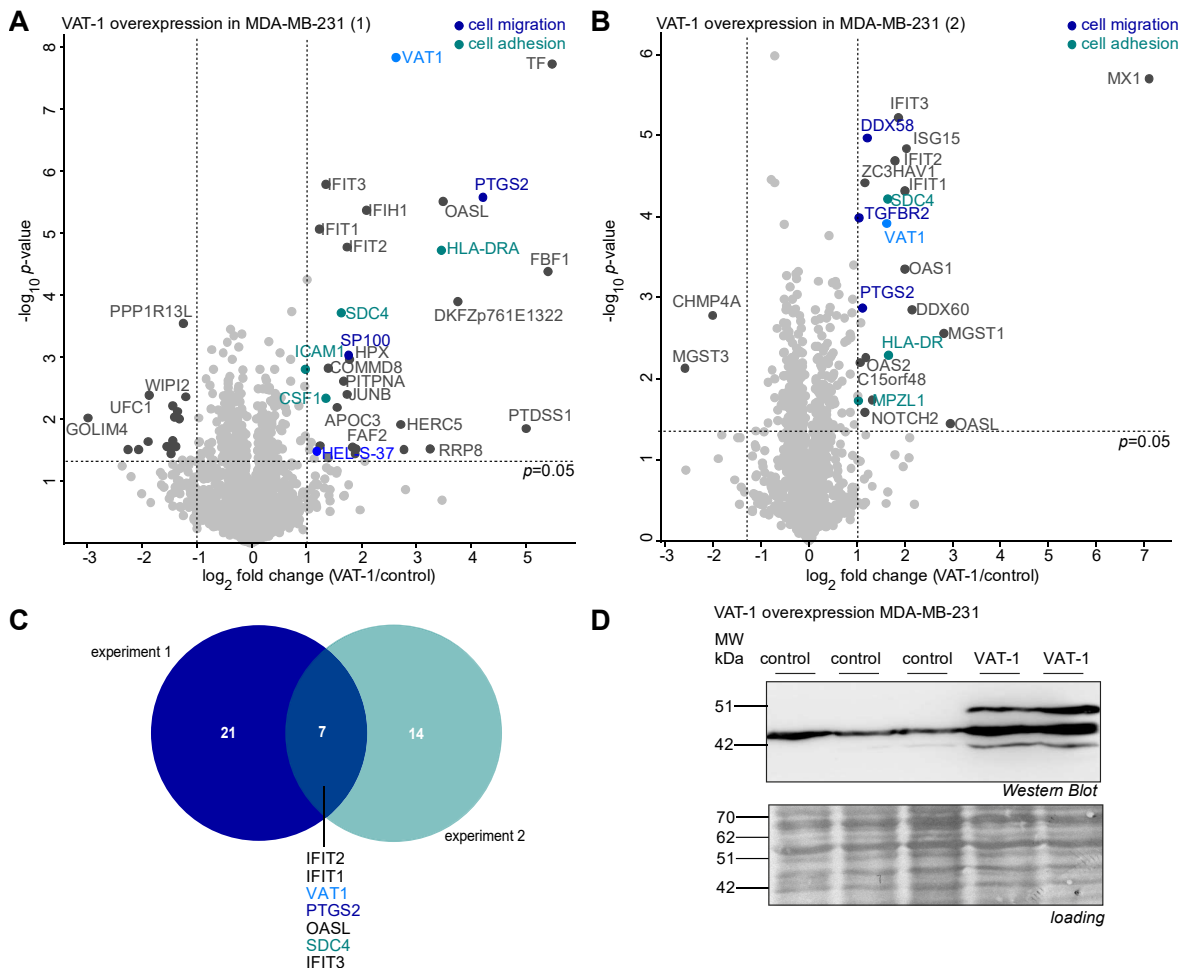
Figure 35: Whole proteome analysis in MDA-MB-231 after VAT-1 overexpression. **A,** Volcano plot of global proteome analysis with LFQ in MDA-MB-231 overexpressing VAT-1 (n=4). Proteins involved in cell migration and adhesion are highlighted among upregulated and depleted proteins. **B,** Volcano plot of global proteome analysis with LFQ in MDA-MB-231 overexpressing VAT-1 (n=3). Proteins involved in cell migration and adhesion are highlighted among upregulated and depleted proteins. **C,** Venn Diagram of upregulated proteins from experiment 1 shown in A and 2 shown in B. **D,** Western blot of cells overexpressing VAT-1 compared to control cells.

Table 9: Upregulated proteins of whole proteome analysis for VAT-1 overexpression shown in Figure 35A. Same color code is used for proteins involved in cell adhesion and cell migration

gene name	protein name	log$_2$ fold change	-log$_{10}$ p-value	coverage [%]
HLA-DRA1	HLA class II histocompatibility antigen, DR alpha chain	3.46	4.72	28.40
SDC4	Syndecan	1.63	3.71	19.00
ICAM1	Intercellular adhesion molecule 1	1.34	2.80	35.00
CSF1	Macrophage colony-stimulating factor 1	0.98	2.32	20.60
PTGS2	Prostaglandin G/H synthase 2	4.21	5.57	45.40
SP100	Nuclear autoantigen Sp-100	1.77	3.03	12.50
HEL-S-37	Plastin-2	1.19	1.47	14.80
TF	Serotransferrin	5.47	7.72	37.50
FBF1	Fas-binding factor 1	5.40	4.37	11.30
PTDSS1	Phosphatidylserine synthase 1	5.00	1.84	7.60
MTPN	Myotrophin	3.75	3.90	33.10
OASL	2-5-oligoadenylate synthase-like protein	3.49	5.50	45.10
RRP8	Ribosomal RNA-processing protein 8	3.25	1.51	11.60
HIST2H2AB	Histone H2A type 2-B	2.77	1.50	42.30
HERC5	E3 ISG15–protein ligase HERC5	2.71	1.91	12.20
VAT1	Synaptic vesicle membrane protein VAT-1 homolog	2.63	7.84	68.20
IFIH1	Interferon-induced helicase C domain-containing protein 1	2.09	5.36	9.80
FAF2	FAS-associated factor 2	1.89	1.52	15.60
PIG60	Mitochondrial carrier homolog 1	1.84	1.55	10.70
HPX	Hemopexin	1.78	2.96	17.50
IFIT2	Interferon-induced protein with tetratricopeptide repeats 2	1.73	4.77	61.40
JUNB	Transcription factor jun-B	1.73	2.39	14.70
PITPNA	Phosphatidylinositol transfer protein alpha isoform	1.68	2.60	19.00
APOC3	Apolipoprotein C-III	1.56	2.19	16.20
COMMD8	COMM domain-containing protein 8	1.39	2.82	19.70
IFIT3	Interferon-induced protein with tetratricopeptide repeats 3	1.35	5.79	74.30
ARMC9	LisH domain-containing protein ARMC9	1.24	1.57	3.30
IFIT1	Interferon-induced protein with tetratricopeptide repeats 1	1.23	5.06	50.20

Table 10: Upregulated proteins of whole proteome analysis for VAT-1 overexpression shown in Figure 35B. Same color code is used for proteins involved in cell adhesion and cell migration

gene names	protein names	log$_2$ fold change	-log$_{10}$ p-value	coverage [%]
HLA-DR	HLA class II histocompatibility antigen, DR beta 4 chain	1.67	2.30	40
SDC4	Syndecan	1.66	4.22	26.2
MPZL1	Myelin protein zero-like protein 1	1.04	1.73	15.6
DDX58	Probable ATP-dependent RNA helicase DDX58	1.22	4.97	46.6
PTGS2	Prostaglandin G/H synthase 2	1.13	2.87	39.6
TGFBR2	TGF-beta receptor type-2	1.05	3.99	10.6
MX1	Interferon-induced GTP-binding protein Mx1	7.10	5.71	56.2
OASL	2-5-oligoadenylate synthase-like protein	2.95	1.45	36.4
MGST1	Microsomal glutathione S-transferase 1	2.83	2.57	70.1
DDX60	Probable ATP-dependent RNA helicase DDX60	2.15	2.85	9.2
ISG15	Ubiquitin-like protein ISG15	2.05	4.85	67.9
OAS1	2-5-oligoadenylate synthase 1	2.01	3.35	20
IFIT1	Interferon-induced protein with tetratricopeptide repeats 1	2.00	4.32	54.6
IFIT3	Interferon-induced protein with tetratricopeptide repeats 3	1.87	5.23	70.8
IFIT2	Interferon-induced protein with tetratricopeptide repeats 2	1.80	4.69	50
VAT1	Synaptic vesicle membrane protein VAT-1 homolog	1.63	3.92	75.6
SLC17A5	Sialin	1.33	1.74	4.3
OAS2	2-5-oligoadenylate synthase 2	1.18	2.26	27.7
ZC3HAV1	Zinc finger CCCH-type antiviral protein 1	1.18	4.43	27.9
NOTCH2	Neurogenic locus notch homolog protein 2	1.17	1.59	3
C15orf48	Normal mucosa of esophagus-specific gene 1 protein	1.06	2.20	97.6

7.5. Effects of VAT-1 downregulation or KO on global proteome

Since some proteins involved in cell migration and cell adhesion were upregulated upon VAT-1 overexpression, VAT-1 was silenced by si-VAT-1 transfection in MDA-MB-231 as a next step for investigation of consequences on the global protein expression levels. Accordingly, VAT-1 was detected among the significantly depleted proteins in the volcano plot (Figure 36A). However, only a three-fold depletion was achieved, since only isoform 1 was downregulated. Therefore, the two other isoforms and the remaining isoform 1 level were still detected in the proteomics data. The depletion of VAT- 1 was also successfully confirmed by Western-blot (Figure 36B). A few proteins associated with GO terms cell adhesion and cell migration were detected mainly among the downregulated proteins (Figure 36A, Table 11).

In detail, among upregulated proteins matching the criteria of $\log_2$ fold change > 1, the Ras-related protein Ral-A (RALA) was detected, which is a multifunctional GTPase involved in cellular processes including cell migration and cell proliferation.[180] Among the significantly downregulated proteins, for example, F11R (Junctional adhesion molecule) was found which is decisive for epithelial tight junction formation.[181] Additionally, CLASP2 was detected as downregulated, which plays a role in cell polarization during cell migration and microtubule stabilization.[182] Again, no change in the protein levels of integrins and TLN1 was detected, which are the main players in cell adhesion. However, only the signaling can be affected but not the expression levels.
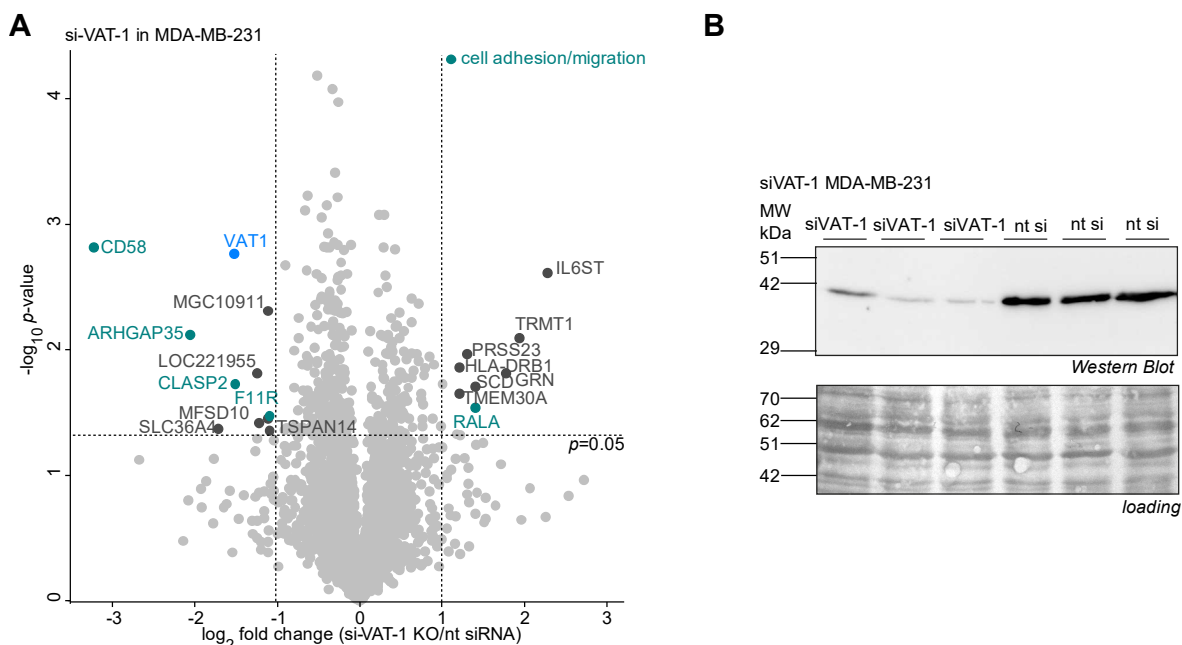
Figure 36: Whole proteome analysis of si-VAT-1 treated MDA-MB-231. A, Volcano plot of global proteome analysis with LFQ in si-VAT-1 MDA-MB-231 cells (n=3). Proteins involved in cell migration and adhesion are highlighted among upregulated and depleted proteins. **B,** Western blot of si-VAT-1 cells compared to control cells.

Table 11: Dysregulated proteins of whole proteome analysis in si-VAT cells shown in Figure 36A. Same color code is used for proteins involved in cell adhesion and cell migration.

gene names	protein names	log$_2$ fold change	-log$_{10}$ p-value	coverage [%]
upregulated				
RALA	Ras-related protein Ral-A	1.40	1.54	44.7
IL6ST	Interleukin-6 receptor subunit beta	2.28	2.61	11.3
TRMT1	tRNA (guanine(26)-N(2))-dimethyltransferase	1.94	2.09	15.4
GRN	Granulins	1.78	1.81	5.9
SCD	Acyl-CoA desaturase	1.41	1.70	14.2
PRSS23	Serine protease 23	1.30	1.97	14.6
HLA-DRB1	HLA class II histocompatibility antigen,	1.21	1.86	49.6
TMEM30A	Cell cycle control protein 50A	1.21	1.65	12.5
depleted				
CD58	Lymphocyte function-associated antigen 3	-3.23	2.82	13.4
ARHGAP35	Rho GTPase-activating protein 35	-2.06	2.12	4.9
CLASP2	CLIP-associating protein 2	-1.51	1.73	8.4
F11R	Junctional adhesion molecule A	-1.09	1.47	14.2
SLC36A4	Proton-coupled amino acid transporter 4	-1.71	1.37	32.4
VAT1	Synaptic vesicle membrane protein VAT-1 homolog	-1.52	2.76	57.5
LOC221955	Sn1-specific diacylglycerol lipase beta	-1.24	1.81	9.2
TSPAN14	Tetraspanin-14	-1.22	1.42	9.3
MFSD10	Major facilitator superfamily domain-containing protein 10	-1.11	1.45	9.8
MGC10911	Proteasome assembly chaperone 3	-1.11	2.31	50

For functional insights, a STRING database (v.11.0) analysis of depleted and upregulated proteins with minimum interaction scores of 0.7 and network edges representing the confidence was performed. For depleted proteins, the KEGG pathway *cell adhesion molecules* (CAMs) (FDR 1.47E-2) was found significantly enriched in the dataset. For upregulated proteins, no overrepresented functional processes were detected. For both upregulated and depleted proteins, functional analysis provided no formation of clusters, indicating that the proteins detected are not connected with each other corresponding to the current knowledge.

Further, a cytoscape[160] BINGO app[170] analysis was carried out for functional enrichment analysis of depleted proteins. Analysis was performed with Benjamini&Hochberg FDR and a significance of 0.05. GO terms associated with cell adhesion and migration which were overrepresented in the dataset compared to the global proteome, are illustrated in Table 12. Here, GO terms such as *regulation of the actin cytoskeleton, regulation of the basement membrane, positive regulation of the ECM disassembly* were detected for the category biological process, while *plasma bounded membrane projection* was found for the namespace cellular compartment (Table 12).

Table 12: Functional enrichment analysis performed by Cytoscape BINGO app for depleted proteins of si-VAT-1 whole proteome analysis listed in Table 11. GO terms involved in cell adhesion and cell migration are listed for analysed categories with corresponding corrected *p*-values and frequencies.

GO-ID	description	corr. *p*-value	frequency global proteome [%]	frequency analyzed data [%]
biological process				
GO:0032956	regulation of actin cytoskeleton organization	1.81E-02	1.89	37.5
GO:0032970	regulation of actin filament-based process	1.86E-02	2.13	37.5
GO:0051493	regulation of cytoskeleton organization	2.71E-02	2.93	37.5
GO:0033043	regulation of organelle organization	2.71E-02	7.02	50
GO:0110011	regulation of basement membrane organization	3.32E-02	0.03	12.5
GO:1904261	positive regulation of basement membrane assembly involved in embryonic body morphogenesis	3.32E-02	0.03	12.5
GO:1904259	regulation of basement membrane assembly involved in embryonic body morphogenesis	3.32E-02	0.03	12.5
GO:0007163	establishment or maintenance of cell polarity	3.76E-02	1.05	25
GO:0090091	positive regulation of extracellular matrix disassembly	3.76E-02	0.04	12.5
molecular function				
GO:0051010	microtubule plus-end binding	3.76E-02	0.10	12.5
cellular compartment				
GO:0044463	cell projection part	2.63E-02	7.60	50
GO:0120025	plasma membrane bounded cell projection	4.81E-02	11.03	50

Overall, the results point towards a slight downregulation of cell migration and cell adhesion after VAT-1 silencing, which is in accordance with the results obtained for VAT-1 upregulation. In general, there are two scenarios which can take place after VAT-1 downregulation: the cells either compensate the function of VAT-1 by upregulation of proteins which replace its function or the cells completely downregulate processes in which VAT-1 is involved, thus, cell adhesion and migration.

Since only a few proteins among the up-or downregulated proteins are involved in cell migration, no clear trend for a compensation of the function of VAT-1 in cell migration or a complete downregulation of migration could be obtained. However, more proteins which are linked to cell migration are depleted, pointing to a short-term downregulation of cell migration after VAT-1 silencing. However, the adaption of the protein expression after downregulation of VAT-1 to compensate its function could last longer than the transfection time. Since si-VAT-1 only evokes a silencing of VAT-1 but not a stable KO, a residual function of VAT-1 is still present and the whole proteome data obtained for si-VAT-1 cells should be further validated. Therefore, whole proteome analysis in HEK-293 VAT-1 KO cells was performed. Even more beneficial would be a whole proteome analysis in MDA-MB-231 VAT-1 KO cells, since all effects were shown for this cell line.

In the context of a downregulation of VAT-1, a whole proteome analysis was performed with the established VAT-1 HEK-293 KO cells for identification of changes on the global proteome. Downregulation of VAT-1 was observed to a much higher extent compared to the si-VAT-1 experiment shown in Figure 36 ($\log_2$ fold change -1.5 *vs.* 5.5) (Figure 37A+B). Proteins dysregulated upon VAT-1 KO cells in comparison HEK-293 cells were identified using a two-sample students *t*-test (Figure 37A). Additionally, fold changes in expression levels between VAT-1 KO cells and HEK-293 control cells – meaning HEK-293 cells which were subjected to the complete CRISPR-Cas9 procedure but did not result in successful knockout of VAT-1 – were elucidated (Figure 37B). In general, 21 significantly upregulated as well as depleted proteins overlap for both experiments, showing that the controls are quite comparable (Figure 37C). VAT-1 KO was further confirmed by a Western-blot, in which isoform 1 is completing missing for KO cells, but isoform 2 and 3 are still present (Figure 37D).

For whole proteome in VAT-1 KO cells compared to control HEK-293 cells, an involvement of proteins in cell migration and cell adhesion was only detected for upregulated hits matching the criteria of $\log_2$ fold change > 1 (Figure 37A+B, Table 13+14) These results indicate that for KO of VAT-1, the cells might compensate the function of VAT-1 by upregulation of other proteins for replacing the role of VAT-1. For upregulated proteins of both experiments, the GO term *ECM component* (FDR 9.0E-3/ 8.2E-3) was overrepresented for the category cellular compartment detected by a STRING database analysis (v.11.0) with high confidence interaction scores. For upregulated proteins illustrated in Figure 37B, *collagen containing ECM* was functionally enriched in the dataset for the category cellular compartment (FDR 4.7E-2).

In detail, laminin subunits (LAMC1, LAMB1) were amongst upregulated proteins which are high-molecular weight glycoproteins of the ECM. They represent a major component of the basement membrane and regulate the attachment as well as migration of cells by interacting with other ECM constituents such as collagen IV or fibronectin.[183, 184] The GO terms *laminin-1* and *laminin-10 complex* (FDR 3.6E-3/3.9E-3) were accordingly overrepresented in the dataset shown by STRING database analysis. Another component of the ECM which was found among upregulated proteins displays COL14A1 (Collagen alpha-1(XIV) chain) with assigned GO terms such as *cell-cell adhesion*, *ECM organization* and *collagen fibril organization*. It plays an adhesive role by integrating collagen fiber bundles.[185] Further, another protein involved in cell adhesion represents NOV (CCN family member 3), which is an ECM-associated signaling protein acting by binding to integrin

receptors[186] or membrane receptors such as NOTCH1[187] thereby regulating cell adhesion and migration.[188]

Overall, in contrast to the whole proteome analysis with si-VAT treatment, proteins involved in GO terms cell adhesion and migration were only found among upregulated proteins. The depletion of VAT-1 in si-VAT-1 treated cells (Figure 36A) was not as high as shown for HEK-293 KO cells (Figure 37A+B), since VAT-1 levels were only reduced. The residual VAT-1 function in si-VAT-1 cells might explain that the functional compensation of VAT-1 by upregulation of other proteins involved in ECM-organization is more pronounced in KO cells compared to si-VAT treated cells. Further, the si-VAT-1 cells might not adapt to the reduced protein levels of VAT-1 during the transfection time. Finally, differences in cell lines regarding protein expression levels and migration behavior might explain the different results obtained for VAT-1 downregulation and a complete KO, too.
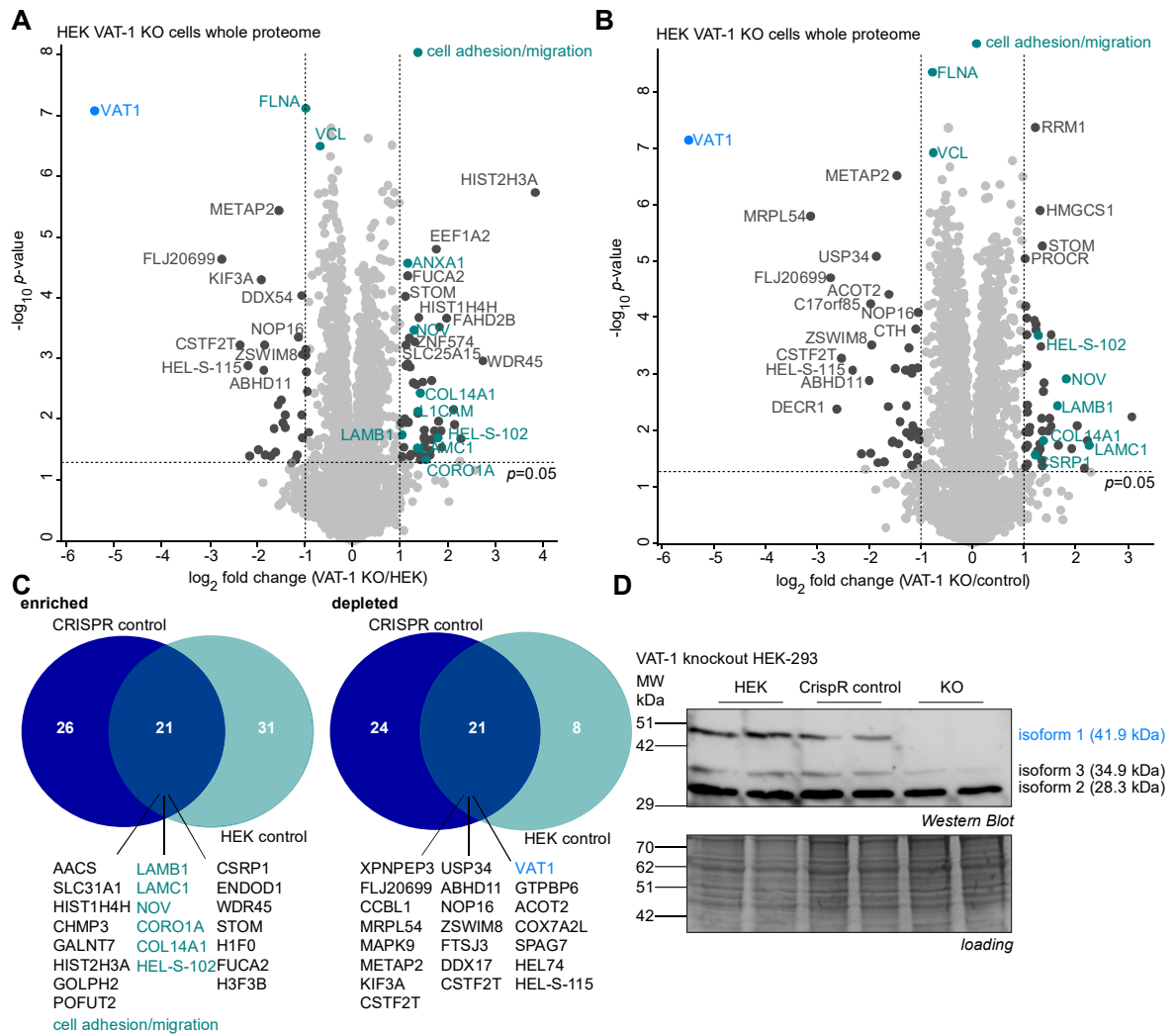
Figure 37: Whole proteome analysis of HEK-293 VAT-1 KO cells. **A,** Volcano plot of global proteome analysis with LFQ in VAT-1 KO cells with HEK-293 cells as a control (n=4). Proteins involved in cell migration and adhesion are highlighted among upregulated and depleted proteins in green. **B,** Volcano plot of global proteome analysis with LFQ in VAT-1 KO cells with HEK-293 control cells as a control (n=4). Proteins involved in cell migration and adhesion are highlighted among upregulated and depleted proteins in green. **C,** Venn Diagram for comparison of upregulated proteins and depleted proteins from **A** and **B** with indicated gene names in the same color code. **D,** Western blot of VAT-1 KO cells compared to control cells.

Table 13: Upregulated proteins of whole proteome analysis in VAT-1 KO cells with HEK-293 cells as a control shown in Figure 37A. (green =proteins involved in cell adhesion and migration matching the criteria $\log_2$ fold change > 1, p-value < 0.05, dark grey = proteins matching the criteria $\log_2$ fold change > 1, p-value < 0.05)

gene names	protein names	$\log_2$ fold change	$-\log_{10}$ p-value	coverage [%]
HEL-S-102	Heat shock protein beta-1	1.80	1.69	60
CORO1A	Coronin	1.54	1.33	12.8
COL14A1	Collagen alpha-1(XIV) chain	1.42	2.43	5.7
L1CAM	Neural cell adhesion molecule L1	1.38	2.13	13.1
LAMC1	Laminin subunit gamma-1	1.36	1.52	14
NOV	Protein NOV homolog	1.30	3.47	14.9
ANXA1	Annexin	1.16	4.56	70.5
LAMB1	Laminin subunit beta-1	1.04	1.74	4
HIST2H3A	Histone H3.2	3.83	5.73	50.7
WDR45	WD repeat domain phosphoinositide-interacting protein 4	2.74	2.97	18.7
MPC1	Mitochondrial pyruvate carrier 1	2.28	1.68	46.8
SLC31A1	High affinity copper uptake protein 1	2.14	1.91	18.7
H1F0	Histone H1.0	2.12	2.16	11.3
FAHD2B	Fumarylacetoacetate hydrolase domain-containing protein 2B	1.98	3.66	42.4
GALNT7	N-acetylgalactosaminyltransferase 7	1.87	1.54	15.4
RFTN1	Raftlin	1.85	1.81	15
MGAT2	Alpha-1,6-mannosyl-glycoprotein 2-beta-N-acetylglucosaminyltransferase	1.81	1.97	15.5
EEF1A2	Elongation factor 1-alpha 2	1.77	4.80	61.1
ELOVL5	Elongation of very long chain fatty acids protein	1.73	1.81	13.8
ENDOD1	Endonuclease domain-containing 1 protein	1.66	2.64	8.8
CEP44	Centrosomal protein of 44 kDa	1.65	1.67	13.1
CD109	CD109 antigen	1.63	1.41	7.8
MGST3	Microsomal glutathione S-transferase 3	1.62	1.49	43.4
PIGU	Phosphatidylinositol glycan anchor biosynthesis class U protein	1.56	1.37	6.2
PTDSS1	Phosphatidylserine synthase 1	1.53	1.62	8.2
AACS	Acetoacetyl-CoA synthetase	1.52	1.68	10.3
POFUT2	GDP-fucose protein O-fucosyltransferase 2	1.51	1.82	12.1
TNFRSF6	Tumor necrosis factor receptor superfamily member 6	1.50	1.71	17.3
PKN3	Serine/threonine-protein kinase N3	1.50	1.53	12.8
ALG9	Alpha-1,2-mannosyltransferase ALG9	1.50	1.39	20.8
FTL	Ferritin light chain;Ferritin	1.48	2.62	18.9
TOP2A	DNA topoisomerase 2-alpha	1.42	1.33	14.2
HIST1H4H	Histone H4	1.39	3.67	67
RAB2B	Ras-related protein Rab-2B	1.37	2.10	50.5
ACTR5	Actin-related protein 5	1.37	1.44	16.1
GOLPH2	Golgi membrane protein 1	1.35	2.57	8.5
ZNF574	Zinc finger protein 574	1.31	3.27	7.2
HEL-S-5	Aminoacylase-1	1.28	2.60	11.3
PRSS21	Testisin	1.22	1.42	6.6
CHMP3	Charged multivesicular body protein 3	1.22	1.40	12.2
H3F3B	Histone H3	1.21	2.86	52.3
HEL-S-43	Protein S100;	1.19	3.34	73.3
ADGRL2	Latrophilin-2	1.18	1.96	4
FUCA2	Plasma alpha-L-fucosidase	1.16	4.36	6.4
BET1	BET1 homolog	1.16	2.91	24.6
RPRC1	MAP7 domain-containing protein 1	1.12	1.95	13.5
SLC25A15	Mitochondrial ornithine transporter 1	1.12	3.22	10.8
STOM	Erythrocyte band 7 integral membrane protein	1.11	4.02	44.8
BPHL	Valacyclovir hydrolase	1.09	2.00	21.9
CSRP1	Cysteine and glycine-rich protein 1	1.07	1.54	38
BIN1	Myc box-dependent-interacting protein 1	1.05	1.38	8.8
TMX4	Thioredoxin-related transmembrane protein 4	1.02	1.94	8.6

Table 14: Upregulated proteins of whole proteome analysis in VAT-1 KO cells with HEK-293 control cells as a control shown in Figure 37A. (green =proteins involved in cell adhesion and migration matching the criteria $\log_2$ fold change> 1, p-value < 0.05, dark grey = proteins matching the criteria $\log_2$ fold change > 1, p-value < 0.05)

gene names	protein names	$\log_2$ fold change	$-\log_{10} p$ value	coverage [%]
LAMC1	Laminin subunit gamma-1	2.26	1.73	14
LAMB1	Laminin subunit beta-1	1.65	2.44	4
CORO1A	Coronin	1.49	2.21	12.8
COL14A1	Collagen alpha-1(XIV) chain	1.37	1.82	5.7
HEL-S-102	Heat shock protein beta-1	1.28	3.69	60
SSRP1	FACT complex subunit SSRP1	1.04	3.99	33.7
HIST2H3A	Histone H3.2	3.08	2.24	50.7
IMPAD1	Inositol monophosphatase 3	2.23	1.82	15
ERGIC3	Endoplasmic reticulum-Golgi intermediate compartment protein 3	2.16	1.33	16.7
WDR45	WD repeat domain phosphoinositide-interacting protein 4	2.03	2.09	18.7
GALNT7	N-acetylgalactosaminyltransferase 7	1.92	1.68	15.4
NOV	Protein NOV homolog	1.81	2.92	14.9
H1F0	Histone H1.0	1.66	1.74	11.3
HIGD1A	HIG1 domain family member 1A, mitochondrial	1.52	3.70	59
CDC123	Cell division cycle protein 123 homolog	1.52	2.08	18.2
MTMR2	Myotubularin-related protein 2	1.46	1.99	16.8
POFUT2	GDP-fucose protein O-fucosyltransferase 2	1.38	2.85	12.1
GOLPH2	Golgi membrane protein 1	1.36	2.69	8.5
RRM2B	Ribonucleoside-diphosphate reductase subunit M2 B	1.36	1.37	24.5
STOM	Erythrocyte band 7 integral membrane protein	1.36	5.27	44.8
STX6	Syntaxin-6	1.36	1.99	23.5
EEF1D	Elongation factor 1-delta	1.34	1.47	37.8
ENDOD1	Endonuclease domain-containing 1 protein	1.34	2.21	8.8
H3F3B	Histone H3	1.33	3.49	52.3
HMGCS1	Hydroxymethylglutaryl-CoA synthase, cytoplasmic	1.31	5.90	51.7
CLPTM1	Cleft lip and palate transmembrane protein 1	1.31	1.66	10
CHMP3	Charged multivesicular body protein 3	1.30	1.76	12.2
AACS	Acetoacetyl-CoA synthetase	1.27	1.59	10.3
PNMA2	Paraneoplastic antigen Ma2	1.26	1.64	19
HIST1H4H	Histone H4	1.23	3.89	67
FDFT1	Squalene synthase	1.23	3.78	39.6
CSRP1	Cysteine and glycine-rich protein 1	1.21	1.57	38
RRM1	Ribonucleoside-diphosphate reductase	1.21	7.37	62.6
CPD	Carboxypeptidase D	1.19	3.96	13.1
AKT1S1	Proline-rich AKT1 substrate 1	1.11	2.05	19.9
FAR1	Fatty acyl-CoA reductase 1	1.09	1.97	14.8
IRAK1	Interleukin-1 receptor-associated kinase 1	1.07	1.73	10.2
SLC31A1	High affinity copper uptake protein 1	1.06	1.40	18.7
ACAA1	3-ketoacyl-CoA thiolase, peroxisomal	1.06	2.46	25
MARC2	Mitochondrial amidoxime reducing component 2	1.06	2.32	10.1
Nbla03646	Delta(24)-sterol reductase	1.04	3.15	13.1
FUCA2	Plasma alpha-L-fucosidase	1.04	3.70	6.4
SUPT16H	FACT complex subunit SPT16	1.04	4.20	29.3
APBB1	Amyloid beta A4 precursor protein-binding family B member 1	1.03	1.97	15.6
KCNAB2	Voltage-gated potassium channel subunit beta-2	1.03	1.70	18.2
NAGK	N-acetyl-D-glucosamine kinase	1.03	1.36	24.4
PROCR	Endothelial protein C receptor	1.02	5.04	12.2

Taken together, for downregulation of VAT-1, the results were unclear. On the one hand, silencing of VAT-1 by si-RNA resulted in no significant overall changes in the whole proteome, but a slight downregulation of cell migration processes, which is in accordance to the observed reduced anti-migratory phenotype after VAT-1 silencing. However, in case of HEK-293 VAT-1 KO cells, an upregulation of proteins involved in cell adhesion and migration was detected.

The cells can either adapt to a downregulation of the protein by upregulation of other proteins to compensate the function of VAT-1 or by downregulating the processes VAT-1 is involved. As a third scenario, a combination of both adaptions is possible. In case of the HEK-293 VAT-1 KO cells, a reduced anti-migratory phenotype was observed as well as an upregulation of proteins involved in cell adhesion and cell migration. Since VAT-1 is completely knocked-out in these cells, the cells can adapt to the loss of the protein as a long-term effect, which was observed in whole proteome analysis of KO cells. Despite of this adaptive feedback, the migratory phenotype of KO cells was still reduced. In case of si-VAT-1 cells, the short-term silencing might not result in an adaption of the global protein expression levels in contrast to VAT-1 KO cells, while a reduced migration was also observed for downregulation of VAT-1.

One drawback of the comparison between silencing and KO is the difference in the cell lines. Therefore, a VAT-1 KO cell line in breast cancer cells would be beneficial. Since experiments regarding cell migration and proliferation were conducted in breast cancer cells due to their high proliferative and motility phenotype, these cells represent the cell line of choice for whole proteome studies. Nevertheless, the HEK-293 VAT-1 KO cells provide a valuable reference point for observation of the functional compensation of VAT-1 effects by ECM associated proteins. Overall, effects of VAT-1 downregulation on cell adhesion need to be Figured out in future studies for linking the hypothesis generated for **NCA** to the role of VAT-1.

8.

ALTERNATIVE PROTEIN TARGET FOR PROLIFRATION

Since VAT-1 is the target protein of **NCA** responsible for inhibition of cell migration, the target relevant for cell proliferation is still unknown. Therefore, alternative target discovery was approached by labeling in VAT-1 KO cells, which did not yield a new protein target. Further, the more active probe **NC-4** was exploited for target discovery, which also didn't provide an alternative target protein, thus suggesting a non-proteinogenic target to be responsible for inhibition of cell proliferation.

Contents:

8. ALTERNATIVE PROTEIN TARGET FOR PROLIFRATION

As already mentioned in the chapter before, VAT-1 was published to have an effect on cell migration but not on cell proliferation. [69] These data were confirmed by a reduced motility phenotype observed in si-VAT-1 MDA-MB-231 and HEK-293 VAT-1 KO cells while cell proliferation was not affected. In contrast, **NCA** caused a high effect on both cell migration and cell proliferation shown in chapter 2. In ABPP experiments performed with probe **NC- 1**, VAT-1 was the only protein which reproducibly turned out to be the most prominent hit in every volcano plot with sufficient competition by **NCA.** So far, it was proposed that VAT-1 is the only proteinogenic target of **NCA** which was detected by probe **NC-1**. In context to the biological activity of **NCA**, the inhibiton of cell migration mediated by **NCA** can be explained by binding to its proteinogenic target VAT-1, which plays a role in cell migration, whereas the reduced proliferation capacity upon **NCA** treatment might be caused by another molecular target. Consequently, human breast cancer cells were screened for an alternative target protein of **NCA** besides VAT-1 for gaining deeper insights into the impaired cell proliferation. The alternative target profiling was attempted by two different strategies.

8.1. Labeling in VAT-1 KO cells for detection of alternative target

As a frist approach, ABPP in HEK-293 VAT-1 KO cells was considered as a possible strategy for the elucidation of further **NCA** targets, which were not as prominent or as abundant as VAT-1 and therefore arise with an higher enrichment factor in proteomics data after VAT-1 KO. Hence, HEK-293 VAT-1 KO cells were investigated in analytical labeling experiments with probe **NC-1**. In control HEK-293 cells – meaning HEK-293 cells which were subjected to the complete CRISPR-Cas9 procedure but did not result in successful knockout of VAT-1 – and HEK-293 cells, the common VAT-1 labeling pattern was observed for 100 and 500 nM probe **NC-1**. Accordingly, no labeling was detected for the DMSO control. For the VAT-1 KO cells, no fluorescent intensity was detected neither for the probe treated cells nor the control (Figure 38A+B). Consquently, no alternative protein target, which could be the key to pathways linked to **NCA**-mediated inhibition of cell proliferation, popped up on the gel. However, the alternative protein target could be of low abundance and therefore, the intensity on the gels might not be sufficient for a detection.
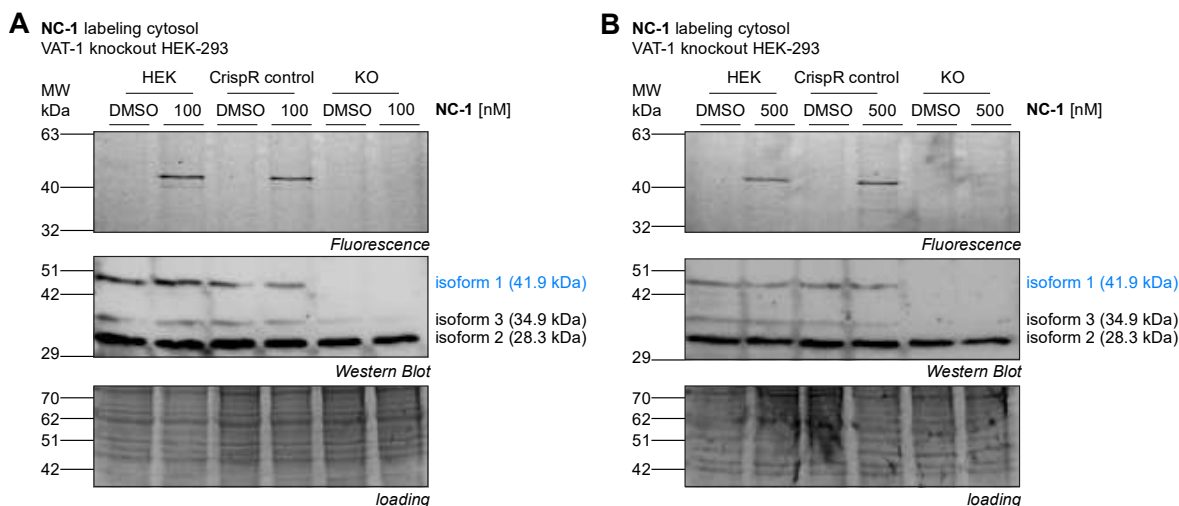
Figure 38: Analytical labeling with probe NC-1 in VAT-1 KO HEK-293 cells. **A,** SDS PAGE and VAT-1 Western blot of analytical labeling with 100 nM of probe **NC-1**. **B,** SDS PAGE and VAT-1 Western blot of analytical labeling with 500 nM of probe **NC-1**.

Consequently, preparative labeling with probe **NC-1** was taken into account for elucidating the alternative proteinogenic target of neocarzilin relevant for inhibition of cell proliferation. Two independent experiments in KO cells were performed (Figure 39A+B). In the first approach, several enriched proteins were detected matching the criteria $\log_2$ enrichment > 1. However, no enriched protein was involved in cell proliferation apart from ZNF503 (Zinc finger protein 503) (Figure 39A). ZNF503 could not be validated as a protein target in the second ABPP approach in KO cells (Figure 39B). Here, only three upregulated proteins were obtained which did not correlate with cell proliferation.

As a control and comparison to breast cancer cells, enrichment was also performed in HEK-293 control cells, in which VAT-1 was again found as the most prominent hit with a high enrichment factor and significance (Figure 39C). Several other proteins were enriched in HEK-293 control cells, which were not detected in MDA-MB-231, probably due to a difference between the cell lines. Since the other upregulated proteins were not detected in MDA-MB-231, these proteins were discarded for further analysis due to low reproducibility. Nevertheless, VAT-1 was the only reproducible hit which was observed for both cell lines.

To sum up, no reproducible protein target was detected in VAT-1 KO cells and VAT-1 was again revealed as the most prominent hit in HEK-293 cells. However, since the effects on cell proliferation were detected in MDA-MB-231 but not in HEK-293 cells, the difference of protein expression levels between the cell lines can be a reason that no alternative protein target for cell proliferation was detected. For detection of an alternative target, preparative labeling in a VAT-1 KO cells established in breast cancer cells could be considered. Consequently, creation of a stable VAT-1 KO clone in a breast cancer cells would be beneficial for elucidation of the mode of action of **NCA** in regard to cell proliferation.
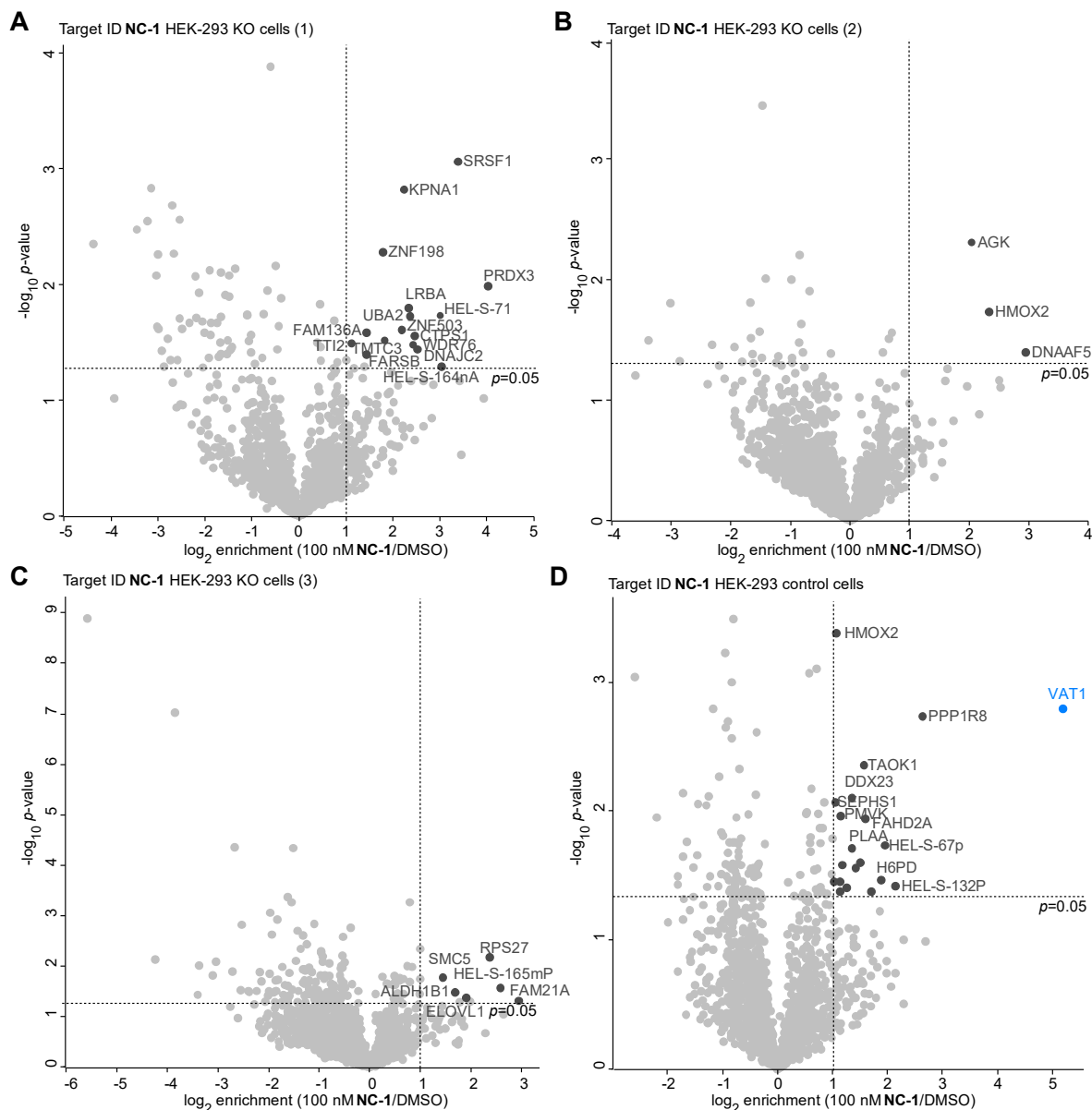
Figure 39: Target ID of probe NC-1 in VAT-1 KO cells. A, Volcano plot of *in situ* LFQ ABPP experiment with 100 nM **NC-1** in HEK-293 VAT-1 KO cells (n=3). Hits matching the criteria log$_2$ enrichment > 1, *p*-value < 0.05 are highlighted in dark grey. **B,** Volcano plot of *in situ* LFQ ABPP experiment with 100 nM **NC-1** (n=3) in HEK-293 VAT-1 KO cells. Hits matching the criteria log$_2$ enrichment > 1, *p*-value < 0.05 are highlighted in dark grey. **C,** Volcano plot of *in situ* LFQ ABPP experiment with 100 nM **NC-1** (n=4) in HEK-293 VAT-1 KO cells. Hits matching the criteria log$_2$ enrichment > 1, *p*-value < 0.05 are highlighted in dark grey. **D,** Volcano plot of *in situ* LFQ ABPP experiment with 100 nM **NC-1** (n=3) in HEK-293 control cells. Hits matching the criteria log$_2$ enrichment > 1, *p*-value < 0.05 are highlighted in dark grey and target protein VAT-1 is shown in blue-

Table 15: Significantly enriched proteins from **NC-1** target ID in VAT-1 KO cells shown in Figure 39A- C with corresponding $\log_2$ enrichment and significance. (dark grey = proteins matching the criteria $\log_2$ enrichment > 1, p-value < 0.05).

gene names	protein names	log₂ fold change	-log₁₀ p-value	coverage [%]
Target ID (100 nM NC-1/DMSO) HEK-293 VAT-1 KO cells Figure **39A**				
PRDX3	Thioredoxin-dependent peroxide reductase, mit.	4.03	1.98	20.7
SRSF1	Serine/arginine-rich splicing factor 1	3.38	3.06	16.5
HEL-S-71	Ubiquitin-conjugating enzyme E2 N	3.00	1.73	19.1
DNAJC2	DnaJ homolog subfamily C member 2 C member 2, N-terminally processed	2.52	1.44	4.5
CTPS1	CTP synthase 1	2.46	1.55	9.8
WDR76	WD repeat-containing protein 76	2.43	1.48	7.9
UBA2	SUMO-activating enzyme subunit 2	2.37	1.73	16.1
LRBA	Lipopolysaccharide-responsive and beige-like anchor protein	2.33	1.80	7.1
KPNA1	Importin subunit alpha;Importin subunit alpha-5	2.24	2.82	11.9
ZNF503	Zinc finger protein 503	2.19	1.61	5.3
TMTC3	Transmembrane and TPR repeat-containing protein 3	1.82	1.51	4.9
ZNF198	Zinc finger MYM-type protein 2	1.79	2.28	8.4
FAM136A	Protein FAM136A	1.44	1.58	10.2
FARSB	Phenylalanine–tRNA ligase beta subunit	1.43	1.39	20.2
PCCB	Propionyl-CoA carboxylase beta chain, mitochondrial	1.39	1.29	17.2
TTI2	TELO2-interacting protein 2	1.12	1.49	9.4
HEL-S-164nA	Neutral alpha-glucosidase AB	1.00	1.35	21.3
Target ID (100 nM NC-1/DMSO) HEK-293 VAT-1 KO cells Figure **39B**				
DNAAF5	Dynein assembly factor 5, axonemal	2.96	1.39	5.6
HMOX2	Heme oxygenase 2	2.34	1.73	28.2
AGK	Acylglycerol kinase, mitochondrial	2.05	2.31	8.4
Target ID (100 nM NC-1/DMSO) HEK-293 VAT-1 KO cells Figure **39C**				
FAM21A	WASH complex subunit FAM21C	2.94	1.31	7.2
HEL-S-165mP	Alcohol dehydrogenase [NADP(+)]	2.59	1.56	17.5
RPS27	40S ribosomal protein S27	2.38	2.18	39.3
PYGB	Alpha-1,4 glucan phosphorylase	1.99	1.30	14.3
ELOVL1	Elongation of very long chain fatty acids protein 1	1.91	1.37	9
ALDH1B1	Aldehyde dehydrogenase X, mitochondrial	1.69	1.48	16.4
SMC5	Structural maintenance of chromosomes protein 5	1.45	1.77	4.4

Table 16: Significantly enriched proteins from **NC-1** target ID in HEK-293 control cells shown in Figure 39D with corresponding $\log_2$ enrichment and significance. (blue = **NC-1** target protein, dark grey = proteins matching the criteria $\log_2$ enrichment > 1, p-value < 0.05).

gene names	protein names	log₂ fold change	-log₁₀ p-value	coverage [%]
VAT1	Synaptic vesicle membrane protein VAT-1 homolog	5.19	2.79	41
PPP1R8	Nuclear inhibitor of protein phosphatase 1	2.63	2.74	17.1
HEL-S-132P	14 kDa phosphohistidine phosphatase	2.14	1.42	36.8
HEL-S-67p	Protein deglycase DJ-1	1.96	1.73	31.2
H6PD	GDH/6PGL endoplasmic bifunctional protein	1.88	1.47	5
PGAM1	Phosphoglycerate mutase	1.71	1.38	42.9
FAHD2A	Fumarylacetoacetate hydrolase domain-containing protein 2A	1.61	1.94	26.1
TAOK1	Serine/threonine-protein kinase TAO1	1.57	2.35	8.2
YARS2	Tyrosine–tRNA ligase, mitochondrial	1.51	1.60	13.4
ALDH6A1	Methylmalonate-semialdehyde dehydrogenase, mit.	1.43	1.56	21.5
DDX23	Probable ATP-dependent RNA helicase DDX23	1.36	2.10	18.6
PLAA	Phospholipase A-2-activating protein	1.35	1.71	12.2
PGM3	Phosphoacetylglucosamine mutase	1.26	1.40	16.2
ANXA7	Annexin	1.18	1.58	14
PMVK	Phosphomevalonate kinase	1.15	1.96	15.1
SART3	Squamous cell carcinoma antigen recognized by T-cells 3	1.14	1.45	26.4
HEL-S-49	Triosephosphate isomerase	1.14	1.38	73.5
HMOX2	Heme oxygenase 2	1.07	3.38	30.6
SEPHS1	Selenide, water dikinase 1	1.06	2.07	24
TLK2	Serine/threonine-protein kinase tousled-like 2	1.03	1.45	7.5

| TFIP11 | Tuftelin-interacting protein 11 | 1.00 | 1.78 | 15.4 |
| VRK1 | Serine/threonine-protein kinase VRK1 | 0.99 | 1.51 | 25 |

8.2. Labeling with probe **NC-4** in breast cancer cells

To avoid discrepancies caused by application of different cell lines, the second approach for detection of the alternative target of **NCA** relevant for the anti-proliferative phenotype is focused on MDA-MB-231. As mentioned in chapter 2, a new probe which is structurally closely related to **NCA** was designed, termed **NC-4**. The probe displayed a high activity in MTT assays. As **NC-4** showed a more pronounced reduction of the metabolic activity of cancer cells than **NC-1**, it might be more beneficial for target profiling studies. But the effects of the probe on cell proliferation and migration still need to be determined for evaluation of its suitability to screen targets responsible for inhibition of proliferation or cell migration. Nevertheless, **NC-4** was tested in first ABPP approaches for the detection of the alternative target protein in concentrations below the IC_{50} in MTT assays (460 nM).

Hence, **NC-4** was applied *in situ* in MDA-MB-231 for analytical and preparative labeling. As shown in Figure 40, **NC-4** was very selective for VAT-1 labeling at a concentration range of 10 – 50 nM. However, more proteins are labeled by the probe at 100 and 500 nM probe concentration compared to **NC-1** at corresponding concentrations. For identification of further target proteins by MS, 50 nM and 100 nM were chosen as suitable concentrations for preparative labeling approaches. The results show that **NC-4** is more reactive than **NC- 1** at similar concentrations, which accordingly goes along with a higher bioactivity observed in MTT assays compared to **NC-1**.
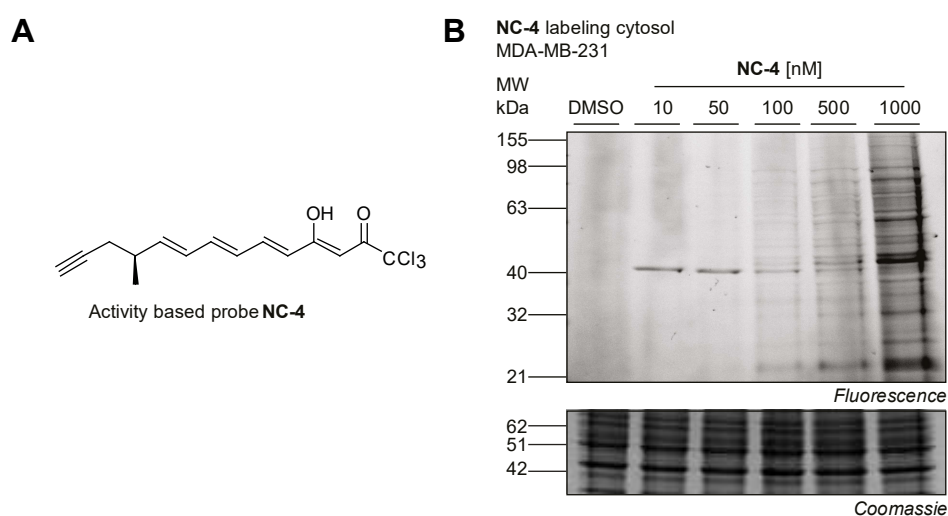
Figure 40: Analytical labeling with probe NC-4. A, Chemical structure of probe **NC-4**. **B,** SDS-PAGE of analytical labeling in MDA-MB-231 for 1 h.

Preparative ABPP was first conducted with 100 nM **NC-4** and a 5-fold access of **NCA** for competition approach. As shown in Figure 41A, VAT-1 was again revealed as prominent hit according to the labeling results on the gel. Several other proteins were enriched matching the criteria $\log_2$ enrichment > 1 and significance of $p < 0.05$. These hits were tested regarding sufficient competition caused by **NCA** binding (Figure 41B). Competition was only revealed for VAT-1, HMOX2 and ELMSAN1, which were also found as hits in the enrichment experiments. The other hits which were upregulated in the competition experiment did not turn out as hits in the enrichment experiment (Figure 41A) and were therefore excluded for possible alternative targets. Competition was also observed for HMOX2 in some **NC-1** based approaches shown in chapter 4, however, it is a highly abundant protein which is often targeted by electrophilic probes and was thus neglected as target protein.[189] ELMSAN1 (ELM2 and SANT domain-containing protein 1)[190] has a DNA binding transcription factor activity but is not linked to the GO term *cell proliferation*. However, the protein was not found amongst hits in the ABPP experiments performed with **NC-1**. For **NC-1**, only slight inhibition of cell proliferation was observed. In case of a higher activity of **NC-4** regarding cell proliferation, which is expected due to the higher activity in MTT assays, the probe would be more appropriate for detection of the target protein involved in cell proliferation. Therefore, it is either suggested that ELMSAN1 is the target protein of **NCA** relevant for the anti-proliferative phenotype which can only be detected by a more active probe than **NC-1** such as **NC-4** or ELMSAN1 is no reproducible target of **NCA**. For deeper insights, concentration dependent labeling with probe **NC-4** was applied.
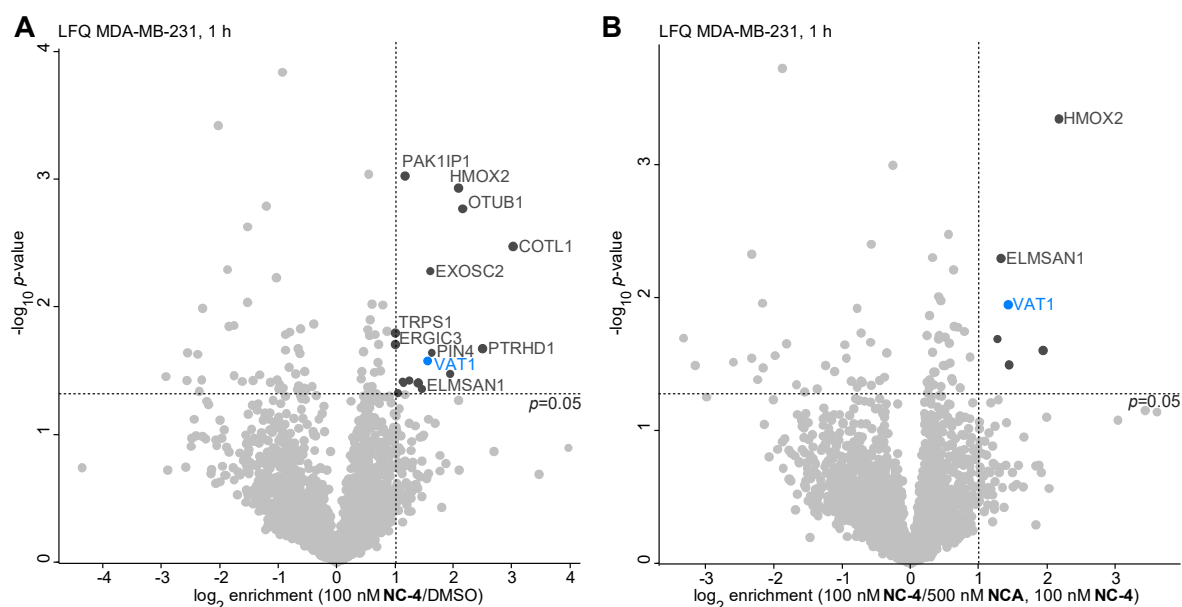
Figure 41: Target ID of probe NC-4 in MDA-MB-231. A, Volcano plot of *in situ* LFQ ABPP experiment with 100 nM **NC-4** (n=4). Hits matching the criteria $\log_2$ enrichment > 1, *p*-value < 0.05 are indicated and highlighted in dark grey and target protein VAT-1 is shown in blue. **B,** Volcano plot of *in situ* competitive LFQ ABPP experiment with 500 nM **NCA** and 100 nM **NC-4** (n=4). Hits matching the criteria $\log_2$ enrichment > 1, *p*- value < 0.05 are highlighted in dark grey and target protein VAT-1 is shown in blue. Enriched proteins from the target ID in **A** which are relevant for competition are indicated, remaining hits are only listed in Table 17.

Table 17: Significantly enriched proteins from **NC-4** target ID and competition experiment shown in Figure 41A+B with corresponding $\log_2$ enrichment and significance. (blue = **NC-1** target protein, dark grey = proteins matching the criteria $\log_2$ enrichment > 1, p- value < 0.05).

gene names	protein names	$\log_2$ fold change	$-\log_{10}$ p-value	coverage [%]
Target ID (100 nM NC-4/DMSO)				
COTL1	Coactosin-like protein	3.03	2.47	21.9
PTRHD1	Putative peptidyl-tRNA hydrolase PTRHD1	2.50	1.67	20.7
OTUB1	Ubiquitin thioesterase OTUB1	2.16	2.77	8.7
HMOX2	Heme oxygenase 2	2.08	2.93	20.1
BOD1L1	Biorientation of chromosomes in cell division protein 1-like 1	1.95	1.48	2.8
PIN4	Peptidyl-prolyl cis-trans isomerase NIMA-interacting 4	1.63	1.64	16
EXOSC2	Exosome complex component RRP4	1.61	2.28	13.3
VAT1	Synaptic vesicle membrane protein VAT-1 homolog	1.56	1.58	31
FNDC3A	Fibronectin type-III domain-containing protein 3A	1.45	1.36	7.3
GPRC5C	G-protein coupled receptor family C group 5 member C	1.41	1.40	7.9
ZW10	Centromere/kinetochore protein zw10 homolog	1.25	1.43	7.1
PAK1IP1	p21-activated protein kinase-interacting protein 1	1.17	3.03	5.9
RASA3	Ras GTPase-activating protein 3	1.15	1.40	4.3
ELMSAN1	ELM2 and SANT domain-containing protein 1	1.13	1.42	8.2
UGP2	UTP–glucose-1-phosphate uridylyltransferase	1.05	1.33	33.7
ERGIC3	Endoplasmic reticulum-Golgi intermediate compartment protein 3	1.01	1.71	17.2
TRPS1	Zinc finger transcription factor Trps1	1.01	1.80	3.3
competition (100 nM NC-4/500 nM NCA, 100 nM NC-4)				
HMOX2	Heme oxygenase 2	2.18	3.34	20.1
DAD1	Dolichyl-diphosphooligosaccharide–protein glycosyltransferase subunit DAD1	1.95	1.60	41.2
FOSL2	Fos-related antigen 2	1.45	1.49	14.9
VAT1	Synaptic vesicle membrane protein VAT-1 homolog	1.43	1.94	31
ELMSAN1	ELM2 and SANT domain-containing protein 1	1.32	2.29	8.2
MYADM	Myeloid-associated differentiation marker	1.27	1.69	18.9

For confirmation of ELMSAN1 as the alternative target of **NCA**, further enrichments with probe **NC-4** in a concentration dependent manner were performed, since concentration dependent output is very informative for target discovery.

Labeling was performed with 50 and 100 nM of **NC-4** for 1 h in MDA-MB-231 shown in Figure 42A+B. For 50 nM probe concentration, several proteins were found as enriched hits matching the criteria of $\log_2$ enrichment > 1 and a significance of p < 0.05. VAT-1 was again detected among the enriched proteins with the highest enrichment factor. Several other proteins were detected as hits, however, without correlation to cell proliferation or unknown function. Further, ELMSAN1, which was obtained as significant hit with sufficient competition in Figure 41A and B was not found among enriched proteins (Figure 42A).

This is the same case for a probe concentration of 100 nM **NC-4**, which was already applied in Figure 41A (Figure 42B). Further, the volcano plot for 100 nM **NC-4** shows a reduced number of enriched proteins compared to 50 nM **NC-4**. The volcano plot obtained for 100 nM **NC-4** is not comparable to that in Figure 41A with the same probe concentration, since the protein identification for these raw files was not as good as before. Therefore, some protein hits might be missing. However, VAT-1 was among the three enriched proteins, showing again, that it displays a highly reproducible target of **NC-4** (Figure 42B). Sufficient competition was only revealed for VAT-1, since the second enriched protein in

the competition volcano plot was not found among overrepresented proteins in Figure 41B (Figure 42C). In Figure 42D, the intensity profile of VAT-1 shows a comparable intensity for 50 nM and 100 nM probe **NC-4**, whereas the intensity was reduced for the competition samples and the DMSO control.

The fact that ELMSAN1 was detected neither for 50 nM nor 100 nM **NC-4** probe concentration points to a background protein which only popped up once as a target protein. In contrast, VAT-1 was enriched in each volcano plot independently of the identification performance and showed sufficient competition. Nevertheless, it would make sense to repeat labeling with 100 nM **NC-4** probe concentration, since the protein identification and the raw files were not comparable to these shown in Figure 40.
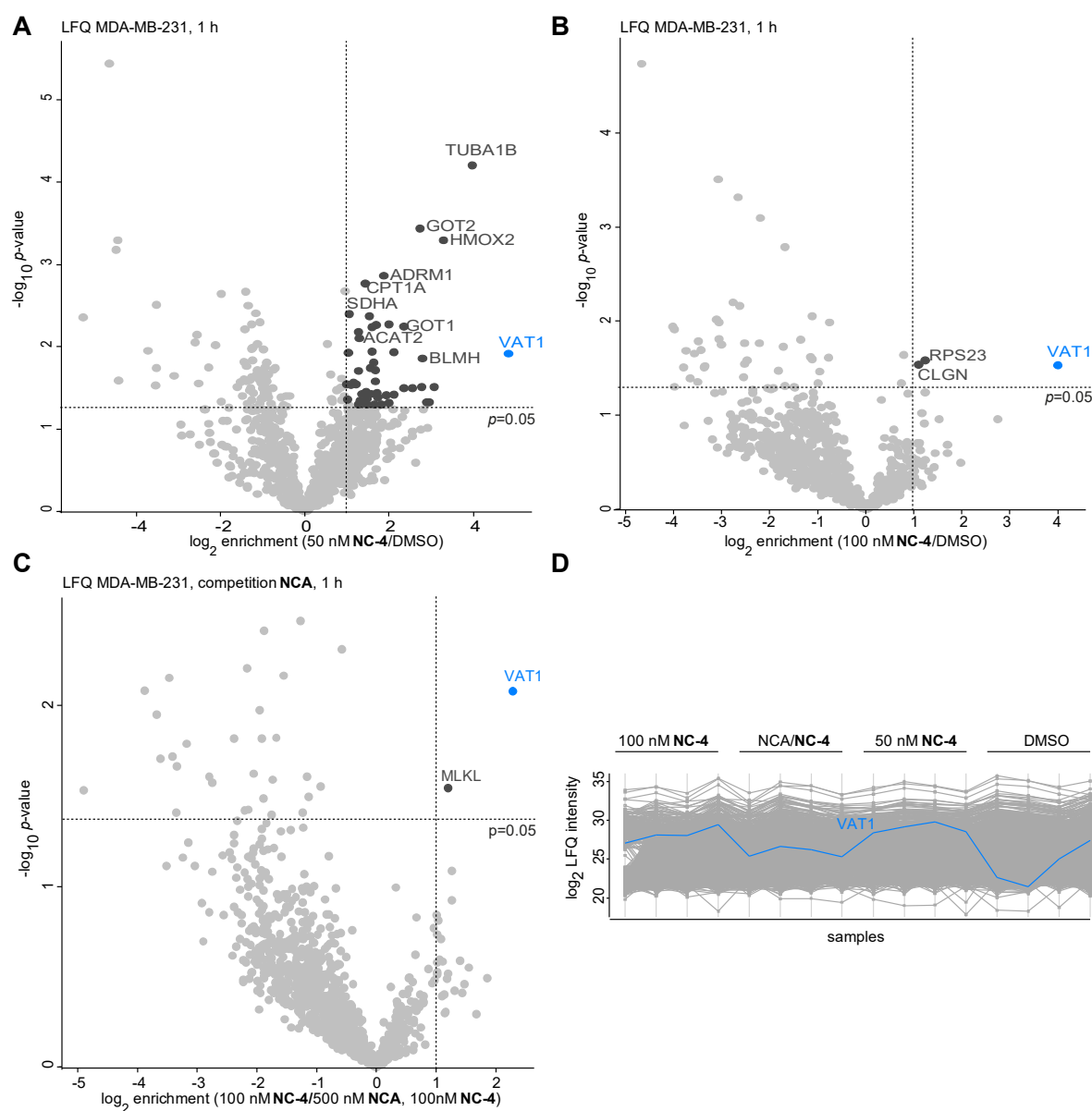
Figure 42: Concentration dependent target ID of probe NC-4 in MDA-MB-231. A, Volcano plot of *in situ* LFQ ABPP experiment with 50 nM **NC-4** (n=4). **B**, Volcano plot of *in situ* LFQ ABPP experiment with 100 nM **NC-4** (n=4). **C,** Volcano plot of *in situ* competitive LFQ ABPP experiment with 500 nM **NCA** and 100 nM **NC-4** (n=4). **A-C,** Hits matching the criteria $\log_2$ enrichment > 1, *p*-value < 0.05 are highlighted in dark grey and target protein VAT-1 is shown in blue. **D,** Profile plot of $\log_2$ intensities over all samples. VAT-1 is shown in blue.

Table 18: Significantly enriched proteins from **NC-4** concentration-dependent target ID and competition experiment in MDA- MB-231 shown in Figure 42A-C with corresponding log$_2$ enrichment and significance. (blue = **NC-1** target protein, dark grey = proteins matching the criteria log$_2$ enrichment > 1, *p*- value < 0.05).

gene names	protein names	log$_2$ fold change	- log$_{10}$ *p*-value	coverage [%]
Target ID (50 nM NC-4/DMSO)				
VAT1	Synaptic vesicle membrane protein VAT-1 homolog	4.82	1.92	31
TUBA1B	Tubulin alpha-1B chain	3.97	4.21	46.9
HMOX2	Heme oxygenase 2	3.28	3.30	29.3
RNPEP	Aminopeptidase B	3.07	1.51	17.3
COPS4	COP9 signalosome complex subunit 4	2.94	1.33	20
NUDC	Nuclear migration protein nudC	2.88	1.33	15.7
BLMH	Bleomycin hydrolase	2.79	1.86	9.1
MBOAT7	Lysophospholipid acyltransferase 7	2.76	1.51	7
GOT2	Aspartate aminotransferase mitochondrial	2.74	3.44	8.9
KNS2	Kinesin light chain 1	2.55	1.49	16.8
GOT1	Aspartate aminotransferase, cytoplasmic	2.36	2.25	28.6
DNAJC3	DnaJ homolog subfamily C member 3	2.35	1.49	5.3
PTPN23	Protein-tyrosine-phosphatase	2.11	1.93	8.7
EPS15L1	Epidermal growth factor receptor substrate 15-like 1	2.11	1.42	14
NSF	Vesicle-fusing ATPase	1.99	1.31	18
CAPRIN1	Caprin-1	1.98	2.27	8.4
LMO7	LIM domain only protein 7	1.92	1.41	6.6
ADRM1	Proteasomal ubiquitin receptor ADRM1	1.87	2.87	10.6
ARHGAP1	Rho GTPase-activating protein 1	1.82	1.30	16.2
USP9X	Probable ubiquitin carboxyl-terminal hydrolase FAF-X	1.73	1.38	3.9
SMARCA4	Transcription activator BRG1	1.70	1.43	6.2
BAIAP2	Brain-specific angiogenesis inhibitor 1-associated protein 2	1.69	2.27	8.6
PMPCA	Mitochondrial-processing peptidase subunit alpha	1.68	1.72	11.6
NUP153	Nuclear pore complex protein Nup153	1.68	1.58	9.4
ARF4	ADP-ribosylation factor 4	1.66	1.30	41.7
PPFIBP1	Liprin-beta-1	1.63	1.81	6.8
SMCHD1	Structural maintenance of chromosomes flexible hinge domain-containing protein 1	1.60	2.23	4.3
GBE1	1,4-alpha-glucan-branching enzyme	1.59	1.94	13.5
SUGT1	Suppressor of G2 allele of SKP1 homolog	1.58	1.43	11.8
BAT3	Large proline-rich protein BAG6	1.56	1.74	5
PLRG1	Pleiotropic regulator 1	1.52	2.37	10.3
DDX18	ATP-dependent RNA helicase DDX18	1.48	1.37	11.9
LRBA	Lipopolysaccharide-responsive and beige-like anchor protein	1.47	1.30	2.2
TES	Testin	1.46	1.45	12.4
CPT1A	Carnitine O-palmitoyltransferase 1, liver isoform	1.43	2.77	4.4
PRRC2C	Protein PRRC2C	1.42	1.33	3.9
SWAP70	Switch-associated protein 70	1.36	1.43	24
ANLN	Actin-binding protein anillin	1.32	1.34	4.1
ACAT2	Acetyl-CoA acetyltransferase, cytosolic	1.30	2.11	11.8
ISG15	Ubiquitin-like protein ISG15	1.28	2.18	9.7
UBE1L2	Ubiquitin-like modifier-activating enzyme 6	1.28	1.71	14.8
SEC61B	Protein transport protein Sec61 subunit beta	1.28	1.30	41.7
RPS23	40S ribosomal protein S23	1.22	1.54	29.4
PYGL	Alpha-1,4 glucan phosphorylase	1.15	1.56	24.3
EPRS	Bifunctional glutamate/proline–tRNA ligase	1.10	1.54	14.5
SDHA	Succinate dehydrogenase [ubiquinone] flavoprotein subunit, mitochondrial	1.05	2.40	11.1
HCTP4	Targeting protein for Xklp2	1.04	1.92	6.9
EIF4G1	Eukaryotic translation initiation factor 4 gamma 1	1.00	1.36	7.8
COPA	Coatomer subunit alpha	1.00	1.55	13.5
Target ID (100 nM NC-4/DMSO)				
VAT1	Synaptic vesicle membrane protein VAT-1 homolog	4.00	1.53	31
CLGN	Calmegin	1.10	1.54	7
RPS23	40S ribosomal protein S23	1.23	1.58	29.4
Competition (100 nM NC-4/500 nM NCA, 100 nM NC-4)				
VAT-1	Synaptic vesicle membrane protein VAT-1 homolog	2.27	2.08	31
MLKL	Mixed lineage kinase domain-like protein	1.19	1.55	5.4

As a conclusion, labeling with the more active probe **NC-4** in breast cancer cells did not provide a reproducible protein hit except VAT-1. For identification of the target protein responsible for cell proliferation, the two valuable approaches described in this chapter could be combined, meaning that **NC-4** is applied in HEK-293 VAT-1 KO cells. Further, a higher concentration of **NC-4** such as 500 nM could be applied for preparative labeling. One reason for the unsuccessful detection of further targets of **NCA** could be explained by the fact that **NCA** causes the effects on cell proliferation by a non-proteinogenic target. For example, it can provoke effects on cell proliferation by interfering with DNA similar to neocarzinostatin, which is produced by the same organism, namely *Streptomyces carzinostaticus*. This suggestion would be supported by the fact that several natural products from *Streptomyces* cause DNA damages resulting in a high cytotoxicity.[37, 49]

9.

CONCLUSION AND OUTLOOK

9. CONCLUSION AND OUTLOOK

The cytotoxic natural product **NCA** was discovered decades ago, however, it has been neglected for several years. Therefore, its potent anti-migratory potential has been overlooked until now.

In this thesis, a proteome wide ABPP approach in the human breast cancer cell line MDA-MB-231 enabled the identification of covalent targets of this polyenone natural product. SILAC as well as LFQ were applied to elucidate cellular targets of a neocarzilin probe bearing an alkyne tag (**NC-1**). The most confident target, synaptic vesicle membrane protein VAT-1 homolog (VAT-1), previously found in the cell line HepG2, was confirmed in the breast cancer cell line MDA-MB-231.[54] Further, a high specificity of **NCA** to its largely uncharacterized target VAT-1 was revealed by competitive approaches, therefore making it an interesting subject to study for further biochemical characterization. The discovery of the target protein of the previously unexplored natural product **NCA** illustrate the power of chemical proteomics approaches.

While the binding mode and the exact binding site **of NCA** was not identified, a proteomics approach for active-site peptide profiling detected a peptide unique for isoform 1 of VAT-1 as the possible site for **NCA** binding. Mutagenesis of the nucleophilic residues of this peptide suggest E113 to be involved in binding. Future studies involving co-crystallization will be performed for confirmation of the binding site. Since VAT-1 has already been crystallized recently, a co-crystal structure with **NCA** will be more easily accessible now.[70]

With derivatives of **NCA** in hand, we investigated the effects on human cancer cells in regard to cell proliferation and cell adhesion. The trichloromethyl group and the stereocenter at C11 position were detected to be crucial for neocarzilin activity. It was found that both migration and proliferation were diminished upon neocarzilin treatment, while **NCA** was the most active compound of the neocarzilin family. Only **NCA** exhibited a strong binding to the target protein VAT-1 accompanied by inhibition of cell migration. Further, it was demonstrated that **NCA** enhances cell adhesion by activation of integrins. This led to the hypothesis that the detachment of the cells is disturbed, which causes a disruption of cell migration. However, no relevant changes in expression levels of proteins involved in cell adhesion were revealed in a global proteome analysis. In case of VAT-1, which has been linked to cell migration in a previous study,[69] silencing or KO of the protein established in HEK-293 cells by CRISPR/Cas resulted in a diminished cell migration, while cell proliferation was unaffected. Therefore, VAT-1 targeting turned out to be responsible for

only the anti-migratory, but not the anti-proliferative effect of **NCA**. In relation to this, overexpression of VAT-1 in human cells resulted in an upregulation of proteins involved in cell adhesion and migration. Accordingly, VAT-1 silencing caused a downregulation of proteins involved cell adhesion and migration. In contrast, VAT-1 KO provoked an upregulation of ECM components and cell adhesion proteins, suggesting a feedback loop for a functional compensation of VAT-1.

For deeper insights, co-IP approaches to detect the role of VAT-1 in cell migration revealed VAT-1 to be part of an intricate network of proteins associated with cell adhesion. Strikingly, TLN1 was found to be a direct interaction partner of VAT-1 both by MS-based co-IP experiments as well as by immunoblotting. TLN1 is one of the key proteins involved in activating integrin signaling, mediating linkage of integrins to the cytoskeleton, formation of focal adhesions and subsequently promoting migration.[169] Western blot analysis indicate that treatment of the cells with **NCA** seemed to enhance the interaction between VAT-1 and TLN1, which would confirm the hypothesis of an enhanced cell adhesion resulting in a diminished migration. However, proteomics results did not support these findings. Despite of these fascinating insights, further extensive studies need to be carried out to detect the function of this interaction within the cell adhesion network on a molecular level.
The observed inhibition of cell migration by enhancement of cell adhesion mediated by **NCA** suggests that the VAT-1 function in cell adhesion is increased by **NCA** instead of inhibited. The role of VAT-1 in cell adhesion needs to be clarified by investigation of integrin activation in si-VAT-1 cells or breast cancer cells with a corresponding VAT-1 KO.

Notably, no other proteins were revealed as significant, reproducible targets of probe **NC-1** proposing that the probe design lacking the methyl-stereocenter at C11 position of **NCA** may have lost affinity for the targets responsible for the anti-proliferative effects. The importance of this stereocenter was confirmed by synthesis of **NCA**' bearing the opposite absolute configuration resulting in a drop of potency. Consequently, another probe which is highly similar to **NCA** bearing the corresponding stereocenter, termed **NC-4**, was applied for profiling of the protein target responsible for inhibition of cell proliferation. However, proteomics analysis did not yield a reproducible target protein which showed sufficient competition. Moreover, labeling with **NC-1** in VAT-1 KO cells was performed for detection of alternative targets, which are less abundant than VAT-1. Again, no protein target linked to cell proliferation was identified. Thus, it is suggested that a non-proteinogenic target might be responsible for inhibition of cell proliferation. Nevertheless, in case of a protein-target relevant for inhibition of cell proliferation, further strategies such as **NC- 4** labeling in HEK-

293 VAT-1 KO cells or the generation of breast cancer VAT-1 KO cells for alternative target profiling will be applied.

An application of small molecules for inhibition of migration would be a breakthrough in cancer therapy, since over 90% of all cancer deaths are related to the formation of metastases.[141] VAT-1 might be an attractive new target for future anti-metastatic drugs since it was identified as a so far unknown player involved in regulation of cell migration. Therefore, further studies should be carried out to elucidate the function of VAT-1 and VAT-1 dependent signaling pathways. In conclusion, VAT-1 is presented as a novel drug target candidate for the prevention of cell migration and thereby metastasis.
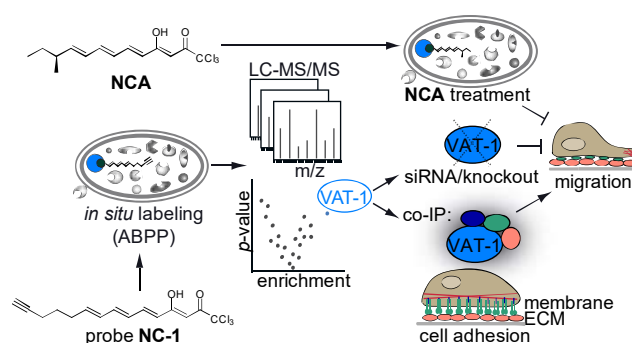
Figure 43: Conclusion of the project: VAT-1 was identified as cellular target protein of the anti-migratory natural product neocarzilin A (**NCA**) by a chemical proteomics ABPP approach and its molecular function was linked to cell adhesion. Adapted from Gleissner *et al.* [134]

10.

EXPERIMENTAL SECTION

10. EXPERIMENTAL SECTION

10.1 Materials

10.1.1 Chemicals

Table 19: Chemicals

chemical	acronym	catalog ID/Lot	manufacturing company
Accutase		A6964	Sigma Aldrich
Agarose		11404	Serva
Agar-Agar		5210.2	Carl Roth
azide-PEG$_3$-biotin		AZ104P4	Jena Bioscience
2-Mercaptoethanol		4227.1	Carl Roth
3-(4,5-Dimethylthiazol-2-yl)-2,5-diphenyltetrazoliumbromide	MTT	M2128	Sigma Aldrich
4-(2-Hydroxyethyl)-1-piperazineethanesulfonic acid	Hepes	HN78.3	Carl Roth
Acetic acid		3738.1	Carl Roth
Acetonitrile	MeCN	Lot 1557305	Fisher Chemical
Acetone		Lot 1668626	Fisher Chemical
Ampicillin	Amp	K029.5	Carl Roth
Avidin Agarose		A9207	Sigma Aldrich
BenchMark™ Fluorescent Protein Standard		LC5928	Invitrogen
Bromphenol blue		18030	Sigma Aldrich
Calcium chloride	CaCl$_2$	2387	
DharmaFECT (Dharmacon)			GE Healthcare
Desthiobiotin-PEG3-Azide		902020	Sigma Aldrich
Dimethylsulfoxid	DMSO	41647	Sigma Aldrich
Disodium hydrogen phosphate	Na$_2$HPO$_4$	P030.1	Carl Roth
Dithiothreitol	DTT	43819	Sigma Aldrich
DNA marker 1 kbp			Carl Roth
Dulbecco's Modified Eagle's Medium (high glucose)	DMEM	D5671	Sigma Aldrich
Dulbecco's Modified Eagle's Medium SILAC		A14431-01	Gibco Life Technologies
Ethanol	EtOH	32205	Sigma Aldrich
Ethylenediaminetetraacetic acid	EDTA	8043.2	Carl Roth
Fetal bovine serum	FBS	F0804	Sigma Aldrich
Formic acid	FA	94318	Sigma Aldrich
Glycerol		3783.1	Carl Roth
Hydrochloride	HCl	4525.1	Carl Roth
Glycine		3790.2	Carl Roth
Imidazole		3899.3	Carl Roth
Iodoacetamide	IAA	I6125	Sigma Aldrich
Isopropyl-β-D-1-thiogalacto-pyranoside	IPTG	CN08.3	Carl Roth
LB		X968	Carl Roth
L-Glutamine		G7513	Sigma Aldrich
Lipofectamine ™ 3000		L3000015	Thermo Fisher Scientific
Magnesium chloride	Mg$_2$Cl	2189.1	Carl Roth
Methanol	MeOH	83638	VWR
Milk powder		T145.3	Carl Roth
NP-40 Alternative		492016	Calbiochem
Non targeting (nt) siRNA (Dharmacon)			GE Healthcare
OpiMEM Medium		11520386	Fisher Scientific
Peptone		8986.2	Carl Roth
Phosphoenolpyruvate	PEP	B20358	Alfa Aesar
Potassium chloride	KCl	6781.1	Carl Roth
Potassium dihydrogen phosphate	KH$_2$PO$_4$	26930	VWR

Protein A/G Agarose		Lot QL227149	Thermo Scientific
Roti®-Mark STANDARD		T851.2	Carl Roth
Rotiphosphorese		3029.1	Carl Roth
Roswell Park Memorial Institute (RPMI) 1640 Medium		R0883-500ML	Sigma Aldrich
Serva Pink Color Protein Standard II		Lot 150047	Serva
Si-VAT-1 (Dharmacon)			GE Healthcare
SOB medium		AE27.1	Carl Roth
Sodium chloride	NaCl	27810295	VWR
Sodium deoxycholate		D6750	Sigma Aldrich
Sodium dodecylsulfate	SDS	CN30.3	Carl Roth
Sodium hydroxide	NaOH	6771.2	Carl Roth
Sulfo-cyanine3 tetrazine		113E0	Lumiprobe
Sypro Orange		S6651	Life Technologies
5-Rh-azide		7807.3	Carl Roth
Tetramethylethylendiamine	TEMED	2367.1	Carl Roth
Thiourea		T7875	Sigma Aldrich
Triethylammoniumbicarbonate	TEAB	17902	Sigma Aldrich
Trifluoroacetic acid	TFA	302031	Sigma
Tris(2-carboxyethyl)phosphine	TCEP	HN95.2	Carl Roth
Tris(hydroxymethyl)-aminomethane hydrochloride	Tris-HCl	9090.3	Carl Roth
Trizma		T1503	Sigma Aldrich
Trypan blue		CN76.1	Carl Roth
Urea		2317.1	Carl Roth
Water		Lot 1683664	Fisher Chemical
Yeast extract		2363.2	Carl Roth

10.1.2. Enzymes and Antibodies

Table 20: Enzymes and Antibodies

enyzmes/antibodies	catalog ID	manufacturing company
Anti-Rabbit Poly-HRP (goat)	32260	Thermo Fisher Scientific
Anti-Mouse Poly-HRP (goat)	32230	Thermo Fisher Scientific
Anti-VAT-1 Homolog (*T. californica*) (C-term) antibody	ABIN2443750	Antibodies online
Anti VAT-1 (E7)	sc-515705	Santa Cruz
Anti- TLN1 (TA-205)	NBP1-21642	Novusbio
Anti- TLN1	MAB1676	Merck
Anti-Fibronectin-1	ab2413	Abcam
Anti-Rac1	05-389	Merck
Anti-PI3 Kinase class III	4263S	Cell Signaling
Rabbit (DA1E) mAb IgG XP isotype control	3900	Cell Signaling
Mouse (G3A1) mAb IgG1 XP isotype control	5415	Cell Signaling
Bovine serum albumin (BSA)	A2152	Sigma Aldrich
HindIII	R0104S	New England Biolabs (NEB)
Chymotrypsin (seq. grade)	V1062	Promega
DpnI	R0176S	New England Biolabs (NEB)
Phusion Polymerase HF	M0530S	New England Biolabs (NEB)
Quick Ligation Kit	M2200S	New England Biolabs (NEB)
Trypsin	V511C	Promega
LysC	125-05061	Wako
XhoI	R0146S	New England Biolabs (NEB)

10.1.3 Buffers and solutions

Table 21: Buffers and solutions

buffer	ingredients
Cutsmart buffer	New England Biolabs (NEB) (lot 0561412)
dNTP solution mix	New England Biolabs (NEB) (lot 0761408)
5x Phusion GC reaction buffer	New England Biolabs (NEB) (lot 0011508)
5x Phusion HF reaction buffer	New England Biolabs (NEB) (lot 0011308)
PBS	140 mM NaCl
	10 mM Na_2HPO_4
	2.7 mM KCl
	1.8 mM KH_2PO_4 in ddH_2O, pH 7.4
Stacking Gel buffer	0.5 M Tris HCl
	pH 6.8 in ddH_2O
Separating Gel buffer	3.0 M Tris HCl
	pH 8.8 in ddH_2O
Tris-glycine running buffer (10x)	0.25 M Tris HCl
	1.92 M glycine
	1% SDS
	pH 8.3 in ddH_2O
2x Laemmli buffer	63 mM Tris HCl
	2% SDS
	10% (v/v) glycerol
	0.0025% bromphenolblue
	5% (v/v) β-mercaptoethanol
Coomassie stain	0.25% (w/v) Coomassie brilliant Blue R250
	9.20% (v/v) AcOH
	45.4% (v/v) EtOH in ddH_2O
Coomassie destain	10%AcOH
	20%EtOH in ddH_2O
Western blotting buffer	48 mM Tris HCl
	39 mM glycine
	20% (v/v) methanol
	0.04% (w/v) SDS in ddH_2O
Lysis buffer	PBS with 1% (v/v) NP40
	1% (w/v) sodium deoxycholate
Trypan blue	5 mg/mL trypan blue
	9 mg/mL NaCl in ddH_2O
VAT-1 His lysis buffer	20 mM Tris HCl
	150 mM NaCl
	1 mM DTT
	10% glycerol
	10 mM imidazole
	pH 8.0
VAT-1 His binding buffer	20 mM Tris HCl
	150 mM NaCl
	1 mM DTT
	10% glycerol
	20 mM imidazole
	pH 8.0
VAT-1 His washing buffer	20 mM Tris HCl
	150 mM NaCl
	1 mM DTT
	10% glycerol
	40 mM imidazole pH 8.0
VAT-1 His elution buffer	20 mM Tris HCl
	150 mM NaCl
	1 mM DTT
	10% glycerol
	500 mM imidazole
	pH 8.0
VAT-1 SEC buffer	20 mM Tris HCl
	150 mM NaCl
	1 mM DTT
	10% glycerol
	pH 8.0

10.1.4 Media

Table 22: Media

media	ingredients
LB media	5 g/L yeast extract
	10 g/L peptone
	5 g/L NaCl
DMEM	D5671 (Sigma)
	supplemented with 10% FBS, 2 mM L-Glutamine
DMEM SILAC	supplemented Lys4/Arg6 or Lys8/Arg10 (Eurisotop)
RPMI	supplemented with 10% FBS, 2 mM L-Glutamine

10.1.5 Cell lines

Table 23: Human cancer cell lines.

cell line	cell type	media for cultivation	cancer type
MDA-MB231 (ECACC)	adherent	DMEM supplemented with 10% FBS, 2 mM L-Glutamine	Breast cancer
HEPG2 (DSMZ)	adherent	RPMI supplemented with 10% FBS, 2 mM L-Glutamine	Liver cancer
MCF-7 (Bayer)	adherent	DMEM supplemented with 10% FBS, 2 mM L-Glutamine	Breast cancer
T24 (DSMZ)	adherent	DMEM supplemented with 10% FBS, 2 mM L-Glutamine	Breast cancer

Table 24: Bacteria

cell line	resistance	media for cultivation
BL21 (DE3)	ampicillin	LB-ampicillin
BL21 Rosetta2	ampicillin, chloramphenicol	LB-ampicillin, chloramphenicol
XL-1 blue	ampicillin	LB-ampicillin

10.2. Methods

10.2.1. Cell culture

10.2.1.1. General cell culture procedures

Cells were incubated at 37 °C and 5% CO_2 (Autoflow, Nuaire, USA). Sterile cell culture was performed under a laminar flow (Herasafe KS, Thermo Scientific, USA) equipped with a vacuum pump (BVC 21, Vacuubrand, Germany) to remove remaining media. A Primo Vert microscope (Zeiss, Germany) was used for cell inspection. Cell counting was carried out in a Neubauer improved chamber. The cell suspension was mixed with trypan blue (1:1), added to the chamber and the cells were counted.

HepG2 cells were purchased from DSMZ and cultured in RPMI-1640 media (Sigma Aldrich) supplemented with 10% (v/v) heat-inactivated fetal bovine serum (FBS) (Sigma Aldrich) and 2 mM L-glutamine (PAA). Urinary bladder cells T24 (DSMZ, kindly provided by the LMU) and adenocarcinoma cells MDA-MB-231 (ECACC) and MCF-7 (Bayer) were all cultured in Dulbecco´s Modified Eagle´s Medium (DMEM) (Sigma Aldrich) supplemented with 10% FBS and 2 mM L-glutamine.

For SILAC experiments, MDA-MB231 cells were passaged at least six times in SILAC-DMEM medium (gibco, Life Technologies) supplemented with 10% dialyzed FBS and 2 mM

L-glutamine as well as L-Arg-HCl (216.60 g/mol) with a final concentration of 214 µM [^{13}C$_6$] L-arginine HCl (Arg6) and 419 µM [4,4,5,5-D$_4$]L-lysine 2 HCl (Lys4) (Cambridge Isotope Laboratories) for light SILAC cells. For heavy SILAC cells, medium was supplemented with 214 µM [^{13}C$_6$,^{15}N$_4$] L-arginine HCl (Arg10) and 419 µM [^{13}C$_6$,^{15}N$_2$] L-lysine 2 HCl (Lys8). All cells were routinely tested for mycoplasma contamination.

10.2.1.2. Thawing and cryopreservation of cells

Cryotubes were thawed as fast as possible after removal from the liquid nitrogen storage (XSS-36/6, VWR, Belgium) in a water bath (MPC, Huber, Germany) at 37 °C and immediately added to 9 mL of prewarmed media. To remove DMSO from cryo storage, cells were harvested at 600 g and r.t. for 5 min (Centrifuge 5810, Eppendorf, Germany). The supernatant was disposed and cells were resuspended in 10 mL of fresh prewarmed media. The mixture was transferred into a T-75 flask and further incubated at 37 °C.

For cryopreservation, cells were pelletized (600 g, r.t., 5 min) and the cell suspension was concentrated to 1-2 million cells/mL in media containing 10% (v/v) DMSO. The cell suspension was transferred to cryo vials and frozen in an isopropanol chamber (Mr. Frosty, Thermo Scientific, USA) at -80 °C (Forma 900, Thermo Scientific). After 1 day, cryo vials were transferred to a liquid nitrogen tank for long term storage (XSS-36/6, VWR, Belgium).

10.2.1.3. Passaging and Splitting

Cells were washed with prewarmed PBS and detached with 1 mL (T-75) or 2 mL (T-175) accutase solution (Sigma). Digestion was carried out at 37 °C for 5-10 min. Detachment of cells was detected under the microscope. Digestion was stopped by adding 9 mL (T-75) or 18 mL (T-175) DMEM or RPMI media to the cells. Depending on the cell density, the suspension was diluted 1:10 to 1:3 with fresh media for further cultivation at 37 °C.

10.2.2. MTT- Assay

The MTT assay was performed in flat bottom 96 well plates (Nunclon™ Delta 96-Well MicroWell™ Plates, Thermo Scientific). For MDA-MB-231, 4000 cells per well were seeded in each well. The assay was performed in triplicates for each compound concentration as well as for DMSO controls. After one day, the medium was removed and 100 µL medium/well containing 0.5 µL DMSO compound stock were added to the cells and incubated for 24 h. 20 µL Thiazolyl Blue Tetrazolium bromide (5 mg/mL in PBS, Sigma Aldrich) were added to the cells and incubated for 4 h until complete consumption was observed. After removal of the medium, the resulting formazan was dissolved in 200 µL DMSO by incubation at r.t. and 400 rpm for about 10 min (Thermomixer comfort, Eppendorf, Germany). Optical density was measured at 570 nm and background subtracted at 630 nm by a TECAN Infinite® M200 Pro reader. For calculation of IC_{50} values, values were normalized to the DMSO control in Microsoft Excel and the mean was calculated with SD Graphpad Prism 6.0. IC_{50} values were calculated by a nonlinear fit (log(inhibitor) vs. response – Variable slope (four parameters), eq. 1) in Graphpad Prism 6.05 and were shown with 95% confidential intervals indicated in brackets.

$$V = \frac{100}{1+10^{(\log{(IC_{50})}-\log{(c)})\cdot N}}$$

(eq.1)

V: viability [%]
c: Inhibitor concentration [M]
N: Hill slope

10.2.3. Proteomics labeling procedures
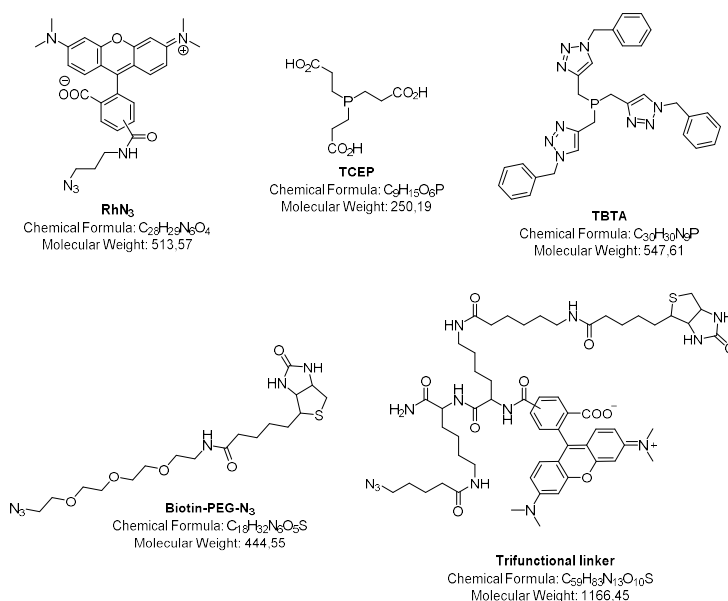
Figure 44: Labeling reagents for click reaction. [54]

10.2.3.1. *In situ* labeling in human cells

Cells were seeded in 6-well plates for analytical and in 10 cm or 15 cm plates for preparative labeling and treated at 90% confluence for 1 h with varying concentrations of probe **NC-1**, **NC-2**, **NC-4** or **NC-5** (stock solution in DMSO, 0.1% end concentration of DMSO for all compounds) or respectively DMSO diluted in PBS at 37 °C and 5% CO_2. For competition experiments, cells were preincubated for 1 h with 100 nM or respectively 500 nM of the natural products **NCA**, **NCB**, **NCC** or derivatives **NCA', NCC'** diluted in PBS before addition of 100 nM **NC-1** for 1 h. Labeling experiments were performed as described before.[191] Briefly, cells were scraped off, pelletized for 3 min at 800 x g and washed with PBS. Cell lysis was performed with 0.1 mL for analytical or respectively 1 mL lysis buffer for preparative labeling (1% (v/v) NP40 and 1% (w/v) sodium deoxycholate in PBS) at 4 °C for 15 min.

10.2.3.2. Analytical *in situ* labeling

For most of the experiments in MDA-MB-231, soluble and insoluble fractions were not separated and whole cell lysate was applied for click chemistry. Otherwise, in case of VAT- 1 KO HEK-293 cells, soluble and insoluble fractions were separated by centrifugation at 20,000 x g and membrane fraction was washed with PBS and resuspended in 100 µL PBS supplemented with 0.2% SDS. Click chemistry was performed with 0.20 mM rhodamine-azide (10 mM stock in DMSO; base click; Rh-N_3), 1.0 mM TCEP (52 mM stock in ddH_2O), 0.10 mM TBTA ligand (1.667 mM stock in 80% tBuOH and 20% DMSO) and 1.0 mM $CuSO_4$ (50 mM stock in ddH_2O). The reaction was incubated at r.t. for 1 h and stopped by addition of 100 µL 2 x SDS loading buffer (63 mM Tris-HCl, 2% (v/v) glycerol, 139 mM sodium dodecylsulfate (SDS), 0.0025% (v/v) Bromophenol blue, 5% (v/v) 2-mercaptoethanol). For gel electrophoresis, 50 µL were applied per gel-lane on a SDS−PAGE gel (12.5% acrylamide). Roti®-Mark STANDARD and BenchMark™ Fluorescent protein standard were applied as markers to determine the protein mass. Gels were developed for 2.5 h with 150 V. Fluorescence was recorded with a Fujifilm Las-4000 luminescent image analyzer with a Fujinon VRF43LMD3 lens and a 575DF20 filter. For determination of relative protein amount, gels were stained with Coomassie stain solution.

10.2.3.3. Preparative *in situ* labeling and quantification *via* SILAC

Both heavy and light labeled MDA-MB-231 cells were treated with 500 nM probe **NC-1** or DMSO, respectively. Soluble and insoluble cell fractions were not separated after cell lysis. Protein concentrations of the lysed cells were measured using a BCA assay (Roti Quant, Roth). Therefore, 10 µL of lysate were mixed with 100 µL ddH$_2$O and 30 µL were measured in a flat-bottom 96 well plate in triplicates. For the bovine serum albumin (BSA) calibration curve, 10 µL of lysis buffer were mixed with 100 µL ddH$_2$O in triplicates representing a concentration of 0 ng/µL. Further, BSA was applied in H$_2$O in a total volume of 30 µL with concentrations of 25, 50, 100, 200 and 400 ng/µL. 100 µL of BCA working solution were added per well. BCA mix was prepared due to the manufacturers' protocol (Carl Roth) (1:15 ratio of solution 1 and 2). The 96 well plate was incubated for 15 min at 60 °C. Afterwards, absorbance was detected at 492 nm using a Tecan reader.

After BCA assay (Roti Quant, Roth), equal protein amounts resulting from "heavy" or "light" cells incubated with the probe and the corresponding DMSO control of the opposite label were pooled and adjusted to a final volume of 1880 µL with lysis buffer (approximately 2 µg). Samples were supplemented with 0.20 mM azide-PEG$_3$-biotin conjugate or trifunctional linker (10 mM stock in DMSO; Jena Bioscience), 0.52 mM TCEP (52 mM stock in ddH$_2$O), 0.050 mM TBTA ligand (1.67 mM stock in 80% tBuOH and 20% DMSO) and 0.50 mM CuSO$_4$ (50 mM stock in ddH$_2$O) (Figure 44). Click reaction was performed at r.t. for 1 h and MS sample preparation was performed as described before.[191] Proteins were precipitated by addition of a 4-fold volume excess of acetone and incubated overnight at -20 °C. Proteins were pelleted at 10000 x g for 15 min at 4 °C. The supernatant was discarded and the pellet washed twice with 500 µL of pre-chilled methanol (resuspension of pellet by sonication: 5-10 sec, 10% intensity, 15 min, 4 °C, 10000 x g). Subsequently, the pellet was dissolved in 1 mL of PBS with 0.2% SDS by sonication. 50 µL avidin-agarose beads were prewashed with 3 mL PBS with 0.4% SDS at 2000 rpm 2 min at rt. Proteins and beads were combined and incubated under gentle mixing at rt for 1 h.

Beads were washed three times with 0.2% SDS in PBS, twice with 6 M urea, three times with PBS and were supplemented with 200 µL denaturation buffer (7 M urea, 2 M thiourea in 20 mM Hepes, pH 8.0). Reduction and alkylation were performed at rt with 1 mM DTT for 45 min, 5.5 mM IAA for 30 min and 4 mM DTT for 30 min. Proteins were digested with 1 µL Lys-C (0.5 mg/mL) at 25 °C for 3 h, diluted in 600 µL 50 mM TEAB buffer and digested with 2 µL Trypsin (0.5 mg/mL, Promega) at 37 °C overnight. Digestion was stopped with a final concentration of 0.75% formic acid (FA) and beads were pelleted at 13000 rpm for 3 min. The peptides were desalted with Sep-Pak C18 1 cc Vac cartridges (Waters Corp.). Therefore, the C18 material was pre-treated with 1 mL MeCN, 0.5 mL elution buffer

(80% MeCN, 0.5% FA in H$_2$O) and 3 x 1 mL 0.1% TFA in H$_2$O prior to sample loading. Peptides bound to the cartridges were washed with 3 x 1 mL 0.1% trifluoroacetic acid (TFA) in H$_2$O, 0.5% FA in H$_2$O and eluted with twice 250 µL elution buffer. Peptides were lyophilized, stored at -80 °C and reconstituted in 30 µL 1% FA for MS/MS measurements.

10.2.3.4. Preparative *in situ* labeling with label-free quantification

Cells were incubated with different concentrations of **NC-1** and **NC-4** for 1 h or 24 h, respectively. For competition experiments, cells were preincubated with 5-fold access of **NCA or NCA'** or DMSO for 1 h. Soluble and insoluble fractions of MDA-MB-231 cells were not separated. Protein amount was adjusted after BCA assay to a final concentration of 1 µg in 1 mL and LFQ samples were further processed separately. Click chemistry and MS sample preparation were performed according to the SILAC labeling with one modification: Beads were not washed with urea but only three times with 0.2% SDS in PBS and five times with PBS.

10.2.3.5. LFQ i*n situ* preparative labeling for binding site peptide identification

In situ labeling in MDA-MB-231 cells with 100 nM **NC-1** was performed as described before with the following modifications: Azide-PEG$_3$-Desthiobiotin (Jena Bioscience) was used for click chemistry and proteins were digested before enrichment. For click chemistry, 150 µg cell lysate of MDA-MB-231 cells was incubated with 0.20 mM azide-PEG$_3$-Desthiobiotin conjugate (5 mM stock in DMSO), 0.52 mM TCEP (52 mM stock in ddH$_2$O), 0.050 mM TBTA ligand (1.67 mM stock in 80% tBuOH and 20% DMSO) and 0.50 mM CuSO$_4$ (50 mM stock in ddH$_2$O). After protein precipitation, proteins were resuspended in 300 µL 0.1 M TEAB supplemented with 8 M urea and digested 1:200 (w/w) with LysC at r.t., diluted with 900 µL 0.1 M TEAB and digested 1:150 (w/w) Trypsin overnight at 37 °C. After digestion, samples were supplemented 1:1 (v/v) with 0.2% NP40 in PBS and enriched for 1 h on 50 µL avidin agarose beads, which were pre-washed with 0.1% NP40. Peptides were washed twice with 0.1% NP40, three times with PBS and twice with H$_2$O. Peptides were eluted twice with 100 µL 80% MeCN, 0.5% FA in ddH$_2$O, were lyophilized and reconstituted in 30 µL 1% FA for MS/MS measurements.

10.2.4 Whole proteome analysis

Cells were seeded in 15 cm plates and were treated at 80% confluence with 500 nM **NCA** or DMSO respectively diluted in DMEM supplemented with FBS for 24 h at 37 °C. For si- VAT-1 cells, cells overexpressing VAT-1 or VAT-1 KO cells, 90% confluent cells were applied directly for global proteome analysis. Cells were scraped off and pelletized for 3 min at 800 x g. The pellets were washed with PBS and lysed in 1 mL lysis buffer at 4 °C for 15 min. Membrane fraction was separated at 20,000 x g at 4 °C for 20 min. Protein concentration of cytosolic fraction was adjusted after BCA assay to 500 µg and proteins were precipitated in 4-fold volume access acetone. Proteins were washed with cold methanol and resuspended in 300 µL denaturation buffer. Reduction and alkylation of disulfides was performed as described for ABPP experiments. Whole proteome was predigested 1:200 (w/w) with LysC at r.t., diluted with 900 µL 50 mM TEAB and digested 1:150 (w/w) Trypsin overnight at 37 °C. Protein digestion was stopped with a final concentration of 0.75% formic acid peptides were desalted with Sep-Pak C18 1 cc Vac cartridges (Waters Corp.). Peptides were lyophilized and were reconstituted in 1% FA in ddH$_2$O to a final concentration of 2 µg/µL.

In case of HILIC fractionization[192] of whole proteome samples, peptides were first dissolved in HILIC buffer A (110 µL, 95% MeCN 5% H$_2$O and 0.1% TFA), sonicated, vortexed and centrifuged at 21,000 x g for 10 min at 4 °C. Peptide fractionation was performed by an UltiMate 3000 HPLC system (*Dionex*) equipped with an YMC-Pack PVA-Sil column (5 µm, 150 x 2.1 mm, 120 Å, *YMC Europe GmbH*). Gradient elution was carried out with 95% MeCN 5% H$_2$O and 0.1% TFA (A) and 95% H$_2$O 5% MeCN and 0.1% TFA (B). 100 µL of peptide sample were separated in a 62.5 min gradient (7.5 min 0% B, 50 min to 30% B, 3.5 min to 50% B and 2.5 min to 100% B) at a flow rate of 0.2 mL/min, followed by a washing and column re-equilibration step (12.5 min 100% B, 0.5 min to 0% B and 22.5 min 0% B). An on-line UV detector set at 215 nm was utilized to monitor peptide mixture elution. Fractions were collected into a 96-well plate (*Eppendorf*) and resulting fractions were pooled into 10 greater fractions. Fractions were dried in a centrifugal vacuum concentrator and fractions 2-9 subjected to LC-MS/MS analysis. Prior to LC-MS/MS analysis, dried peptide samples were reconstituted in 1% FA in ddH$_2$O (10 µL).[193]

10.2.5. Immunoprecipitation based methods

10.2.5.1. Co-Immunoprecipitation (co-IP) coupled to mass spectrometry

MS-based co-IP was performed either with DSSO crosslinking or without. For co-IP without crosslinker, MDA-MB-231 were grown in 15 cm dishes to 80-90% confluence, the medium was removed and the cells were washed twice with cold PBS before cell lysis.

In case of co-IP with DSSO crosslinker, cells were seeded in 15 cm plates and were applied at 90% confluence for co-IP using disuccinimidyl sulfoxide (DSSO) crosslinker. Co-IP with MS sample preparation was performed as described before.[159] Synthesis of DSSO and crosslinking was carried out as described previously.[82] Briefly, cells were washed with PBS, scraped off in PBS and pelletized. Crosslinking reaction was performed with 2 mM DSSO in 1 mL PBS at 37 °C and 250 rpm for 1 h. Crosslinking reaction was quenched with 50 mM Tris-HCl pH 8.0

Cells were lysed in 1 mL co-IP lysis buffer (50 mM Tris-HCl, 150 mM NaCl, 10% glycerol, 1 mM $MgCl_2$, 1% NP40, pH 8.0) for 30 min at 4 °C while rotating and membrane fraction was pelleted at 21,000 x g and 4° C for 20 min.

Protein concentration of cytosolic fraction was adjusted after BCA assay to 500 µg. A volume of 30 µL of Protein AG beads (Pierce) were equilibrated with 1 mL wash buffer (50 mM Tris-HCl, 150 mM NaCl, 10% glycerol, 0.05% NP40, pH 8.0) and were incubated with 500 µg protein lysate and 1:100 (w/w) specific antibody or the corresponding amount of IgG isotype control for 3 h at 4 °C Beads were washed twice with wash buffer and twice with basic buffer (50 mM Tris-HCl, 150 mM NaCl, 10% glycerol pH 8.0). For MS sample preparation, 25 µL of elution buffer I (50 mM Tris-HCl, 2 M urea, 1 mM DTT, 0.5 ng/µL trypsin) was added to the beads for 30 min at rt. Subsequently, the beads were treated with 100 µL elution buffer II (50 mM Tris-HCl, 2 M urea, 5 mM IAA) overnight at 37 °C. Protein digestion was stopped by adjusting a final concentration of 0.75% TFA and peptides were desalted using stage-tips (self-made pipette tips containing two layers of C18 disks) according to the standard protocol.[194] Therefore, C18 materials was washed with 70 µL MeOH, three times with 70 µL 0.5% FA in ddH$_2$O, samples were loaded, again washed three times with 70 µL 0.5% FA in ddH$_2$O and peptides were eluted with 80% MeCN, 0.5% FA in ddH$_2$O. The solvent was evaporated in a speedvac and the peptides stored at -80 °C.

10.2.5.2. Immunoprecipitation coupled with analytical labeling

For labeling with a subsequent immunoprecipitation, cells were first labeled *in situ* with **NC 1** in 15 cm plates. Afterwards, cells were lysed with co-IP lysis buffer, insoluble fraction was separated, and proteins were enriched on 60 µL Protein A/G beads with 5 µL VAT-1 antibody (antibodies.online) as described before. After incubation for 3 h at 4 °C, beads

were washed with co-IP was buffer and co-IP basic buffer. Beads were separated into two parts and click reaction was performed directly on the beads in 97 μL PBS with 0.20 mM rhodamine-azide (10 mM stock in DMSO; base click; Rh-N$_3$), 1.0 mM TCEP (52 mM stock in ddH$_2$O), 0.10 mM TBTA ligand (1.667 mM stock in 80% tBuOH and 20% DMSO) and 1.0 mM CuSO$_4$ (50 mM stock in ddH$_2$O) for 1 h at r.t. After click reaction, supernatant was removed and proteins were eluted by either 4% SDS in PBS or an acidic solution with 2 M glycine, pH 2.5. Beads were separated from the protein solution by centrifugation at 13000 rpm for 2 min. For acidic elution, solution was neutralized before SDS-PAGE. Finally, proteins were supplemented with 2 x Laemmli and analytical SDS-PAGE was performed with a subsequent Western-blot to confirm the identity of the pulled-down proteins.

10.2.6. MS/MS measurement Orbitrap Fusion

For MS measurements, peptide samples were first dissolved in 30 μL 1% FA in H$_2$O, sonicated for 15 min and filtered with 0.22 μm Ultrafree-MC® centrifugal filters (Merck, UFC30GVNB) equilibrated with 1% FA in H$_2$O.

Samples were analyzed by LC-MS/MS using an UltiMate 3000 nano HPLC system (Dionex) equipped with an Acclaim C18 PepMap100 75 μm ID x 2 cm trap and an Acclaim Pepmap RSLC C18 separation column (75 μm ID x 50 cm) in an EASY-spray setting coupled to an Orbitrap Fusion (Thermo Fisher Scientific Inc.). Approximately 8 μg were loaded on the trap column with a flow rate of 5 μL/min with 0.1% TFA buffer and then transferred onto the separation column at a flow rate of 0.3 μL/min. Samples were separated using a 152 min gradient (buffer A: H$_2$O with 0.1% FA, buffer B: MeCN with 0.1% FA, gradient: to 5% buffer B in 7 min, from 5% to 22% buffer B in 105 min, then to 32% buffer B in 10 min, to 90% buffer B in 10 min and hold at 90% buffer B for 10 min, then to 5% buffer B in 0.1 min and hold 5% buffer B for 9.9 min). Peptides were ionized using a nanospray source at 1.7-1.9 kV and a capillary temperature of 275 °C. The instrument was operated in a top speed data dependent mode with a cycle time between master scans of 3 s. MS full scans were performed in the orbitrap with quadrupole isolation at a resolution of R = 120,000 and an automatic gain control (AGC) ion target value of 2e5 in a scan range of 300 – 1500 m/z with a maximum injection time of 50 ms. Internal calibration was performed using the ion signal of fluoranthene cations (EASY-ETD/IC source). Besides two experiments, all samples were measured on the Orbitrap Fusion instrument for the publication.

Dynamic exclusion time was set to 60 s with a mass tolerance of 10 ppm (low/high). Precursors with intensities higher than 5e3 and charge states 2 – 7 were selected for fragmentation with HCD (30%). MS^2 scans were recorded in the ion trap operating in a rapid mode with an isolation window of 1.6 m/z. For enriched samples, the AGC target was set to 1.0e4 with a maximum injection time of 100 ms and the "inject ions for all available

parallelizable time" was enabled. For complex samples, AGC target of 1.0e4 with a maximum injection time of 35 ms was applied.

10.2.7. MS/MS measurement Q Exactive

Samples clicked to desthiobiotin-azide and 24 h **NC-1** labeling in MDA-MB-231 were analyzed *via* an UltiMate 3000 nano HPLC system (Dionex) using Acclaim C18 PepMap100 75 µm ID x 2 cm trap and Acclaim PepMap RSLC C18 (75 µm ID x 50 cm) separation columns in an EASY-spray setting coupled to a Q Exactive Plus (Thermo Fisher). After reconstitution of the samples in 1% FA in ddH$_2$O and filtering, 5 µL peptide samples were loaded on the trap column with a flow rate 5 µL/min in 0.1% TFA, and were subsequently transferred to the separation column at a flow rate of 0.3 µL/min. Separation was performed with a 152 min gradient (buffer A: H$_2$O with 0.1% FA, buffer B: MeCN with 0.1% FA) increasing buffer B to 5% within 7 min, to 22% the next 105 min, to 32% the next 10 min and to 90% the next 10 min. Buffer B was held another 10 min at 90% and was then decreased to 5% in 0.1 min and held until end of the run. Peptide samples were ionized at spray voltage of 1.6 kV and a capillary temperature of 275 °C. Q Exactive Plus was operated in a TopN data dependent mode of 12. Full scans were performed in the orbitrap mass analyzer with a resolution of R = 140,000 and an AGC target of 3.0 e6 with a maximum injection time of 80 ms. The scan range was set to 300-15000 m/z. Peptide fragments were generated by HCD with a normalized collision energy of 27%.

MS^2 scans were recorded in the orbitrap at a resolution of 17,500 with an AGC target of 1e5 and a maximum injection time of 100 ms scan range. Isolation was performed in the quadrupole using a window of 1.6 m/z. Dynamic exclusion duration was set to 60 s. Precursors with charge states >1, intensities higher than 1e4 and a minimum AGC target of 1.00e3 were selected for fragmentation.

10.2.8. Bioinformatics and statistics

MS data was processed with the software MaxQuant[128, 129] version 1.6.0.1 or 1.6.2.10. For peptide identification, MS/MS spectra were searched against the Uniprot database for *homo sapiens* (taxon identifier: 9606, canonical version, reviewed and unreviewed proteome downloaded on 05.04.2018 or 28.10.2019) using the Andromeda search engine.[195]

MaxQuant was run using mostly default settings (trypsin/P set as the digest enzyme, max. 2 missed cleavages, oxidation (M) and protein N-term acetylation as variable modifications, carbamidomethylation as fixed modification, min. peptide length 7, 4.5 ppm for precursor mass tolerance (FTMS MS/MS match tolerance) and 0.5 Da for fragment mass tolerance (ITMS MS/MS match tolerance)). For protein identification the following settings were used:

PSM FDR 0.01, Protein FDR 0.01, min. razor + unique peptides: 2, razor protein FDR enabled, second peptides enabled. The match between run option with a matching window of 0.7 min and alignment time window of 20 min was enabled for all experiments. LFQ samples were processed using the built-in label-free quantification algorithm in the MaxQuant software (MaxLFQ)[148] with a minimal ratio count of 2.

For SILAC experiments, multiplicity was set to 2, parameter groups were defined and corresponding labels were selected: For light labels, Arg6 and Lys4 was selected for samples which have been treated with probe **NC-1** in Arg10 Lys8 medium and heavy labels were set to Arg10 Lys8. For samples which have been treated with **NC-1** in Arg6 Lys4 medium, light labels were set to Arg10 Lys8 and heavy labels to Arg6 Lys4. The re-quantify option was enabled for SILAC samples. The mass spectrometry proteomics data have been deposited to the ProteomeXchange Consortium[196] *via* the PRIDE[197] partner repository with the dataset identifier PXD012952.

Resulting data was statistically analyzed further with Perseus software[198] (version 1.6.2.3). The *protein groups* table in the *txt* folder was selected and the rows containing the normalized ratios were filtered by "filtering by categorical columns", namely the columns "identified by site", "reverse" and "contaminants". Ratios were $\log_2$ transformed and categorical annotation of treated samples and control was performed for LFQ samples. Matrices were further filtered against 70% of valid values in at least one group and missing values were imputed from normal distribution (width 0.3, down shift 0.9, for the total matrix. For LFQ experiments, two-sided student's *t*-tests with background as single control group and Benjamini-Hochberg false discovery rate correction (FDR 0.05) were applied. Volcano plots were generated by plotting student's *t*-test difference (treated/control) against *t*-test *p*-value (treated/control).

For SILAC experiments, rows were filtered against 70% of valid values in total after $\log_2$ transformation and a one-sample Student's *t*-test was performed

Heat map was generated in GraphPad Prism 8.0 with $\log_2$ enrichments of peptides obtained for each of the 7 independent target ID experiment by statistical analysis in Perseus. Experiments visualized in the heat map were evaluated in one MaxQuant run with the match between run option enabled. Missing value imputation of unfiltered peptides and a two-sample student's *t*-test was performed in Perseus. Peptides which did not occur in target ID experiments but were found in co-IP data were included in the heat map and are shown as colorless.

10.2.9. Gene ontology enrichment analysis

Gene Ontology enrichment analysis was performed in Cytoscape[160] version 3.7.1. using the BiNGO app[170] 3.0.3. Human gene association (.gaf) and ontology[163] (.obo) files were downloaded from http://www.geneontology.org/ (31/01/2019). An overrepresentation among the proteins of interest was selected and a hypergeometric test with a significance level of 0.05 and Benjamini & Hochberg False Discovery Rate (FDR) correction was performed. Biological process name space was used to select the terms molecular function, biological process and cellular compartment. Whole annotations were used as reference set. STRING database (v.11.0) was used for network analysis of enriched or depleted proteins in the multiple proteins option for human proteins. For minimum interaction scores, high confidence setting (0.7) was applied and the number of edges represented the confidence. Human whole proteome was used as a background for enrichment analysis.

10.2.10. Binding site identification by mass spectrometry

In order to determine the binding mode of **NCA** to VAT-1 and to identify the respective binding site, recombinant VAT-1 was incubated with a 50-fold excess of **NCA** for 2 h at rt. For binding site localization, labeled and DMSO treated recombinant VAT-1 was reduced, alkylated and digested o/n with chymotrypsin or trypsin, which was added in a ratio of 1:100 (w/w) to the protein amount. Acidifying the sample with FA to a final concentration of 0.75% stopped the digest. Peptides were subjected to LC-MS/MS analysis on an Orbitrap Fusion as described previously.

Identification of **NCA**-modified peptides and localization of the site was performed using MaxQuant version 1.6.1.0. Oxidation of methionine, Carbamidomethylation of cysteines and binding of **NCA** to variable amino acids were added as variable modifications. Chymotrypsin or trypsin, respectively, was specified as the proteolytic enzyme with two missed cleavages allowed. The match between runs option was enabled.

10.2.11. Intact protein MS

LC-MS analysis of intact proteins was performed on a Dionex UltiMate 3000 HPLC system coupled to a Thermo LTQ-FT Ultra mass spectrometer with an electrospray ionization source (capillary temp 275 °C, spray voltage 4.0 kV, tube lens 110 V, capillary voltage 48 V, sheath gas 60 arb, aux gas 10 arb, sweep gas 0.2 arb). Desalting was carried out with Massprep online desalting cartridges (Waters Corp.). Briefly, proteins were loaded in 1% FA and eluted in a 5 min gradient from 6 to 95% acetonitrile, 1% FA. The mass spectrometer was operated in positive mode collecting full scans at high resolution (R = 200,000) from

m/z = 600 to m/z = 2000. Data analysis and deconvolution was performed using *Thermo Xcalibur Xtract* software.

10.2.12. Cloning procedures

10.2.12.1. Cloning of VAT-1 for overexpression in *E. coli*

10.2.12.1a) Gateway Cloning

A BL21 strain expressing the gene sequence encoding human VAT-1 (hVAT-1) was obtained by W. Heydenreuter.[54] Therefore, hVAT-1 was inserted in the expression vector pET300 by using the Invitrogen™ Gateway® Technology (Life Technologies Corp.). The target gene was amplified from the corresponding cDNA (GeneCopoeia, GC-T3028) by PCR with a Phusion® HF DNA Polymerase. For Gateway® Technology, *att*B1 forward primer and *att*B2 reverse primer were designed to yield *att*B-PCR products. Primers are listed in the table below. The expression construct for hVAT1 (Uniprot-ID: Q99536) with protein purification tags was N-Start-His-attB1-TEV-Start-VAT1-Stop-attB2-C. Obtained protein sequence is shown in Table 31.

Table 25: Primer for Gateway Cloning

primer name	sequence
for_attB1_VAT1	5'-ggggacaagtttgtacaaaaaagcaggctttgagaatctttattttcagggctccgac gagagagaggtagc-3'
rev_attB1_VAT1	5'-ggggaccactttgtacaagaaagctgggtgctagttctccttctctggccc-3'

10.2.12.1. b) QuikChange PCR for *in vitro* mutagenesis of bacterial constructs

QuikChange™ PCR was applied for the creation of bacterial VAT-1 mutants. Human His-TEV-VAT-1 in pET300 was applied as a template DNA for PCR. PCR was performed in a CFX96™ Real-Time PCR System (Bio-Rad) according to Phusion® HF DNA Polymerase (NEB) manufacturer´s PCR protocol (Table 26) and thermocycling conditions for a routine PCR (Table 27). Primers are listed in the Table 28. Mutants are named corresponding to the location in the native VAT-1 protein (Table 31). Location in the His- TEV-VAT-1 construct is always shifted 23 residues to the c-terminus and is shown in brackets (Table 28, sequence Table 31). After PCR, constructs were digested with DpnI (NEB) according to the manufacturer´s protocol, transformed in *E. coli* XL1-blue cells and grown on LB agar plates with ampicillin. Clones were isolated, grown in LB media with ampicillin and purified using an E.Z.N.A.® Plasmid Mini Kit I (Omega Bio-Tek Inc.). DNA concentrations were measured using an Infinite® M200 Pro multiplate reader. After sequencing, constructs were transformed in *E. coli* Top10 cells and were purified by QIAGEN Plasmid Midi Kit according

to the manufacturer´s protocol. Sequencing services, sequencing primers, and PCR primers were provided by Eurofins Genomics GmbH (Ebersberg).

Table 26: PCR reaction mix

ingredients	amount
5x HF buffer/5x GC buffer	10 µL
10 mM dNTPs	1 µL
10 (pmol/µL) primer fwd/rev	each 0.75 µL
Template DNA	50 ng
DMSO	1.5 µL
autoclaved ddH2O	ad 50 µL
Phusion polymerase (NEB)	0.5 µL

Table 27: PCR temperature protocol

cycle	step	temperature	time
1	**Initial denaturation**	98 °C	30 sec
2 – 34	**Denaturation**	98 °C	10 sec
	Annealing	62 °C	30 sec
	Elongation	72 °C	3 min
35	**Final elongation**	72 °C	5 min
	Storage	4 °C	∞

Table 28: Primer sequences

primer name	sequence
C50S fwd (C66S)	5'-tgagcactagggagcgcagcagtggc-3'
C50S rev (C66S)	5'-gccactgctgcgctccctagtgctca-3'
C104S fwd (C102S)	5'-tgagcccggaggcccgcagacgc-3'
C104S rev (C102S)	5'-gcgtctgcgggcctccgggctca-3'
C209S fwd (C225S)	5'-cactgtacgggacagctgcacggcagc-3'
C209S rev (C225S)	5'-gctgccgtgcagctgtcccgtacagtg-3'
C324S fwd (C340S)	5'-tggaagccagacacagcccggttggcc-3'
C324S rev (C340S)	5'-ggccaaccgggctgtgtctggcttcca-3'
E113Q fwd (E136Q)	5'-acccgcgccctgcatgcccggag-3'
E113Q rev (E136Q)	5'-ctccgggcatgcagggcgcgggt-3'
R128K fwd (R151K)	5'-ccggtctcctgccttcttgtcgctgactccctc-3'
R128K rev (R151K)	5'-gagggagtcagcgacaagaaggcaggagaccgg-3'
R128Q fwd (R151Q)	5'-cggtctcctgccttctggtcgctgactccc-3'
R128Q rev (R151Q)	5'-gggagtcagcgaccagaaggcaggagaccg-3'
R128N fwd (R151N)	5'-cggtctcctgccttgttgtcgctgactccctc-3'
R128N rev (R151N)	5'-gagggagtcagcgacaacaaggcaggagaccg-3'

10.2.12.2. Cloning of VAT-1 and point mutants in human vector

The gene of interest His-TEV-tagged VAT-1 was cloned in the human vector pRK5SV40 bearing an ampicillin resistance and the restriction sites XhoI and HindIII, which was generously provided by the MPI of Psychiatry (Munich). The vector pET300 encoding His-TEV-tagged VAT-1 (section before) was applied as a template for PCR according to Phusion® HF DNA Polymerase (New England Biolabs) manufacturer´s PCR protocol. Applied primers for the transfer in the human vector are listed in the Table 26. PCR product and vector were digested with the restriction enzyme XhoI (NEB) and HindIII (NEB) according to the manufacturer´s protocol. The digested vector was extracted from a 1% agarose gel by E.Z.N.A.® Gel Extraction Kit (Omega Bio-Tek Inc.) and the gene of interest was purified by E.Z.N.A. MicroElute Cycle Pure Kit (Omega Bio-Tek Inc.). Vector and gene were ligated with Quick Ligation Kit (New England Biolabs), transformed in *E. coli* Top10 and grown on LB agar plates supplemented with ampicillin (100 µg/mL).

Further, QuikChange™ PCR was applied for the creation of the human VAT-1 mutants. Primers are listed in the Table 29. After sequencing, constructs were transformed in *E. coli* Top10 cells and were purified by QIAGEN Plasmid Midi Kit according to the manufacturer´s protocol with endotoxin-free reagents for a transfection in human cells.

Table 29: Primer for human VAT-1 expression construct

primer name	sequence
Xho1_TEV_VAT-1_WT fwd	5'-ccgctcgagatgcatcatcatcatcatcacatcacaagttt-3'
HindIII_VAT-1_WT rev	5'-gggaagcttctagttctccttctctggccctg-3'
T109V fwd (T132V)	5'-cgcctctgcctgtcgttccgggcatggagg-3'
T109V rev (T132V)	5'-cctccatgcccggaacgacaggcagaggcg-3'
E113Q fwd (E136Q)	5'-acccgcgccctgcatgcccggag-3'
E113Q rev (E136Q)	5'-ctccgggcatgcagggcgcgggt-3'
E123Q fwd (E146Q)	5'-cgctgactccctggcccactgcgat-3'
E123Q rev (E146Q)	5'-atcgcagtgggccagggagtcagcg-3'
S126A fwd (S149A)	5'-tgccttgcggtcggcgactccctcgccc-3'
S126A rev (S149A)	5'-gggcgagggagtcgccgaccgcaaggca-3'
D127N fwd (D150N)	5'-cctgccttgcggttgctgactccctcg-3'
D127N rev (D150N)	5'-cgagggagtcagcaaccgcaaggcagg-3'
R128K fwd (R151K)	5'-ccggtctcctgccttcttgtcgctgactccctc-3'
R128K rev (R151K)	5'-gagggagtcagcgacaagaaggcaggagaccgg-3'
R'28Q fwd (R151Q)	5'-cggtctcctgccttctggtcgctgactccc-3'
R128Q rev (R151Q)	5'-gggagtcagcgaccagaaggcaggagaccg-3'
R128N fwd (R151N)	5'-cggtctcctgccttgttgtcgctgactccctc-3'
R128N rev (R151N)	5'-gagggagtcagcgacaacaaggcaggagaccg-3'

10.2.13. Protein expression of VAT-1 in MDA-MB-231

10.2.13.1. si-RNA or plasmid transfection of human cells

MDA-MB-231 and 4T1-luc2 cells were transfected with non-targeting control siRNA or siRNA targeting VAT-1 (Dharmacon™, GE Healthcare) for 48 h using DharmaFECT™ transfection reagent according to manufacturer's protocol (Dharmacon™, GE Healthcare). For plasmid transfection, MDA-MB-231 were seeded in 12-well plates and were transfected at 90% confluence. Cells were transfected with Lipofectamin3000 (ThermoFisher Scientific) according to the manufacturer's instructions. 1 or 2 µg of plasmid DNA which was purified by QUIAGEN MidiPrep Kit was applied for complex formation in serum-fee Opti-MEM medium (ThermoFisher Scientific) per well. Transfection was performed at 37 °C for 48 h in DMEM supplemented with FBS.

10.2.13.2. Analytical labeling of VAT-1 point mutants in human cells

After 48 h of plasmid or si-RNA transfection, cells were labeled with 100 nM **NC-1** according to section 10.2.3.1. for 1 h in PBS. Downregulation or overexpression of VAT-1 was confirmed by Western blot.

10.2.14. Protein expression of VAT-1 in *E. coli*

10.2.14.1. Analytical labeling in *E. coli*

E. coli BL21 (DE3) cells transformed with pET300-TEV-VAT-1 or point mutants were grown in LB medium supplemented with ampicillin (100 µg/mL) and target gene expression was induced with 500 µM isopropyl β-D-thiogalactopyranoside (IPTG) at 22 °C for 3 h. Cells were harvested at 6000 x g for 15 min at 4 °C. The cells were resuspended in PBS to a theoretical OD_{600} of 40 and 200 µL were labeled with 2 or 5 µM probe **NC-1** (1% DMSO) for 1 h at rt. For cysteine mutant labeling, 100 µL of bacterial suspension were diluted 1:1 in PBS before labeling for reduction of protein amount. A control with no induction of protein expression was additionally added to each experiment. Cells were pelletized, washed with 800 µL PBS and lysed by sonication on ice (3 x 20 sec, 85% of maximal intensity). Membrane and cytosol fraction were separated by centrifugation at 21,000 x g for 30 min at 4 °C and membrane fraction was additionally washed with 800 µL PBS. Membrane fraction was resuspended in 100 µL PBS. For click reaction, 50 µL of membrane or respectively cytosolic fraction were incubated with 0.10 mM rhodamine-azide (5 mM stock in DMSO; base click; Rh-N_3), 1.0 mM TCEP (52 mM stock in ddH_2O), 0.10 mM TBTA ligand (1.667 mM stock in 80% tBuOH and 20% DMSO) and 1.0 mM $CuSO_4$ (50 mM stock in

ddH$_2$O).Reaction was carried at r.t. for 1 h and was quenched by addition of 50 µL 2 x SDS loading buffer before SDS-PAGE.

10.2.14.2. Recombinant protein purification

E. coli BL21 (DE3) cells were transformed with a pET300 expression vector encoding the human VAT-1 with a N-terminal His-TEV tag. The cells were grown in two liters of LB medium supplemented with ampicillin (100 µg/mL) at 37 °C to OD$_{600}$ ~ 0.6 and protein expression was induced with 500 µM IPTG for 3 h at 22 °C. Cells were harvested at 6000 x g for 15 min at 4 °C, washed in PBS (140 mM NaCl, 10 mM Na$_2$HPO$_4$, 2.7 mM KCl, 1.8 mM KH$_2$PO$_4$, pH 7.6), resuspended in His-binding buffer (20 mM Tris, 150 mM NaCl, 10% glycerin, 1 mM DTT, 10 mM imidazole, pH 8.0) and lysed on ice by ultrasonication (20 min in total, 80% of maximal intensity) (Bandolin sonupuls). Cell debris was pelletized at 18,000 rpm (30 min, 4 °C) for 30 min at 4 °C and cell lysates were loaded onto a HisTrap HP (5 mL, GE Healthcare) by an Äkta system (GE Healthcare). The protein of interest was washed with 20 mM and 40 mM imidazole and was eluted in His-elution buffer (20 mM Tris, 150 mM NaCl, 10% glycerin, 1 mM DTT, 500 mM imidazole, pH 8.0). Protein containing fractions were loaded onto a Superose6 prep grade column (130 mL, GE Healthcare) with gel filtration buffer (20 mM Tris, 150 mM NaCl, 1 mM DTT, 10% glycerol, pH 8.0). Fractions containing VAT-1 were pooled and concentrated using centrifugal filter tubes with a molecular weight cut-off (MWCO) of 30 kDa. Protein concentration was determined by absorbance measurement at 280 nm with a Nanoquant plate in an Infinite F200 Pro reader (Tecan). Proteins were stored at -80 °C for further use. Protein size and identity were verified by Western blot and intact protein mass spectrometry measurements.

10.2.15. Biochemical characterization of VAT-1

10.2.15.1. VAT-1 *in vitro* labeling

For validation of covalent binding, 2 µM of recombinant TEV-VAT-1 were labeled in a final volume of 50 µL PBS with 1 µL of the probe **NC-1** (DMSO stock) at various concentrations for 1 h at r.t. Heat control and no enzyme control were included. Click chemistry was performed with 0.2 mM Rh-N$_3$ (10 mM in DMSO), 1 mM TCEP (52 mM stock in ddH$_2$O), 0.1 mM TBTA ligand (1.667 mM stock in 80% tBuOH and 20% DMSO), 1.0 mM CuSO$_4$ (50 mM stock in ddH$_2$O) for 1 h at r.t. Reaction was quenched with 50 µL 2 x SDS loading buffer and SDS-PAGE was performed as described before.

10.2.15.2. Western blot analysis

Western blotting was performed according to standard procedures after separation of proteins *via* SDS-gel electrophoresis. Cell lysates were transferred onto a Roti®-PVDF 2.0 pore size 0.2 µm membrane (Carl Roth) with blotting buffer (48 mM Tris base, 39 mM glycine, 20% (v/v) MeOH, ddH$_2$O) in a Trans-Blot® SD Semi-Dry Transfer cell (Bio-Rad) for 50 min at 20 V. Membranes were blocked with 5% milk powder (Carl Roth) in PBS-T (PBS buffer with 0.5% Tween-20®, pH 7.4) for 1 h and incubated overnight at 4 °C 1:1000 with the respective primary antibody. Afterwards, membranes were washed with PBS-T and incubated with the corresponding horseradish peroxidase (HRP)-conjugated secondary antibody 1:10.000 for 1 h at r.t. Protein bands were visualized using enhanced luminol/enhancer and peroxide solution (Clarity TM Western ECL Substrate, Bio-Rad,) with a Fujifilm LAS 4000 luminescent image analyser with a Fujinon VRF43LMD3 lens in chemiluminescence mode.

11. REFERENCE LIST

1. Bray, F.; Ferlay, J.; Soerjomataram, I.; Siegel, R. L.; Torre, L. A.; Jemal, A., Global cancer statistics 2018: GLOBOCAN estimates of incidence and mortality worldwide for 36 cancers in 185 countries. *CA Cancer J Clin* **2018,** *68* (6), 394-424.

2. Dagenais, G. R.; Leong, D. P.; Rangarajan, S.; Lanas, F.; Lopez-Jaramillo, P.; Gupta, R.; Diaz, R.; Avezum, A.; Oliveira, G. B. F.; Wielgosz, A.; Parambath, S. R.; Mony, P.; Alhabib, K. F.; Temizhan, A.; Ismail, N.; Chifamba, J.; Yeates, K.; Khatib, R.; Rahman, O.; Zatonska, K.; Kazmi, K.; Wei, L.; Zhu, J.; Rosengren, A.; Vijayakumar, K.; Kaur, M.; Mohan, V.; Yusufali, A.; Kelishadi, R.; Teo, K. K.; Joseph, P.; Yusuf, S., Variations in common diseases, hospital admissions, and deaths in middle-aged adults in 21 countries from five continents (PURE): a prospective cohort study. *Lancet* **2019**.

3. Siegel, R. L.; Miller, K. D.; Jemal, A., Cancer statistics, 2019. *CA Cancer J Clin* **2019,** *69* (1), 7-34.

4. Hanahan, D.; Weinberg, R. A., Hallmarks of cancer: the next generation. *Cell* **2011,** *144* (5), 646-74.

5. Hanahan, D.; Weinberg, R. A., The hallmarks of cancer. *Cell* **2000,** *100* (1), 57-70.

6. Prasetyanti, P. R.; Medema, J. P., Intra-tumor heterogeneity from a cancer stem cell perspective. *Mol Cancer* **2017,** *16* (1), 41.

7. Baskar, R.; Lee, K. A.; Yeo, R.; Yeoh, K. W., Cancer and radiation therapy: current advances and future directions. *Int J Med Sci* **2012,** *9* (3), 193-9.

8. Chabner, B. A.; Roberts, T. G., Jr., Timeline: Chemotherapy and the war on cancer. *Nat Rev Cancer* **2005,** *5* (1), 65-72.

9. Palumbo, M. O.; Kavan, P.; Miller, W. H., Jr.; Panasci, L.; Assouline, S.; Johnson, N.; Cohen, V.; Patenaude, F.; Pollak, M.; Jagoe, R. T.; Batist, G., Systemic cancer therapy: achievements and challenges that lie ahead. *Front Pharmacol* **2013,** *4*, 57.

10. Miller, K. D.; Nogueira, L.; Mariotto, A. B.; Rowland, J. H.; Yabroff, K. R.; Alfano, C. M.; Jemal, A.; Kramer, J. L.; Siegel, R. L., Cancer treatment and survivorship statistics, 2019. *CA Cancer J Clin* **2019,** *69* (5), 363-385.

11. Fernando Jenny, J. R., The principles of cancer treatment by chemotherapy. *Surgery* **2015,** *33* (3), 131-135.

12. Vanneman, M.; Dranoff, G., Combining immunotherapy and targeted therapies in cancer treatment. *Nat Rev Cancer* **2012,** *12* (4), 237-51.

13. Arnold, M.; Rutherford, M. J.; Bardot, A.; Ferlay, J.; Andersson, T. M.; Myklebust, T. A.; Tervonen, H.; Thursfield, V.; Ransom, D.; Shack, L.; Woods, R. R.; Turner, D.; Leonfellner, S.; Ryan, S.; Saint-Jacques, N.; De, P.; McClure, C.; Ramanakumar, A. V.; Stuart-Panko, H.; Engholm, G.; Walsh, P. M.; Jackson, C.; Vernon, S.; Morgan, E.; Gavin, A.; Morrison, D. S.; Huws, D. W.; Porter, G.; Butler, J.; Bryant, H.; Currow, D. C.; Hiom, S.; Parkin, D. M.; Sasieni, P.; Lambert, P. C.; Moller, B.; Soerjomataram, I.; Bray, F., Progress in cancer survival, mortality, and incidence in seven high-income countries 1995-2014 (ICBP SURVMARK-2): a population-based study. *Lancet Oncol* **2019,** *20* (11), 1493-1505.

14. Biemar, F.; Foti, M., Global progress against cancer-challenges and opportunities. *Cancer Biol Med* **2013,** *10* (4), 183-6.

15. Spano, D.; Heck, C.; De Antonellis, P.; Christofori, G.; Zollo, M., Molecular networks that regulate cancer metastasis. *Semin Cancer Biol* **2012,** *22* (3), 234-49.

16. Mackay, C. R., Moving targets: cell migration inhibitors as new anti-inflammatory therapies. *Nat. Immunol.* **2008,** *9* (9), 988-998.

17.   Fontebasso, Y.; Dubinett, S. M., Drug Development for Metastasis Prevention. *Crit Rev Oncog* **2015,** *20* (5-6), 449-73.

18.   Chambers, A. F.; Groom, A. C.; MacDonald, I. C., Dissemination and growth of cancer cells in metastatic sites. *Nat Rev Cancer* **2002,** *2* (8), 563-72.

19.   Bravo-Cordero, J. J.; Hodgson, L.; Condeelis, J., Directed cell invasion and migration during metastasis. *Curr Opin Cell Biol* **2012,** *24* (2), 277-83.

20.   Gupta, G. P.; Massague, J., Cancer metastasis: building a framework. *Cell* **2006,** *127* (4), 679-95.

21.   Vignjevic, D.; Montagnac, G., Reorganisation of the dendritic actin network during cancer cell migration and invasion. *Semin Cancer Biol* **2008,** *18* (1), 12-22.

22.   Raftopoulou, M.; Hall, A., Cell migration: Rho GTPases lead the way. *Dev Biol* **2004,** *265* (1), 23-32.

23.   Onishi, K.; Higuchi, M.; Asakura, T.; Masuyama, N.; Gotoh, Y., The PI3K-Akt pathway promotes microtubule stabilization in migrating fibroblasts. *Genes Cells* **2007,** *12* (4), 535-46.

24.   Hood, J. D.; Cheresh, D. A., Role of integrins in cell invasion and migration. *Nat Rev Cancer* **2002,** *2* (2), 91-100.

25.   Hamidi, H.; Ivaska, J., Every step of the way: integrins in cancer progression and metastasis. *Nat Rev Cancer* **2018,** *18* (9), 533-548.

26.   Moser, M.; Legate, K. R.; Zent, R.; Fassler, R., The tail of integrins, talin, and kindlins. *Science* **2009,** *324* (5929), 895-9.

27.   Klapholz, B.; Brown, N. H., Talin - the master of integrin adhesions. *J Cell Sci* **2017,** *130* (15), 2435-2446.

28.   Ley, K.; Rivera-Nieves, J.; Sandborn, W. J.; Shattil, S., Integrin-based therapeutics: biological basis, clinical use and new drugs. *Nat Rev Drug Discov* **2016,** *15* (3), 173-83.

29.   Barthel, S. R.; Gavino, J. D.; Descheny, L.; Dimitroff, C. J., Targeting selectins and selectin ligands in inflammation and cancer. *Expert Opin Ther Targets* **2007,** *11* (11), 1473-91.

30.   Raab-Westphal, S.; Marshall, J. F.; Goodman, S. L., Integrins as therapeutic targets: successes and cancers. *Cancers (Basel)* **2017,** *9* (9).

31.   Radisky, E. S.; Raeeszadeh-Sarmazdeh, M.; Radisky, D. C., Therapeutic potential of matrix metalloproteinase inhibition in breast cancer. *J. Cell. Biochem.* **2017,** *118* (11), 3531-3548.

32.   Sarwar, M. S.; Zhang, H. J.; Tsang, S. W., Perspectives of plant natural products in inhibition of cancer invasion and metastasis by regulating multiple signaling pathways. *Curr. Med. Chem.* **2018,** *25* (38), 5057-5087.

33.   Dias, D. A.; Urban, S.; Roessner, U., A historical overview of natural products in drug discovery. *Metabolites* **2012,** *2* (2), 303-36.

34.   Mishra, B. B.; Tiwari, V. K., Natural products: an evolving role in future drug discovery. *Eur J Med Chem* **2011,** *46* (10), 4769-807.

35.   Amaral, R., dos Santos, S., Andrade, L., Severino, P. & Carvalho, A., Natural Products as Treatment against Cancer: A Historical and Current Vision. *Clinics in Oncology* **2019,** *4*.

36.   Bernardini, S.; Tiezzi, A.; Laghezza Masci, V.; Ovidi, E., Natural products for human health: an historical overview of the drug discovery approaches. *Nat Prod Res* **2018,** *32* (16), 1926-1950.

37.   Demain, A. L.; Vaishnav, P., Natural products for cancer chemotherapy. *Microb Biotechnol* **2011,** *4* (6), 687-99.

38.   Harvey, A. L.; Edrada-Ebel, R.; Quinn, R. J., The re-emergence of natural products for drug discovery in the genomics era. *Nat Rev Drug Discov* **2015,** *14* (2), 111-29.

39.   Rodrigues, T.; Reker, D.; Schneider, P.; Schneider, G., Counting on natural products for drug design. *Nat Chem* **2016,** *8* (6), 531-41.

40.   Newman, D. J.; Cragg, G. M., Natural products as sources of new drugs from 1981 to 2014. *J. Nat. Prod.* **2016,** *79* (3), 629-661.

41.   J., C. G. M. a. N. D., Biodiversity: A continuing source of novel drug leads. *Pure Appl. Chem.* **2005,** *77* (1), 7-24.

42.   Jain, C. K.; Majumder, H. K.; Roychoudhury, S., Natural Compounds as Anticancer Agents Targeting DNA Topoisomerases. *Curr Genomics* **2017,** *18* (1), 75-92.

43.   Risinger, A. L.; Du, L., Targeting and extending the eukaryotic druggable genome with natural products: cytoskeletal targets of natural products. *Nat Prod Rep* **2019**.

44.   Koehn, F. E.; Carter, G. T., The evolving role of natural products in drug discovery. *Nat Rev Drug Discov* **2005,** *4* (3), 206-20.

45.   Liu, R.; Deng, Z.; Liu, T., Streptomyces species: Ideal chassis for natural product discovery and overproduction. *Metab Eng* **2018,** *50*, 74-84.

46.   Sivalingam, P.; Hong, K.; Pote, J.; Prabakar, K., Extreme Environment Streptomyces: Potential Sources for New Antibacterial and Anticancer Drug Leads? *Int J Microbiol* **2019,** *2019*, 5283948.

47.   Ikeda, H.; Kazuo, S. Y.; Omura, S., Genome mining of the Streptomyces avermitilis genome and development of genome-minimized hosts for heterologous expression of biosynthetic gene clusters. *J Ind Microbiol Biotechnol* **2014,** *41* (2), 233-50.

48.   Pham, J. V.; Yilma, M. A.; Feliz, A.; Majid, M. T.; Maffetone, N.; Walker, J. R.; Kim, E.; Cho, H. J.; Reynolds, J. M.; Song, M. C.; Park, S. R.; Yoon, Y. J., A Review of the Microbial Production of Bioactive Natural Products and Biologics. *Front Microbiol* **2019,** *10*, 1404.

49.   Salas, J. A.; Mendez, C., Genetic manipulation of antitumor-agent biosynthesis to produce novel drugs. *Trends Biotechnol* **1998,** *16* (11), 475-82.

50.   Kiyoto Edo, M. M., Yoshio Koide, Haruo Seto, Kazuo Furihata, Noboru Ōtake , Nakao Ishida, The structure of neocarzinostatin chromophore possessing a novel bicyclo-[7,3,0]dodecadiyne system. *Tetrahedron Letters* **1985,** *26* (3), 331-334.

51.   Jean, M.; Tomasi, S.; van de Weghe, P., When the nine-membered enediynes play hide and seek. *Org Biomol Chem* **2012,** *10* (37), 7453-7456.

52.   Liu, W.; Nonaka, K.; Nie, L.; Zhang, J.; Christenson, S. D.; Bae, J.; Van Lanen, S. G.; Zazopoulos, E.; Farnet, C. M.; Yang, C. F.; Shen, B., The neocarzinostatin biosynthetic gene cluster from Streptomyces carzinostaticus ATCC 15944 involving two iterative type I polyketide synthases. *Chem Biol* **2005,** *12* (3), 293-302.

53.   Nozoe, S., Ishii, N., Kusano, G., Kikuchi, K., Ohta, T., Neocarzilins A and B, novel polyenones from Streptomyces carzinostaticus. *Tetrahedron Lett.* **1992,** *33*, 7547-7550.

54.   Heydenreuter, W. Target identification of natural products by activity based protein profiling and a whole proteome inventory of background photocrosslinker binding. 2016.

55.   Otsuka, M.; Ichinose, K.; Fujii, I.; Ebizuka, Y., Cloning, sequencing, and functional analysis of an iterative type I polyketide synthase gene cluster for biosynthesis of the antitumor chlorinated polyenone neocarzilin in "Streptomyces carzinostaticus". *Antimicrob. Agents Chemother.* **2004,** *48* (9), 3468-3476.

56.   Nozoe, S., Kikuchi, K., Ishii, N., Ohta, T., Synthesis of neocarzilin A: An absolute stereochemistry. *Tetrahedron Lett.* **1992,** *33*, 7551-7552.

57.   Linial, M.; Miller, K.; Scheller, R. H., VAT-1: an abundant membrane protein from Torpedo cholinergic synaptic vesicles. *Neuron* **1989,** *2* (3), 1265-73.

58.   Loeb-Hennard, C.; Cousin, X.; Prengel, I.; Kremmer, E., Cloning and expression pattern of vat-1 homolog gene in zebrafish. *Gene Expr Patterns* **2004,** *5* (1), 91-6.

59.   Linial, M.; Levius, O., VAT-1 from Torpedo is a membranous homologue of zeta crystallin. *FEBS Lett* **1993,** *315* (1), 91-4.

60.   Linial, M.; Levius, O., The protein VAT-1 from Torpedo electric organ exhibits an ATPase activity. *Neurosci. Lett.* **1993,** *152* (1-2), 155-157.

61.   Linial, M., VAT-1 from Torpedo electric organ forms a high-molecular-mass protein complex within the synaptic vesicle membrane. *Eur J Biochem* **1993,** *216* (1), 189-97.

62.   Levius, O.; Linial, M., VAT-1 from Torpedo synaptic vesicles is a calcium binding protein: a study in bacterial expression systems. *Cell Mol Neurobiol* **1993,** *13* (5), 483-92.

63.   Linial, M.; Levius, O.; Ilouz, N.; Parnas, D., The effect of calcium levels on synaptic proteins. A study on VAT-1 from Torpedo. *J Physiol Paris* **1995,** *89* (2), 103-12.

64.   Persson, B.; Zigler, J. S., Jr.; Jornvall, H., A super-family of medium-chain dehydrogenases/reductases (MDR). Sub-lines including zeta-crystallin, alcohol and polyol dehydrogenases, quinone oxidoreductase enoyl reductases, VAT-1 and other proteins. *Eur J Biochem* **1994,** *226* (1), 15-22.

65.   Hayess, K.; Kraft, R.; Sachsinger, J.; Janke, J.; Beckmann, G.; Rohde, K.; Jandrig, B.; Benndorf, R., Mammalian protein homologous to VAT-1 of Torpedo californica: isolation from Ehrlich ascites tumor cells, biochemical characterization, and organization of its gene. *J Cell Biochem* **1998,** *69* (3), 304-15.

66.   Eura, Y.; Ishihara, N.; Oka, T.; Mihara, K., Identification of a novel protein that regulates mitochondrial fusion by modulating mitofusin (Mfn) protein function. *J Cell Sci* **2006,** *119* (Pt 23), 4913-25.

67.   Koch, J.; Foekens, J.; Timmermans, M.; Fink, W.; Wirzbach, A.; Kramer, M. D.; Schaefer, B. M., Human VAT-1: a calcium-regulated activation marker of human epithelial cells. *Arch. Dermatol. Res.* **2003,** *295* (5), 203-210.

68.   Junker, M.; Rapoport, T. A., Involvement of VAT-1 in Phosphatidylserine Transfer from the Endoplasmic Reticulum to Mitochondria. *Traffic* **2015,** *16* (12), 1306-17.

69.   Mertsch, S.; Becker, M.; Lichota, A.; Paulus, W.; Senner, V., Vesicle amine transport protein-1 (VAT-1) is upregulated in glioblastomas and promotes migration. *Neuropathol Appl Neurobiol* **2009,** *35* (4), 342-52.

70.   Watanabe, Y.; Tamura, Y.; Kakuta, C.; Watanabe, S.; Endo, T., Structural basis for inter-organelle phospholipid transport mediated by VAT-1. *J Biol Chem* **2020**.

71.   Fang, H. Y.; Chang, C. L.; Hsu, S. H.; Huang, C. Y.; Chiang, S. F.; Chiou, S. H.; Huang, C. H.; Hsiao, Y. T.; Lin, T. Y.; Chiang, I. P.; Hsu, W. H.; Sugano, S.; Chen, C. Y.; Lin, C. Y.; Ko, W. J.; Chow, K. C., ATPase family AAA domain-containing 3A is a novel anti-apoptotic factor in lung adenocarcinoma cells. *J Cell Sci* **2010,** *123* (Pt 7), 1171-80.

72.   Gilquin, B.; Taillebourg, E.; Cherradi, N.; Hubstenberger, A.; Gay, O.; Merle, N.; Assard, N.; Fauvarque, M. O.; Tomohiro, S.; Kuge, O.; Baudier, J., The AAA+ ATPase ATAD3A controls mitochondrial dynamics at the interface of the inner and outer membranes. *Mol Cell Biol* **2010,** *30* (8), 1984-96.

73.   Wang, X.; Devaiah, S. P.; Zhang, W.; Welti, R., Signaling functions of phosphatidic acid. *Prog Lipid Res* **2006,** *45* (3), 250-78.

74.   Faugaret, D.; Chouinard, F. C.; Harbour, D.; El azreq, M. A.; Bourgoin, S. G., An essential role for phospholipase D in the recruitment of vesicle amine transport protein-1 to membranes in human neutrophils. *Biochem Pharmacol* **2011,** *81* (1), 144-56.

75.   Friedman, L. S.; Ostermeyer, E. A.; Lynch, E. D.; Welcsh, P.; Szabo, C. I.; Meza, J. E.; Anderson, L. A.; Dowd, P.; Lee, M. K.; Rowell, S. E.; et al., 22 genes from chromosome 17q21: cloning, sequencing, and characterization of mutations in breast cancer families and tumors. *Genomics* **1995,** *25* (1), 256-63.

76.   Miki, Y.; Swensen, J.; Shattuck-Eidens, D.; Futreal, P. A.; Harshman, K.; Tavtigian, S.; Liu, Q.; Cochran, C.; Bennett, L. M.; Ding, W.; et al., A strong candidate for the breast and ovarian cancer susceptibility gene BRCA1. *Science* **1994,** *266* (5182), 66-71.

77.   Ransom, C. B.; Sontheimer, H., BK channels in human glioma cells. *J Neurophysiol* **2001,** *85* (2), 790-803.

78. Mori, F.; Tanigawa, K.; Endo, K.; Minamiguchi, K.; Abe, M.; Yamada, S.; Miyoshi, K., VAT-1 is a novel pathogenic factor of progressive benign prostatic hyperplasia. *Prostate* **2011,** *71* (14), 1579-86.

79. Miura, K., An Overview of Current Methods to Confirm Protein-Protein Interactions. *Protein Pept Lett* **2018,** *25* (8), 728-733.

80. Zhang, H.; Tang, X.; Munske, G. R.; Zakharova, N.; Yang, L.; Zheng, C.; Wolff, M. A.; Tolic, N.; Anderson, G. A.; Shi, L.; Marshall, M. J.; Fredrickson, J. K.; Bruce, J. E., In vivo identification of the outer membrane protein OmcA-MtrC interaction network in Shewanella oneidensis MR-1 cells using novel hydrophobic chemical cross-linkers. *J Proteome Res* **2008,** *7* (4), 1712-20.

81. Selbach, M.; Mann, M., Protein interaction screening by quantitative immunoprecipitation combined with knockdown (QUICK). *Nat Methods* **2006,** *3* (12), 981-3.

82. Fux, A.; Korotkov, V. S.; Schneider, M.; Antes, I.; Sieber, S. A., Chemical cross-linking enables drafting ClpXP proximity maps and taking snapshots of in situ interaction networks. *Cell Chem. Biol.* **2019,** *26* (1), 48-59 e7.

83. Arkin, M. R.; Wells, J. A., Small-molecule inhibitors of protein-protein interactions: progressing towards the dream. *Nat Rev Drug Discov* **2004,** *3* (4), 301-17.

84. Bojadzic, D.; Buchwald, P., Toward Small-Molecule Inhibition of Protein-Protein Interactions: General Aspects and Recent Progress in Targeting Costimulatory and Coinhibitory (Immune Checkpoint) Interactions. *Curr Top Med Chem* **2018,** *18* (8), 674-699.

85. Cravatt, B. F.; Wright, A. T.; Kozarich, J. W., Activity-based protein profiling: from enzyme chemistry to proteomic chemistry. *Annu Rev Biochem* **2008,** *77*, 383-414.

86. Evans, M. J.; Cravatt, B. F., Mechanism-based profiling of enzyme families. *Chem. Rev.* **2006,** *106* (8), 3279-3301.

87. Cunningham, M. J., Genomics and proteomics: the new millennium of drug discovery and development. *J Pharmacol Toxicol Methods* **2000,** *44* (1), 291-300.

88. Schenone, M.; Dancik, V.; Wagner, B. K.; Clemons, P. A., Target identification and mechanism of action in chemical biology and drug discovery. *Nat Chem Biol* **2013,** *9* (4), 232-40.

89. Tyers, M.; Mann, M., From genomics to proteomics. *Nature* **2003,** *422* (6928), 193-7.

90. Cox, J.; Mann, M., Is proteomics the new genomics? *Cell* **2007,** *130* (3), 395-8.

91. Aebersold, R.; Mann, M., Mass spectrometry-based proteomics. *Nature* **2003,** *422* (6928), 198-207.

92. Su, Y.; Ge, J.; Zhu, B.; Zheng, Y. G.; Zhu, Q.; Yao, S. Q., Target identification of biologically active small molecules via in situ methods. *Curr Opin Chem Biol* **2013,** *17* (5), 768-75.

93. Daniel Martinez Molina, R. J., Marina Ignatushchenko, Takahiro Seki, E. Andreas Larsson, Chen Dan, Lekshmy Sreekumar, Yihai Cao, Pär Nordlund, Monitoring Drug Target Engagement in Cells and Tissues Using the Cellular Thermal Shift Assay. *Science* **2013,** *341* (84), 84-87.

94. Savitski, M. M.; Reinhard, F. B.; Franken, H.; Werner, T.; Savitski, M. F.; Eberhard, D.; Martinez Molina, D.; Jafari, R.; Dovega, R. B.; Klaeger, S.; Kuster, B.; Nordlund, P.; Bantscheff, M.; Drewes, G., Tracking cancer drugs in living cells by thermal profiling of the proteome. *Science* **2014,** *346* (6205), 1255784.

95. Franken, H.; Mathieson, T.; Childs, D.; Sweetman, G. M.; Werner, T.; Togel, I.; Doce, C.; Gade, S.; Bantscheff, M.; Drewes, G.; Reinhard, F. B.; Huber, W.; Savitski, M. M., Thermal proteome profiling for unbiased identification of direct and indirect drug targets using multiplexed quantitative mass spectrometry. *Nat Protoc* **2015,** *10* (10), 1567-93.

96. Li, N.; Overkleeft, H. S.; Florea, B. I., Activity-based protein profiling: an enabling technology in chemical biology research. *Curr Opin Chem Biol* **2012,** *16* (1-2), 227-33.

97.   Sadaghiani, A. M.; Verhelst, S. H.; Bogyo, M., Tagging and detection strategies for activity-based proteomics. *Curr Opin Chem Biol* **2007,** *11* (1), 20-8.

98.   Kobe, B.; Kemp, B. E., Active site-directed protein regulation. *Nature* **1999,** *402* (6760), 373-6.

99.   Khan, A. R.; James, M. N., Molecular mechanisms for the conversion of zymogens to active proteolytic enzymes. *Protein Sci* **1998,** *7* (4), 815-36.

100.   Speers, A. E.; Adam, G. C.; Cravatt, B. F., Activity-based protein profiling in vivo using a copper(i)-catalyzed azide-alkyne [3 + 2] cycloaddition. *J. Am. Chem. Soc.* **2003,** *125* (16), 4686-4687.

101.   Sieber, S. A.; Cravatt, B. F., Analytical platforms for activity-based protein profiling--exploiting the versatility of chemistry for functional proteomics. *Chem Commun (Camb)* **2006,** (22), 2311-9.

102.   Anna E. Speers, B. F. C., Profiling Enzyme Activities In Vivo Using Click Chemistry Methods. *Chemistry & Biology* **2004,** *11* (4), 535-546.

103.   Speers, A. E.; Cravatt, B. F., Chemical strategies for activity-based proteomics. *Chembiochem* **2004,** *5* (1), 41-7.

104.   Ahmed S. Abuelyaman, D. H., Susan L. Woodard, James C. Powers, Fluorescent Derivatives of Diphenyl [1-(N-Peptidylamino)alkyl]phosphonate Esters: Synthesis and Use in the Inhibition and Cellular Localization of Serine Proteases. *Bioconjugate Chem.* **1994,** *5* (5), 400-405.

105.   Kam, C. M.; Abuelyaman, A. S.; Li, Z.; Hudig, D.; Powers, J. C., Biotinylated isocoumarins, new inhibitors and reagents for detection, localization, and isolation of serine proteases. *Bioconjug Chem* **1993,** *4* (6), 560-7.

106.   Liu, Y.; Patricelli, M. P.; Cravatt, B. F., Activity-based protein profiling: the serine hydrolases. *Proc Natl Acad Sci U S A* **1999,** *96* (26), 14694-9.

107.   Greenbaum, D.; Medzihradszky, K. F.; Burlingame, A.; Bogyo, M., Epoxide electrophiles as activity-dependent cysteine protease profiling and discovery tools. *Chem Biol* **2000,** *7* (8), 569-81.

108.   Fonovic, M.; Bogyo, M., Activity-based probes as a tool for functional proteomic analysis of proteases. *Expert. Rev. Proteomics* **2008,** *5* (5), 721-730.

109.   Li, N.; Kuo, C. L.; Paniagua, G.; van den Elst, H.; Verdoes, M.; Willems, L. I.; van der Linden, W. A.; Ruben, M.; van Genderen, E.; Gubbens, J.; van Wezel, G. P.; Overkleeft, H. S.; Florea, B. I., Relative quantification of proteasome activity by activity-based protein profiling and LC-MS/MS. *Nat Protoc* **2013,** *8* (6), 1155-68.

110.   Bottcher, T.; Sieber, S. A., Beta-lactones as privileged structures for the active-site labeling of versatile bacterial enzyme classes. *Angew Chem Int Ed Engl* **2008,** *47* (24), 4600-3.

111.   Weerapana, E.; Wang, C.; Simon, G. M.; Richter, F.; Khare, S.; Dillon, M. B.; Bachovchin, D. A.; Mowen, K.; Baker, D.; Cravatt, B. F., Quantitative reactivity profiling predicts functional cysteines in proteomes. *Nature* **2010,** *468* (7325), 790-5.

112.   Wirth, T.; Schmuck, K.; Tietze, L. F.; Sieber, S. A., Duocarmycin analogues target aldehyde dehydrogenase 1 in lung cancer cells. *Angew Chem Int Ed Engl* **2012,** *51* (12), 2874-7.

113.   Kolb, H. C.; Sharpless, K. B., The growing impact of click chemistry on drug discovery. *Drug Discov Today* **2003,** *8* (24), 1128-37.

114.   Meldal, M.; Tornoe, C. W., Cu-catalyzed azide-alkyne cycloaddition. *Chem Rev* **2008,** *108* (8), 2952-3015.

115.   Rostovtsev, V. V.; Green, L. G.; Fokin, V. V.; Sharpless, K. B., A stepwise huisgen cycloaddition process: copper(I)-catalyzed regioselective "ligation" of azides and terminal alkynes. *Angew. Chem. Int. Ed. Engl.* **2002,** *41* (14), 2596-2599.

116.   Himo, F.; Lovell, T.; Hilgraf, R.; Rostovtsev, V. V.; Noodleman, L.; Sharpless, K. B.; Fokin, V. V., Copper(I)-catalyzed synthesis of azoles. DFT study predicts unprecedented reactivity and intermediates. *J Am Chem Soc* **2005,** *127* (1), 210-6.

117. Adam, G. C.; Sorensen, E. J.; Cravatt, B. F., Trifunctional chemical probes for the consolidated detection and identification of enzyme activities from complex proteomes. *Mol Cell Proteomics* **2002,** *1* (10), 828-35.

118. Schulze, W. X.; Usadel, B., Quantitation in mass-spectrometry-based proteomics. *Annu Rev Plant Biol* **2010,** *61*, 491-516.

119. Rabilloud, T.; Lelong, C., Two-dimensional gel electrophoresis in proteomics: a tutorial. *J Proteomics* **2011,** *74* (10), 1829-41.

120. Wasinger, V. C.; Zeng, M.; Yau, Y., Current status and advances in quantitative proteomic mass spectrometry. *Int J Proteomics* **2013,** *2013*, 180605.

121. Chen, X.; Wei, S.; Ji, Y.; Guo, X.; Yang, F., Quantitative proteomics using SILAC: Principles, applications, and developments. *Proteomics* **2015,** *15* (18), 3175-92.

122. Werner, T.; Sweetman, G.; Savitski, M. F.; Mathieson, T.; Bantscheff, M.; Savitski, M. M., Ion coalescence of neutron encoded TMT 10-plex reporter ions. *Anal Chem* **2014,** *86* (7), 3594-601.

123. Ong, S. E.; Blagoev, B.; Kratchmarova, I.; Kristensen, D. B.; Steen, H.; Pandey, A.; Mann, M., Stable isotope labeling by amino acids in cell culture, SILAC, as a simple and accurate approach to expression proteomics. *Mol. Cell. Proteomics* **2002,** *1* (5), 376-386.

124. Gygi, S. P.; Rist, B.; Gerber, S. A.; Turecek, F.; Gelb, M. H.; Aebersold, R., Quantitative analysis of complex protein mixtures using isotope-coded affinity tags. *Nat Biotechnol* **1999,** *17* (10), 994-9.

125. Boersema, P. J.; Aye, T. T.; van Veen, T. A.; Heck, A. J.; Mohammed, S., Triplex protein quantification based on stable isotope labeling by peptide dimethylation applied to cell and tissue lysates. *Proteomics* **2008,** *8* (22), 4624-32.

126. Ross, P. L.; Huang, Y. N.; Marchese, J. N.; Williamson, B.; Parker, K.; Hattan, S.; Khainovski, N.; Pillai, S.; Dey, S.; Daniels, S.; Purkayastha, S.; Juhasz, P.; Martin, S.; Bartlet-Jones, M.; He, F.; Jacobson, A.; Pappin, D. J., Multiplexed protein quantitation in Saccharomyces cerevisiae using amine-reactive isobaric tagging reagents. *Mol Cell Proteomics* **2004,** *3* (12), 1154-69.

127. Cox, J.; Hein, M. Y.; Luber, C. A.; Paron, I.; Nagaraj, N.; Mann, M., Accurate proteome-wide label-free quantification by delayed normalization and maximal peptide ratio extraction, termed MaxLFQ. *Mol Cell Proteomics* **2014,** *13* (9), 2513-26.

128. Tyanova, S.; Temu, T.; Cox, J., The MaxQuant computational platform for mass spectrometry-based shotgun proteomics. *Nat Protoc* **2016,** *11* (12), 2301-2319.

129. Cox, J.; Mann, M., MaxQuant enables high peptide identification rates, individualized p.p.b.-range mass accuracies and proteome-wide protein quantification. *Nat Biotechnol* **2008,** *26* (12), 1367-72.

130. Asara, J. M.; Christofk, H. R.; Freimark, L. M.; Cantley, L. C., A label-free quantification method by MS/MS TIC compared to SILAC and spectral counting in a proteomics screen. *Proteomics* **2008,** *8* (5), 994-9.

131. Wong, J. W.; Cagney, G., An overview of label-free quantitation methods in proteomics by mass spectrometry. *Methods Mol Biol* **2010,** *604*, 273-83.

132. Griffin, N. M.; Yu, J.; Long, F.; Oh, P.; Shore, S.; Li, Y.; Koziol, J. A.; Schnitzer, J. E., Label-free, normalized quantification of complex mass spectrometry data for proteomic analysis. *Nat Biotechnol* **2010,** *28* (1), 83-9.

133. Fetzer, C.; Korotkov, V. S.; Thanert, R.; Lee, K. M.; Neuenschwander, M.; von Kries, J. P.; Medina, E.; Sieber, S. A., A Chemical Disruptor of the ClpX Chaperone Complex Attenuates the Virulence of Multidrug-Resistant Staphylococcus aureus. *Angew Chem Int Ed Engl* **2017,** *56* (49), 15746-15750.

134. Gleissner, C. M.; Pyka, C. L.; Heydenreuter, W.; Gronauer, T. F.; Atzberger, C.; Korotkov, V. S.; Cheng, W.; Hacker, S. M.; Vollmar, A. M.; Braig, S.; Sieber, S. A., Neocarzilin A Is a Potent Inhibitor of Cancer Cell Motility Targeting VAT-1 Controlled Pathways. *ACS Cent Sci* **2019,** *5* (7), 1170-1178.

135. Wright, M. H.; Tao, Y.; Drechsel, J.; Krysiak, J.; Chamni, S.; Weigert-Munoz, A.; Harvey, N. L.; Romo, D.; Sieber, S. A., Quantitative chemoproteomic profiling reveals multiple target interactions of spongiolactone derivatives in leukemia cells. *Chem Commun (Camb)* **2017,** *53* (95), 12818-12821.

136. Pyka, C., The potential of the natural compound Neocarzilin A as inhibitor of cell migration in breast cancer cells. *Dissertation (LMU Munich)* **2019**.

137. Chavez, K. J.; Garimella, S. V.; Lipkowitz, S., Triple negative breast cancer cell lines: one tool in the search for better treatment of triple negative breast cancer. *Breast Dis* **2010,** *32* (1-2), 35-48.

138. Berridge, M. V.; Herst, P. M.; Tan, A. S., Tetrazolium dyes as tools in cell biology: new insights into their cellular reduction. *Biotechnol Annu Rev* **2005,** *11*, 127-52.

139. Mosmann, T., Rapid colorimetric assay for cellular growth and survival: application to proliferation and cytotoxicity assays. *J Immunol Methods* **1983,** *65* (1-2), 55-63.

140. Feoktistova, M.; Geserick, P.; Leverkus, M., Crystal Violet Assay for Determining Viability of Cultured Cells. *Cold Spring Harb Protoc* **2016,** *2016* (4), pdb prot087379.

141. Palmer, T. D.; Ashby, W. J.; Lewis, J. D.; Zijlstra, A., Targeting tumor cell motility to prevent metastasis. *Adv Drug Deliver Rev* **2011,** *63* (8), 568-581.

142. Wells, A.; Grahovac, J.; Wheeler, S.; Ma, B.; Lauffenburger, D., Targeting tumor cell motility as a strategy against invasion and metastasis. *Trends Pharmacol Sci* **2013,** *34* (5), 283-289.

143. Riccardi, C.; Nicoletti, I., Analysis of apoptosis by propidium iodide staining and flow cytometry. *Nat. Protoc.* **2006,** *1* (3), 1458-1461.

144. Braig, S.; Kressirer, C. A.; Liebl, J.; Bischoff, F.; Zahler, S.; Meijer, L.; Vollmar, A. M., Indirubin derivative 6BIO suppresses metastasis. *Cancer Res.* **2013,** *73* (19), 6004-6012.

145. Gandalovicova, A.; Rosel, D.; Fernandes, M.; Vesely, P.; Heneberg, P.; Cermak, V.; Petruzelka, L.; Kumar, S.; Sanz-Moreno, V.; Brabek, J., Migrastatics-Anti-metastatic and Anti-invasion Drugs: Promises and Challenges. *Trends Cancer* **2017,** *3* (6), 391-406.

146. Piggott Andrew M., K. P., Quality not Quantity: The Role of Marine Natural Products in Drug Discovery and Reverse Chemical Proteomics. *Mar Drugs* **2005,** *3* (2), 36-63.

147. Liu, Y.; Guo, M., Chemical proteomic strategies for the discovery and development of anticancer drugs. *Proteomics* **2014,** *14* (4-5), 399-411.

148. Cox, J.; Hein, M. Y.; Luber, C. A.; Paron, I.; Nagaraj, N.; Mann, M., Accurate proteome-wide label-free quantification by delayed normalization and maximal peptide ratio extraction, termed MaxLFQ. *Mol. Cell. Proteomics* **2014,** *13* (9), 2513-2526.

149. Gleissner, C., Validation of VAT-1 as a target of tumor cell migration. *master thesis, TU Munich* **2017**.

150. Bern, M.; Kil, Y. J.; Becker, C., Byonic: advanced peptide and protein identification software. *Curr Protoc Bioinformatics* **2012,** *Chapter 13*, Unit13 20.

151. Adam, G. C.; Burbaum, J.; Kozarich, J. W.; Patricelli, M. P.; Cravatt, B. F., Mapping enzyme active sites in complex proteomes. *Journal of the American Chemical Society* **2004,** *126* (5), 1363-1368.

152. Zanon, P. R. A.; Lewald, L.; Hacker, S. M., Isotopically Labeled Desthiobiotin Azide (isoDTB) Tags Enable Global Profiling of the Bacterial Cysteinome. *Angew Chem Int Ed Engl* **2020,** *59* (7), 2829-2836.

153. Swaney, D. L.; Wenger, C. D.; Coon, J. J., Value of using multiple proteases for large-scale mass spectrometry-based proteomics. *J Proteome Res* **2010,** *9* (3), 1323-9.

154. Backus, K. M.; Correia, B. E.; Lum, K. M.; Forli, S.; Horning, B. D.; Gonzalez-Paez, G. E.; Chatterjee, S.; Lanning, B. R.; Teijaro, J. R.; Olson, A. J.; Wolan, D. W.; Cravatt, B. F., Proteome-wide covalent ligand discovery in native biological systems. *Nature* **2016,** *534* (7608), 570-574.

155. Bar-Peled, L.; Kemper, E. K.; Suciu, R. M.; Vinogradova, E. V.; Backus, K. M.; Horning, B. D.; Paul, T. A.; Ichu, T. A.; Svensson, R. U.; Olucha, J.; Chang, M. W.; Kok, B. P.; Zhu, Z.; Ihle, N. T.; Dix, M. M.; Jiang, P.; Hayward, M. M.; Saez, E.; Shaw, R. J.; Cravatt, B. F., Chemical proteomics identifies druggable vulnerabilities in a genetically defined cancer. *Cell* **2017,** *171* (3), 696-709 e23.

156. Lanning, B. R.; Whitby, L. R.; Dix, M. M.; Douhan, J.; Gilbert, A. M.; Hett, E. C.; Johnson, T. O.; Joslyn, C.; Kath, J. C.; Niessen, S.; Roberts, L. R.; Schnute, M. E.; Wang, C.; Hulce, J. J.; Wei, B.; Whiteley, L. O.; Hayward, M. M.; Cravatt, B. F., A road map to evaluate the proteome-wide selectivity of covalent kinase inhibitors. *Nat. Chem. Biol.* **2014,** *10* (9), 760-767.

157. Mertsch, S.; Becker, M.; Lichota, A.; Paulus, W.; Senner, V., Vesicle amine transport protein-1 (VAT-1) is upregulated in glioblastomas and promotes migration. *Neuropathol. Appl. Neurobiol.* **2009,** *35* (4), 342-352.

158. Linial, M.; Levius, O., VAT-1 from Torpedo is a membranous homologue of zeta crystallin. *FEBS Lett.* **1993,** *315* (1), 91-94.

159. Keilhauer, E. C.; Hein, M. Y.; Mann, M., Accurate protein complex retrieval by affinity enrichment mass spectrometry (AE-MS) rather than affinity purification mass spectrometry (AP-MS). *Mol. Cell. Proteomics* **2015,** *14* (1), 120-135.

160. Shannon, P.; Markiel, A.; Ozier, O.; Baliga, N. S.; Wang, J. T.; Ramage, D.; Amin, N.; Schwikowski, B.; Ideker, T., Cytoscape: a software environment for integrated models of biomolecular interaction networks. *Genome Res.* **2003,** *13* (11), 2498-2504.

161. Thoresen, S. B.; Pedersen, N. M.; Liestol, K.; Stenmark, H., A phosphatidylinositol 3-kinase class III sub-complex containing VPS15, VPS34, Beclin 1, UVRAG and BIF-1 regulates cytokinesis and degradative endocytic traffic. *Exp Cell Res* **2010,** *316* (20), 3368-78.

162. Maritzen, T.; Schachtner, H.; Legler, D. F., On the move: endocytic trafficking in cell migration. *Cell Mol Life Sci* **2015,** *72* (11), 2119-2134.

163. Ashburner, M.; Ball, C. A.; Blake, J. A.; Botstein, D.; Butler, H.; Cherry, J. M.; Davis, A. P.; Dolinski, K.; Dwight, S. S.; Eppig, J. T.; Harris, M. A.; Hill, D. P.; Issel-Tarver, L.; Kasarskis, A.; Lewis, S.; Matese, J. C.; Richardson, J. E.; Ringwald, M.; Rubin, G. M.; Sherlock, G., Gene ontology: tool for the unification of biology. The Gene Ontology Consortium. *Nat Genet* **2000,** *25* (1), 25-9.

164. Sun, H. Q.; Yamamoto, M.; Mejillano, M.; Yin, H. L., Gelsolin, a multifunctional actin regulatory protein. *J Biol Chem* **1999,** *274* (47), 33179-82.

165. Sato, Y.; Akitsu, M.; Amano, Y.; Yamashita, K.; Ide, M.; Shimada, K.; Yamashita, A.; Hirano, H.; Arakawa, N.; Maki, T.; Hayashi, I.; Ohno, S.; Suzuki, A., The novel PAR-1-binding protein MTCL1 has crucial roles in organizing microtubules in polarizing epithelial cells. *J Cell Sci* **2013,** *126* (Pt 20), 4671-83.

166. Watanabe, T.; Noritake, J.; Kaibuchi, K., Regulation of microtubules in cell migration. *Trends Cell Biol* **2005,** *15* (2), 76-83.

167. Tu, H.; Sasaki, T.; Snellman, A.; Gohring, W.; Pirila, P.; Timpl, R.; Pihlajaniemi, T., The type XIII collagen ectodomain is a 150-nm rod and capable of binding to fibronectin, nidogen-2, perlecan, and heparin. *J Biol Chem* **2002,** *277* (25), 23092-9.

168. Vasilescu, J.; Guo, X.; Kast, J., Identification of protein-protein interactions using in vivo cross-linking and mass spectrometry. *Proteomics* **2004,** *4* (12), 3845-54.

169. Klapholz, B.; Brown, N. H., Talin - the master of integrin adhesions. *J. Cell. Sci.* **2017,** *130* (15), 2435-2446.

170. Maere, S.; Heymans, K.; Kuiper, M., BiNGO: a Cytoscape plugin to assess overrepresentation of gene ontology categories in biological networks. *Bioinformatics* **2005,** *21* (16), 3448-3449.

171. Mostowy, S.; Cossart, P., Septins: the fourth component of the cytoskeleton. *Nat Rev Mol Cell Biol* **2012,** *13* (3), 183-94.

172.   Mori, F.; Tanigawa, K.; Endo, K.; Minamiguchi, K.; Abe, M.; Yamada, S.; Miyoshi, K., VAT-1 is a novel pathogenic factor of progressive benign prostatic hyperplasia. *Prostate* **2011,** *71* (14), 1579-1586.

173.   Weed, S. A.; Karginov, A. V.; Schafer, D. A.; Weaver, A. M.; Kinley, A. W.; Cooper, J. A.; Parsons, J. T., Cortactin localization to sites of actin assembly in lamellipodia requires interactions with F-actin and the Arp2/3 complex. *J Cell Biol* **2000,** *151* (1), 29-40.

174.   Huttenlocher, A.; Ginsberg, M. H.; Horwitz, A. F., Modulation of cell migration by integrin-mediated cytoskeletal linkages and ligand-binding affinity. *J Cell Biol* **1996,** *134* (6), 1551-62.

175.   Smith, W. L.; Urade, Y.; Jakobsson, P. J., Enzymes of the cyclooxygenase pathways of prostanoid biosynthesis. *Chem Rev* **2011,** *111* (10), 5821-65.

176.   Mayoral, R.; Fernandez-Martinez, A.; Bosca, L.; Martin-Sanz, P., Prostaglandin E2 promotes migration and adhesion in hepatocellular carcinoma cells. *Carcinogenesis* **2005,** *26* (4), 753-61.

177.   Subramanian, S. V.; Fitzgerald, M. L.; Bernfield, M., Regulated shedding of syndecan-1 and -4 ectodomains by thrombin and growth factor receptor activation. *J Biol Chem* **1997,** *272* (23), 14713-20.

178.   Fensterl, V.; Sen, G. C., The ISG56/IFIT1 gene family. *J Interferon Cytokine Res* **2011,** *31* (1), 71-8.

179.   Ishibashi, M.; Wakita, T.; Esumi, M., 2',5'-Oligoadenylate synthetase-like gene highly induced by hepatitis C virus infection in human liver is inhibitory to viral replication in vitro. *Biochem Biophys Res Commun* **2010,** *392* (3), 397-402.

180.   Kashatus, D. F., Ral GTPases in tumorigenesis: emerging from the shadows. *Exp Cell Res* **2013,** *319* (15), 2337-42.

181.   Sobocka, M. B.; Sobocki, T.; Banerjee, P.; Weiss, C.; Rushbrook, J. I.; Norin, A. J.; Hartwig, J.; Salifu, M. O.; Markell, M. S.; Babinska, A.; Ehrlich, Y. H.; Kornecki, E., Cloning of the human platelet F11 receptor: a cell adhesion molecule member of the immunoglobulin superfamily involved in platelet aggregation. *Blood* **2000,** *95* (8), 2600-9.

182.   Akhmanova, A.; Hoogenraad, C. C.; Drabek, K.; Stepanova, T.; Dortland, B.; Verkerk, T.; Vermeulen, W.; Burgering, B. M.; De Zeeuw, C. I.; Grosveld, F.; Galjart, N., Clasps are CLIP-115 and -170 associating proteins involved in the regional regulation of microtubule dynamics in motile fibroblasts. *Cell* **2001,** *104* (6), 923-35.

183.   Timpl, R.; Martin, G. R.; Bruckner, P.; Wick, G.; Wiedemann, H., Nature of the collagenous protein in a tumor basement membrane. *Eur J Biochem* **1978,** *84* (1), 43-52.

184.   Timpl, R.; Rohde, H.; Robey, P. G.; Rennard, S. I.; Foidart, J. M.; Martin, G. R., Laminin--a glycoprotein from basement membranes. *J Biol Chem* **1979,** *254* (19), 9933-7.

185.   Schuppan, D.; Cantaluppi, M. C.; Becker, J.; Veit, A.; Bunte, T.; Troyer, D.; Schuppan, F.; Schmid, M.; Ackermann, R.; Hahn, E. G., Undulin, an extracellular matrix glycoprotein associated with collagen fibrils. *J Biol Chem* **1990,** *265* (15), 8823-32.

186.   Lin, C. G.; Chen, C. C.; Leu, S. J.; Grzeszkiewicz, T. M.; Lau, L. F., Integrin-dependent functions of the angiogenic inducer NOV (CCN3): implication in wound healing. *J Biol Chem* **2005,** *280* (9), 8229-37.

187.   Wagener, J.; Yang, W.; Kazuschke, K.; Winterhager, E.; Gellhaus, A., CCN3 regulates proliferation and migration properties in Jeg3 trophoblast cells via ERK1/2, Akt and Notch signalling. *Mol Hum Reprod* **2013,** *19* (4), 237-49.

188.   Lin, C. G.; Leu, S. J.; Chen, N.; Tebeau, C. M.; Lin, S. X.; Yeung, C. Y.; Lau, L. F., CCN3 (NOV) is a novel angiogenic regulator of the CCN protein family. *J Biol Chem* **2003,** *278* (26), 24200-8.

189.   Gronauer, T. F.; Mandl, M. M.; Lakemeyer, M.; Hackl, M. W.; Messner, M.; Korotkov, V. S.; Pachmayr, J.; Sieber, S. A., Design and synthesis of tailored

human caseinolytic protease P inhibitors. *Chem Commun (Camb)* **2018,** *54* (70), 9833-9836.

190.   Itoh, T.; Fairall, L.; Muskett, F. W.; Milano, C. P.; Watson, P. J.; Arnaudo, N.; Saleh, A.; Millard, C. J.; El-Mezgueldi, M.; Martino, F.; Schwabe, J. W., Structural and functional characterization of a cell cycle associated HDAC1/2 complex reveals the structural basis for complex assembly and nucleosome targeting. *Nucleic Acids Res* **2015,** *43* (4), 2033-44.

191.   Kleiner, P.; Heydenreuter, W.; Stahl, M.; Korotkov, V. S.; Sieber, S. A., A whole proteome inventory of background photocrosslinker binding. *Angew. Chem. Int. Ed. Engl.* **2017,** *56* (5), 1396-1401.

192.   Boersema, P. J.; Mohammed, S.; Heck, A. J., Hydrophilic interaction liquid chromatography (HILIC) in proteomics. *Anal Bioanal Chem* **2008,** *391* (1), 151-9.

193.   Kirsch, V., Molecular target elucidation of vioprolide A in human cancer cells and -omics insights into the ClpXP machinery of *Staphylococcus aureus*. *Dissertation (LMU Munich)* **2020**.

194.   Rappsilber, J.; Mann, M.; Ishihama, Y., Protocol for micro-purification, enrichment, pre-fractionation and storage of peptides for proteomics using StageTips. *Nat. Protoc.* **2007,** *2* (8), 1896-1906.

195.   Cox, J.; Neuhauser, N.; Michalski, A.; Scheltema, R. A.; Olsen, J. V.; Mann, M., Andromeda: a peptide search engine integrated into the MaxQuant environment. *J. Proteome Res.* **2011,** *10* (4), 1794-1805.

196.   Vizcaino, J. A.; Deutsch, E. W.; Wang, R.; Csordas, A.; Reisinger, F.; Rios, D.; Dianes, J. A.; Sun, Z.; Farrah, T.; Bandeira, N.; Binz, P. A.; Xenarios, I.; Eisenacher, M.; Mayer, G.; Gatto, L.; Campos, A.; Chalkley, R. J.; Kraus, H. J.; Albar, J. P.; Martinez-Bartolome, S.; Apweiler, R.; Omenn, G. S.; Martens, L.; Jones, A. R.; Hermjakob, H., ProteomeXchange provides globally coordinated proteomics data submission and dissemination. *Nat. Biotechnol.* **2014,** *32* (3), 223-226.

197.   Vizcaino, J. A.; Csordas, A.; Del-Toro, N.; Dianes, J. A.; Griss, J.; Lavidas, I.; Mayer, G.; Perez-Riverol, Y.; Reisinger, F.; Ternent, T.; Xu, Q. W.; Wang, R.; Hermjakob, H., 2016 update of the PRIDE database and its related tools. *Nucleic Acids Res.* **2016,** *44* (22), 11033.

198.   Tyanova, S.; Temu, T.; Sinitcyn, P.; Carlson, A.; Hein, M. Y.; Geiger, T.; Mann, M.; Cox, J., The Perseus computational platform for comprehensive analysis of (prote)omics data. *Nat. Methods* **2016,** *13* (9), 731-740.

12. LIST OF ABBREVIATIONS

ABPP	activity-based protein profiling
ACN	acetonitrile
AfBPP	affinity-based protein profiling
Amp	ampicillin
ASPP	active site peptide profiling
BCA	bicinchoninic acid
BSA	bovine serum albumin
CETSA	cellular thermal shift assay
CM	chloramphenicol
dd	double distilled
DMEM	Dulbecco's modified Eagle's medium
DMSO	dimethylsulfoxide
DNA	deoxyribonucleic acid
DTT	dithiothreitol
ECM	extracellular matrix
E. coli	*Escherichia coli*
EDTA	ethylenediaminetetraacetic acid
e.g.	Exempli gratia
ER	endoplasmic reticulum
ESI	electro spray ionization
et al.	et alii
FA	formic acid
FBS	fetal bovine serum
FDR	false discovery rate
Glu	glutamine
GO	gene ontology
HILIC	hydrophilic liquid interaction chromatography
HPLC	high-performance liquid chromatography
HR-MS	high resolution mass spectrometry
HTS	high throughput screening
IAA	iodoacetamide
IC_{50}	concentration of 50% inhibition
iTRAQ	isobaric tags for relative and absolute quantitation
IPTG	isopropyl β-d-1-thiogalactopyranoside
KEGG	kyoto encyclopedia of genes and genomes
KD	knockdown
KO	knockout
LysC	endoproteinase lys-C
LB	lysogeny broth
LC	liquid chromatography
LC-MS	liquid chromatography coupled to mass spectrometry
LFQ	label-free quantification
LysC	Endoproteinase Lys-C
MALDI	matrix-assisted laser desorption/ionization
MeCN	acetonitrile
MeOH	methanol
min	minutes
MMP	matrix metalloproteases
MS	mass spectrometry
MS/MS	tandem mass spectrometry
MTT	3-(4,5-dimethylthiazol-2-yl)-2,5-diphenyltetrazolium bromide
MWCO	molecular weight cut-off
m/z	mass to charge
NCA	neocarzilin A
NCA'	stereoisomer of **NCA**
NCB	neocarzilin B
NCC	neocarzilin C
NCC'	stereoisomer of **NCC**
NC-1	neocarzilin 1 probe
NC-4	neocarzilin 4 probe

|	
NC-2	neocarzilin 2 probe
NC-5	neocarzilin 5 probe
nt siRNA	non-targeting small interfering RNA
OD	optical density
on	overnight
PA	phosphatidic acid
PBS	phosphate buffered saline
PTM	posttranslational modification
PEG	polyethylene glycol
PKC	Protein kinase C
PCR	polymerase chain reaction
pH	power of hydrogen
PLD	phospholipase d
ppm	parts per million
PS	phosphatidylserine
RhN$_3$	rhodamine azide
RNA	ribonucleic acid
RPMI	Roswell Park Memorial Institute
r.t.	room temperature
SAR	structure-activity relationship
SDS-PAGE	sodium dodecyl sulfate – polyacrylamide gel electrophoresis
SEC	size exclusion chromatography
sec	seconds
SILAC	stable isotope labeling with amino acids in cell culture
siRNA	small interfering RNA
SPR	surface plasmon resonance
Src	cellular und sarcoma
S. carzinostaticus	*Streptomyces carzinostaticus*
STRING	Search tool for the retrieval of interacting genes/proteins
TEAB	triethylammoniumbicarbonat
T. californica	*Torpedo californica*
TCEP	tris(2-carboxyethyl)phosphine
TEV	tobacco etch virus
TBTA	tris(benzyltriazolylmethyl)amine
TFA	trifluoro acetic acid
TFL	trifunctional linker
TMT	tandem mass tag
UV	ultraviolet
v/v	volume/volume
vs.	versus
wt	wildtype
w/v	weight/volume

13. APPENDIX

Neocarzilin A and C
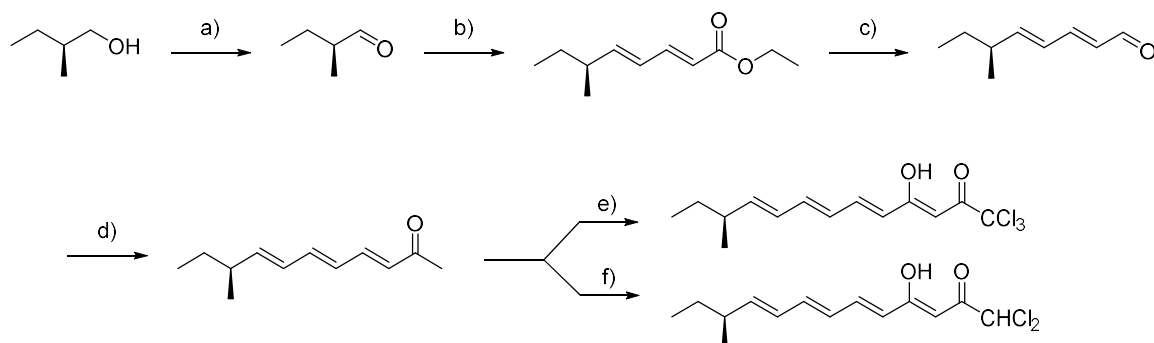
Scheme S1: Synthesis of **NCA** and **NCC**: a) TEMPO (1 mol-%), KBr (0.10 eq), NaOCl (2.00 eq), CH2Cl2/carbonate-buffer pH = 8.6, 0 °C, 45 min, 85%; b) 1. LiHMDS (1.00 eq), 2. ethyl (E)-4-(diethoxyphosphoryl)-but-2-enoate (1.00 eq),THF, -78 °C → -40 °C, 3 h, 76%; c) DIBAL-H (2.10 eq) MnO2 (20.0 eq), THF, hexane,-78 °C → rt, 5 h, 72% over 2 steps; d) 1-(Triphenylphosphoranylidene)-2-propanone (2.00 eq), toluene, 100 °C, 16 h, 59%; e) 1. LiHMDS (1.05 eq); 2. Trichloroacetic anhydride (2.00 eq), THF, -78 °C, 3 h, 71%; f) 1. LiHMDS (1.05 eq), 2. Dichloroacetic anhydride (2.00 eq), THF, -78 °C, 3 h, 44%. Synthesis was performed by Thomas Gronauer and Dr. Wolfgang Heydenreuter.

Neocarzilin B
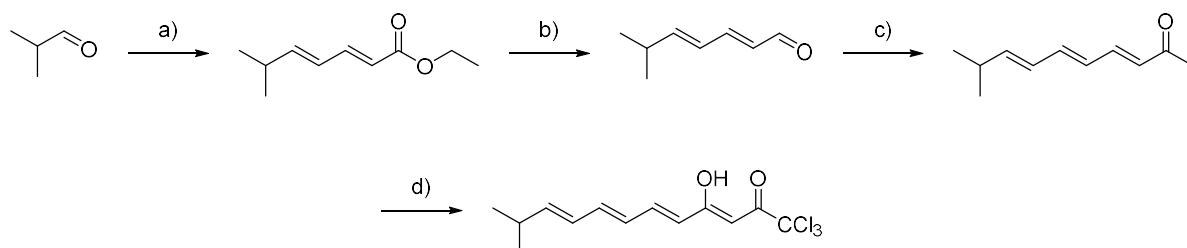
Scheme S2: Synthesis of **NCB**: a) LiHMDS (1.00 eq) ethyl (E)-4-(diethoxyphosphoryl)-but-2-enoate (4.15) (1.00 eq), THF, -78 °C → rt, 4 h, 51%; b) DIBAL-H (2.10 eq), MnO2 (20.0 eq), THF, hexane, -78 °C → rt, 5 h, 83% over 2 steps; c) 1-(Triphenylphosphoranylidene)-2-propanone (2.00 eq), toluene,100 °C, 16 h, 60%; d) 1. LiHMDS (1.00 eq), 2. trichloroacetic anhydride (2.00 eq), THF, -78 °C, 3 h, 83%. Synthesis was performed by Thomas Gronauer and Dr. Wolfgang Heydenreuter.

Neocarzilin A'
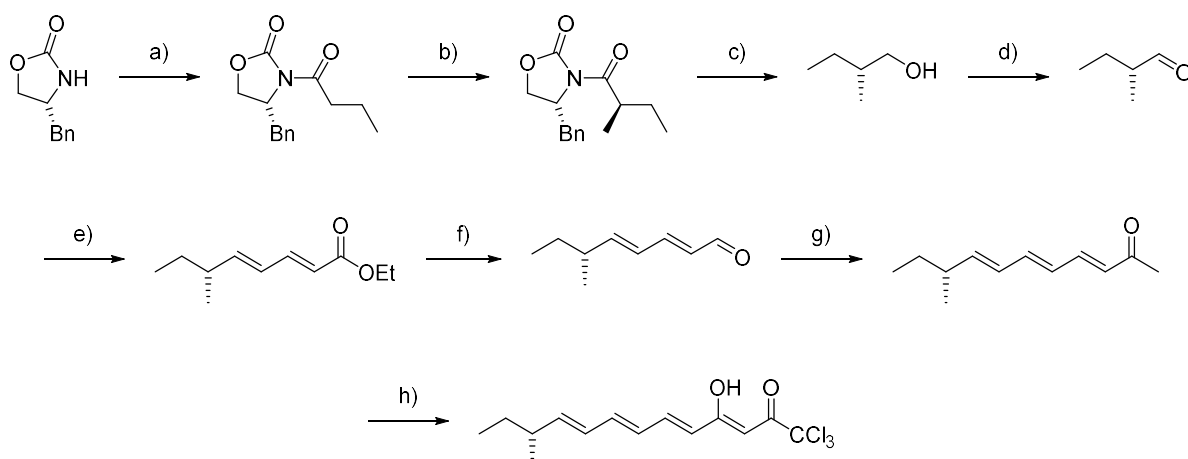
Scheme S3: Synthesis of **NCA'**: a) 1.) n-BuLi (1.10 eq), THF, -78 °C, 0.5 h, 2.) butyryl chloride, -78 °C, 0.5 h, -78 °C – rt, 0.5 h, 68%; b) 1.) NaHMDS (1.20 eq), THF, -78 °C, 1 h, 2.) MeI (2.50 eq), -78 °C, 2.5 h, 77%; c) LiBH4 (0.70 eq), MeOH (1.48 eq), Et2O, -20 °C → rt, 2 h, 66%; d) (COCl)2 (1.50 eq), DMSO (2.50 eq), NEt3 (5.00 eq), CH2Cl2, -78 °C, 0.5 h, rt, 2 h, 56%; e) 1. LiHMDS (1.50 eq), 2. ethyl (E)-4-(diethoxyphosphoryl)-but-2-enoate (1.50 eq),THF, -78 °C → -40 °C, 3 h, 30%; f) DIBAL-H (2.50 eq) MnO2 (20.0 eq), THF, hexane,-78 °C → rt, 5 h, 78% over 2 steps; g) 1-(Triphenylphosphoranylidene)-2-propanone (2.00 eq), toluene, 100 °C, 16 h, 77%; h) 1. LiHMDS (1.10 eq); 2. Trichloroacetic anhydride (2.00 eq), THF, -78 °C, 3 h, 60%. Synthesis was performed by Thomas Gronauer.

ABPP probe NC-1
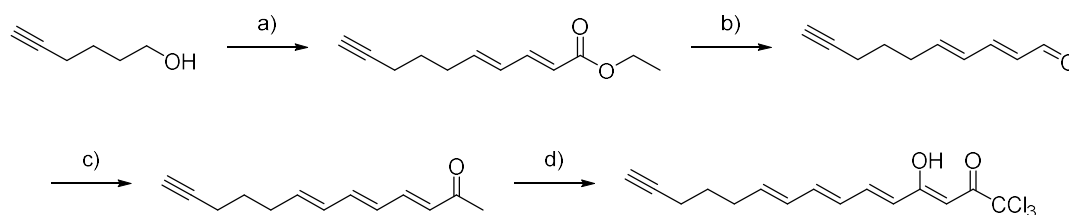
Scheme S4: Synthesis of probe **NC-1**: a) 1.DMSO (2.22 eq), (COCl)2 (1.11 eq), NEt3 (4.50 eq); 2. LiHMDS (1.00 eq), ethyl (E)-4-(diethoxyphosphoryl)-but-2-enoate (1.00 eq), CH2Cl2,THF, -78 °C → rt, 4 h, 38% over 2 steps; b) DIBAL-H (2.10 eq), MnO2 (20.0 eq), THF, hexane, -78 °C → rt, 5 h, 54% over 2 steps; c) 1-(Triphenyl-phosphoranylidene)-2-propanone (2.00 eq), toluene,100 °C, 16 h, 54%; d) 1. LiHMDS (2.00 eq); 2. trichloroacetic anhydride (1.00 eq), THF, -78 °C, 3 h, 45%. Synthesis was performed by Thomas Gronauer and Dr. Wolfgang Heydenreuter.
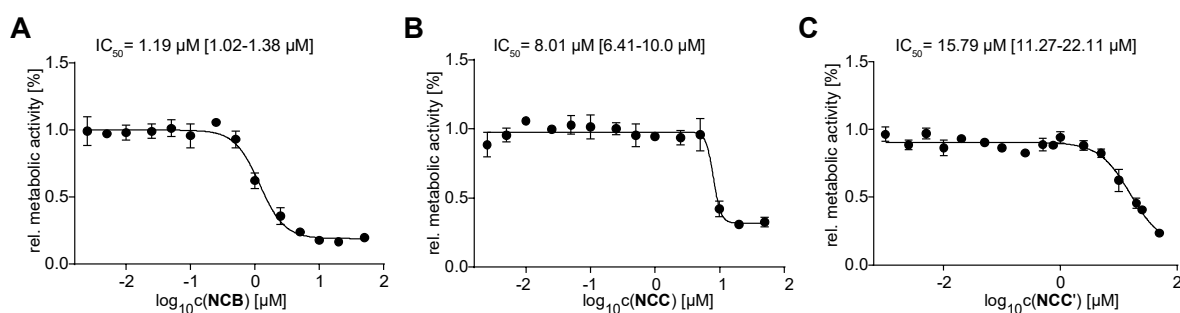

Figure 45: Cytotoxicity of remaining natural products in MDA-MB-231. A, MTT assay of **NCB**. **B,** MTT assays of **NCC**. **C,** MTT assay of **NCC'**. One representative plot of three independent experiments is shown. 95% confidential intervals are shown in brackets of a non-linear curve fit performed by Prism 6.5.
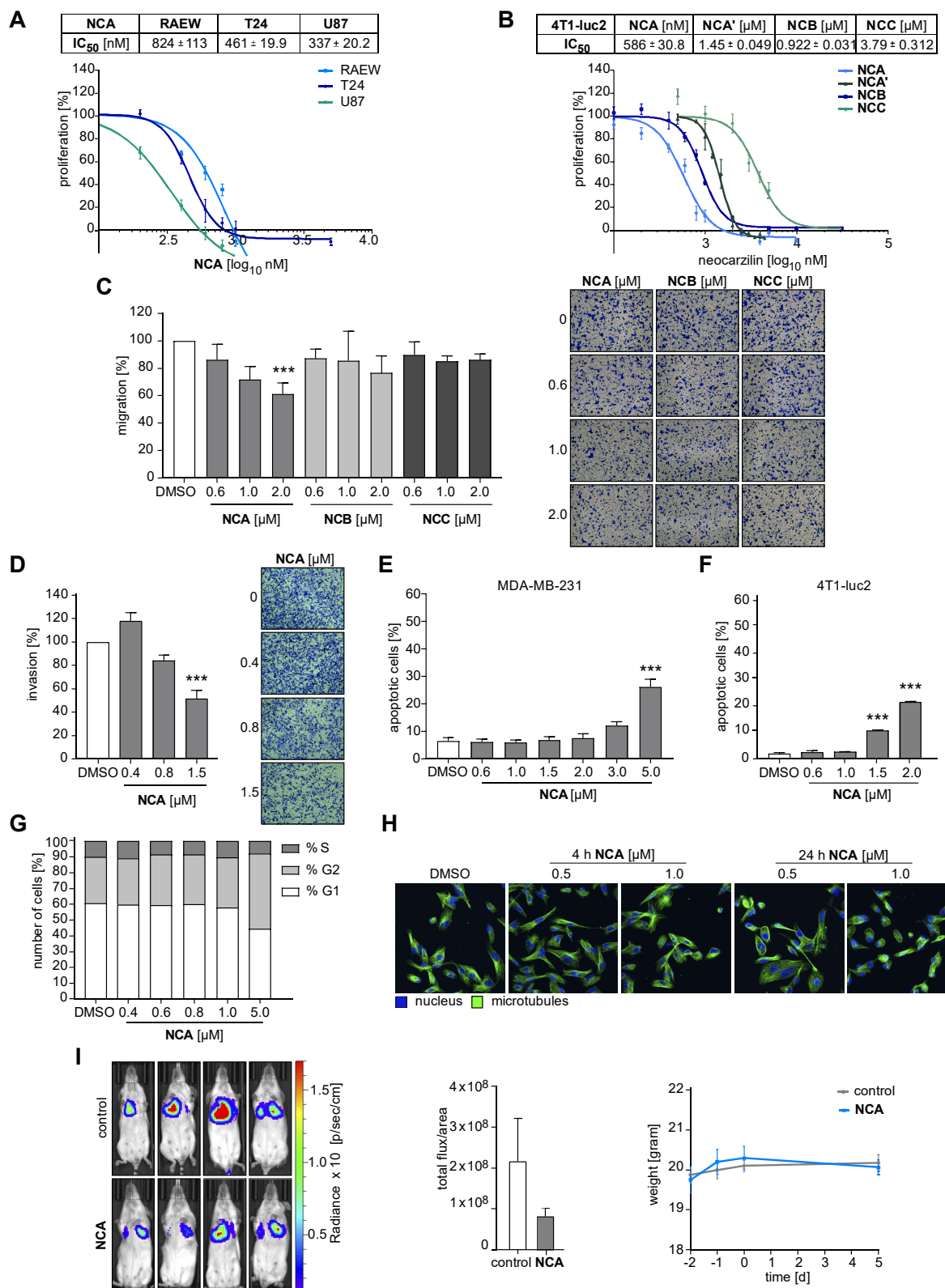
Figure 46: Effect of NCA on cancer cells. A, The anti-proliferative effect of **NCA** on T24 human bladder carcinoma cells and the glioblastoma cell lines RAEW and U87 was determined by crystal violet staining after 72 h. **B,** Proliferative capacity of 4T1-luc2 murine breast carcinoma cells treated with **NCA**, **NCA'**; **NCB** and **NCC** was determined by crystal violet staining after 72 h. **C,** Transwell migration of 4T1-luc2 cells treated with **NCA**, **NCB** or **NCC** determined by Boyden Chamber assay. **A-C,** Bars always represent the mean ± SEM of at least three independent experiments performed in duplicates/triplicates, one-way ANOVA, Dunnett's test, ***P < 0.001 compared with DMSO control (**C**). **D**, Effect of **NCA** on the invasiveness of MDA-MB-231 cells was determined *via* Boyden Chamber assay using Matrigel-coated membrane inserts. The bar diagram shows the number of invasive cells normalized to the control. **E-F,** MDA-MB-231 (**E**) or 4T1-luc2 cells (**F**) were treated with

indicated concentrations of **NCA**. Cells were permeabilized and stained with propidiumiodide using the method described by Nicoletti *et al.*[143]. The percentage of dying cells was determined by flow cytometry. **D-F,** Bars always represent the mean ± SEM of at least three independent experiments performed in duplicates/triplicates, one-way ANOVA, Dunnett's test, ***P < 0.001 compared with DMSO control. **G,** The effect of **NCA** on the cell cycle progression of MDA-MB-231 cells was determined by propidiumiodide staining using the method described by Nicoletti *et al.*[143]. The cell cycle analysis was performed with the FlowJo 7.4 program using the Watson pragmatic model. **H,** MDA-MB-231 cells were seeded in eight-well microscopic slides and stimulated with **NCA** or DMSO as indicated. α-Tubulin (green) and nuclei (blue) were visualized by immunocytochemistry. Representative images out of 3 independent experiments are shown. **I,** Dissemination of 4T1-luc2 cells injected into the tail vein of control and **NCA**-treated Balb/c mice into the lungs and bodyweight changes in control and **NCA**-treated mice. Representative in vivo bioluminescent images of 4 out of 8 mice on day 5 are shown. Bar diagram shows corresponding signal intensities with bars representing the mean ± SEM of 8 mice, two-tailed unpaired Student's *t* test, not significant. Experiments were performed by Dr. Carolin Pyka (LMU). Adapted from Gleissner *et al.* [134]
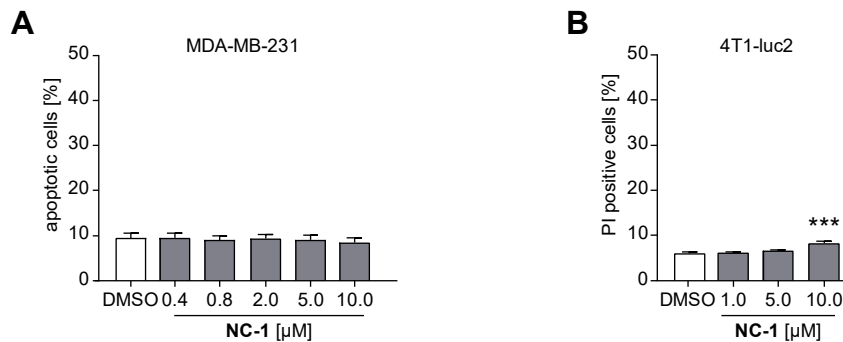
Figure 47: Apoptosis induction by probe NC-1. A-B, MDA-MB-231 (**A**) and 4T1-luc2 cells (**B**) treated with indicated concentrations of **NC-1**. Cells were either permeabilized and stained with propidiumiodide using the method described by Nicoletti *et al.*[143] (**A**) or stained with propidiumiodide (**B**). The percentage of dying cells was determined by flow cytometry. **A-B,** Bars represent the mean ± SEM of three independent experiments performed in duplicates/triplicates, one-way ANOVA, Dunnett's test, ***P < 0.001 compared with DMSO control. Experiments were performed by Dr. Carolin Pyka (LMU). Adapted from Gleissner *et al.* [134]
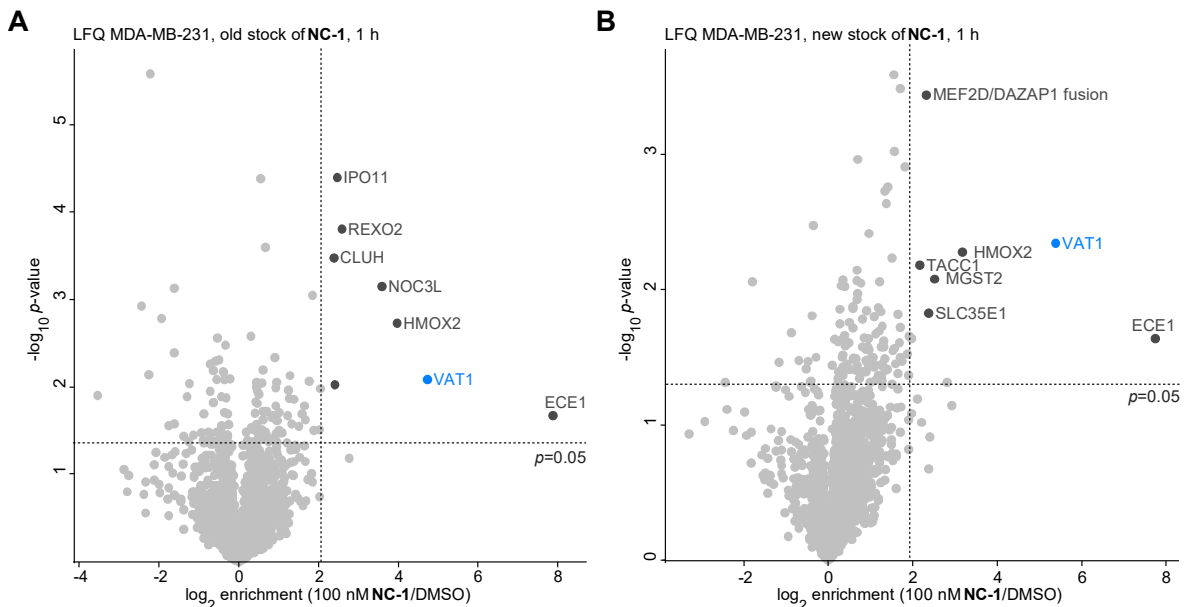
Figure 48: Comparison between old and new stock of probe NC-1. A, Volcano plot showing the results of a two-sample *t*-test of **NC-1** enrichment against DMSO background (n=4). Old stock of **NC-1** was applied **B,** Volcano plot showing the results of a two-sample *t*-test of **NC-1** enrichment against DMSO background. New stock of **NC-1** was applied. **A-B,** Hits matching the criteria log₂ enrichment > 2 and *p*-value < 0.05 are highlighted in grey, target protein VAT-1 is shown in blue.

A **NC-1** labeling cytosol + membrane
MS preparation stability test
MDA-MB-231

B **NC-1** labeling cytosol + membrane
Transfection of His-TEV-VAT-1 contruct, R128 mutants
MDA-MB-231
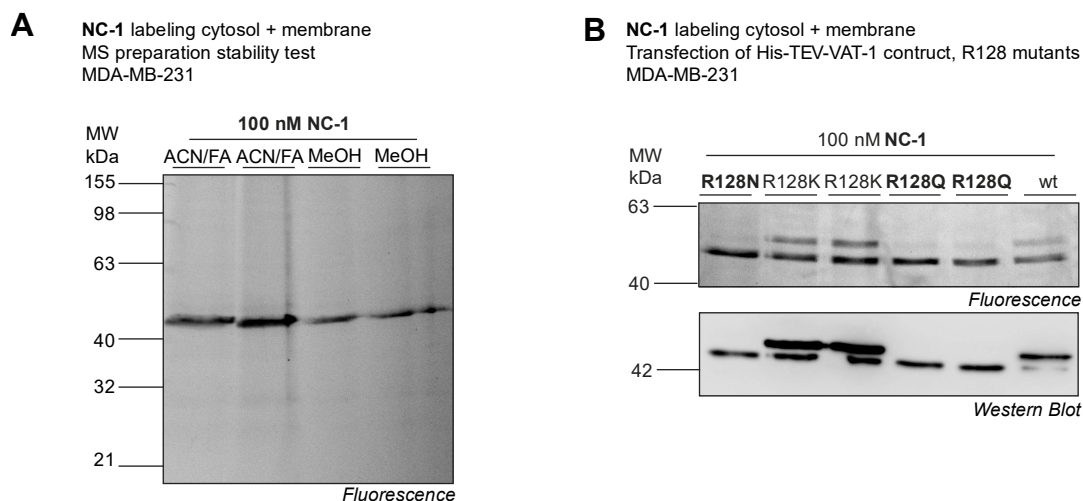
Figure 49: Additional validation of binding site peptides. A, MS sample preparation test for evaluation of VAT-1-**NC-1** binding stability. Cells were labeled *in situ* with **NC-1**, were clicked to rhodamine azide and were precipitated with acetone, washed with MeOH and were resuspended with MeCN/FA. SDS-PAGE of samples is shown. **B,** MDA-MB-231 cells were transfected with binding site point mutants and were labeled *in situ* with **NC-1**. SDS PAGE and Western blot analysis is shown.
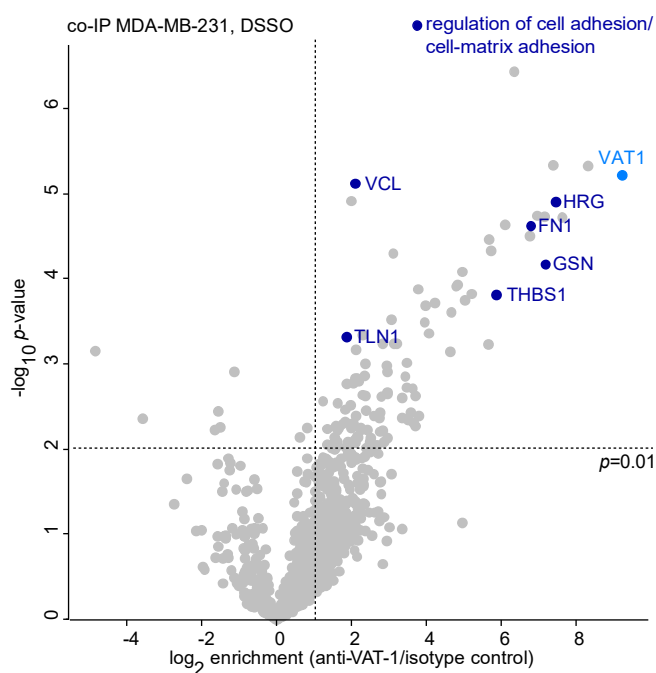
Figure 50: VAT-1 crosslink co-IP in MDA-MB-231. Volcano plot showing results of two-sample *t*-test of VAT- 1 co-IP with 2 mM DSSO crosslinker (n=5). Rabbit isotype control was applied as a control. Proteins involved in cell adhesion are highlighted in dark blue and VAT-1 is shown in blue. Hits matching the criteria log$_2$ enrichment > 1 and *p*-value < 0.01 are potential VAT-1 interaction partners.

Figure 51: Control of DSSO crosslink target ID approach. Volcano plot showing the results of a two-sample *t*-test of **NC-1** enrichment without DSSO crosslinker (n=3). Hits matching the criteria log$_2$ enrichment > 1 and *p*- value < 0.05 are highlighted in grey and were excluded as potential VAT-1 interaction partners for Figure 31. Target protein VAT-1 is shown in blue.
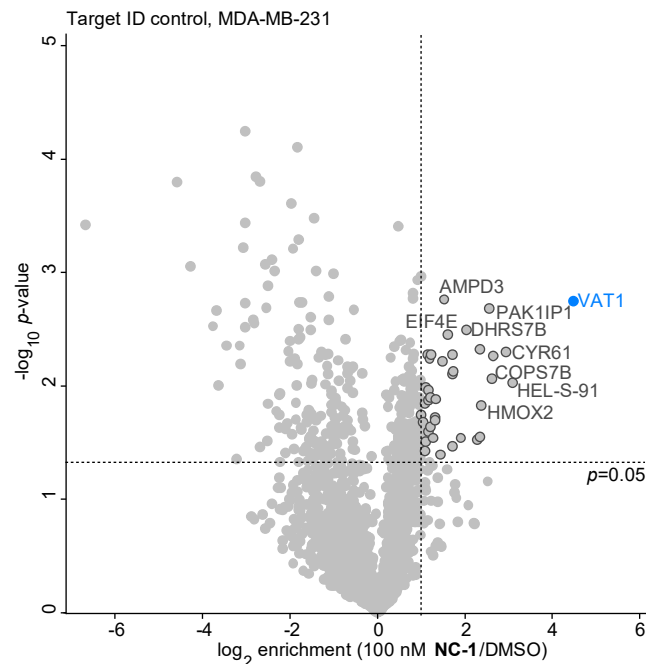
Table 30: Enriched proteins in control volcano plot from crosslink target ID in MDA- MB-231 shown in Figure 31 with corresponding log$_2$ enrichment and significance. (blue = **NC-1** target protein, dark grey = proteins matching the criteria log$_2$ enrichment > 1, *p*- value < 0.05).

gene names	protein names	log$_2$ fold change	-log$_{10}$ *p*-value	coverage [%]
VAT1	Synaptic vesicle membrane protein VAT-1 homolog	4.48	2.74	41.2
HEL-S-91	Serine/arginine-rich splicing factor 6	3.09	2.03	9.9
CYR61	Protein CYR61	2.94	2.30	15.1
COPS7B	COP9 signalosome complex subunit 7b	2.64	2.26	22.6
PCCA	Propionyl-CoA carboxylase alpha chain, mitochondrial	2.61	2.06	29.3
PAK1IP1	p21-activated protein kinase-interacting protein 1	2.55	2.68	8.7
HMOX2	Heme oxygenase 2	2.38	1.83	26.3
CALM3	Calmodulin-3	2.34	2.32	52.4
NADK2	NAD kinase 2, mitochondrial	2.34	1.55	23.5
ORMDL3	ORM1-like protein 3	2.28	1.52	20.2
DHRS7B	Dehydrogenase/reductase SDR family member 7B	2.02	2.49	15.2
FOXK1	Forkhead box protein K1	1.91	1.54	17.2
CPSF2	Cleavage and polyadenylation specificity factor subunit 2	1.73	2.13	15.9
GPRC5C	G-protein coupled receptor family C group 5 member C	1.72	2.27	9.3
PLXNA1	Plexin-A1	1.72	1.47	3.5
EED	Polycomb protein EED	1.71	2.10	15.5
EIF4E	Eukaryotic translation initiation factor 4E	1.61	2.46	20.7
AMPD3	AMP deaminase 3	1.52	2.76	7.2
PAFAH1B3	Platelet-activating factor acetylhydrolase IB subunit gamma	1.49	2.22	26.4
CDYL	Chromodomain Y-like protein	1.43	1.39	16.4
BCS1L	Mitochondrial chaperone BCS1	1.33	1.88	6.9
RAB43	Ras-related protein Rab-43	1.32	1.69	24.5
CPT1A	Carnitine O-palmitoyltransferase 1, liver isoform	1.31	1.72	8.9
DAG1	Dystroglycan;Alpha-dystroglycan;Beta-dystroglycan	1.27	1.54	4.9
LOC221955	Sn1-specific diacylglycerol lipase beta	1.25	1.30	9
IFIT1	Interferon-induced protein with tetratricopeptide repeats 1	1.22	2.27	18.6
SHCBP1	SHC SH2 domain-binding protein 1	1.22	1.64	7.4
MAP4K5	Mitogen-activated protein kinase kinase kinase kinase	1.20	1.89	12.9
RTN4	Reticulon-4	1.19	2.24	9.1
NT5C2	Cytosolic purine 5-nucleotidase	1.19	1.33	14.7

HID1	Protein HID1	1.17	1.88	11.6
HEL-S-132P	14 kDa phosphohistidine phosphatase	1.16	1.60	16
FKBP1A	Peptidyl-prolyl cis-trans isomerase FKBP1A	1.16	1.96	28.7
ATP6V1G1	V-type proton ATPase subunit G 1	1.14	2.27	22
HIBADH	3-hydroxyisobutyrate dehydrogenase	1.14	1.97	31.5
HIP1R	Huntingtin-interacting protein 1-related protein	1.14	1.87	11.6
GNAS	Guanine nucleotide-binding protein G(s) subunit alpha isoforms short	1.11	1.63	16.3
SMG8	Protein SMG8	1.10	1.99	6.1
KIAA1598	Shootin-1	1.10	1.51	7.4
TDRD3	Tudor domain-containing protein 3	1.09	1.84	5.1
CCDC93	Coiled-coil domain-containing protein 93	1.08	1.42	13.5
TACC1	Transforming acidic coiled-coil-containing protein 1	1.05	1.68	18.3
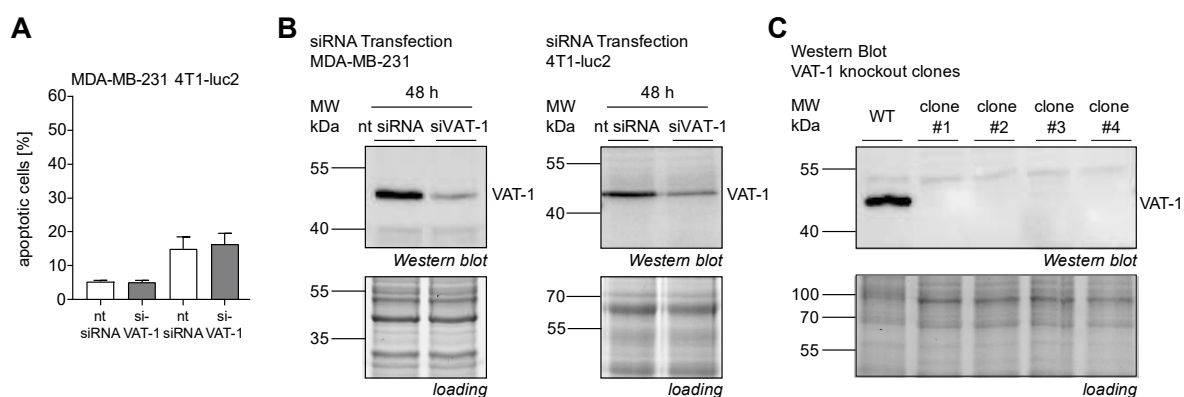
Figure 52: Knockdown or knockout of VAT-1. A, MDA-MB-231 or 4T1-luc2 cells were transfected with siRNA targeting VAT-1 for 48 h. Cells were permeabilized and stained with propidiumiodide using the method described by Nicoletti *et al.*[143] The percentage of dying cells was determined by flow cytometry. Bars represent the mean ± SEM of three independent experiments performed in triplicates, two-tailed unpaired Student's *t* test. **B,** Western Blot showing VAT-1 protein levels in non-targeting (nt) and VAT-1 siRNA MDA-MB-231 after 48 h of siRNA transfection. **C,** Western Blot showing VAT-1 protein levels in HEK-293 WT cells and HEK-293 VAT-1 knockout clones generated *via* the CRISPR-Cas9 method. Adapted from Gleissner *et al.* [134]
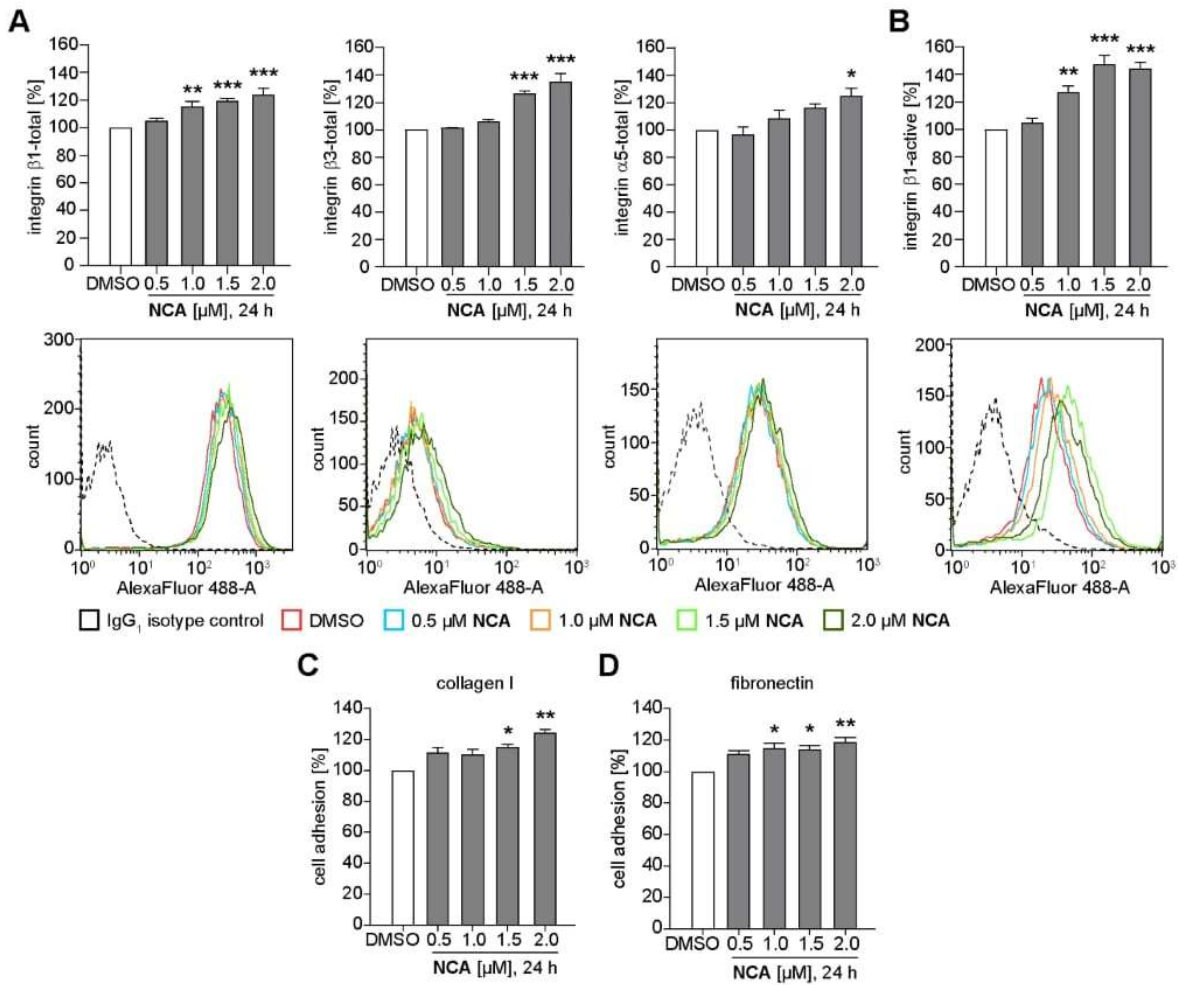
Figure 53: Impact of NCA on integrin expression and cell-matrix adhesion. A, Surface expression of total integrin β1, β3, and α5 was determined *via* antibody staining and FACS analysis in MDA-MB-231 cells after 24 h treatment with **NCA**. **B,** The effect of **NCA** on the activation of integrin β1 in MDA-MB-231 was analyzed by immunostaining and FACS analysis in MDA-MB-231 cells after 24 h. **A-B,** Data was analyzed using FlowJo 7.6.5 software. **C-D,** Influence of **NCA** on the adhesion of MDA-MB-231 cells to collagen I © and fibronectin D, determined *via* plate-and-wash adhesion assay. **A-D,** Bar diagrams showing results normalized to the DMSO control as mean ± SEM of at least three independent experiments performed in triplicate are presented, one-way ANOVA, Dunnett's test, *P < 0.033, **P < 0.002, ***P < 0.001 compared with DMSO control. Experiments were performed by Dr. Carolin Pyka (LMU).[136]

A

B

Figure 54: Effect of NCA on the cellular level of selected interaction partners of VAT-1. **A-B,** MDA-MB-231 cells were treated with the indicated concentrations of **NCA** or DMSO for 4 h (**A**) or 24 h (**B**), respectively. Cellular protein levels were detected by Western blot analysis and results normalized t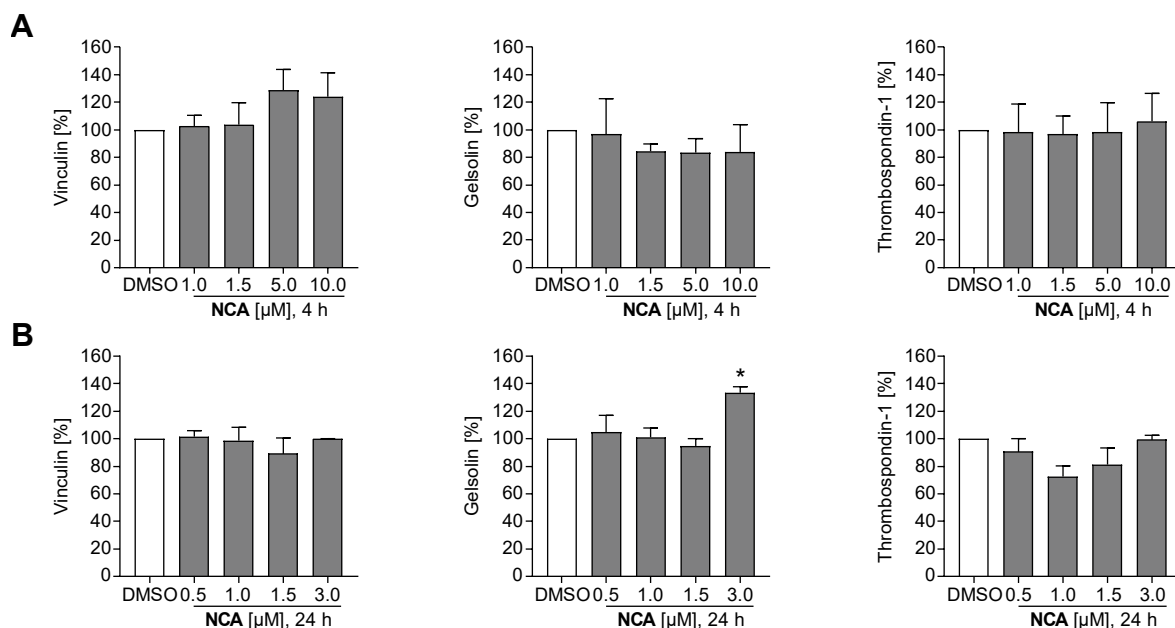o DMSO treated cells. Bars represent the mean ± SEM of three independent experiments, one-way ANOVA, Dunnett's test, *P < 0.033 compared with DMSO control. Experiments were performed by Dr. Carolin Pyka (LMU). Adapted from Gleissner *et al.* [134]

Table 31: VAT-1 sequences for point mutant numeration**:** VAT-1 isoform 1 from uniprot was applied for numeration, VAT-1 with His-TEV tag was applied for overexpression in *E. coli* and human cells.

gene	protein sequence
VAT-1 uniprot Q99536	MSDEREVAEAATGEDASSPPPKTEAASDPQHPAASEGAAAAAASPPLLRCLVLTGFGG YDKVKLQSRPAAPPAPGPGQLTLRLRACGLNFADLMARQGLYDR**LPPLPVTPGMEGAG VVIAVGEGVSDR**KAGDRVMVLNRSGMWQEEVTVPSVQTFLIPEAMTFEEAAALLVNYIT AYMVLFDFGNLQPGHSVLVHMAAGGVGMAAVQLCRTVENVTVFGTASASKHEALKEN GVTHPIDYHTTDYVDEIKKISPKGVDIVMDPLGGSDTAKGYNLLKPMGKVVTYGMANLLT GPKRNLMALARTWWNQFSVTALQLLQANRAVCGFHLGYLDGEVELVSGVVARLLALYN QGHIKPHIDSVWPFEKVADAMKQMQEKKNVGKVLLVPGPEKEN
His-TEV-VAT-1 (*E. coli* and human)	MHHHHHHITSLYKKAGFENLYFQGSDEREVAEAATGEDASSPPPKTEAASDPQHPAAS EGAAAAAASPPLLRCLVLTGFGGYDKVKLQSRPAAPPAPGPGQLTLRLRACGLNFADLM ARQGLYDR**LPPLPVTPGMEGAGVVIAVGEGVSDR**KAGDRVMVLNRSGMWQEEVTVPS VQTFLIPEAMTFEEAAALLVNYITAYMVLFDFGNLQPGHSVLVHMAAGGVGMAAVQLCR TVENVTVFGTASASKHEALKENGVTHPIDYHTTDYVDEIKKISPKGVDIVMDPLGGSDTA KGYNLLKPMGKVVTYGMANLLTGPKRNLMALARTWWNQFSVTALQLLQANRAVCGFHL GYLDGEVELVSGVVARLLALYNQGHIKPHIDSVWPFEKVADAMKQMQEKKNVGKVLLVP GPEKEN

14. LICENCES

ELSEVIER LICENSE

TERMS AND CONDITIONS

Apr 20, 2020

This Agreement between TUM Munich -- Carolin Gleissner ("You") and Elsevier ("Elsevier") consists of your license details and the terms and conditions provided by Elsevier and Copyright Clearance Center.

License Number	4798780806668
License date	Mar 30, 2020
Licensed Content Publisher	Elsevier
Licensed Content Publication	Trends in Biotechnology
Licensed Content Title	yGenetic manipulation of antitumor-agent biosynthesis to produce novel drugs
Licensed Content Author	José A Salas,Carmen Méndez
Licensed Content Date	Nov 1, 1998
Licensed Content Volume	16
Licensed Content Issue	11
Licensed Content Pages	8
Start Page	475
End Page	482
Type of Use	reuse in a thesis/dissertation

Portion	figures/tables/illustrations
Number of figures/tables/illustrations	1
Format	both print and electronic
Are you the author of this Elsevier article?	No
Will you be translating?	No
Title	Investigation of the role of VAT-1 as a target of the natural product Neocarzilin A in tumor cell migration
Institution name	TUM Munich
Expected presentation date	Apr 2020
Portions	Figure 1
Requestor Location	TUM Munich Lichtenbergstraße 4 Garching, other 85748 Germany Attn: TUM Munich
Publisher Tax ID	GB 494 6272 12
Total	0.00 EUR

ELSEVIER LICENSE
TERMS AND CONDITIONS

Apr 20, 2020

This Agreement between TUM Munich -- Carolin Gleissner ("You") and Elsevier ("Elsevier") consists of your license details and the terms and conditions provided by Elsevier and Copyright Clearance Center.

License Number	4798780974792
License date	Mar 30, 2020
Licensed Content Publisher	Elsevier
Licensed Content Publication	Cell
Licensed Content Title	Hallmarks of Cancer: The Next Generation
Licensed Content Author	Douglas Hanahan,Robert A. Weinberg
Licensed Content Date	Mar 4, 2011
Licensed Content Volume	144
Licensed Content Issue	5
Licensed Content Pages	29
Start Page	646
End Page	674
Type of Use	reuse in a thesis/dissertation
Portion	figures/tables/illustrations

Number of figures/tables/illustrations	1
Format	both print and electronic
Are you the author of this Elsevier article?	No
Will you be translating?	No
Title	Investigation of the role of VAT-1 as a target of the natural product Neocarzilin A in tumor cell migration
Institution name	TUM Munich
Expected presentation date	Apr 2020
Portions	Figure 6
Requestor Location	TUM Munich Lichtenbergstraße 4 Garching, other 85748 Germany Attn: TUM Munich
Publisher Tax ID	GB 494 6272 12
Total	0.00 EUR

Copyright Clearance Center — Marketplace™

Royal Society of Chemistry - License Terms and Conditions

This is a License Agreement between Carolin Gleissner, TUM ("You") and Royal Society of Chemistry ("Publisher") provided by Copyright Clearance Center ("CCC"). The license consists of your order details, the terms and conditions provided by Royal Society of Chemistry, and the CCC terms and conditions.

All payments must be made in full to CCC.

Order Date	04-Aug-2020	Type of Use	Republish in a thesis/dissertation
Order license ID	1053151-1	Publisher	ROYAL SOCIETY OF CHEMISTRY
ISSN	1477-0539	Portion	Chart/graph/table/figure

LICENSED CONTENT

Publication Title	Organic & biomolecular chemistry	Country	United Kingdom of Great Britain and Northern Ireland
Author/Editor	Royal Society of Chemistry (Great Britain)	Rightsholder	Royal Society of Chemistry
Date	01/01/2003	Publication Type	e-Journal
Language	English	URL	http://www.rsc.org/is/journals/current/obc/obcpub.htm

REQUEST DETAILS

Portion Type	Chart/graph/table/figure	Distribution	Worldwide
Number of charts / graphs / tables / figures requested	1	Translation	Original language of publication
Format (select all that apply)	Print, Electronic	Copies for the disabled?	No
Who will republish the content?	Academic institution	Minor editing privileges?	No
Duration of Use	Life of current edition	Incidental promotional use?	No
Lifetime Unit Quantity	Up to 499	Currency	EUR
Rights Requested	Main product		

NEW WORK DETAILS

Title	Investigation of the role of VAT-1 as a target of the natural product neocarzilin A in tumor cell migration	Institution name	TU Munich
		Expected presentation date	2020-08-09
Instructor name	Carolin Gleissner		

ADDITIONAL DETAILS

Order reference number	N/A	The requesting person / organization to appear on the license	Carolin Gleissner, TUM

REUSE CONTENT DETAILS

Title, description or numeric reference of the portion(s)	Figure 1	Title of the article/chapter the portion is from	When the nine-membered enediynes play hide and seek
Editor of portion(s)	N/A	Author of portion(s)	Royal Society of Chemistry (Great Britain)
Volume of serial or monograph	N/A	Issue, if republishing an article from a serial	N/A
Page or page range of portion	7453	Publication date of portion	2012-08-12

Copyright Clearance Center — Marketplace™

American Soc for Biochemistry & Molecular Biology - License Terms and Conditions

This is a License Agreement between Carolin Gleissner, TUM ("You") and American Soc for Biochemistry & Molecular Biology ("Publisher") provided by Copyright Clearance Center ("CCC"). The license consists of your order details, the terms and conditions provided by American Soc for Biochemistry & Molecular Biology, and the CCC terms and conditions.

All payments must be made in full to CCC.

Order Date	30-Mar-2020	Type of Use	Republish in a thesis/dissertation
Order license ID	1025704-1	Publisher	AMERICAN SOCIETY FOR BIOCHEMISTRY AND MOLECULAR BI
ISSN	1083-351X	Portion	Chart/graph/table/figure

LICENSED CONTENT

Publication Title	Journal of biological chemistry	Country	United States of America
Author/Editor	AMERICAN SOCIETY FOR BIOCHEMISTRY & MOLECULAR BIOL	Rightsholder	American Soc for Biochemistry & Molecular Biology
Date	01/01/1905	Publication Type	e-Journal
Language	English	URL	http://www.jbc.org/

REQUEST DETAILS

Portion Type	Chart/graph/table/figure	Distribution	Worldwide
Number of charts / graphs / tables / figures requested	2	Translation	Original language of publication
Format (select all that apply)	Print, Electronic	Copies for the disabled?	No
Who will republish the content?	Academic institution	Minor editing privileges?	No
Duration of Use	Life of current edition	Incidental promotional use?	No
Lifetime Unit Quantity	Up to 499	Currency	EUR
Rights Requested	Main product		

NEW WORK DETAILS

Title	Investigation of the role of VAT-1 as a target of the natural product Neocarzilin A in tumor cell migration	Institution name	TUM Munich
		Expected presentation date	2020-04-23
Instructor name	Carolin Gleissner		

ADDITIONAL DETAILS

Order reference number	N/A
The requesting person / organization to appear on the license	Carolin Gleissner, TUM

REUSE CONTENT DETAILS

Title, description or numeric reference of the portion(s)	Figure 2A, Figure 3A	Title of the article/chapter the portion is from	Structural basis for inter-organelle phospholipid transport mediated by VAT-1
Editor of portion(s)	N/A	Author of portion(s)	AMERICAN SOCIETY FOR BIOCHEMISTRY & MOLECULAR BIOL
Volume of serial or monograph	N/A		
Page or page range of portion	19-20	Issue, if republishing an article from a serial	N/A
		Publication date of portion	1905-01-01

ACS — Chemistry for Life®

Dear Carolin Gleissner,

Your permission requested is granted and there is no fee for this reuse. In your planned reuse, you must cite the ACS article as the source, add this direct link https://pubs.acs.org/doi/10.1021/acscentsci.9b00266, and include a notice to readers that further permissions related to the material excerpted should be directed to the ACS.

If you need further assistance, please let me know.

Sincerely,

Raquel Picar-Simpson
ACS Publications Support
Customer Services & Information

15. CURRICULUM VITAE

Carolin Marie-Luise Gleißner, born 15th august 1991 in Cham, Germany

Academic Education

05.2017 – 05.2020	**Doctoral Studies** under Prof. Dr. Stephan A. Sieber, Chair of Organic Chemistry II (OC2), TU München: *Investigation of the role of VAT-1 as a target of the natural product neocarzilin A in tumor cell migration*
10.2014 – 03.2017	**Master of Science** in Biochemistry, TU München (Grade 1.1) Bioorganic chemistry and pharmacology and toxicology *Project: Validation of VAT-1 as a cellular target of tumor cell migration* Chair of organic chemistry II (OC2) Prof. Stephan A. Sieber
10.2011 – 05.2014	**Bachelor of Science** in Biochemistry, TU München (Grade 1.7) *Project: Transduction efficiency of AAV6 containing the shortEF1 and CMV promotor in cardiac fibroblast in vivo* Institute of pharmacology and toxicology Munich Prof. Stephan Engelhardt

Research internship in industry

01.2016 - 06.2016	**Boehringer Ingelheim**, Analytical Development, Biberach, Germany

School Education

09.2002 – 05.2011	Higher education entrance qualification ("Abitur"), Gymnasium Cham, Germany (Grade 1.5)

Conferences and workshops:

02.2020	Introduction into drug discovery, Kurt Ritter, TUM Graduate school, Munich, Germany
02.2020	Job application, TUM Graduate school, Munich, Germany
11.2019	Communication in teams and difficult situations, TUM Graduate school, Munich, Germany
10.2019	Scientific Octoberfest, CIPSM, Munich, Germany
06.2019	Bioorganic chemistry, Gordon research conference, Andover, USA
06.2019	Bioorganic chemistry, Gordon research seminar, Chemical tools for understanding biological systems Andover, USA
10.2018	Effizienztraining für Naturwissenschaftler, TUM Graduate School, Raitenhaslach, Germany
07.2018	MaxQuant Summer School, Barcelona, Spain
02.2017	New developments in the research of the pharma industry, TUM Graduate School, Munich, Germany
11.2016	Mass-Spec Proteomics on Campus 2016, Martinsried, Germany